HOMOGENEOUS PRECIPITATION OF BARIUM CHROMATE

A Thesis Submitted

by

Rohan Lakdasa De Silva

for the Degree of Doctor of Philosophy

DEPARTMENT OF CHEMICAL ENGINEERING

UNIVERSITY OF ASTON IN BIRMINGHAM

OCTOBER 1982

THE UNIVERSITY OF ASTON IN BIRMINGHAM

HOMOGENEOUS PRECIPITATION OF BARIUM CHROMATE

R.L. De Silva Ph.D. 1982

SUMMARY

The crystallisation of barium chromate in a batch stirred vessel, using the technique of precipitation from homogeneous solution (PFHS) was investigated. Experimental conditions that were varied included rate of change of solubility, operating temperature and stirrer speed. The results were fitted to an empirical model for growth rate per unit surface area (R_G), of the form:

$$R_G = k_1(a_{H^+})^{k_2}(\Delta C_t)^{k_4}$$

where, a_{H^+} was the hydrogen ion activity (kmol/m^3); ΔC_t was the supersaturation based on barium ion concentrations (kmol/m^3); and, R_G was expressed in kg/m^{2}s. The value of k_4 was 2 for all experimental conditions, while k_1 ranged from 0.6×10^{-2} to 7.2×10^{-2}, and k_2 from -0.56 to -0.39. Growth rate was independent of both crystal size, expressed in terms of mean equivalent volume diameters, and stirrer speed. Activation energies for crystal growth were in excess of 100 kJ/mol and strongly dependent on the amount of urea used for PFHS. This evidence led to the conclusion that crystal growth was surface integration controlled with the probable rate determining step being removal of the inner hydration sphere of the barium ion. The results of Falangas (5), obtained under comparable conditions, were also shown to follow the above empirical model.

The solubility of barium chromate was obtained by fitting the data of Skander (4) and Falangas (5), two former members of the research school at Aston, to the semi-empirical model,

$$C_e = S_1 \exp(S_2/T)(a_{H^+})^{S_3}$$

where, C_e was the solubility (kmol/m^3); T was the absolute temperature (K); and, S_1, S_2 and S_3 were empirical parameters.

Experiments to achieve epitaxial growth of barium chromate on fine polydisperse metal particulate substrates, using a batch stirred vessel and a batch fluidised bed, proved unsuccessful. This was attributed to lack of lattice match between substrate and overgrowth, and to deleterious experimental conditions. The substrates investigated were copper, hafnium, molybdenum, nickel, tantalum, titanium and tungsten.

Keywords

Barium Chromate
Batch Crystallisation
Precipitation from Homogeneous Solution
Solubility
Epitaxy

ACKNOWLEDGEMENT

I would like to express my appreciation and thanks to the following:

Professor P.E. Barker, who took over as my supervisor at a critical point in the project, and provided invaluable guidance and encouragement throughout the final stage of my work.

Dr. D.E. Creasy, who was my supervisor for the major part of this project, and until his departure to take up a new post in Australia, was always available with apposite academic and technical help as well as propitious personal advice.

Dr. M.C. Jones, of the Department of Chemical Engineering, for constructive suggestions and stimulating discussions during the latter part of this work.

The Department of Chemical Engineering, for providing the necessary facilities to carry out this project; in particular the technical staff, for a prompt and efficient service.

The Department of Metallurgy and Materials, for use of the facilities for scanning electron microscope photomicrography.

The Association of Commonwealth Universities for the award of a Commonwealth Scholarship.

The Vice Chancellor and the senior staff of the Department of Chemical Engineering, at the University of Moratuwa, Sri Lanka, for granting an adequate period of study leave to permit completion of this work.

TABLE OF CONTENTS

LIST OF TABLES

LIST OF GRAPHS

LIST OF FIGURES

CHAPTER ONE

INTRODUCTION

Time delay fuses are usually composed of a physical mixture of a fuel and an oxidant. Conventionally, the fuel is a metal and the oxidant is a heavy metal chromate. These physical mixtures have been found to give non-reproducible burning rates over certain composition ranges and this has been attributed to segregation processes occurring during fuse manufacture (1). It was considered that one way to overcome this problem while also improving the shelf life of the product was to grow the oxidant on each fuel particle, thereby encapsulating it. Tungsten powder and barium chromate were chosen as a typical working combination for investigation. Furthermore, it was decided to apply to the process, the technique of precipitation from homogeneous solution (P.F.H.S.) (2,3), in which supersaturation is generated homogeneously throughout the bulk of the solution, and epitaxial nucleation followed by growth occurs on the metal substrate which is kept in suspension in the solution.

The work reported here is a continuation of previous work by Skander (4) and Falangas (5). Skander investigated the solubility of barium chromate in hydrochloric acid and derived values for the equilibrium constants of the different complex equilibria which involve chromate ions in acidic

solutions. The feasibility of using urea hydrolysis to cause a controlled generation of supersaturation, thereby enabling the production of barium chromate crystals of 100 μm nominal size, as opposed to the much finer commercially available size of about 2 μm, was also established.

Falangas studied the crystal growth of barium chromate in a batch stirred vessel using the technique of precipitation from homogeneous solution and attempted epitaxial growth of barium chromate on tungsten particles in a batch fluidised bed crystalliser. Further studies on the solubility of barium chromate in a variety of acidic media, and an investigation of the kinetics of urea hydrolysis were also carried out.

Precipitation from homogeneous solution has hitherto been extensively used in analytical chemistry to separate barium from strontium and radium (2,6,7), but the technique does not appear to have been applied to the quantitative study of the kinetics of crystal growth of barium chromate. Most previous nucleation and growth studies on barium chromate have been carried out by the direct mixing of solutions of soluble salts containing the barium cation and the chromate anion. Usually the solutions used were very dilute and a slow rate of addition coupled with rapid mixing was employed to prevent build-up of high supersaturations which cause massive nucleation but little growth.

The aim of this work was to achieve the epitaxial growth of barium chromate on particulate metal substrates, with tungsten being chosen as a typical substrate. It was also intended to establish the most suitable production technique for carrying out epitaxial growth. If epitaxy was successfully achieved the product was to be used to prepare time delay fuses for burning tests in order to investigate the effect of product composition and particle size on burning rate and its reproducibility.

The lack of success experienced with epitaxial growth experiments using tungsten, lead to a broadening of the work after the first year of research. In the first instance it was decided to investigate other particulate metal substrates, which may have a more favourable crystal lattice for epitaxy. These were hafnium, molybdenum, tantalum and titanium of different nominal sizes. It was further decided to study the kinetics of crystal growth of barium chromate to attempt to resolve possible reasons for the difficulties encountered in the early part of the work.

A subsidiary aim of the work was to resolve the conflicting solubility measurements of Skander (4) and Falangas (5), by the use of an 'in situ' method of checking barium chromate solubility, such as a barium ion selective electrode.

CHAPTER TWO

CRYSTALLISATION LITERATURE

2.0 INTRODUCTION

The process of solute crystallisation from solution primarily involves two basic steps; namely nucleation of crystal embryos and their subsequent growth (8,9). However, the attainment of a driving force or supersaturated state is an essential prerequisite for both processes. It is possible, though not necessarily desirable, that the processes of generation of supersaturation, nucleation and crystal growth may occur simultaneously (9).

The literature review presented in this chapter has focussed on:

1. an examination of the theoretical aspects of nucleation and crystal growth;
2. the methods for controlled generation of supersaturation applicable to the crystallisation of barium chromate; and
3. previous studies on the crystal growth of barium chromate.

2.1 NUCLEATION

Current understanding on the phenomenon of nucleation recognises several different modes of nucleation (10). These are primary homogeneous nucleation, primary heterogeneous nucleation and secondary nucleation. Secondary nucleation can in

turn be sub-divided further according to its manner of occurrence (11). The mechanism of nucleation and theoretical and empirical nucleation models have been reviewed by many authors including De Jong (10), Mullin (9,12), Nielsen (13), Ohara and Reid (14) and Walton (15). Secondary nucleation has been reviewed by Botsaris (16), Garside and Davey (17) and Strickland-Constable (11,18).

2.1.1 Primary Homogeneous Nucleation

Homogeneous nucleation is considered to take place as a result of a statistical clustering process involving solute molecules or ions in solution. A stable nucleus is thought to arise when a cluster, formed by an essentially random process, exceeds a certain critical diameter ($d_{crit.}$) which is given by (9,10):

$$d_{crit.} = \frac{4\sigma_s M}{RT\rho \ln(S_{rel.}+1)} \quad \ldots\ldots\ldots\ldots\ldots\ldots \quad (2.1)$$

where, σ_s is the surface energy; M is the molecular weight; R is the universal gas constant; T is the absolute temperature; ρ is the density; and, $S_{rel.}$ is the relative supersaturation ($S_{rel.} = (a/a_e)-1$, where a is the solute activity and a_e is the equilibrium activity of the solute at saturation).

The rate of steady state homogeneous nucleation (R_H) is given by the Becker-Doring equation (19,20) and is equal to the net flux of clusters passing the critical nucleus size (10).

i.e. $R_H = K_H \exp\left(\frac{-\Delta G_{crit.}}{RT}\right)$ ..... (2.2)

where, K_H is a constant. $\Delta G_{crit.}$ is the free energy of formation of a critical nucleus which is given by (9,10):

$$\Delta G_{crit.} = \frac{16\sigma_s^2 M^2}{3R^2T^2\rho^2[\ln(S_{rel.}+1)]^2} \text{ ..... } (2.3)$$

The constant K_H is a complex function of temperature, surface energy and the diffusion coefficient of the solute (10,13). Walton (3) has stated that the approximation, $K_H \approx 10^{25}$ is appropriate for most purposes.

Homogeneous nucleation has been found to take place at a significant rate only above a certain limiting supersaturation (3,9). Since heterogeneous nucleation usually occurs at much lower supersaturations and because favourable conditions for heterogeneous nucleation generally prevail in real crystallisation systems (10), homogeneous nucleation rarely occurs in practice, except under special experimental conditions.

2.1.2 Primary Heterogeneous Nucleation

In heterogeneous nucleation the presence of foreign bodies or surfaces lowers the energy barrier associated with the formation of critical nuclei, and thus catalyses the process. The lowering of this energy barrier favours heterogeneous nucleation at low supersaturation. The critical free energy for heterogeneous nucleation ($\Delta G^*_{crit.}$) can be expressed

in terms of that for homogeneous nucleation (9,10).

i.e. $\Delta G^{*}_{crit.} = \Omega \Delta G_{crit.}$ ..... (2.4)

The factor Ω can take on a value between zero and unity. When the foreign body or surface has no effect on the energy barrier, Ω is unity and homogeneous nucleation takes place. When, for example, a supersaturated solution is seeded with minute crystals of the solute no nucleation is required and hence Ω is zero. Intermediate values of Ω correspond to heterogeneous nucleation. The value of Ω can be related to the affinity between the extraneous surface and the crystalline substance (3,9,10,13). Since the physical properties of the foreign substrate and crystalline solid necessary for computing Ω are unknown in most cases, the usual practice is to use an empirical power law model for primary nucleation rate (R_N) (10):

$$R_N = K_N S^{p}_{rel.} \quad \text{..... (2.5)}$$

where, K_N and p are constants. The constant p signifies the 'order' of primary nucleation. Supersaturation ($\Delta a = a - a_e$) or supersaturation ratio ($S_r = a/a_e$) is frequently used instead of relative supersaturation, ($S_{rel.} = \Delta a/a_e = S_r - 1$).

A special case of primary heterogeneous nucleation is epitaxy in which the growth of nuclei on the foreign body follows a specific orientation. Epitaxy has been reviewed in Chapter 3.

2.1.3 Secondary Nucleation (11,16,17,18,21)

The phenomenon, of nucleation taking place in the presence of solute crystals, at much lower supersaturations than required for primary nucleation, has been termed secondary nucleation. Secondary nucleation can occur in a variety of different ways, which may operate simultaneously.

2.1.3.1 Collision Breeding (11,17,18,21)

Collision breeding, or contact nucleation as it is also termed, takes place in agitated crystallisers of all types in the presence of suspended crystals. The mechanism is thought to involve collisions between crystals and between crystals and impeller or vessel walls, but is not yet clearly understood. The nuclei produced are usually, though not always, submicroscopic in size. Collision breeding has been studied in many systems (11,18,21). Ottens et al (22,23), Evans et al (24), Garside et al (25) and Yamamoto and Harano (26) have reported work carried out in agitated vessels. In general these studies have concluded that the rate of collision nucleation depended on supersaturation and the energy dissipated in agitation of the system. However, Garside et al (25) found that the number of nuclei smaller than about 4 μm, was relatively insensitive to supersaturation. Secondary contact nucleation has recently been reviewed in detail by Garside and Davey (17) and by Larson (21).

2.1.3.2 Dendritic and Polycrystalline Breeding (11,18)

At high supersaturation dendritic crystal growth can occur. In stirred systems such crystals can easily break giving secondary crystals large enough to be visible. Such a process is termed dendritic breeding. Under similar conditions of high supersaturation in agitated systems polycrystals can sometimes form. These too break up easily giving macroscopic secondary crystals. Both these mechanisms are usually swamped by ordinary collision breeding.

2.1.3.3 Crystal Fracture (11)

Under conditions of violent agitation crystals can be broken into macroscopic pieces. A shower of submicroscopic secondary nuclei has been found to be produced concurrently with these macroscopic secondary crystals.

2.1.3.4 Initial Breeding (11,18)

Initial nucleation is the term applied to the secondary nucleation that is observed when a dry crystal is introduced into a supersaturated solution. The source of this nucleation is considered to be crystal dust present on the surface of a dry crystal.

2.1.3.5 Other Sources of Secondary Nucleation

Several studies have revealed that secondary nucleation could have taken place in an impurity concentration gradient resulting from the rapid

incorporation of dissolved impurities in growing crystals (27,28). The claim has also been made that the shearing action of solution flowing over a crystal face is a possible source of secondary nucleation (11,18,29,30). Some experimental evidence seems to indicate however, that fluid shear alone is an insufficient factor at low supersaturations (18). Finally, it is possible that secondary nucleation may occur by a process different from all those elucidated above. Mullin and Leci (31) have investigated one such system.

2.2 FACTORS AFFECTING NUCLEATION

Experimental studies of nucleation have been competently reviewed by De Jong (10). The effects of temperature, cooling rate, supersaturation, thermal history of the solution, stirrer speed, number and size of seed crystals and impurity concentration have been studied, but in most work it was not clear which of these specific mechanisms were being examined or whether the effects on nucleation were separated from the effects on growth.

A certain supersaturation in excess of equilibrium saturation is required for nucleation. In figure 2.1, the saturation curve represents equilibrium conditions while the supersaturation curve, which is usually not well defined, represents conditions of spontaneous nucleation. A metastable region exists between these two curves and its width has been found to decrease

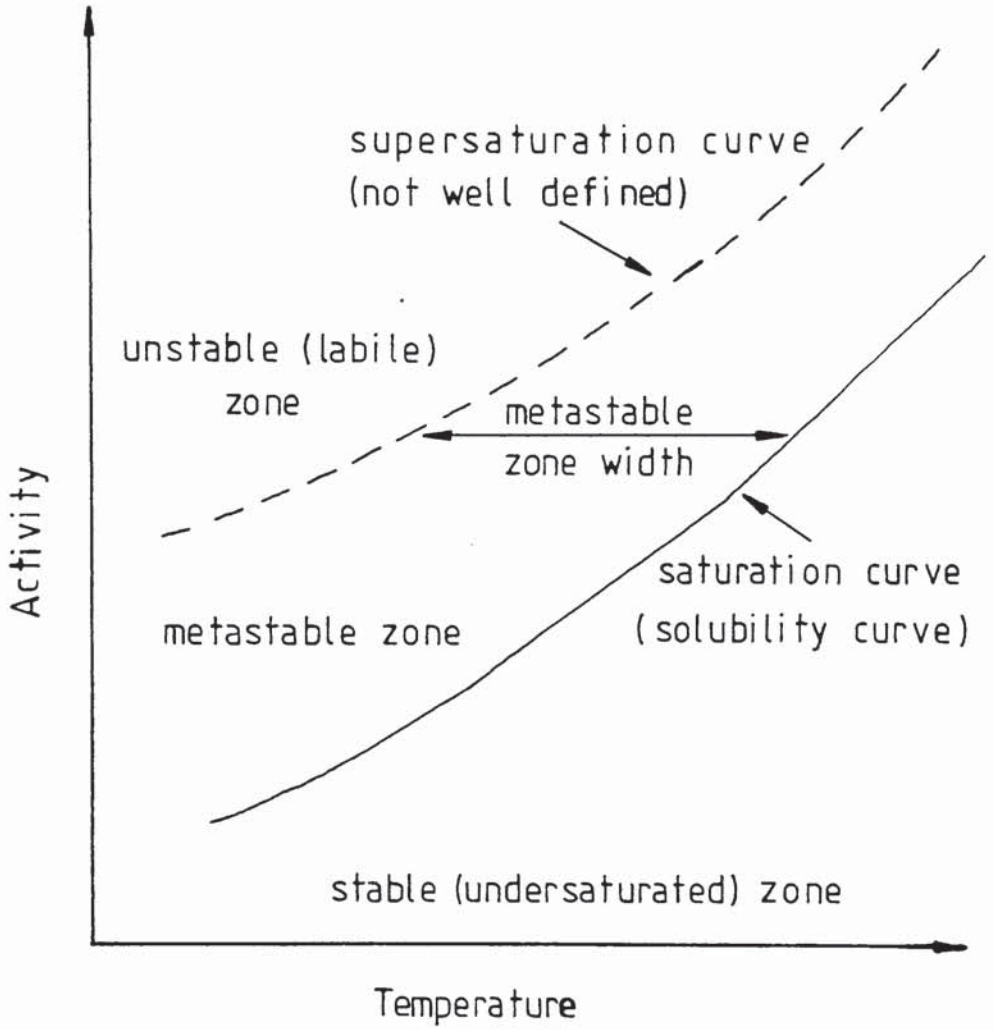

Figure 2.1 Solubility - Supersolubility Diagram

with increasing temperature, decreasing cooling rate, and increasing concentration of seed crystals (10,32). A study of the effect of solvent properties on metastable zone width in urea crystallisation revealed a direct dependence on solvent viscosity, molecular weight and density and an inverse dependence on surface tension, dielectric constant and solute concentration (33). The effect of agitation on nucleation and metastable zone width is a subject of some controversy. It appears that nucleation increases with agitation at moderate and very rapid stirrer speeds but decreases at intermediate speeds (9,10,34,35). This discontinuity has been attributed by Mullin and Raven (34,35) to two conflicting effects; namely, the tendency of macroscopic crystals to break up as a result of agitation, giving two or more growth centres, and the likelihood of destroying clusters of near critical nucleus size by agitation (36). Different impurities have been found to both increase or decrease the metastable zone width (10,37). Furthermore, vapour or gas bubbles in solution may affect both primary and secondary nucleation (10).

2.3 CRYSTAL GROWTH

Numerous theories of crystal growth are available in the literature (3,9,13,14,38). The multiplicity of crystal growth theories reflect the lack of adequate understanding of growth mechanisms (36). This is bourne out by the fact that these theories are mathematically complex and none of them yield results

that describe or predict crystal growth rate as straightforward functions of relevant independent system parameters (14). Recent developments in crystal growth theories have been reviewed by Aquilano (39), Bennema (40,41), Mullin (12,42) and Rousseau (43).

The incorporation of new solute upon a crystal face is considered to take place by a series of simple stages which are (8):

1. transport of the growth units to the crystal surface from the bulk solution;
2. physical or chemical adsorption on the crystal surface;
3. diffusion to energetically more favourable positions on the surface;
4. incorporation into the crystal lattice with concomitant dehydration if necessary.

Theories of crystal growth usually assume nucleation itself or one of these stages to be the rate determining step.

2.3.1 Nucleation Controlled Growth (3,13,14)

These growth theories assume that the rate controlling factor is concerned with the critical nucleus. A number of different mechanisms have been proposed for the manner in which the nucleus forms and grows (14). In mononuclear two dimensional nucleation it is assumed that once a nucleus is formed it has an infinitely rapid rate of lateral growth across the surface. In this case, growth rate (R_M) normal

to any crystal face of total area, A and having a growth step height of h is given by (14):

$$R_M = AhR_N \quad \ldots\ldots\ldots\ldots\ldots\ldots\ldots\ldots \quad (2.6)$$

where, R_N is the nucleation rate.

If the assumption of zero spreading velocity is made, growth occurs by the accumulation of critical nuclei. This constitutes the polynuclear two dimensional nucleation model for which the growth rate is given by (14):

$$R_M = a_n hR_N \quad \ldots\ldots\ldots\ldots\ldots\ldots\ldots\ldots \quad (2.7)$$

where, a_n is the surface area occupied by a single nucleus.

For intermediate spreading velocities a range of models, termed birth and spread models (14) are possible. For these, growth rate is not dependent upon crystal surface area but is a complex function of supersaturation and temperature.

The main drawback of all nucleation controlled growth models is that at low supersaturation little or no growth is predicted which is contrary to experimental evidence (3,14).

2.3.2 Surface Diffusion and Dislocation Controlled Growth (3,9,13,14)

The failure of nucleation controlled growth models to predict finite growth rates at low supersaturation, lead to the idea of growth taking place on stepped

growth spirals on the crystal surface, in such a manner that the spiral sources were self perpetuating. This model was first introduced by Burton, Cabrera and Frank (44) in their pioneering work which still forms the basis of most surface kinetic models. The BCF growth spirals are thought to originate at dislocations of both the screw and edge types which are common in almost all crystals. The main shortcoming of the BCF model is that it cannot be tested directly because it yields expressions for growth rate which involve parameters such as surface equilibrium concentrations, surface diffusivities, straight step velocities and mean spacing between steps (14), which cannot be measured separately. The BCF theory, which was originally derived for deposition from the vapour phase, has been extended and generalised in recent years, partly by means of computer simulations (8,45).

2.3.3 Mass Transfer Limited Growth (9,13,14)

An important class of crystal growth models assumes that bulk diffusion of solute to the growing crystal surface is the rate limiting step. Ordinarily, mass transfer involves eddy and molecular diffusion (9,14), whereas older mass transfer theories such as the Burton-Cabrera-Frank bulk diffusion model (44) and the Chernov model (46) only considered molecular diffusion.

Hence, the use of general relations involving empirical mass transfer coefficients, familiar in chemical engineering practice, usually results in more

reliable rate equations for crystal growth (14).

i.e. $R_M = K_M A S$ ..... (2.8)

where, A is the crystal surface area; S is the driving force; and, K_M is the empirical mass transfer coefficient, which accounts for crystal geometry, fluid dynamics and other relevant physical properties involved. The growth rate (R_M) is expressed in mass or molar units per unit time.

For regular geometric shapes, experimental evidence exists (46-50) to suggest that the following dimensionless correlation is applicable to mass transfer.

i.e. $Sh = F_1 + F_2 Re^{m_1} Sc^{m_2}$ ..... (2.9)

where, Sh, Re and Sc are the Sherwood, Reynolds and Schmidt numbers respectively; and, F_1, F_2, m_1 and m_2 are empirical constants. For spheres F_1 is 2, while for tetrahedra and octahedra its value is $2\sqrt{6}$ and $2\sqrt{2}$ respectively (14). Ranz and Marshall (46,47) found that, for spheres,

$$Sh = 2 + 0.60\ Re^{0.5}\ Sc^{0.33} \quad \ldots\ldots\ldots\ldots \quad (2.10)$$

Frossling (51) was the first to propose an equation of this type but gave F_2 as 0.552 instead of 0.60. A review of their own and previously published data by Rowe et al (49) yielded a value for F_2 of 0.69 in air and 0.79 in water. Investigation of mass transfer to particles suspended in a stirred vessel, by Levins and Glastonbury (50) resulted in a slightly different

correlation.

i.e. $Sh = 2 + 0.44\ Re^{0.5}\ Sc^{0.38}$ ..... (2.11)

2.3.4 Other Growth Models (14)

A recent feature of published literature on crystal growth has been the increasing use of probabilistic models. Ohara and Reid (14) have reviewed some of these models but have noted that the results predicted are frequently not in accord with established experimental evidence.

2.4 FACTORS AFFECTING CRYSTAL GROWTH

2.4.1 Temperature

The temperature of crystallisation usually has a greater effect on nucleation than on crystal growth. For cases of mass transfer limited growth the empirical mass transfer coefficient has been found to depend on temperature according to an Arrhenius type equation (9). In general, growth rate increases with temperature (14).

2.4.2 Solvent

Experimental evidence exists to indicate that crystal growth of a given substance in different solvents occurs at widely different rates (42). The phenomenon of molecular roughness of the crystal-solution interface has been invoked to explain this effect (41,52).

2.4.3 Crystal Size

Particle size appears to be important only in mass transfer limited growth (14). However, many empirical crystal growth models make some allowance for crystal size. Tavare et al (53,54) and Blickle and Halasz (55) have analysed different modes of operation of batch crystallisers using both size independent and linear-size-dependent power law growth models. A size dependent growth model widely used in the analysis of continuous crystallisers (56,57) has been that developed by Abegg et al (58). A number of experimental studies have indicated that the growth rates of small crystals are much lower than those of larger macroscopic crystals. Garside (59) has reviewed these growth studies and has suggested that crystals smaller than about 20 μm grow very slowly.

2.4.4 Agitation

The rate of crystal growth has been found to increase with agitation in many cases. However, this increase does not occur indefinitely and for any given size of solid particle, a critical degree of agitation exists at which the particle-fluid relative velocity is a maximum (36). Nienow et al (60) have described the use of particle-fluid slip velocities to correlate agitated vessel crystal growth data with single crystal and fluidised bed growth. Levins and Glastonbury (50, 61) have applied the same concept to particle-liquid mass transfer in a stirred vessel. Since

secondary nucleation is also strongly dependent upon agitation it has been suggested that optimum impeller speed in agitated vessels should be the minimum required for efficient crystal suspension (62). It has been found that this optimum speed is considerably influenced by vessel geometry (63).

2.4.5 Impurities

Numerous studies of the effects of impurities on both nucleation and growth have been carried out and these have been discussed in recent reviews by Broul and Nyvlt (64) and Mullin (42). Studies on the effect of impurities present in ppm level concentrations have produced conflicting results (65,66,67). It is thought that the observed effects are due either to the influence the impurities exert on the nucleation rate, or, in the case of non-nucleation controlled growth, to the blocking of active sites thereby preventing the advance of growth steps. It has also been pointed out by Mullin (42) that the solvent itself represents a massive impurity in the system and is capable of interaction with the solute.

2.4.6 pH

It is known that pH modifies the nature and concentration of ions in solution and this can be of particular importance to crystallisation kinetics in the presence of impurities (42). The pH also influences ionic ratios which determine the degree

of ion association (68). This can have a marked effect on the thermodynamic driving force for nucleation and growth. Pazourek (69), Davey and Mullin (70), Lewin and Vance (71) and Phillips et al (72) have investigated the action of pH in modifying the crystal habit of a variety of substances. Such observed effects have been generally attributed to the change in relative face growth rates with bulk solution pH, due to differential adsorption of hydrated hydrogen ionic species. Kuznetsov and Hodorowicz (73) have cited experimental evidence from a variety of sources that growth rate may increase by as much as threefold when hydrogen ion concentration increases tenfold. They have advanced a hypothesis, based on thermal vibration frequencies of molecules and ions which depend on pH, to explain this effect.

2.5 THERMODYNAMIC DRIVING FORCE FOR CRYSTALLISATION

The need to formulate a more fundamental basis for the driving force for crystal growth has for long been a neglected aspect. However, a major advance in this respect was made by Mullin and co-workers in a series of papers (74-77), in which they set down the proper thermodynamic driving force for crystal growth from solution. Binary systems and those with hydrates, partially dissociated electrolytes, mixed electrolytes and non-stoichiometric quantities of ions in solution were all considered. The driving force for crystallisation

was expressed as,

$$\frac{\phi^*}{RT} = \nu \ln(a/a_e) \quad \ldots\ldots\ldots\ldots\ldots\ldots \quad (2.12)$$

where, ϕ^* is the molar growth affinity; R is the universal gas constant; T is the absolute temperature; and, ν is the number of ions in a molecular unit. The solute activity (a) and the equilibrium solute activity at saturation (a_e) could be expressed on the basis of molarity, molality or mole fraction. The driving force was also expressed in terms of concentration and activity coefficient ratios, expressed on a common basis.

$$\text{i.e.} \quad \frac{\phi^*}{RT} = \nu \ln \frac{\gamma C}{\gamma_e C_e} = \nu \ln(\xi\zeta_c) \quad \ldots\ldots\ldots \quad (2.13)$$

$$\text{or,} \quad \frac{\phi^*}{RT} = \nu \ln(1 + S_{rel.}) \quad \ldots\ldots\ldots\ldots\ldots \quad (2.14)$$

In these equations, γ and γ_e are the activity coefficients of solute in solution and at equilibrium saturation respectively; C and C_e are the corresponding solute concentrations; ξ is the activity coefficient ratio; ζ_c is the concentration ratio; and, $S_{rel.}$ is the relative supersaturation based on activities (i.e. $S_{rel.} = (a/a_e) - 1$).

It was shown that the presence of other electrolytes only affected the driving force by their effect on the activity coefficients, and if the electrolytes contained a common ion the driving force should be based on individual ion activities.

Sohnel and Garside (77) evaluated different methods for estimating these activity coefficients in aqueous solution. Their results indicated that the estimated activity coefficient ratio deviated more from its true value at higher supersaturation. None of the correlations evaluated gave consistently low deviations. However, it has been suggested that in the absence of information on activity coefficients, molal concentration units are preferable due to their simplicity and temperature independence (74).

When considering hydrates and partially dissociated electrolytes, Sohnel and Mullin (76) stated that the degree of dissociation was not relevant. However, Christoffersen et al (78) have claimed that this is incorrect and have pointed out that neglect of ion association can result in errors of upto 30% in calculation of the growth affinity. Van Leeuwen (79) has presented approximate relations for driving force in melt and solution growth, based on equation 2.12, and compared the ensuing results with experimental measurements. Van Leeuwen and Blomen (80) derived a similar relation for the growth affinity of sparingly soluble salts, and, by comparison with experimental data for gypsum and barium sulphate, have shown that the relation is applicable upto very high supersaturations. The relation is of the form,

$$\frac{\phi^*}{RT} = \xi_o \ln(1 + S_{c,rel.}) \quad \ldots\ldots\ldots\ldots\ldots \quad (2.15)$$

where, $S_{c,rel.}$ is the relative supersaturation in concentration units and ξ_o is an effective value for the number of particles, formed per molecule of solute, and present in the solution. Sohnel and Garside (81) assessed the range of utility of this expression for a number of easily soluble anhydrous salts and concluded that for relative supersaturations in excess of 0.1 the method used by van Leeuwen and Blomen to calculate ξ_o would lead to unacceptable errors. It has been demonstrated, however, that for low relative supersaturations, (say below 0.1) (74), equation 2.14 reduces to:

$$\frac{\phi^*}{RT} \approx \nu S_{rel.} = \xi_o S_{c,rel.} \quad \ldots\ldots\ldots\ldots \quad (2.16)$$

2.6 METHODS FOR GENERATION OF SUPERSATURATION

Investigation of crystal growth of low solubility materials poses several special problems. To obtain a reasonable rate of production from a given volume of solution, it becomes necessary to continuously balance the loss of solute due to crystal growth by some means of generation of supersaturation. This can be done either by the continuous production of solute in solution or by the reduction of solute solubility. Both methods can also be applied concurrently. Possible methods for generating supersaturation in barium chromate crystallisation are reviewed in this section.

2.6.1 Direct Mixing of Reagents

It is possible to maintain supersaturation by controlled addition of a soluble chromate and a soluble barium salt. However, this might cause local concentration gradients, resulting in fresh nucleation rather than growth on existing crystals. Use of very dilute solutions together with highly turbulent mixing may overcome this problem but even under such conditions high localised concentration gradients will probably exist at the feed solutions inlet points. Moreover, high turbulence would enhance secondary nucleation and dilute solutions would yield low product masses for a given volume of solution. It is significant that studies by Nielsen (82) of crystal growth of a range of sparingly soluble inorganic compounds including barium chromate, gave homogeneous nucleation at high supersaturation, even with very rapid mixing of solutions.

2.6.2 Controlled Generation of Chromate Ions

One way of generating supersaturation for the crystallisation of barium chromate is by producing chromate ions homogeneously within a system in which barium ions are already present. A number of possible methods exist for achieving this.

2.6.2.1 Hydrolysis of Organic Chromium Compounds

The important class of organic reactions known as Etard reactions (83) produce stable chromium

complexes termed Etard adducts. Aqueous hydrolysis of an Etard adduct produces chromate ions as a byproduct. However, hydrolysis occurs very rapidly and generates considerable heat (84). Hence, controlled generation of chromate ions is not possible. Both chromyl chloride and chromyl acetate give chromate ions on hydrolysis (84). However, the process is vigorously exothermic and therefore unsuitable.

2.6.2.2 Redox Reactions

A number of redox reactions can be used to oxidise trivalent chromium species to hexavalent chromate and dichromate. The use of hydrogen peroxide to carry out this oxidation has been investigated by Knoblowitz and Morrow (85) who presented reaction mechanisms and rate constants. Aerobic oxidation at a pH above 12 can also be used for this purpose (86). Another possible method is the redox reaction between tetravalent cerium ionic species and trivalent chromium ions, the kinetics and mechanism of which has been studied by Tong and King (87). A further possibility is to use a soluble bromate to carry out the oxidation. The reaction is pH and temperature dependent and involves the formation of bromine gas (88,89,90). Chromate generation occurs slowly at 90-95^{o}C and stops completely at pH values above 4. Ramette (88) used the technique for quantitative precipitation of lead chromate.

2.6.2.3 Other Methods of Generating Chromate Ions

The use of high energy γ-rays to oxidise chromic ions to chromate ions in solution has been reported (91,92,93). It is also possible that some form of electrochemical oxidation (94) may be applicable. Mellor (95) has described an electrochemical method for the production of lead chromate. However, there appears to be a risk of continual nucleation being caused by the electrodes (96) in such a process.

2.6.3 Controlled Generation of Barium Ions

An alternative to homogeneous generation of chromate ions is the generation of barium ions in a system containing chromate ions. This can be achieved by complexing the barium ions with ethylenediamine tetra-acetic acid (EDTA) and then gradually causing their release by decomposition of the complex with hydrogen peroxide. Takiyama (97) has applied this method to the precipitation of barium sulphate and Benes (98) has used it for barium chromate. A drawback of the technique is that, due to the low solubility of EDTA, the hold-up of barium ions in solution is limited causing low productivity. Heyn and Schupak (99) used the property of the barium-EDTA complex of being unstable below a pH value of 9, for precipitation of barium sulphate, by causing a controlled change in pH, with the aid of the hydrolysis of ammonium peroxydisulphate at about 60°C. This method has also

been described by Gordon et al (2).

2.6.4 Generation of Supersaturation by a Controlled Solubility Change

The technique of precipitation from homogeneous solution (2) can be applied to the crystallisation of barium chromate by utilising the strong dependence of barium chromate solubility on pH. The principle of this technique is that, as the supersaturation is relieved by crystal growth, it tends to be maintained by the reduction of solubility due to an increase in pH (124,138). The method has been used for the precipitation of a great variety of sparingly soluble substances (2,100-102). It has also been used for the precipitation of barium chromate (4-7). The hydrolysis of urea has commonly been used to change pH but other reactions are possible.

2.6.4.1 Hydrolysis of Urea (5,103-109)

Warner (103) first proposed that urea hydrolysis was a pseudo-first order reaction, due to the reaction indicated by equation 2.18 (below) being achieved very rapidly. In the pH range 1.5 to 5.0, the rate constant depended only on temperature. The suggested reaction mechanisms were:

$$CO(NH_2)_2 \rightleftharpoons NH_4^+ + OCN^- \quad \ldots\ldots\ldots\ldots \quad (2.17)$$

$$OCN^- + H_3O^+ \longrightarrow NH_3 + CO_2 \uparrow \quad \ldots\ldots\ldots\ldots \quad (2.18)$$

Welles et al (108) investigated urea hydrolysis at high urea concentrations upto 8.0 M and at temperatures below 50°C. Their results agreed with Warner's (103) on extrapolation to higher temperatures. Shaw and Bordeaux (109) investigated urea hydrolysis rate in aqueous and acidic media in the temperature range 60°C to 100°C. These studies also compared well with those of Warner, although being slightly lower. Falangas's (5) experiments were carried out in nitric, citric and formic acids, in mixtures of these acids, and in the presence of barium chromate. The first order rate constants derived were of the same order of magnitude as those of Warner but slightly larger. Falangas also suggested a zero order reaction model for pH above 2.5. However, this analysis disregarded the buffering action of the ammonium salt produced in the reaction (110), due to which the change in pH, at higher pH values, no longer represented the production of ammonia from urea.

2.6.4.2 Other Methods of Changing pH

One shortcoming of the urea hydrolysis reaction is the outgassing of carbon dioxide (equation 2.18). A possible alternative hydrolysis reaction is that of hexamethylene tetramine (111).

i.e. $(CH_2)_6N_4 + 6H_2O \rightleftharpoons 4NH_3 + 6HCHO$ ..... (2.19)

However, hydrolysis was suppressed by an increase in pH and also by the reaction product formaldehyde. When pH was low enough to permit complete hydrolysis, the rate was very rapid. Furthermore, the formaldehyde formed is a potential health hazard when in contact with hydrochloric acid (112,113) and may adversely affect crystal habit and growth rate.

2.7 PREVIOUS WORK ON CRYSTALLISATION OF BARIUM CHROMATE

Several investigations of the crystallisation of barium chromate have been reported in the literature.

2.7.1 Work of Benes, Bindra, Rychly and Adamski

Benes (98) precipitated barium chromate by using EDTA to complex barium ions and found a strong temperature dependence on rate of precipitation. Bindra (114) studied the growth kinetics of barium chromate in neutral solutions at 20°C and 25°C, by the rapid mixing of soluble salts and concluded that the growth mechanism changed from diffusion control to interface control with an intermediate stage in which both mechanisms were operative. Final crystal sizes obtained were about 5 μm. Rychly (115) found that for crystallisation carried out by mixing dilute solutions of barium hydroxide and chromic acid in concentrations of about 3×10^{-4} kmol/m^3, larger crystals grew more slowly than smaller ones. Adamski (116-119) used a modified technique ('synchronised precipitation') but no specific growth rate measurements

were made.

2.7.2 Work of Packter et al

Packter (120) found that for slow precipitation of barium chromate at 20°C, in well stirred solutions of final concentration about 0.002 kmol/m^3, the growth rate was dependent on the square of the supersaturation. Packter et al (121) investigated crystal size of barium chromate on precipitation by rapid mixing of solutions of barium nitrate and sodium chromate, to give solute concentrations of 10^{-4} to 10^{-2} kmol/m^3. Crystal size was less than 5 μm, decreased to a minimum at about 200 r.p.m. and increased with the temperature of precipitation. A study of growth rate at 25°C, under similar conditions of mixing and for initial solute concentrations from 10^{-4} to 10^{-3} kmol/m^3, revealed that for barium chromate the rate controlling step was surface deposition (122). A second order dependence of growth rate on supersaturation was found to apply to this study and also to similar experiments by Packter and Alleem (123), carried out at 22°C in acid solutions of pH below 5. Packter and Sahay (124) investigated nucleation rates of barium chromate at 20°C to 95°C. Supersaturation was generated by the slow direct addition of an aqueous solution of sodium chromate to a barium nitrate solution or by precipitation from a homogeneous barium chromate solution in excess acid, using urea hydrolysis. Heterogeneous nucleation was observed

in both cases. Nucleation rate constants were found to be lower for precipitation from homogeneous solution. Rate constants also decreased at higher precipitation temperatures. Furthermore, Packter (125) examined growth and nucleation rates of barium chromate during the induction period when precipitation was achieved by rapid mixing at 22°C. A sixth and second order dependence on barium chromate concentration was found for nucleation and growth respectively. In subsequent experiments under similar conditions but over a pH range from 3 to 8 (123), homogeneous nucleation was found to predominate at pH values from 8 to 5, while at pH below 5 heterogeneous nucleation was found to occur. Work by Packter and Sahay (126), showed that on slow addition of anion to the cation solution at 20°C, heterogeneous nucleation occurred at first but as solute concentration increased, homogeneous nucleation became predominant. Homogeneous nucleation followed by diffusion controlled crystal growth was also observed by Nielsen (82) at high supersaturation when solutions of anion and cation were rapidly mixed in a special turbulent vortex mixing chamber. Supersaturation ratios of the order of 10^2 to 10^3 were achieved. The critical barium chromate nucleus was estimated to be comprised of 14 ions.

2.7.3 Work of Skander (4)

Skander initially employed a mixed suspension mixed product removal (MSMPR) crystalliser at 30°C operating in the pH range 0.1 to 1.0. However, operation was unstable with the seed crystals used tending to periodically dissolve. This was attributed to the low growth rate of barium chromate and insufficient temperature control. Apparent linear growth rates of the order of 10^{-4} and 10^{-3} μm/s were observed for crystals smaller than and larger than about 4 μm, respectively. Skander also conducted preliminary tests in a batch crystalliser and demonstrated the feasibility of growing 100 μm sized crystals but no growth rate information was derived.

2.7.4 Work of Falangas (5)

The work of Falangas (5) was carried out in a 1 dm^3 batch stirred crystalliser at 100°C. Hydrochloric acid of initial strength from 0.06 to 0.12 kmol/m^3 was used. Initial barium chromate holdup was between 2 and 10 g and initial urea concentration was 20 kg/m^3. Stirrer speeds of 200, 400 and 800 r.p.m. were investigated. Growth rate was correlated empirically and the following relation was obtained.

$$R_M = K.L^{(0.5 \pm 0.04)} . w^{(1.2 \pm 0.1)} . S_{c,rel.}^{(0.83 \pm 0.15)} \quad \ldots\ldots\ldots\ldots\ldots\ldots (2.19)$$

where, K is a constant; L is a mass mean characteristic crystal dimension; w is stirrer speed; and, $S_{c,rel.}$ is

the relative supersaturation. The effect of pH was found to be negligible. Despite an unusual, higher than unity stirrer speed index, this correlation indicates bulk diffusion controlled growth. Falangas suggested 'a stationary particle growth model' in which smaller particles, produced by attrition and other forms of breeding, grew much faster than larger ones, to explain the apparent lack of fines tails in his experimental crystal size distributions.

Although Reiss (127) has shown that polydisperse colloids similarly tend to become more monodispersed during diffusional growth, much experimental evidence exists to indicate that small crystals, particularly those produced by secondary nucleation mechanisms, grow more slowly than larger crystals (59). Repeat analyses of some of Falangas's crystalline products have revealed the existence of considerable fines, and the apparent lack of fines on initial analysis was probably due to an arbitrary detection limit being imposed by the analytical technique used.

CHAPTER THREE

EPITAXIAL GROWTH LITERATURE

3.0 INTRODUCTION

Epitaxy or oriented overgrowth has been defined by van der Merwe (128) as the formation of a crystalline overgrowth on a different crystalline substrate in such a manner that the orientation of the overgrowth is related to that of the substrate, even though their normal lattices do not match at the substrate-overgrowth interface. Epitaxy is closely related to heterogeneous nucleation and could be considered to be a special case of primary heterogeneous nucleation (129,130). Epitaxy is of primary interest in studies of single crystal film growth. It also plays an important part in scale formation (131-135) and in normal and pathological biological mineralisation (8,129,130,136).

3.1 REVIEWS ON EPITAXIAL GROWTH

Numerous reviews on epitaxy have appeared in the literature (8,15,129,137-144). However, these deal primarily with film growth on ideal substrates rather than epitaxial growth from solution, which is more relevant to this current work. The role of epitaxy in crystal nucleation and growth from solution has been considered by Nancollas (8) and Walton (15,129). The problems of nucleus formation in epitaxy and the role of the substrate have been examined by Ickert (142,143), while Dankov (144) has reviewed the factors affecting

orientation of the overgrowth.

3.2 THEORETICAL ASPECTS OF EPITAXY

The classical theory of oriented overgrowth was developed by Frank and van der Merwe (145,146,147). The theory was based on the properties of a one dimensional dislocation model and led to predictions regarding the conditions necessary for embroyo formation in epitaxy (138). The extension of the model to two dimensions has been shown to be justified (146, 147). The classical theory predicted a certain critical difference in lattice spacing between substrate and overgrowth, below which a monolayer overgrowth, in its minimum energy state, was deformed into an exact fit with the substrate, and above which it was only slightly deformed but had many dislocations at the interface. The limiting misfit (relative to the substrate lattice) was ∿9% for an average case (138,146) but could be as high as ∿14% at low temperatures (138). Dankov showed that the critical misfit was given by (144):

$$\delta = \{2\alpha_o\sigma_o/(E_1+E_2)\}^{\frac{1}{2}} \quad \ldots\ldots\ldots\ldots\ldots\ldots \quad (3.1)$$

where, α_o is the relevant lattice spacing of the overgrowth; σ_o is its surface tension; and, E_1 and E_2 are its moduli of elasticity in mutually perpendicular directions. Using typical values for these parameters, Dankov found that the critical misfit amounted to ∿9% in confirmation with the Frank-van der Merwe model.

However, Zalkin (148) has pointed out that Dankov's work disregarded the adhesive forces between deposit and substrate which provide an additional source of energy for oriented crystallisation. When this factor was considered critical misfits higher than 9% were found to apply in some cases. Blisnakov (149) has considered the effect of temperature on critical misfit and has derived expressions for the dependence of misfit on temperature, which also involve the moduli of elasticity, the work of removal and deformation of an embryo and surface concentration.

3.3 FACTORS AFFECTING EPITAXY

3.3.1 Lattice Misfit

Lattice misfit is probably the single most important factor affecting epitaxy. It has been suggested that misfit plays a prominent role in conditioning the growth morphology, in initiating epitaxy and in inducing structural defects in epitaxial crystals (128). Lattice misfit has been quantitatively defined relative to the substrate (128,138,144,146,148), the overgrowth (8,128,130,150), and even the average of the lattice spacings of substrate and overgrowth (128).

It has been postulated that misfit has an effect on growth morphology (i.e. whether epitaxy occurs in the form of 2-dimensional layer by layer growth or by 3-dimensional island growth), by affecting the adhesion energy of an epitaxial overlayer on a substrate. A low adhesion energy would favour 3-dimensional

growth. However, if the energy of cohesion between monolayers of the overgrowth was lower 2-dimensional growth would be favoured.

As shown by the theories of epitaxial growth it appears that an upper limit to misfit of around 10-20% (130) exists for epitaxial growth, and in general the tendency for epitaxy is improved by a reduced misfit. However, a small misfit alone is neither a necessary nor a sufficient condition for epitaxy. Misfits of 30% and more have been reported (129,130,138). On the other hand no overgrowth has occurred in some cases where misfit in two orthogonal directions has been less than 4% (with ideal matching in one of these directions) (138).

In cases where lattice misfit exceeds the critical value unoriented overgrowth can occur with arrays of misfit dislocations at the substrate-overgrowth interface accommodating the misfit between the lattices. The extent of misfit to be accommodated largely governs the nature of these dislocations.

3.3.2 Supersaturation

Oriented overgrowth from solution usually occurs only above a certain critical supersaturation of the epitaxial growth phase (128,151). The critical supersaturation depends in turn, upon lattice misfit and strain and upon the surface characteristics of the substrate. Other conditions being favourable, if misfit is large a high supersaturation is generally

required for epitaxy (130).

3.3.3 Temperature

The influence of temperature on epitaxy is by means of its effect on lattice misfit (149), and critical supersaturation (129). Critical misfit is larger at lower temperatures (146). It has also been found that substances that are not usually good substrates can sometimes be activated by heating (152,153).

3.3.4 Properties of Substrate Surface

A number of experimental studies have shown that substrates possessing low index lattice planes at their surfaces facilitate epitaxial growth (151,154,155). Furthermore, it is evident that the intensity of interaction between the substrate and the epitaxial overlayer plays an important part in determining critical misfit (148) and growth morphology (128). A low net surface charge favours epitaxy, but if individual substrate surface atoms are highly charged nucleation can still be inhibited (156). The size of the substrate is also of importance in overgrowth from solution. It has been found that for primary heterogeneous nucleation in general, solid particles in the size range 0.1 to 1.0 μm are most effective (9,129). Theoretical considerations have shown that sizes below 0.1 μm are not effective as heterogeneous nucleators (157,158).

3.3.5 Properties of Solution

In epitaxial growth from solution, where the overgrowth phase is the solute dissolved in a suitable solvent, the concentration of potential determining ions in solution (131,156) and the dielectric constant of the solvent (138) can be of importance. The critical misfit can be increased by the use of solvents of lower dielectric constant and experimental verification of this has been obtained by Willems (159) and by Sloat and Menzies (160). Adsorption of ions in solution onto active sites on the substrate can prevent epitaxy by hindering nucleation (156).

3.3.6 Other Factors

The physical nature of the substrate and the overgrowth has also been found to influence epitaxy. Some experimental evidence exists (138) to show that critical misfit in cases where both substrate and overgrowth are ionic is greater than when one of these is non ionic or metallic (138). Hence, the limiting misfits permissible for the formation of ionic overgrowths on metallic substrates, could be smaller than in the case of other substrates.

3.4 EPITAXIAL GROWTH FROM SOLUTION

3.4.1 Biological Mineralisation

Biological mineralisation of both the physiological and pathological types often involves epitaxial growth from solution (8,129). Overgrowths of hydroxyapatite

on collagen substrates in bone growth, and of calcium oxalate and phosphates on mucoid substrates in kidney and bladder stone formation are common examples of physiological and pathological mineralisation respectively. Nancollas et al (130,136) investigated the solution growth of various calcium phosphate phases on seed crystals of hydroxyapatite and also the growth of hydroxyapatite on crystals of dicalcium phosphate dihydrate, calcium fluoride and calcite at low supersaturations. The closé lattice match between substrate and overgrowth was supported in each case by observed epitaxial growth. The misfit did not exceed 15% in all these cases.

3.4.2 Scale Formation

The growth of scale on metal surfaces or on other crystalline deposits is usually a form of epitaxy. Calcium sulphate dihydrate (gypsum) and barium sulphate (barite) are common components of scale which forms in many industrial environments. Liu and Nancollas (132) have studied the growth of gypsum on gypsum substrates, while Nancollas et al (133,134,135) have investigated growth from solution of barite on barite and calcite on calcite. However, deposition can occur on substrates different from the depositing material. Thus, Gill and Nancollas (131) investigated solution growth of gypsum on seeds of barite and calcite. The growth rates on the foreign substrates were found to be faster than on gypsum itself. Since epitaxy occurred despite

the lack of a close lattice fit, it was suggested that other factors such as surface charge or potential determining ions in solution played an important part.

Studies of growth of barium sulphate on barite substrates of different morphologies showed that substrate structure had no effect on the growth kinetics of barium sulphate (133). In the work with calcite, barite and gypsum in which the substrate was the same as the depositing substance, it was found that surface nucleation only occurred at relatively high supersaturation. At low supersaturation and with a high seed crystal concentration, growth on the seeds took place rather than fresh nucleation.

3.4.3 Other Systems (138,139)

Other studies of epitaxial growth from solution have involved the use of substrates such as cleavage planes of mica, ionic or metallic single crystals or films and polished and etched polycrystalline metal surfaces (155,160-162). The method usually adopted was to place a drop of a saturated solution of the proposed overgrowth on the prepared substrate, which was slowly cooled while observing it microscopically. Schulz (155) studied overgrowths of alkali halides on substrates which were cleavage surfaces of calcium carbonate and nitrate. The overgrowths always adopted orientations that minimised the misfit with at least one of the lattice directions of the substrate surface. Epitaxial growth of alkali halides on single crystals

and polycrystalline specimens of various metals has been obtained by Johnson (161). These overgrowths were found to have permissible misfits of the same order of magnitude as for purely ionic pairs. Newkirk and Turnbull (150) investigated epitaxial growth of ammonium iodide on freshly cleaved mica surfaces and showed that the relationship between supersaturation and critical misfit was in general agreement with the theory of Turnbull and Vonnegut (151). Schulz (162) also studied the solution growth of alkali halides on mica and determined that the overgrowths were oriented with their [111] lattice direction normal to the substrate. These results were almost identical to those of vapour growth studies with the same substances. Numerous other similar studies of epitaxial growth from solution have been published and these are listed in the comprehensive compilations of van der Merwe (138) and Grunbaum (139).

3.5 COPRECIPITATION

The term coprecipitation is applied rather loosely to the process of obtaining overgrowths through adherence of developed crystals, or otherwise, by incorporation within a crystalline matrix, such as in occlusion or inclusion. The process has been studied in conjunction with the formation of overgrowths of alums (163) and in analytical chemistry (2), such as in the simultaneous precipitation of silver chromate and calcium carbonate, where a silver chromate crystal

is occluded between two crystals of calcite (164), and in the coprecipitation of radium and barium chromate from homogeneous solution (6).

Coprecipitation is of importance in the formulation of igniferous compositions and pyrotechnic time delay fuses (1,165). Incorporation of the fuel component of the composition in a matrix of the oxidant instead of mixing the fuel and oxidant mechanically prevents segregation of the ingredients, facilitates intimate contact between fuel and oxidant and protects the fuel from the atmosphere. Miller (1) used lead and barium chromates as the oxidant and tungsten, molybdenum, titanium, silicon, tantalum and boron as the fuel, in a variety of compositions all of which were prepared by precipitating the oxidant in sufficiently massive form to permit incorporation of the fuel into the crystalline matrix, rather than by oriented overgrowth of the oxidant on the fuel substrate. The method used by Miller (1) was the addition of solutions of soluble salts to an acidic suspension of the fuel particles.

CHAPTER FOUR

PROPERTIES OF MATERIALS USED IN HOMOGENEOUS PRECIPITATION AND EPITAXIAL GROWTH EXPERIMENTS

4.0 INTRODUCTION

The substances used in precipitating barium chromate from homogeneous solution are, in addition to barium chromate itself, urea, hydrochloric acid and distilled water. Also, the epitaxial growth experiments involved the use of various metal wires and powders as potential substrates. Relevant physical and chemical properties of these substances are surveyed.

4.1 BARIUM CHROMATE

4.1.1 Physical Properties of Barium Chromate

Barium chromate has an orthorhombic crystal structure with lattice parameters having the following values (166,167,168): a_o = 9.103 ± 0.010 Å; b_o = 5.526 ± 0.010 Å; and, c_o = 7.337 ± 0.010 Å. The lattice co-ordinates have coefficients of thermal expansion of 1.65 x 10^{-5}, 3.38 x 10^{-5} and 2.04 x 10^{-5} K^{-1} (167) respectively. The specific gravity has been reported as: 4.296-4.304 (95); 4.49 (95); 4.498 (95,169); 4.5044 (95); and, 4.60 (95, 170). The surface energy was determined by Nielsen (82) and found to be 0.12 J/m^2. The heat of formation is -1.429x10^6 kJ/kmol (-341.3 kcal/mole) (169) and the heat of solution is -2.706x10^4 kJ/kmol (-6.4 kcal/mole) (171).

4.1.2 Chemical Properties of Barium Chromate

Barium chromate is a yellow precipitate and has a molecular weight of 253.34 (169). No phase change or decomposition of barium chromate occurs below 813°C (167). It is a toxic substance which acts as an irritant to the skin, eyes, nose and throat (172). Occupational contact with barium chromate solutions is known to cause skin cancer (172). Skander (4) has noted several authors as specifying the solubility product to be $(1.3 \pm 0.3) \times 10^{-10}$ $(kmol/m^3)^2$. Barium chromate is nearly insoluble in water but solubility is dependent strongly on pH (4,5,95,173) and less markedly on temperature (4,5). Although there is some doubt about the value for the heat of solution given above, it translates into an increase of solubility with temperature of ∿4%/K (4). Skander (4) gives an extensive survey of the literature on the solubility of barium chromate in various media.

Two types of barium chromate were used for homogeneous crystallisation and epitaxial growth experiments:

1. B.D.H. Chemicals Ltd., Laboratory Reagent Grade-
   Iodometric minimum assay : 98%
   Maximum limits of impurities:
   Chloride (Cl) = 0.005%
   Sulphate (SO_4) = 0.1%
2. Hopkin and Williams General Purpose Reagent Grade-
   Minimum Assay : 99%

Maximum limits of impurities:

Chloride (Cl) = 0.001%

Sulphate (SO_4) = 0.02%

Potassium (K) = 0.01%

Sodium (Na) = 0.01%

4.2 SUBSTRATES USED FOR EPITAXIAL GROWTH EXPERIMENTS

True epitaxy requires a certain degree of lattice match between the substrate and the preferred overgrowth (129). Therefore, the choice of materials for epitaxial growth experiments was based on: the degree of lattice match with barium chromate; the suitability of the substrate as the 'fuel' component in the final 'fuel/oxidant' product (1); the need for the substrate chosen to be relatively inexpensive; the importance of the material chosen being preferably non-toxic in powder form and safe to handle; and, the resistance of the material to acid attack. The metals chosen were: copper, hafnium, molybdenum, nickel, tantalum, titanium (α form) and tungsten (α form). Of these copper and nickel had poor resistance to hot acid and were discarded. Furthermore, several samples of tungsten of different nominal sizes were used. Some relevant physical and chemical properties of these materials are summarised in table 4.1, while table 4.2 gives details of lattice structure and misfit with the barium chromate crystal lattice. Finally, table 4.3 contains particulars of particle size data for the metal powders used as substrates in the epitaxial growth

TABLE 4.1

Physical and Chemical Properties of Substrates for Epitaxial Growth

Metal	Atomic Weight (174)	Specific Gravity (174)	Resistance to Acid Attack (175)	Melting Point (°C) (174)
Copper	63.55	8.93	dissolves in HNO_3 and in other acids at high temperature	1356
Hafnium	178.49	13.3	soluble in HF only	2423
Molybdenum	95.94	10.2	soluble in hot HNO_3 and H_2SO_4	2880
Nickel	58.71	8.90	dissolves in HNO_3 and in other acids at high temperature	1726
Tantalum	180.95	16.6	dissolves only in HF	3269
α-Titanium	47.90	4.54	soluble in HF and in some hot acids	1948
α-Tungsten	183.85	19.32	dissolves only in mixed acids at high temperature	3650

TABLE 4.2

Lattice Structural Properties of Substrates for Epitaxial Growth (166,168,176)

Metal	Crystal Structure	Lattice Parameters (Å)	Lattice Planes for Best Match		Mutually Perpendicular Directions for Best Match		Best Misfit in Mutually Perpendicular Directions (% Relative to $BaCrO_4$)
			$BaCrO_4$ Lattice	Metal Lattice	$BaCrO_4$ Lattice	Metal Lattice	
Copper	f.c.c.	a_o=3.615	(010)	(110)	[001] [100]	[110] [100]*	- 7.5 - 1.5
Hafnium	h.c.p.	a_o=3.197 c_o=5.058	(001)	(1100)	[100] [010]	[1000]* [0001]*	-12.9 11.1
Molybdenum	b.c.c.	a_o=3.147	(001)	(110)	[100] [010]	[001]* [110]	-14.2 - 2.2
Nickel	f.c.c.	a_o=3.524	(010)	(110)	[001] [100]	[110] [100]*	- 9.8 - 4.0
Tantalum	b.c.c.	a_o=3.306	(001)	(110)	[100] [010]	[001]* [110]	- 9.9 2.7
α-Titanium	h.c.p.	a_o=2.295 c_o=4.686	(100)	(1100)	[001] [010]	[1000]* [0001]*	6.8 3.0
α-Tungsten	b.c.c.	a_o=3.165	(001)	(110)	[100] [010]	[001]* [110]*	-13.7 - 1.7

* - Alternate Rows of Atoms Considered when Calculating Misfit

TABLE 4.3

Particle Size Data of Metal Powders Used as Substrates for Epitaxial Growth

Metal	Supplier	Nominal Size Specification (μm)	Coulter Counter Particle Size Measurement (μm)		Andreasen Sedimentation Particle Size Measurement (in 50/50 (mass) Glycerol -Water Medium) (μm)	
			Size Range	Mass Mean Size	Size Range	Mass Mean Size
Hafnium	NMC	-	-	-	0-68	21.3
Molybdenum	NMC	1-5	-	-	2-94	27.1
Tantalum	NMC	-	-	-	0-60	20.7
α-Titanium	KLL	<150	-	-	0-180+	78.3+
Type 1 Tungsten	HW	∿1	1-21	8.28	0-15*	3.98*
Type 2 Tungsten	NMC	∿0.4	1-18	4.93	0-20	2.74
Type 3 Tungsten	NMC	0-2.5	1-15	4.11	0-52	3.77
Type 4 Tungsten	NMC	0-3.5	1-19	4.98	0-52	4.09
Type 5 Tungsten	NMC	0-10	0.5-22	6.03	0-52	8.87
Type 6 Tungsten	NMC	43-63	-	-	0-90+	46.3+

* - Andreasen sedimentation carried out in water
\+ - Values based on sieve analysis
NMC - New Metals and Chemicals Ltd
KLL - Koch-Light Laboratories Ltd
HW - Hopkin and Williams

TABLE 4.3 (Continued)

Particle Size Data of Metal Powders Used as Substrates for Epitaxial Growth

Metal	Supplier	Nominal Size Specification (μm)
Tungsten-M1	MOD	∿0.5*
Tungsten-M2	MOD	∿0.37*
Tungsten-M3	MOD	∿1.5*
Tungsten-M4	MOD	∿2.5*

MOD - Ministry of Defence, U.K.

* - Only small quantities of the metal powders were available. These were used up in the epitaxial growth experiments. Hence, no Coulter counter or Andreasen sedimentation particle size analyses were carried out for these samples.

experiments. The tungsten types 1 and 2 listed here correspond to tungsten types I and II respectively, of Falangas (5).

4.3 OTHER CHEMICALS USED

The other major chemicals used in both epitaxial growth tests and homogeneous precipitation were urea and hydrochloric acid.

Urea of Analar grade was obtained from either Hopkin and Williams or B.D.H. Chemicals Ltd. Both sources had the same specifications which were:

Minimum assay: 99.5%

Melting point: 132 to 133^{o}C

Maximum limits of impurities:

insoluble matter	= 0.003%
acidity	= 0.05 ml N%
alkalinity	= 0.05 ml N%
sulphated ash	= 0.005%
chloride (Cl)	= 0.0005%
sulphate (SO_4)	= 0.001%
copper (Cu)	= 0.0001%
iron (Fe)	= 0.0001%
lead (Pb)	= 0.0002%
biuret ($C_2H_5N_3O_2$)	= 0.05%

Hydrochloric acid of Analar grade was obtained from Hopkin and Williams, and had the following specifications:

Minimum assay: 35.4% (w/w)

Maximum limits of impurities:

non-volatile matter = 0.001%

free chlorine (Cl) = 0.0002%

sulphate (SO_4) = 0.0005%

sulphite (SO_3) = 0.0001%

aluminium (Al) = 0.00005%

ammonium (NH_4) = 0.0003%

arsenic (As) = 0.000002%

copper (Cu) = 0.00001%

iron (Fe) = 0.00004%

lead (Pb) = 0.00005%

Weight per ml. : 1.18 grammes

CHAPTER FIVE

EPITAXIAL GROWTH EXPERIMENTS AND RESULTS

5.0 INTRODUCTION

The experiments and results described in this chapter detail the methods and materials used in an attempt to achieve epitaxial growth of barium chromate on a substrate of fine metal particles. Although unsuccessful, these experiments took nearly one year to perform.

5.1 10-LITRE BATCH FLUIDISED BED CRYSTALLISER

A batch fluidised bed crystalliser, having a 10 dm^3 feed reservoir, which had been constructed by Falangas (5), was modified by removing superfluous pipe work, adding in-line bayonet heaters to shorten heating up time, repositioning the fluidised bed itself, and fitting a bleed line from the main circulating pump inlet to the feed reservoir, with bleed flow maintained by a peristaltic pump. This last modification was required to prevent failure of the circulating pump, due to gas lock caused by carbon dioxide generation. Figure 5.1 shows a photograph of the rig and figure 5.2 depicts its flow diagram.

Experiments were carried out on this rig with tungsten powder used as the bed material. The feed reservoir contained barium chromate, dissolved in hydrochloric acid solution and containing urea to provide the controlled generation of supersaturation

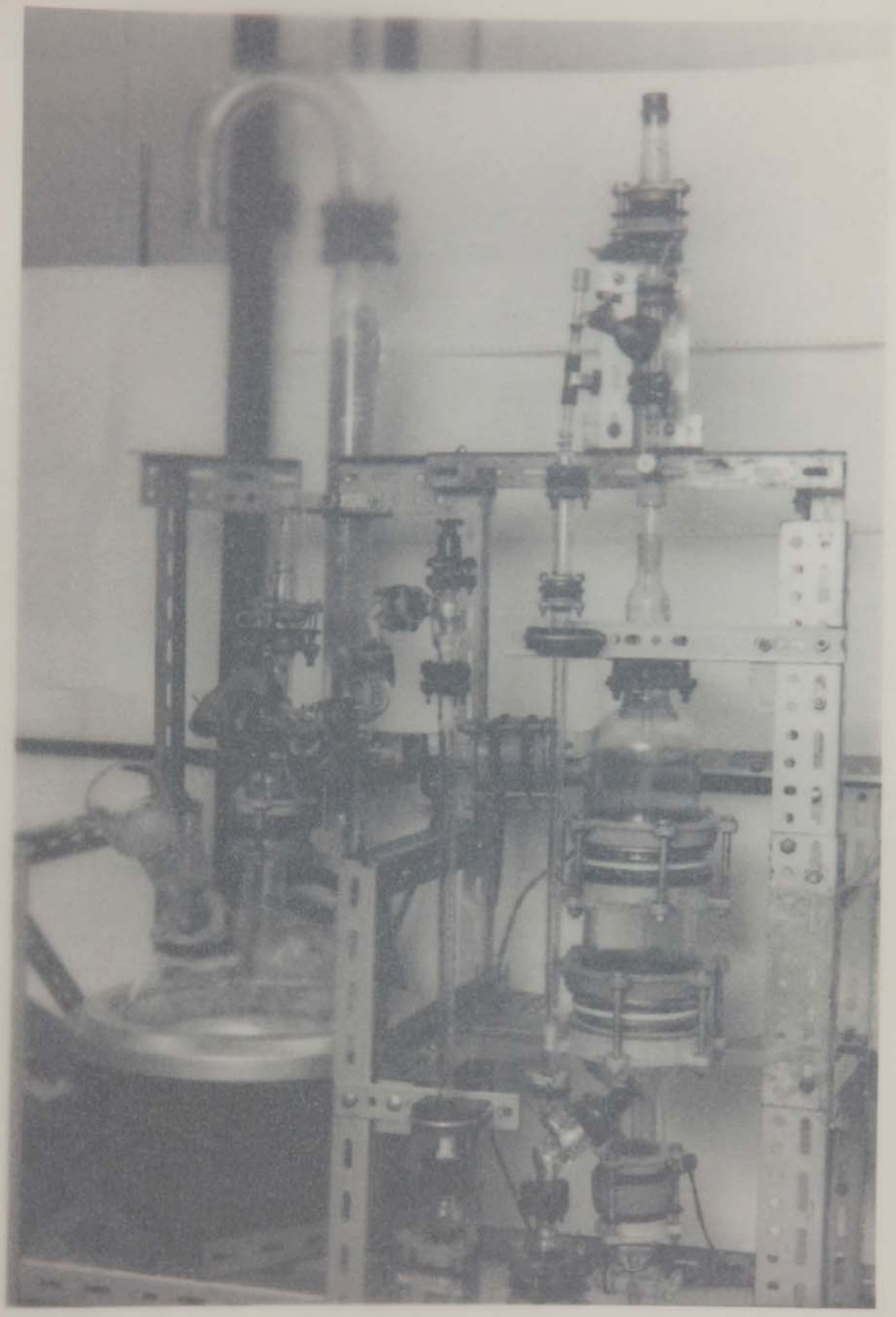

Figure 5.1 - Batch Fluidised Bed Crystalliser Rig
with 10-Litre Feed Reservoir

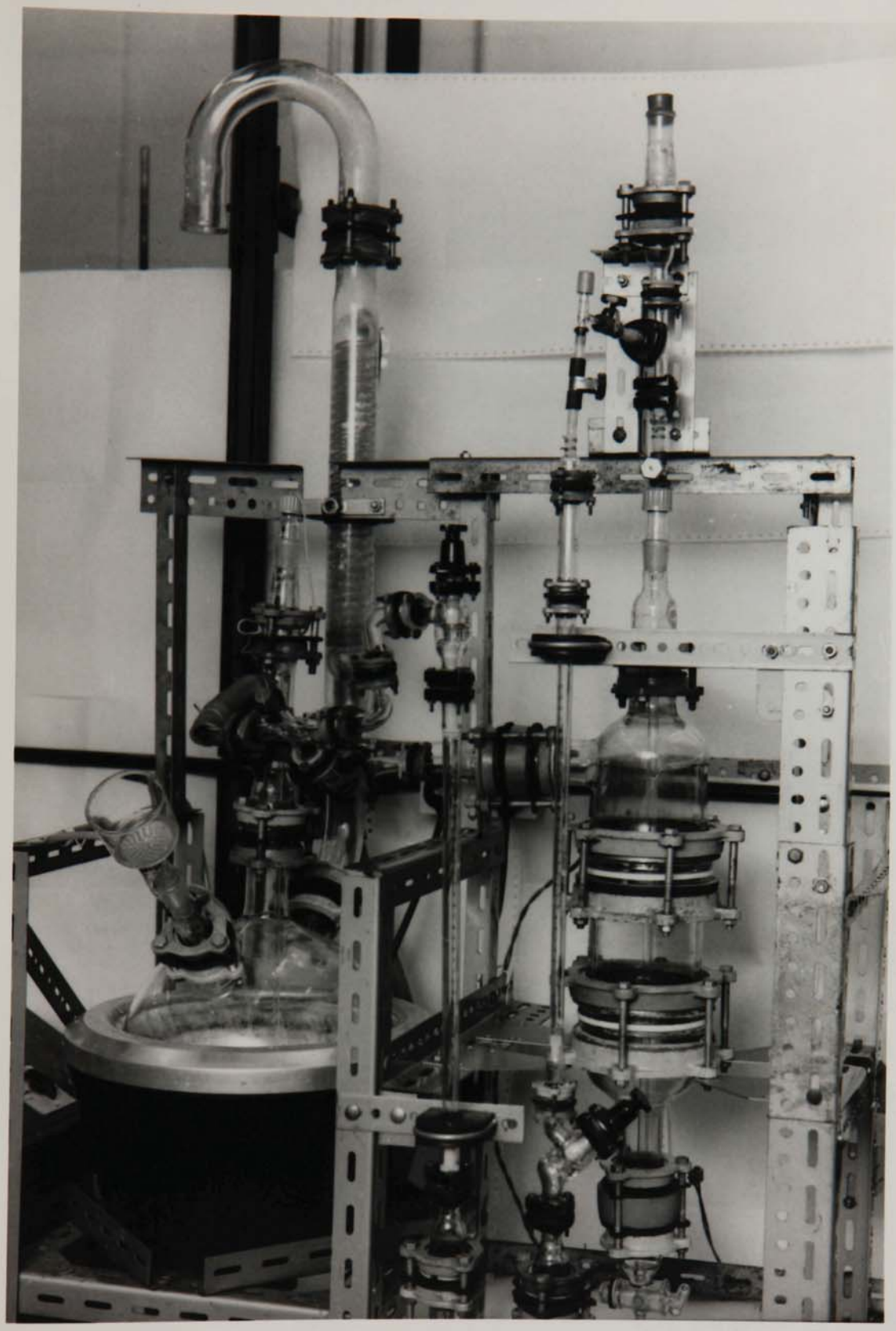

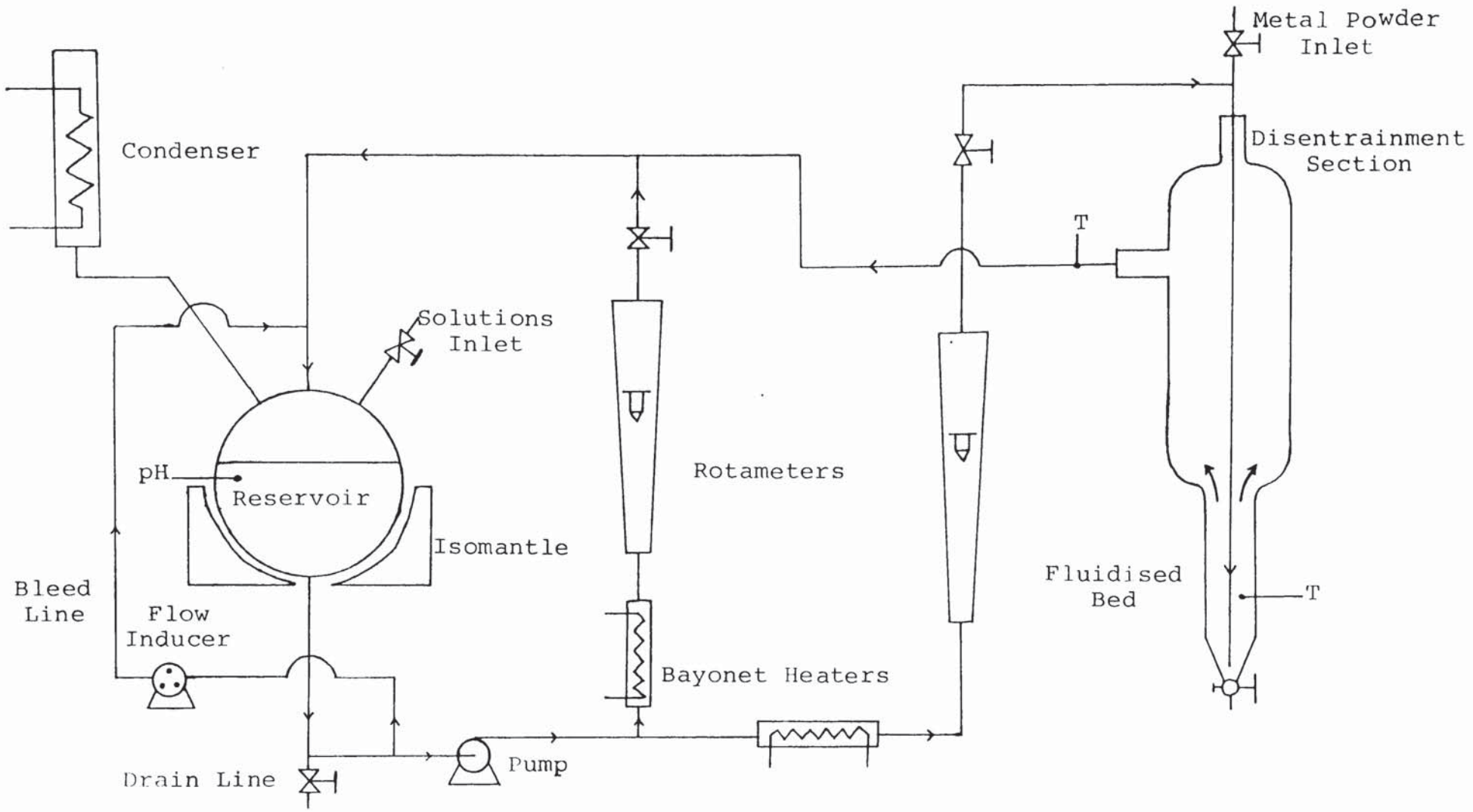

Figure 5.2 Flow Diagram of 10-Litre Batch Fluidised Bed Crystalliser Rig

by hydrolysis. The tungsten powders used were types 1 and 2 (see Chapter 4). Between 0.5 and 13 grammes of tungsten were used in the 40 mm diameter bed. Initial acid strength was varied from 0.03 to 0.10 N; initial mass of barium chromate in solution from 10 to 40 grammes, and initial concentration of urea from 6 to 20 kg/m^3. After the initial heating up period, the reservoir temperature reached 101 ± 1°C, and the bed temperature was usually 98 ± 1°C. Experiments were carried out until the reservoir turned pale yellow-green indicating that most of the barium chromate had come out of solution.

These experiments produced poor results usually with considerable nucleation taking place throughout the rig. Nucleation was extensive in the liquid reservoir but little or no nucleation occurred in the bed itself and almost certainly no epitaxial growth occurred. Even operation with very low rates of hydrolysis of urea, and hence, with low rates of change of solubility, did not result in any improvement. There were also problems in maintaining a stable bed; the distribution of particle sizes in the tungsten powders used resulted in significant removal of fines from the bed and this material eventually entered the reservoir and also the flow lines, settling at points where the liquid velocity was relatively low. The low operating flow rates required for bed stability were difficult to maintain, particularly because of fluctuations due to degassing of carbon dioxide.

The product obtained from the fluidised bed was a dark dirty green in colour while the material recovered from the reservoir of the rig was yellow-green in colour. The bed product was examined under an optical microscope and a scanning electron microscope, and was observed to be made up of a mixture of metal particles and crystal agglomerates. The barium chromate crystals in these agglomerates appeared to be less than 20 μm in size. Scanning electron microscopy clearly revealed the presence of uncoated metal particles (see figure 5.3). Many of the crystal agglomerates were physically broken up during microscopic observation, using a stiff metal wire fused onto the end of a glass rod, but no evidence of the inclusion of a tungsten particle within an agglomerate was detected.

5.2 2-LITRE BATCH FLUIDISED BED CRYSTALLISER

A smaller batch fluidised bed crystalliser was constructed to examine the effects of various operating conditions on a small scale. The feed reservoir capacity was approximately 2 dm^3. In an attempt to restrict nucleation to the fluidised bed alone, a jacket cooler cum disentrainment section was introduced immediately downstream of the bed section. Subsequently, the rig was further modified to provide a jacket cooler for the whole of the bed and disentrainment section. The bed diameter was 20 mm. Figure 5.4 shows a photograph of the rig and figure 5.5 depicts the flow diagram.

Figure 5.3 - Bed Product from 10-Litre Batch Fluidised Bed Crystalliser


20HM

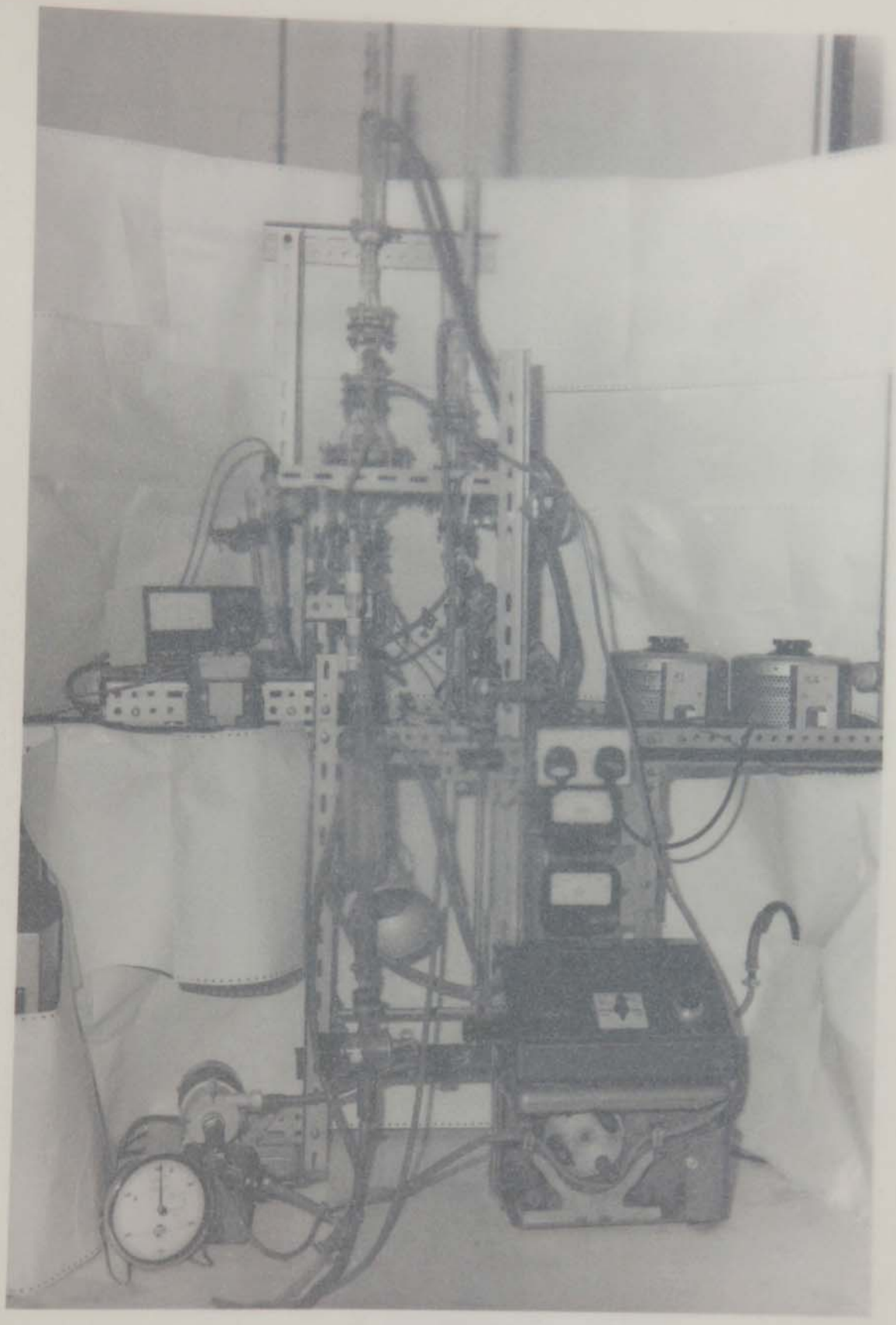

Figure 5.4 - Batch Fluidised Bed Crystalliser Rig
with 2-Litre Feed Reservoir

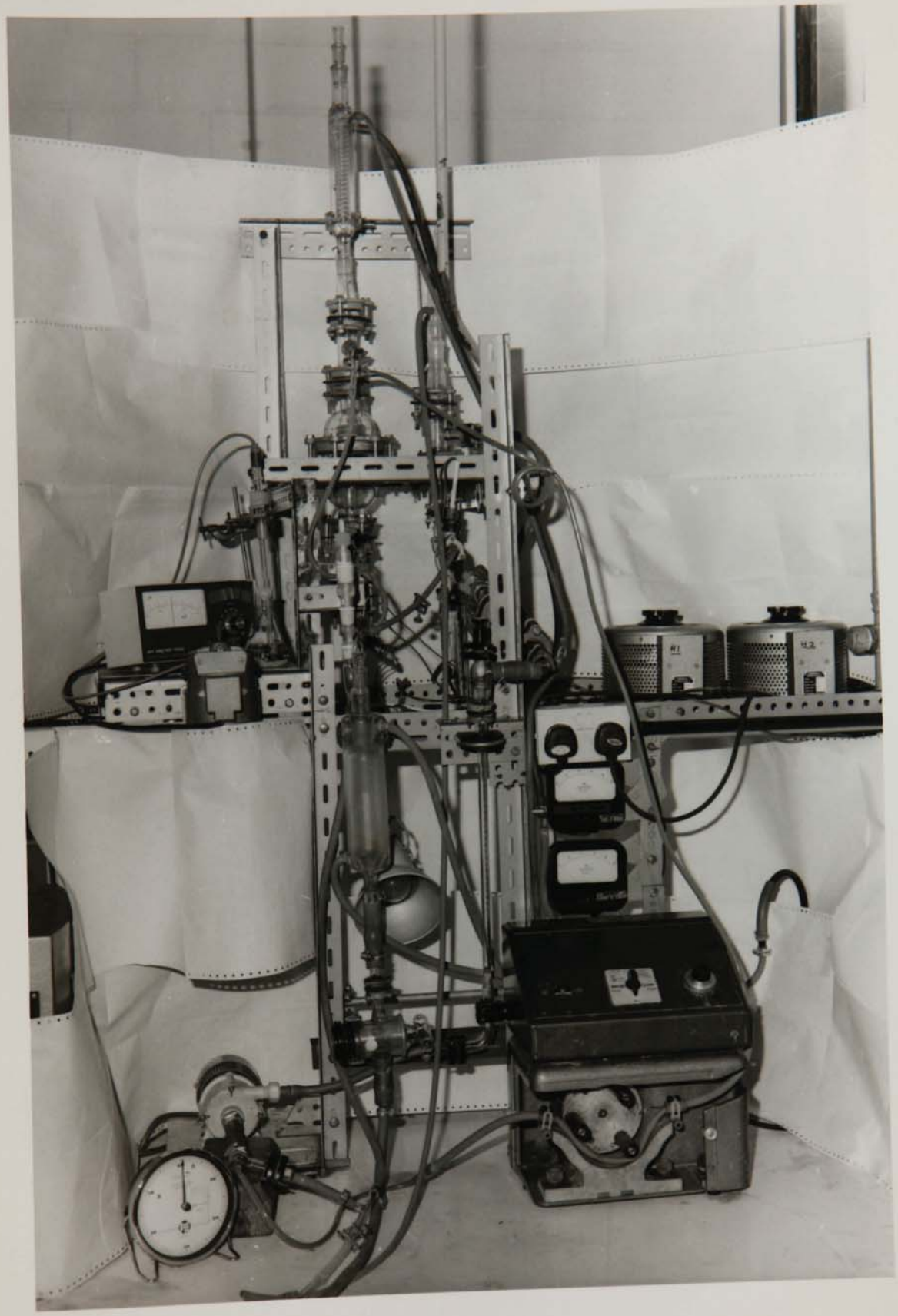

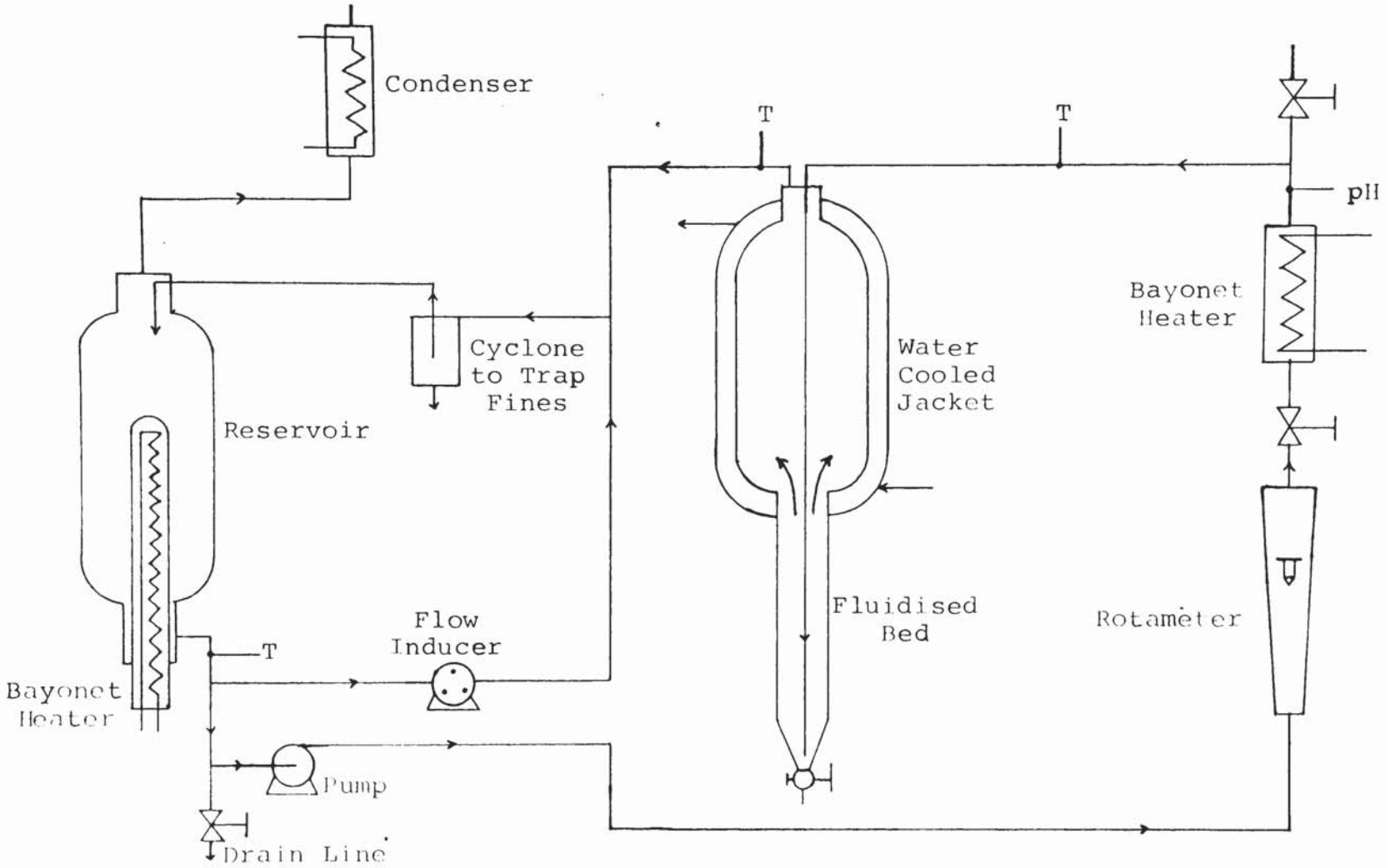

Figure 5.5 Flow Diagram of 2-Litre Batch Fluidised Bed Crystalliser Rig

In the experiments carried out on this rig, the metal powder was introduced into the bed section at the start of each run, instead of doing so when hydrolysis had commenced, as was the case with the 10 litre rig. Furthermore, the metal powders used were conditioned in concentrated hydrochloric acid for at least 24 hours before a test. The metal powders used were tungsten types 2 and 6 (see Chapter 4), a +45 μm to -53 μm sieve fraction of type 6 tungsten, and a -44 μm sieve fraction of the same material. Between 1 and 6 grammes of metal powder were used in these experiments. Initial acid strength was varied from 0.05 to 0.70 N; initial mass of barium chromate in solution was varied from 5 to 10 grammes; and, initial concentration of urea was varied from 25 to 134 kg/m^3. After the initial heating up period, bed inlet temperature remained at a value in the range 96 ± 2 ^{o}C.

These tests failed to achieve epitaxial growth. Nucleation took place mainly on the walls of the jacket cooler rather than on the bed material itself. Considerable unwanted nucleation eventually occurred in other sections of the rig, particularly in the heater unit immediately upstream of the bed. Entrainment of the bed material tended to take place even at flow rates below the theoretical entrainment velocity of spherical particles of similar size.

Microscopic observation of the bed products showed that these were similar to those obtained with the 10 litre rig. Uncoated metal particles and

barium chromate crystal agglomerates, made up of generally equiaxed crystals of varying size, were observed.

5.3 MIXED SUSPENSION CLASSIFIED PRODUCT REMOVAL (MSCPR) CRYSTALLISER (38)

In view of the lack of success of the 10 litre fluidised bed rig in achieving epitaxial growth, the rig was modified to a MSCPR configuration. In this rig, a flow diagram of which is shown in figure 5.6, the metal powder was introduced directly into the reservoir and was kept in suspension, and in contact with the whole of the solution, by means of a stirrer and the upward flow of recirculating liquid. It was expected that only crystals large enough to settle against this upward flow would collect at the reservoir outlet, therefore giving a product of narrow size range. This arrangement, however, did not work as expected because it proved impossible to prevent the tungsten being carried away into the recirculation line, and settling at dead spots in the pipework. Attempts at using larger sized tungsten powder were also unsuccessful because the powder available was too coarse to keep suspended within the reaction vessel. It was clear that the presence of metal powder in the reactor itself did not lead to preferential nucleation on it. Nucleation occurred throughout the rig and epitaxial growth did not occur.

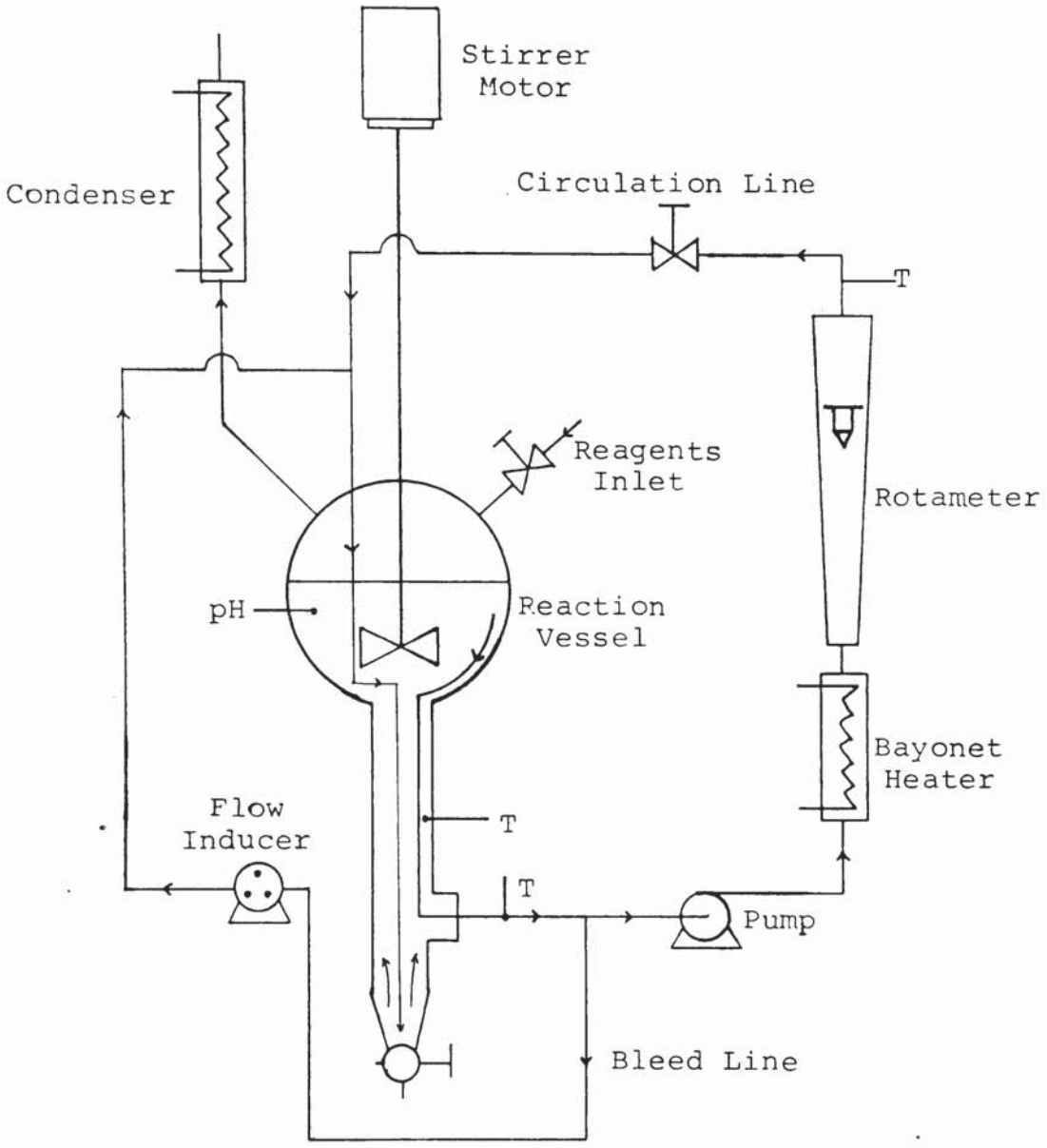

Figure 5.6 Flow Diagram of Mixed Suspension Classified Product Removal Crystalliser Rig

5.4 MATHEMATICAL MODEL OF FLUIDISED BED CRYSTALLISER

The problems experienced with the fluidised bed crystallisers, led to the development of a mathematical model for the process. This model is set down in Appendix 6.

The model confirmed the difficulty of balancing the conflicting requirements of having a sufficiently high flow velocity to the fluidised bed in order to ensure the removal of the supersaturation generated by the solubility change, due to urea hydrolysis, while at the same time having a suitably low velocity to prevent the removal of the extremely small metal particles from the bed. This model has shown that even at the lowest possible urea hydrolysis rates, the flow rates required to prevent a build-up of supersaturation were too high to maintain a stable fluidised bed of reasonable diameter.

5.5 EPITAXIAL GROWTH EXPERIMENTS USING METAL WIRES

A series of experiments was carried out in a 1 dm^3 capacity spherical stirred vessel, in order to test the suitability of various metals for use in powder form for epitaxial growth of barium chromate. The experimental rig is depicted schematically in figure 5.7. In each experiment a different metal wire, each 1 mm in diameter, was immersed in solution and the process of precipitation from homogeneous solution was carried out. Moderate agitation of the solution took place by means of an inclined double bladed

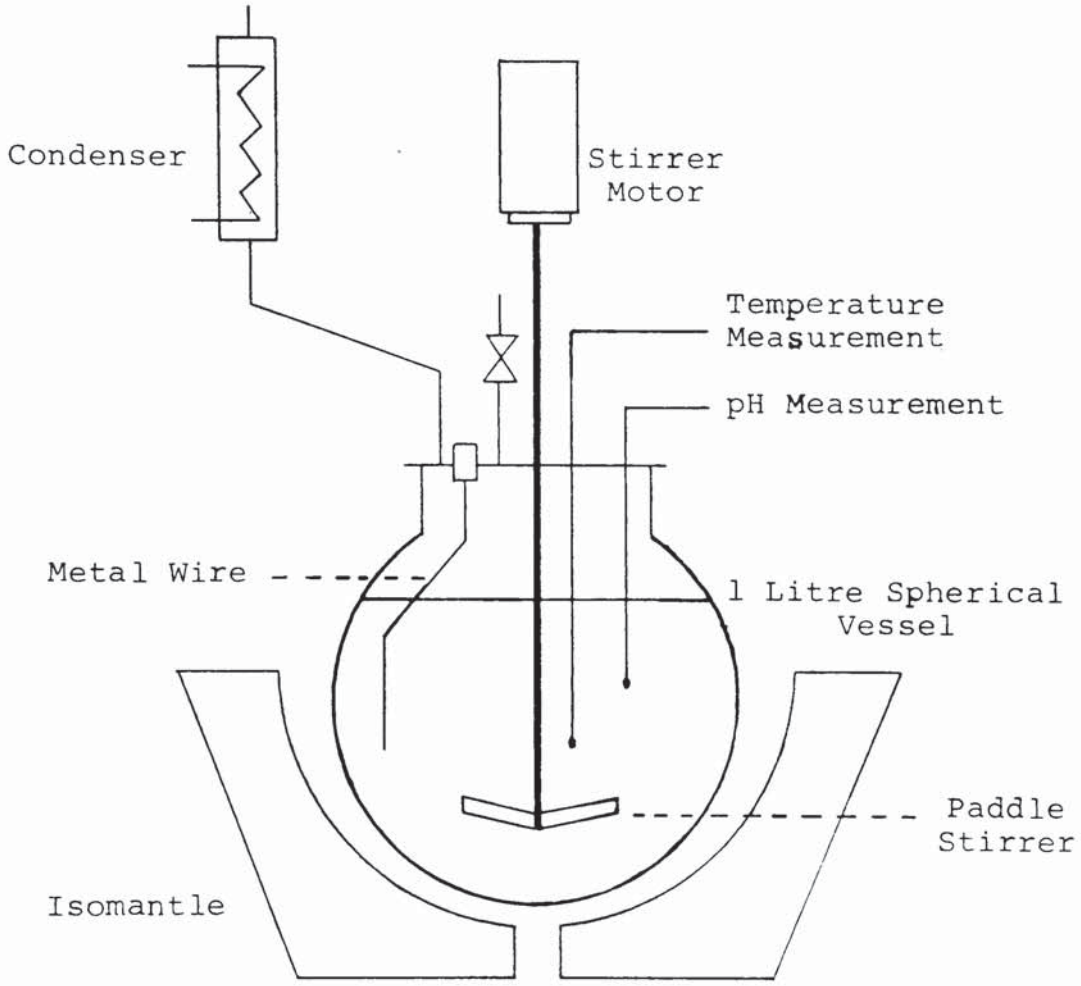

Figure 5.7 Schematic Diagram of Batch Stirred Vessel used for Epitaxial Growth Experiments on Metal Wires and Metal Powders

paddle. The metals tested were copper, molybdenum, nickel, tantalum, titanium and tungsten. In each case the metal wire was conditioned by immersion in concentrated hydrochloric acid in an attempt to remove any surface oxide layer, prior to the test. Three different initial acid strengths, 1.2N, 5.0N and 10.0N were used in experiments with tungsten. The other experiments were carried out with an initial acid strength of 1.2N. Initial urea concentrations depended on the acid strength and were in the range 150 to 750 kg/m^3 (i.e. 2.5 to 12.5M).

These tests showed that the copper and nickel wires were attacked by the hot acidic solution and were therefore unsuitable as substrates for epitaxy. The other tests produced sparse and non-uniform overgrowths on the metal wires. The overgrowth tended to break away very easily on touch and appeared, on microscopic examination, to be made up of clusters of small crystals of barium chromate attached to the wire. The best overgrowths occurred on the titanium and molybdenum wires. The former gave the most uniform overgrowth while the latter had the thickest deposit.

All these experiments resulted in the major proportion of barium chromate originally in solution precipitating out on its own rather than nucleating on the metal wire. It was also observed that parts of the wire that had been in relatively still solution usually showed a thicker encrustation. These observations probably indicate that true epitaxy did not

occur but that the overgrowth obtained was due to crystals deposited on the wires rather than due to those nucleated on their surfaces.

5.6 EPITAXIAL GROWTH EXPERIMENTS USING METAL POWDERS

A further series of experiments was carried out in the rig used for the metal wire tests (figure 5.7) to examine the possibility of achieving epitaxial growth on particles of different metal powders suspended in the solution in which homogeneous precipitation was taking place.

The powders used in these experiments were hafnium, molybdenum, tantalum, titanium and tungsten types 2,3,4,5 and 6 (see Chapter 4). Subsequently four further samples of tungsten powder supplied by the Ministry of Defence (U.K.), were also tested. In each experiment, the powder was kept suspended by a sufficiently rapid rate of agitation, using a collapsible flat paddle in all except the tests on the relatively large sized type 6 tungsten, for which a short shaft three-blade propellor was used. Initial acid strength was between 1.0 and 1.2 N. Initial urea concentration varied from 60 to 200 kg/m^3 (i.e. 1.0 M to 6.7 M). The initial mass of barium chromate was either 5 or 10 grammes. Operating temperatures were in the range 99 to 101^{o}C. The metal powders used were conditioned in hydrochloric acid for more than 24 hours before each test.

The products from these experiment were different shades of green in colour. The tests with the titanium and tungsten powders gave products that could clearly be seen to be a mixture of barium chromate crystals and metal powder. Optical microscopy confirmed this and also indicated that a smaller proportion of uncoated metal particles was evident in the products from the other tests. On physically breaking up some of the agglomerates in these products it was possible to observe that at least some of these had metal particles included in them. In other cases metal particles were observed adhering to a cluster of barium chromate crystals. Scanning electron microscope photographs of the products obtained with tungsten powders showed them to be mixtures of metal particles and crystals. The other products photographed did not, however, reveal the presence of much uncoated metal powder. Figures 5.8, 5.9, 5.10 and 5.11 are some of the photographs showing these test products.

Experiments were also carried out using four samples of tungsten supplied by the Ministry of Defence (U.K.), two of which had been used by Miller in his work on igniferous compositions (1). The products from these seemed to have less uncoated metal particles, on microscopic observation, than the other tungsten experiments. Physical break-up of crystalline agglomerates in these products yielded some metal particles but no clear evidence of epitaxy.

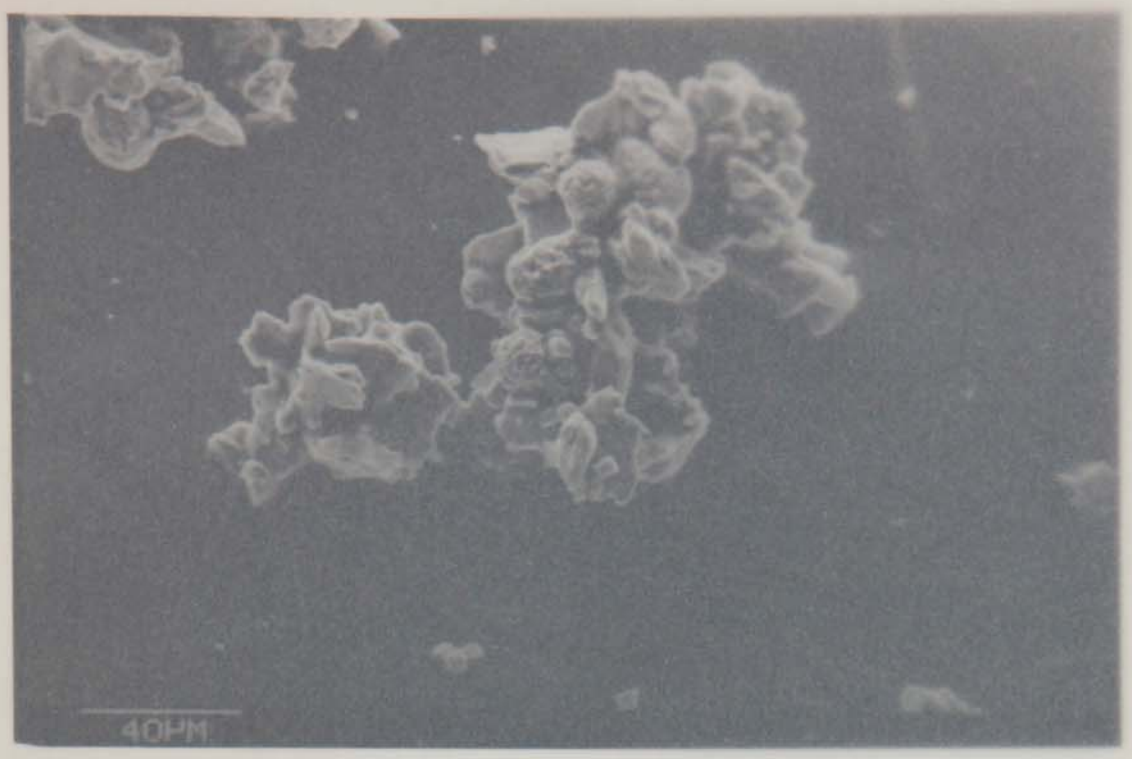

Figure 5.8 - Product from Batch Stirred Vessel Test Using a Tungsten Powder, Showing Uncoated Metal Particles

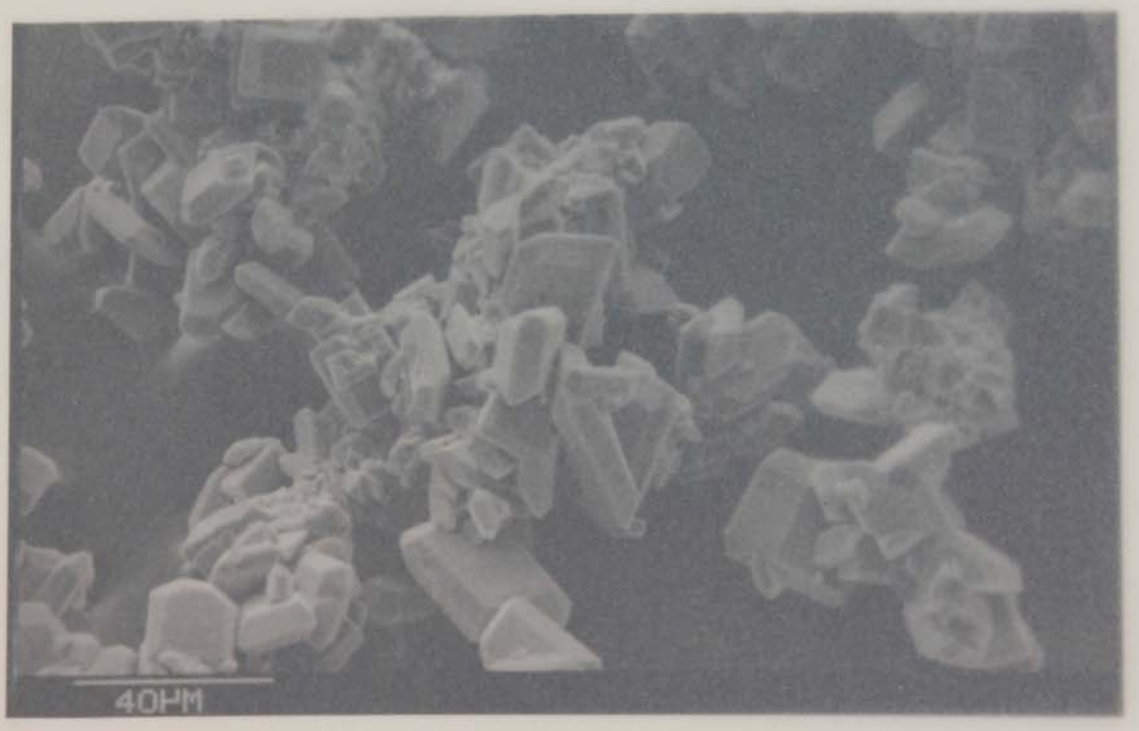

Figure 5.9 - Crystalline Agglomerates Obtained with Tantalum Powder in a Batch Stirred Vessel Test

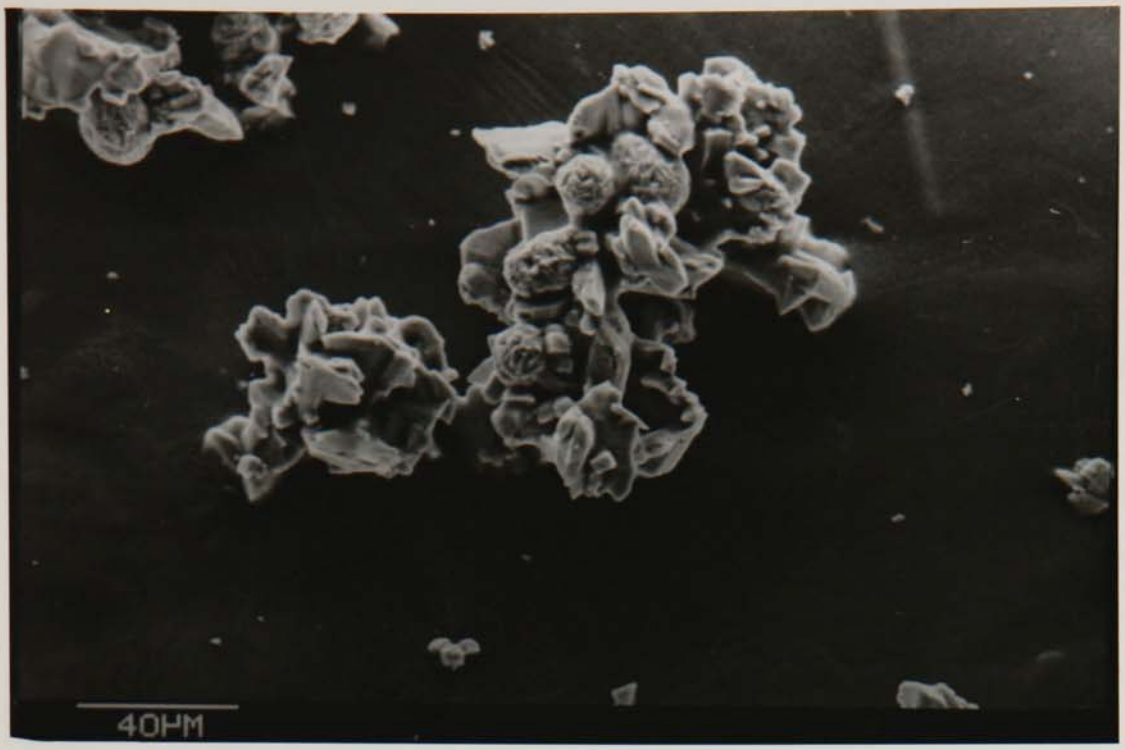
40μM

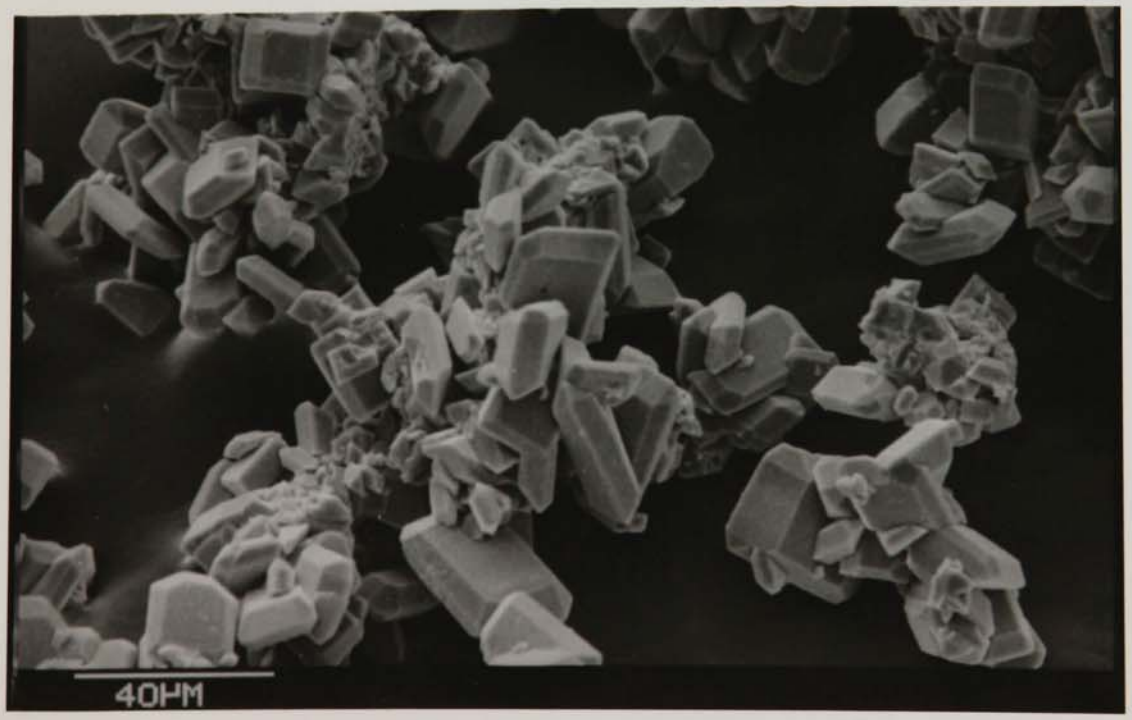
40μM

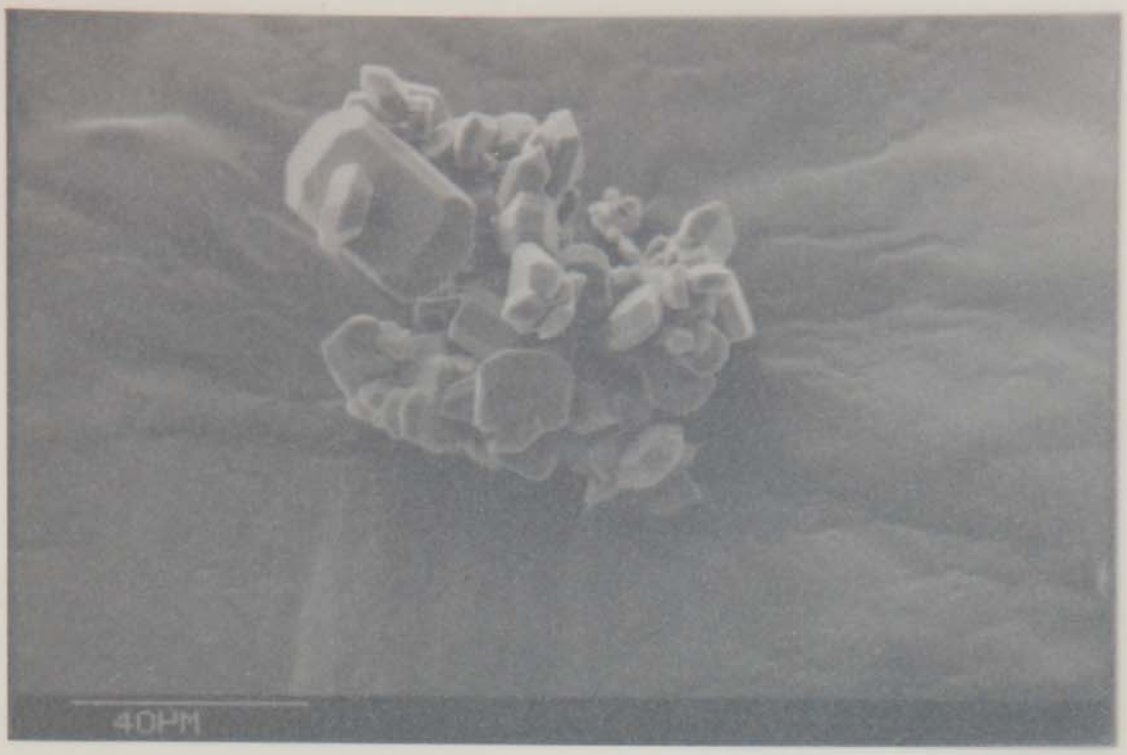

Figure 5.10 - A Single Crystalline Agglomerate in the Product Obtained with Hafnium Powder in a Batch Stirred Vessel Test

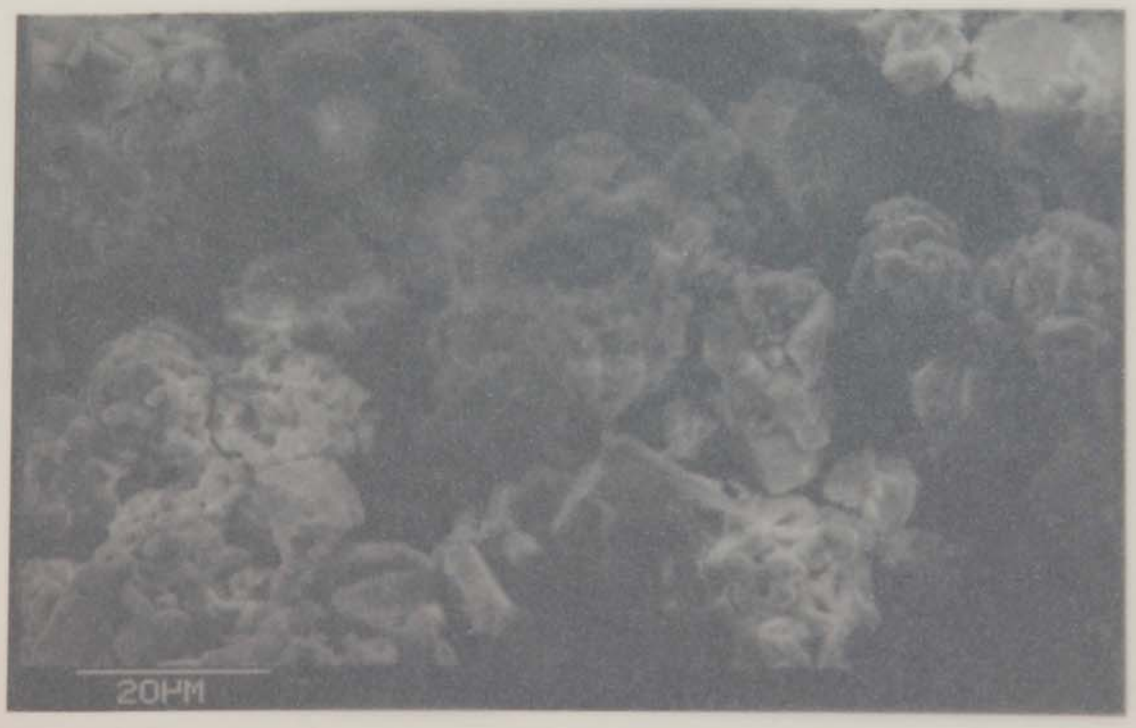

Figure 5.11 - Crystalline Agglomerates Obtained with Molybdenum Powder in a Batch Stirred Vessel Test

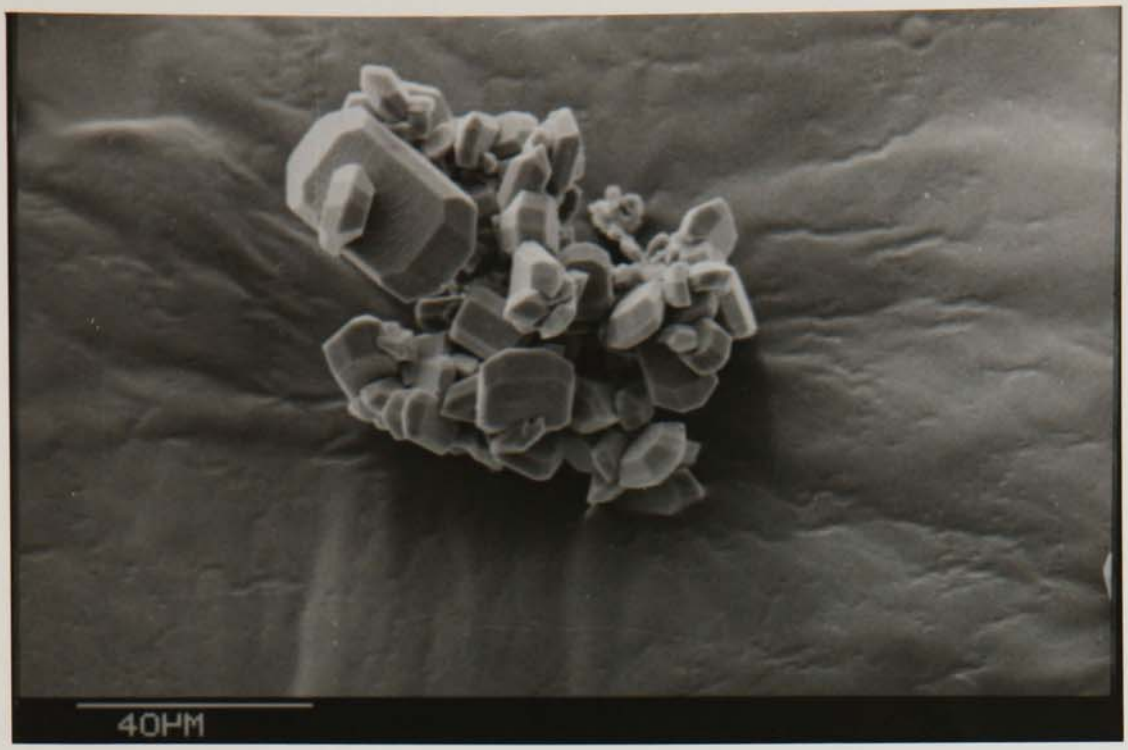
40HM


20HM

5.7 GENERAL CONCLUSIONS

The experiments described above showed that hydrodynamic restrictions made the use of a fluidised bed for epitaxial growth impracticable. The MSCPR crystalliser experiments and the metal powder tests showed that the available tungsten powders did not act as preferential sites for nucleation. There may have been partial epitaxial growth with some of the other metal powders and with the Ministry of Defence tungsten samples. However, the products obtained were probably merely barium chromate agglomerates, with precipitation at times taking place in sufficiently massive form to physically include the metal particles. It is possible that epitaxy, even if favoured by lattice match and substrate size (129), is hindered by the vigorous agitation prevailing in the batch stirred vessel experiments, due to the evolution of carbon dioxide and mechanical stirring. The carbon dioxide might also act to prevent epitaxy by facilitating nucleation in solution and/or being adsorbed on the substrate surface.

CHAPTER SIX

BARIUM CHROMATE BATCH CRYSTALLISATION EXPERIMENTS

6.0 INTRODUCTION

The experimental rig used for the barium chromate batch crystallisation experiments, along with its associated instrumentation, is described in this chapter. The experimental technique used and the different series of experiments are also reported.

6.1 BATCH CRYSTALLISATION RIG

A Quickfit, type FR1LF, spherical, glass reaction flask of nominal capacity 1 dm^3, was used as the vessel for batch crystallisation. The vessel was fitted with a Quickfit, type MAF3/52, multi-socket, flat flange, glass lid having one central and four peripheral openings. Details of these openings are given in Appendix 11. ; A Quickfit, type JC1OOF, metal clip was used to clamp the lid to the vessel. A coil type Quickfit water cooled condenser (type: C3/22) having an approximate surface area of 0.04 m^2 and an overall length of 460 mm was fitted to opening P4 (see Appendix 11) by means of a Quickfit multiple adaptor, type MA1/2 . The condenser and adaptor both had cone and socket joint specifications of 19/26. Quickfit cone/screwthread adaptors (types ST52/13, ST52/24 and ST53/24) were used to insert the different measuring instruments used, through the other openings in the lid.

Figure 6.1 shows a close-up view of the batch crystallisation vessel and the type MUL/1L, 240V, 300W isomantle laboratory heater. An overall view of the whole rig and some of its instrumentation is provided in figure 6.2, while figure 6.3 is a schematic diagram of the rig.

6.2 INSTRUMENTATION AND ACCESSORIES

6.2.1 Heating System

A type MUL/1L, 240V, 300W, isomantle laboratory heater was used to achieve operating temperatures. The heater was connected to an Ether 'mini' type 17-90B/1, proportional temperature controller. The controller employed a resistance thermometer, having a sensitivity of 0.5°C, which was introduced into the crystallisation vessel through the opening, P3 in the lid. The controller had a nominal working range of 0 to 100°C. In practice it was found that temperature control under stable ambient conditions was better than ±0.5°C.

6.2.2 Temperature Measurement

A conventional mercury in glass thermometer graduated to 0.1°C, and hence capable of reading to the nearest 0.05°C, was used as the primary mode of temperature measurement. The thermometer was inserted into the crystallisation vessel through opening P2 in the lid. A standard chromel-alumel thermocouple in a glass sheath was also introduced into the vessel

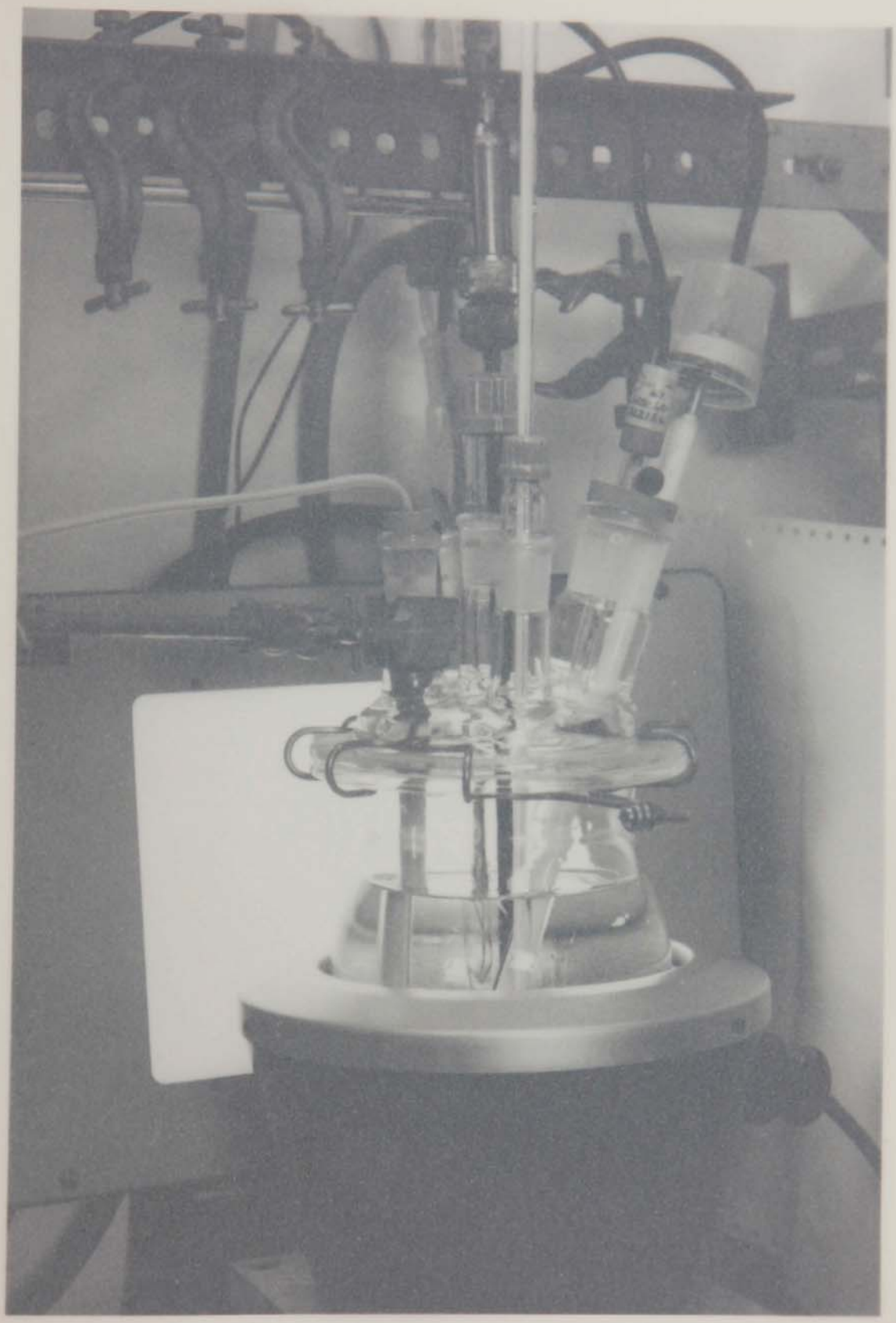

Figure 6.1 - Close-Up View of Batch Crystallisation Vessel

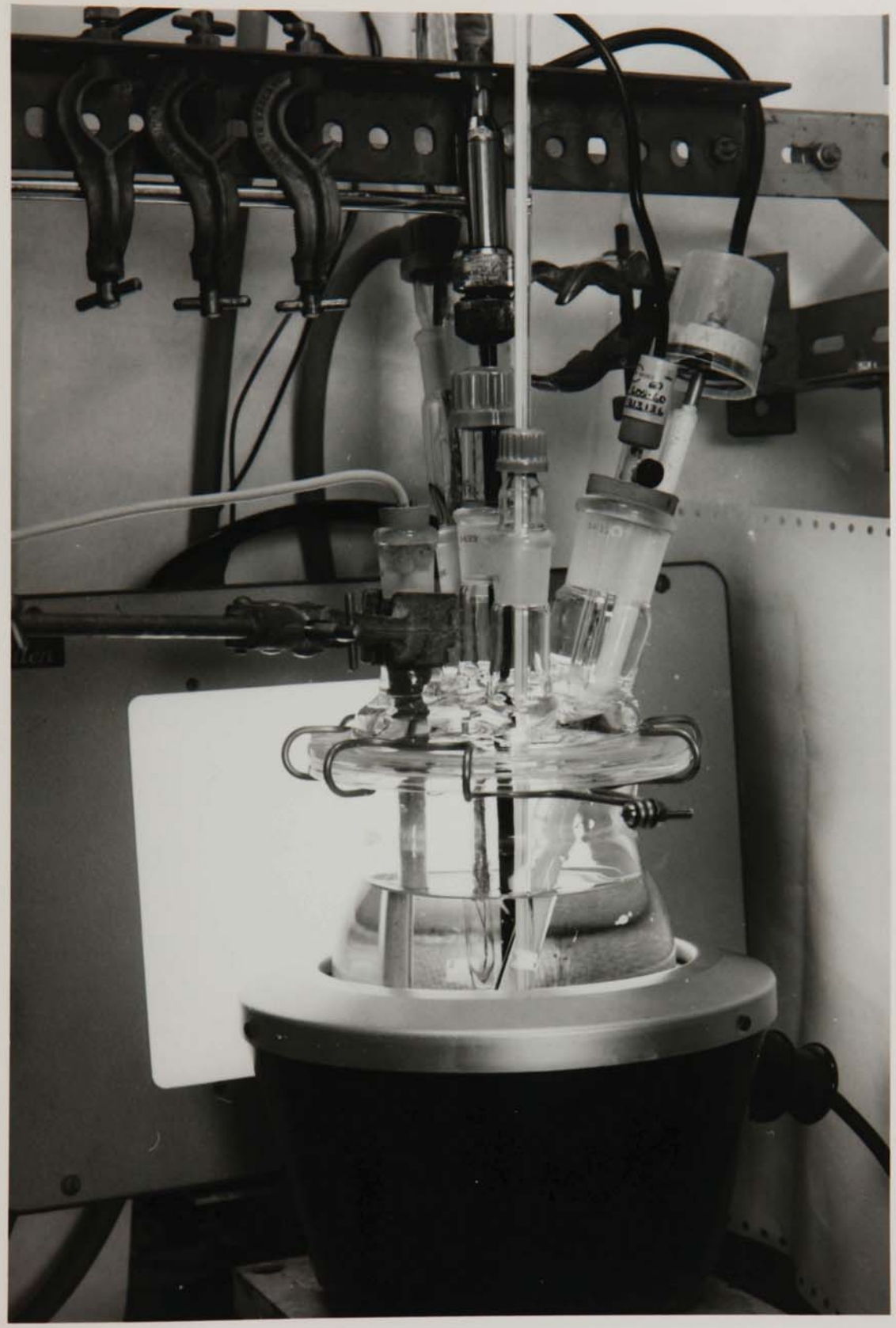

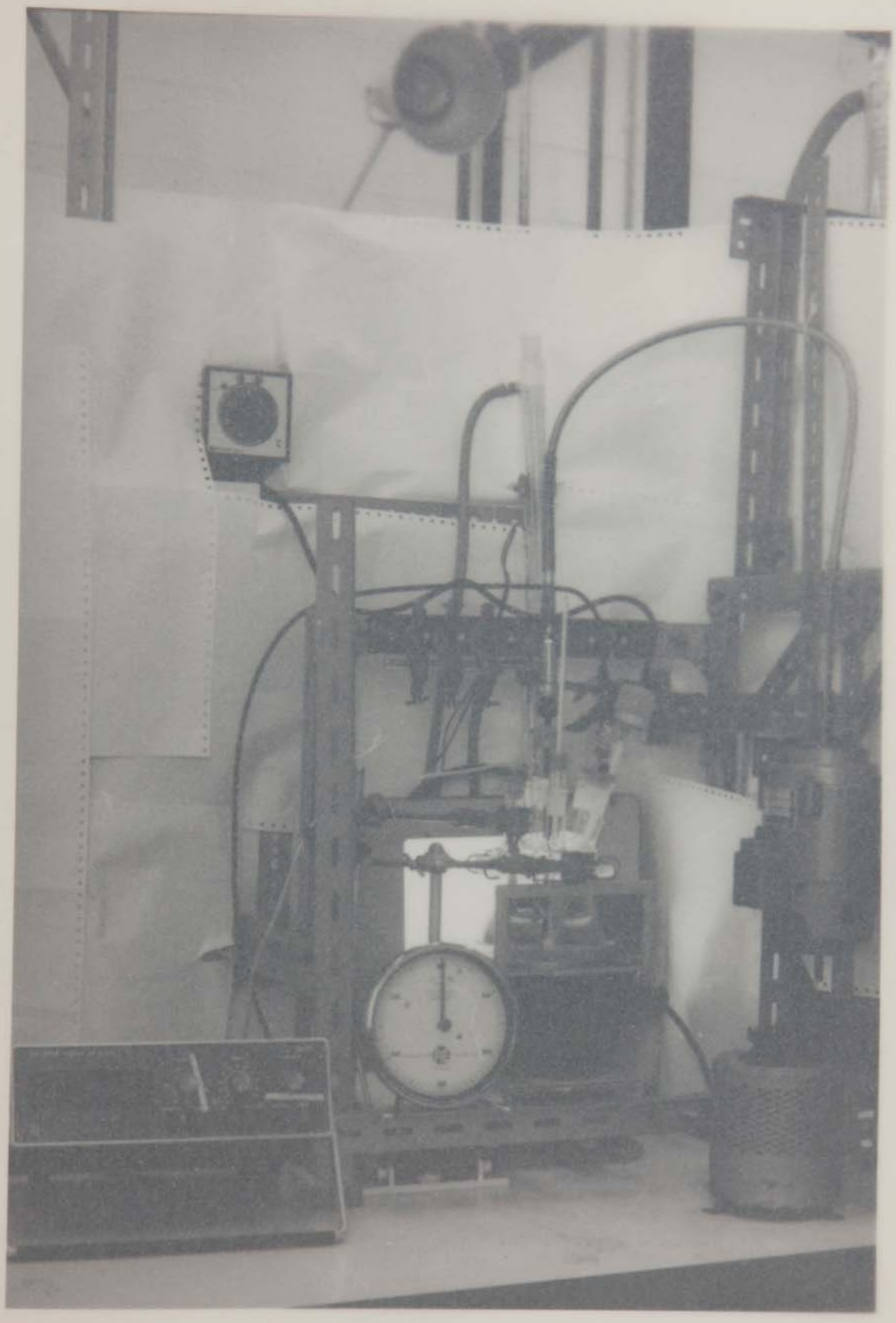

Figure 6.2 - Overall View of Batch Crystallisation Rig

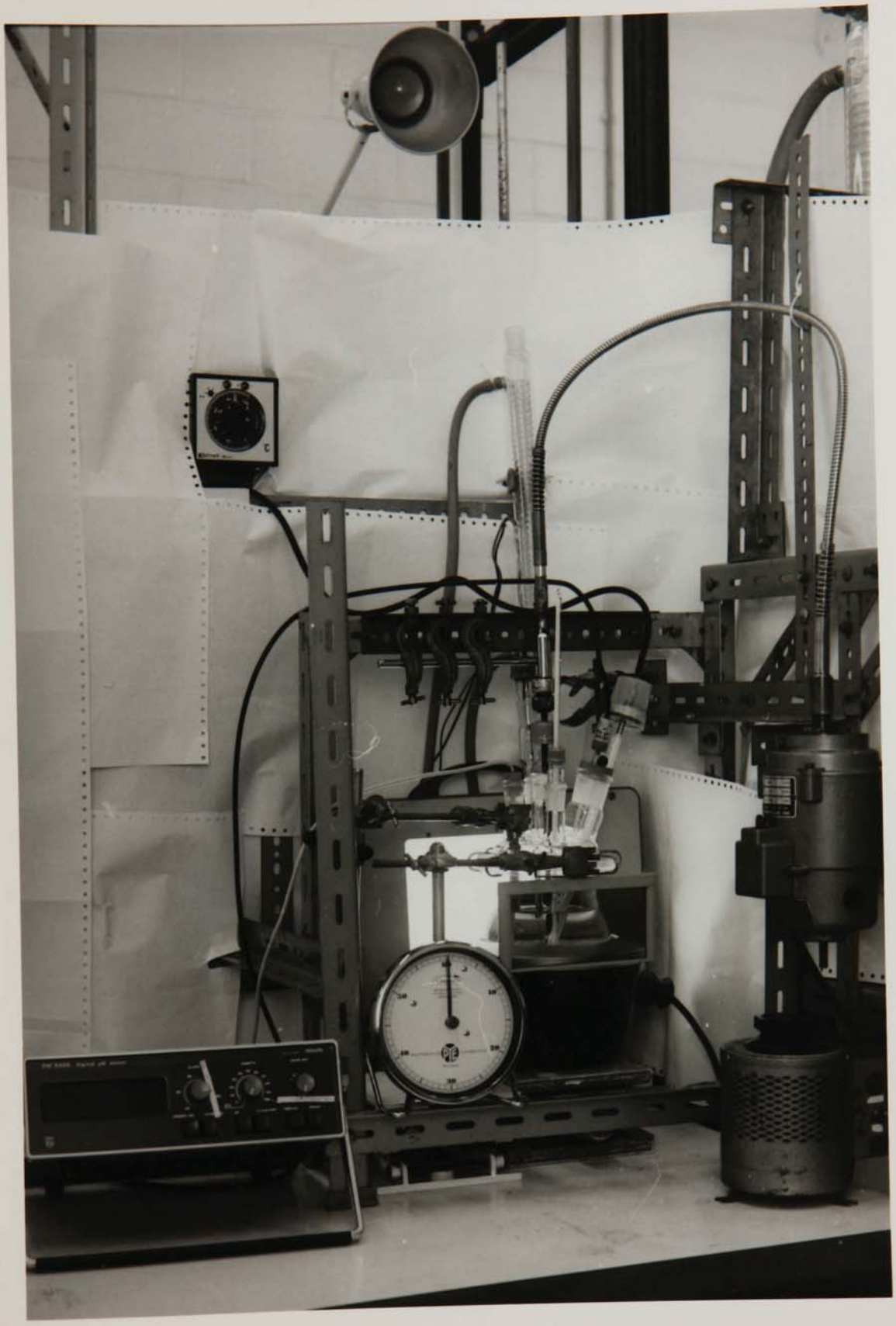

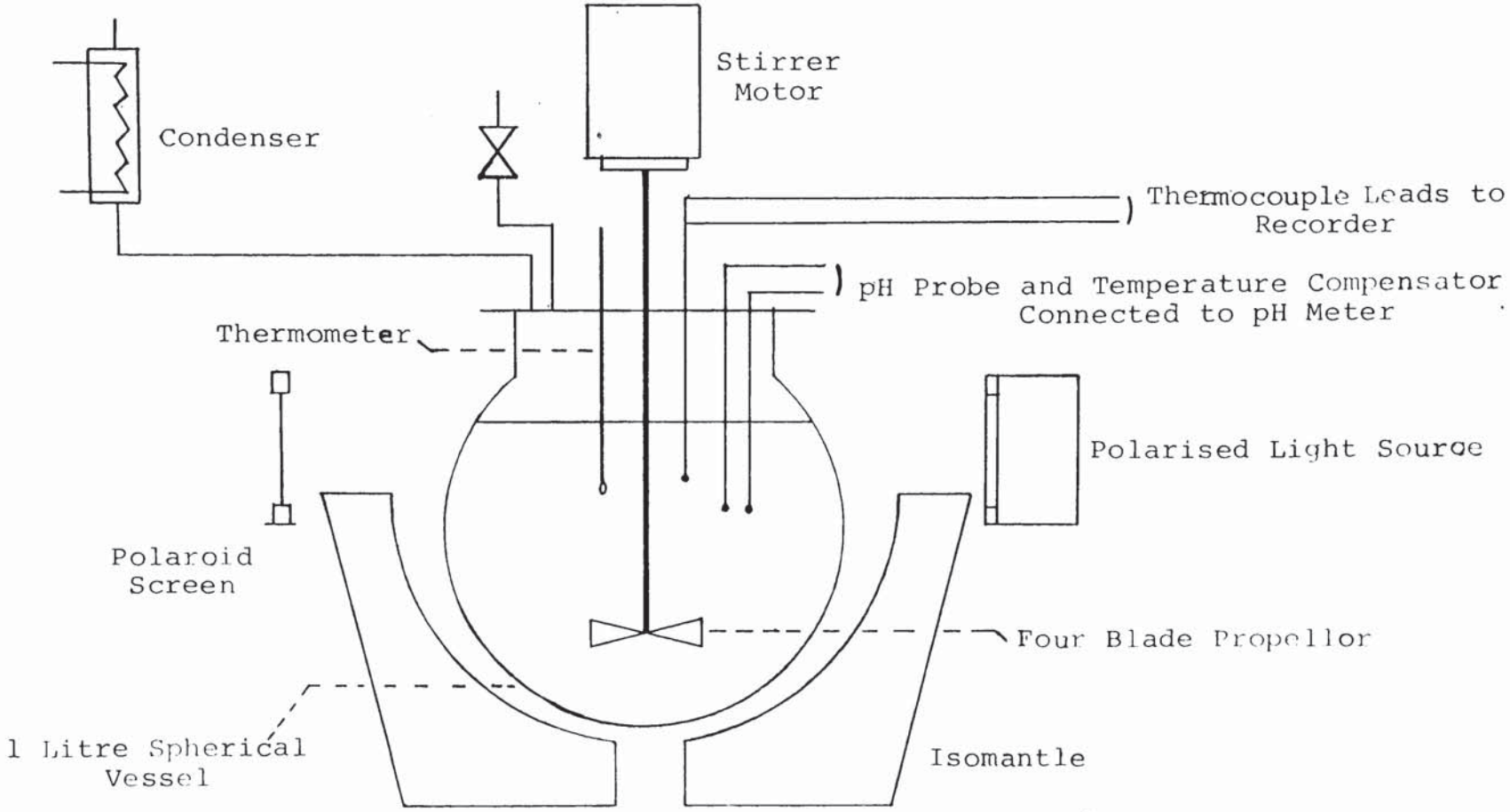

Figure 6.3 Schematic Diagram of Batch Crystallisation Rig

through the multiple adaptor used to connect the condenser. This thermocouple was connected to a Kent-Mark 3, 16 point multi range millivolt recorder. The recorder was used with its reference junction placed in a vacuum flask containing water at 20°C. The reference temperature was checked periodically during any test run. The purpose of the recorder was to provide a permanent record of the temperature changes during a crystallisation and to monitor the temperature to determine if it remained steady during the period of crystal growth. The instrument was found to be accurate to ±0.5°C. A typical temperature record is shown in figure 6.4.

6.2.3 pH Measurement

During each crystallisation experiment pH was monitored continuously using a Philips PW9409 digital pH meter. The instrument had a resolution of 0.005 pH units over a measuring range from 0 to 19.99 pH units and a response of 10 mV/pH unit. The pH probe was a Pye-Unicam laboratory combined electrode (type: 405-60) with an operating range of 0 to 12 pH units and specially rated for use at temperatures from 10 to 130°C. The probe was filled with a saturated solution of Analar grade potassium chloride in distilled water. Automatic temperature compensation was employed by means of a Philips Pt 100 resistance thermometer, operable over the temperature range from -10 to 150°C, which was directly connected to the pH meter. The

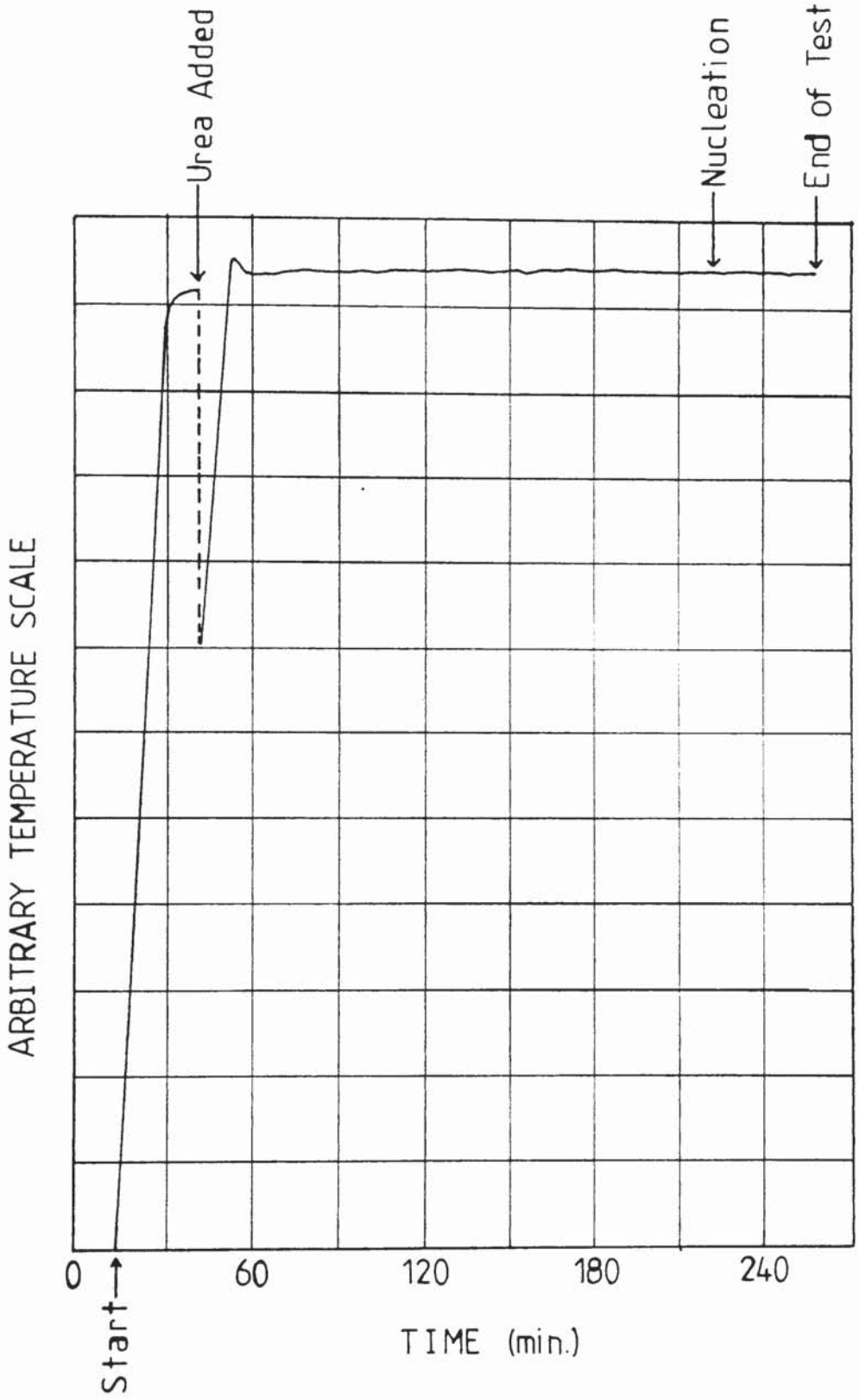

Figure 6.4 Typical Temperature Record from a Batch Crystallisation Experiment (Series G; Crystallisation Time: 2070 s)

pH probe was introduced into the crystalliser through opening P3 in its lid while the temperature compensator was inserted through opening P1.

The pH measuring instrumentation was calibrated at regular intervals during the course of the crystallisation experiments, and after each time the pH probe was refilled. Calibration was carried out according to the recommended procedure (177) using freshly prepared buffer solutions of pH 4 and 7, maintained at a steady temperature. The buffer solutions were prepared from sachets of Pye-Unicam buffer powders.

6.2.4 Agitation

The stirrer used for the batch crystallisation experiments was a four blade propellor of diameter 38 mm, having a pitch of 30^{o} and a shaft of diameter 6.5 mm and length 325 mm. The stirrer was completely coated with a 0.18 $\pm$ 0.02 mm thick layer of PTFCE for acid resistance.

The stirrer was inserted into the crystalliser through the central opening in the lid which was fitted with a Quickfit adaptor (type: ST53/24) to reduce the clearance between the shaft and the glass to a minimum. A Voss 1/8 h.p. (93W), 250V electric motor having a maximum rating of 3000 r.p.m. was used to drive the stirrer by means of a flexible shaft coupling. Speed control was achieved by means of a Cressall Torovolt voltage regulator fitted to the

motor. In practice smooth control of speed below about 400 r.p.m. proved to be difficult.

Stirrer speed was measured using a Comark, type 2101 stroboscopic tachometer having a measuring range of upto 30,000 r.p.m. Usually measurements were made on an intermediate scale with full scale deflection corresponding to 3000 r.p.m. On this scale the measurements were accurate to within ±10 r.p.m.

6.2.5 Other Equipment

An Allen, type LV28, polarised-light source and a polaroid sheet were used to observe the contents of the crystalliser in transmitted polarised light to facilitate detection of the onset of nucleation.

A Pye mechanical stopclock graduated in seconds was used to measure time during the course of each experiment.

6.3 EXPERIMENTAL PROCEDURE

The properties of the chemicals used for crystallisation experiments have been covered in Chapter 4. In addition freshly distilled water which had been filtered through a Sartorius 0.45 μm membrane filter was used to prepare all solutions. Concentrated hydrochloric acid solution was prepared using Analar grade acid and standardised with a 0.1N solution of Analar grade di-sodium tetraborate decahydrate (borax). Appropriate quantities of barium chromate and urea were weighed to the nearest 0.01 gramme.

Prior to the commencement of a crystallisation run 5g of barium chromate was introduced into the crystalliser through opening P2. Sufficient concentrated hydrochloric acid to make the initial acid strength of the system, approximately 0.11M, prior to commencement of crystallisation, was also added (e.g. 22 cm^3 of 5.27N acid). A further 550 cm^3 of distilled water was then added and the stirrer, the temperature recorder, the pH meter, cooling water to the condenser, and the heater, with the controller set point preset, were all turned on. The system was left until all barium chromate had dissolved and the solution had attained a steady temperature. This process usually required approximately 20 minutes. The pH reading at this stage was usually 0.98 $\pm$ 0.05.

The preweighed quantity of urea was first dissolved in 150 cm^3 of distilled water. Before adding the urea solution 150 cm^3 of distilled water was added to momentarily reduce the temperature of the contents of the crystalliser so that rapid hydrolysis of urea did not occur immediately on its addition. The urea solution was then introduced and finally sufficient distilled water to make up the nominal system volume to 1 dm^3. The stopclock was started at this time, and temperature, stirrer speed and pH were all noted. These readings were also noted at regular intervals during the whole experiment. The onset of nucleation was detected by observing the solution in transmitted polarised light and noting

the characteristic cloudiness caused by the initial burst of fine crystallites. Although a visual method, this technique was found to be adequate for detection of nucleation.

Each experiment was terminated at a predetermined time by switching off the heater and adding 200-250 cm^3 of distilled water at ambient temperature (16-20^{o}C). This caused a rapid drop in system temperature to below 85^{o}C and thus effectively stopped urea hydrolysis. Preliminary experiments using different quantities of distilled water showed that this technique did not cause any significant extra nucleation at the end of a run. Experiments using dilute acid instead of distilled water in a bid to compensate for the increase in supersaturation, due to the temperature drop, by decreasing the solution pH to cause a counteracting increase in solubility, were unsuccessful since it was found that this caused dissolution of some of the precipitated barium chromate.

At the end of each run the crystalliser lid was removed and the contents of the vessel were rapidly vacuum filtered using a 170 mm Buchner funnel and Whatman grade 542, hardened ashless filter paper. Any precipitate sticking onto objects that had been immersed in the crystalliser was removed, using a fine water jet from a wash bottle, and recovered. The precipitate was washed with a small quantity of distilled water (<30 cm^3), dried in an oven at below 40^{o}C, weighed, and subjected to size analysis as

described in Chapter 8. The process of filtration and washing was carried out in less than 5 minutes. The recovered precipitate varied in colour from bright yellow to dark amber according to increasing crystal size.

Two spherical vessels of the same specifications were used alternately during the main series of experiments. After each experiment the vessel was filled with dilute hydrochloric acid and left for at least 24 hours before washing and drying. This was found to prevent deposition of the barium chromate precipitate on the walls of the vessel during subsequent experiments.

6.4 DETAILS OF EXPERIMENTAL CONDITIONS

6.4.1 Main Batch Crystallisation Experiments

Table 6.1 summarises the experimental conditions employed for the five main series of batch crystallisation experiments which were carried out. This table gives the total number of runs carried out in a particular series, inclusive of runs that failed. Successive experiments in each series lasted for progressively shorter durations of time. The major experimental data are tabulated in Appendix 2.

6.4.2 Experiments of a Qualitative Nature

Prior to the commencement of the main crystallisation experiments a set of five preliminary experiments was carried out under conditions used for series A (see

TABLE 6.1

Experimental Conditions for Batch Crystallisation Experiments

Series	Number of Experiments (-)	Initial Mass of Barium Chromate (g)	Initial Mass of Urea (g)	Crystallisation Temperature (^{o}C)	Stirrer Speed (r.p.m.)	Initial HCl Acid Strength (M)
A	12	5.00	20.00	100	500	0.1075
D	14	5.00	20.00	90	500	0.1070
E	24	5.00	10.00	100	500	0.1070
F	30	5.00	10.00	90	500	0.1071
G	20	5.00	20.00	90	750	0.1070

table 6.1). These were performed to perfect the experimental technique and to test the method used for detection of nucleation. A similar set of eight preliminary tests, under conditions used for series E, was also carried out. These preparatory experiments are not reported in Appendix 2.

Several experiments were also carried out, under conditions used for series A, in which seeding was attempted. The seed material used was 0.5 grammes of the -53 μm to +44 μm sieve fraction of recrystallised barium chromate from previous experiments. The seeds were introduced at the instant in time just prior to when nucleation would have otherwise occurred, in order to minimise the possibility of the seeds dissolving before growth commenced. However, seeding did not prevent secondary nucleation and no significant difference in product size distribution was observed for the seeded experiments. The seeds were washed in dilute hydrochloric acid (∿0.12m) before addition in order to remove any fine crystalline dust on the surface, which might have caused a shower of secondary nuclei, but this too did not prevent subsequent nucleation. Therefore, a seeding technique was not considered suitable for the main series of experiments.

A set of five experiments were also carried out, under conditions corresponding to long duration runs of series A, D, E, F and G, using recrystallised barium chromate from previous runs as the feed material. This material was considered to be purer than the

general purpose reagent grade material otherwise used. Experimental results from these tests are also presented in Appendix 2.

6.5 MICROSCOPIC OBSERVATION OF CRYSTAL PRODUCTS

The optical microscopy carried out in determining shape factors for conversion of sieve diameters to equivalent spherical diameters, is described in Chapter 8 (section 8.5). In addition to this, microscopic observations of a number of different crystal products were carried out to observe crystal form and habit, and to check for evidence of agglomerate formation.

It was observed that for all series of experiments, the crystal products were comprised of a mixture of discrete crystals and agglomerates. This was also the case for experiments carried out using recrystallised barium chromate. Agglomerates were found to be present when product recovery was by means of filtration, followed by washing with water and oven drying at a moderate temperature ($<40^{o}C$). Similar agglomerates were also detected in products recovered by filtration, followed by washing with methanol and hot air drying, thus indicating that the agglomerates were not necessarily a consequence of the method of product recovery.

Photomicrographs of some of the crystal products observed are shown in figures 6.5, 6.6, 6.7, 6.8, 6.9 and 6.10. A typical mixture of discrete crystals and

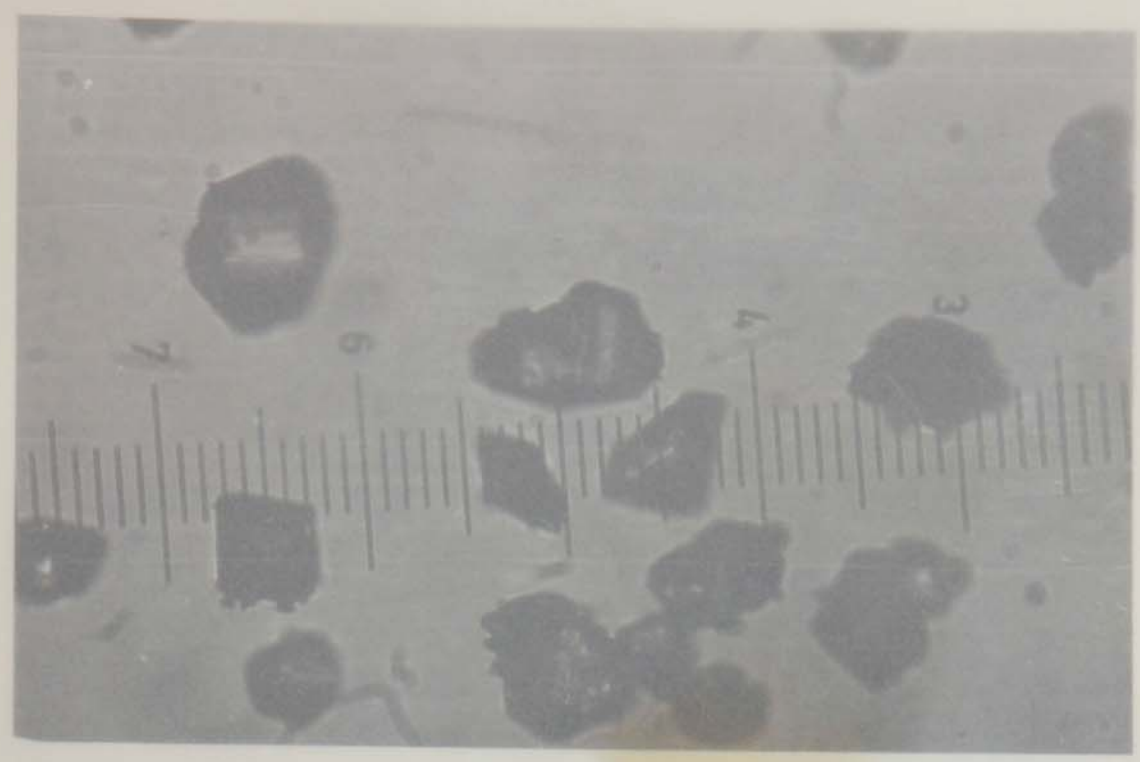

Figure 6.5 - Crystal Product from an Experiment in Series A (Duration 1545 s) (Scale: 1 Sub-Division of Superimposed Scale = 5.5 μm)

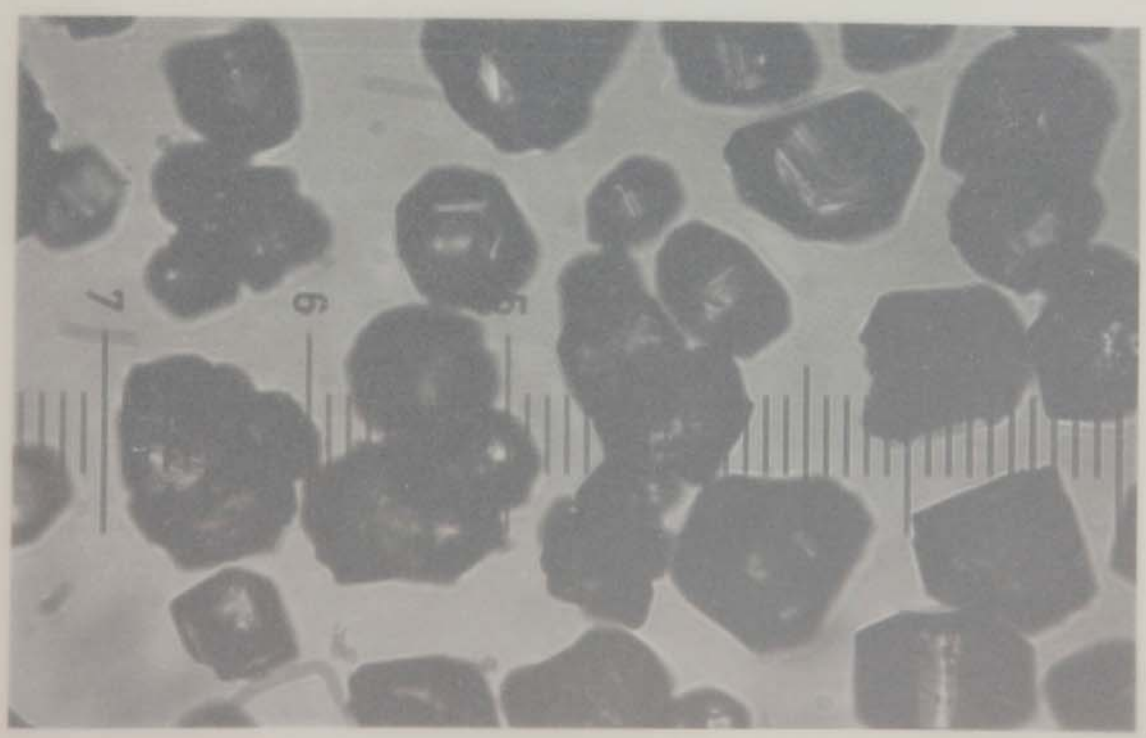

Figure 6.6 - Mixture of Discrete Crystals and Agglomerates in a Product Obtained Using Recrystallised Barium Chromate, Under Series D Conditions (Duration 10440 s) (Scale: 1 Sub-Division of Superimposed Scale = 5.5 μm)


7
6
4
3

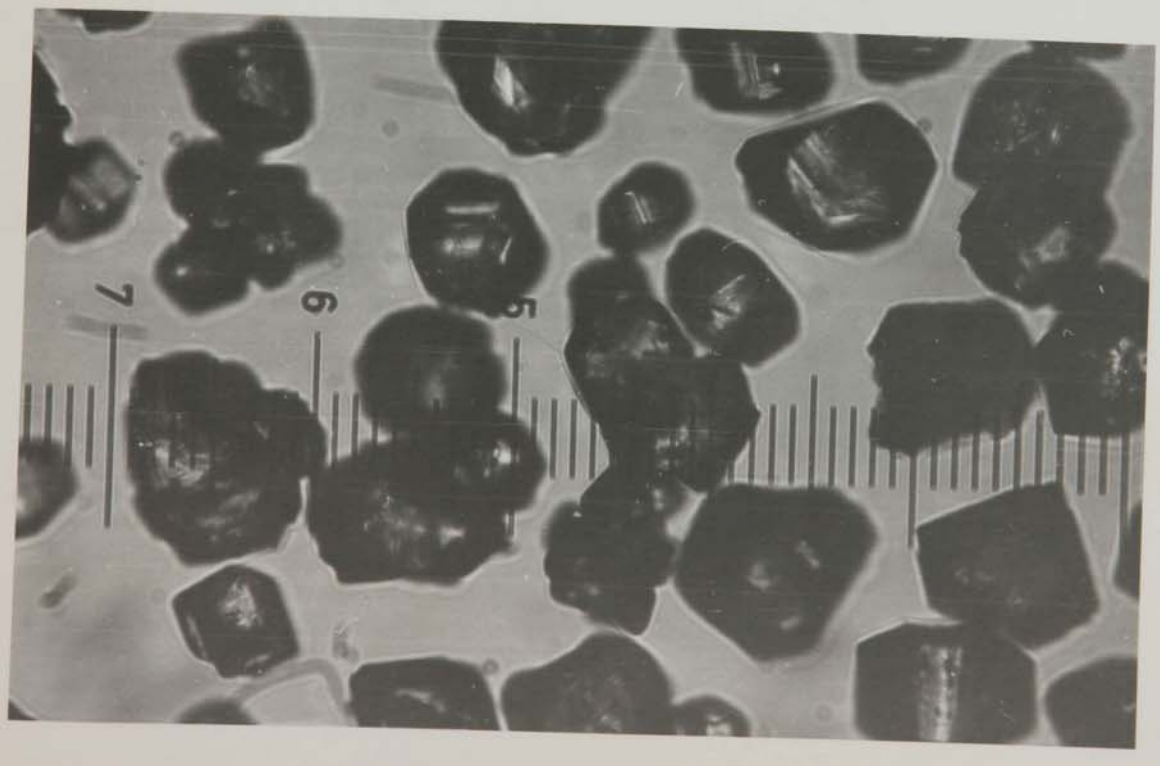
7
6
5

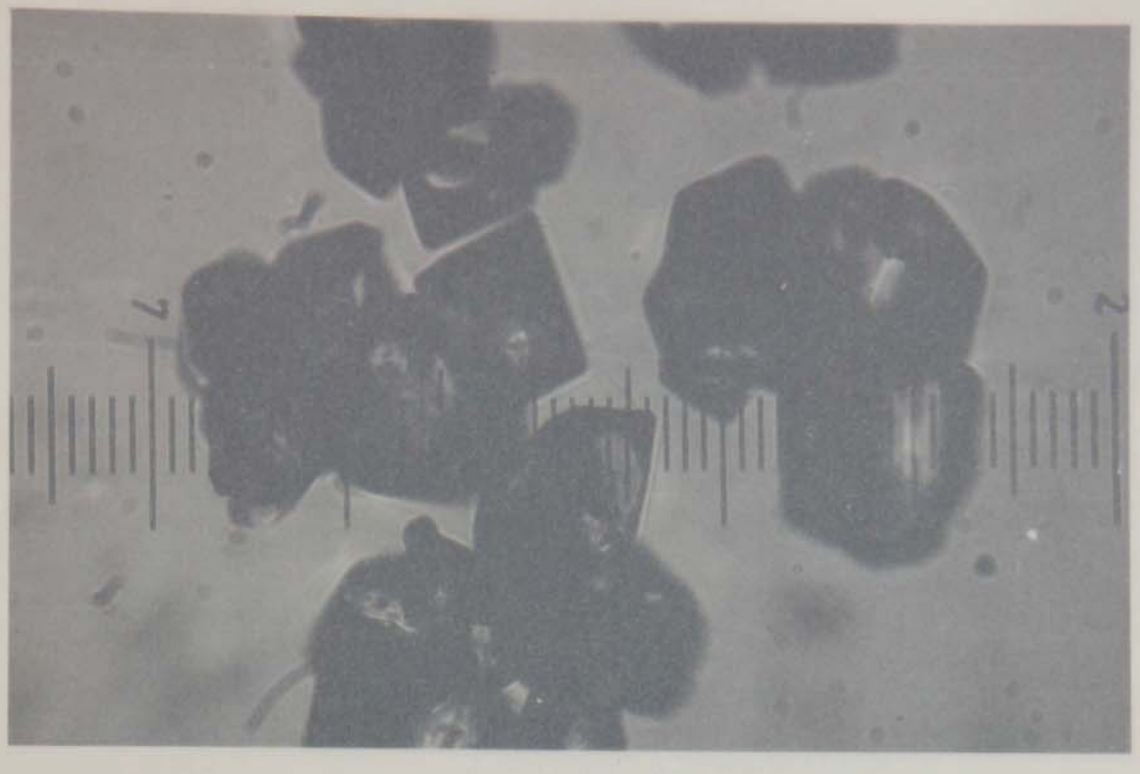

Figure 6.7 - Crystal Agglomerates in a Product from Series E (Duration 3385 s) (Scale: 1 Sub-Division of Superimposed Scale = 5.5 μm)

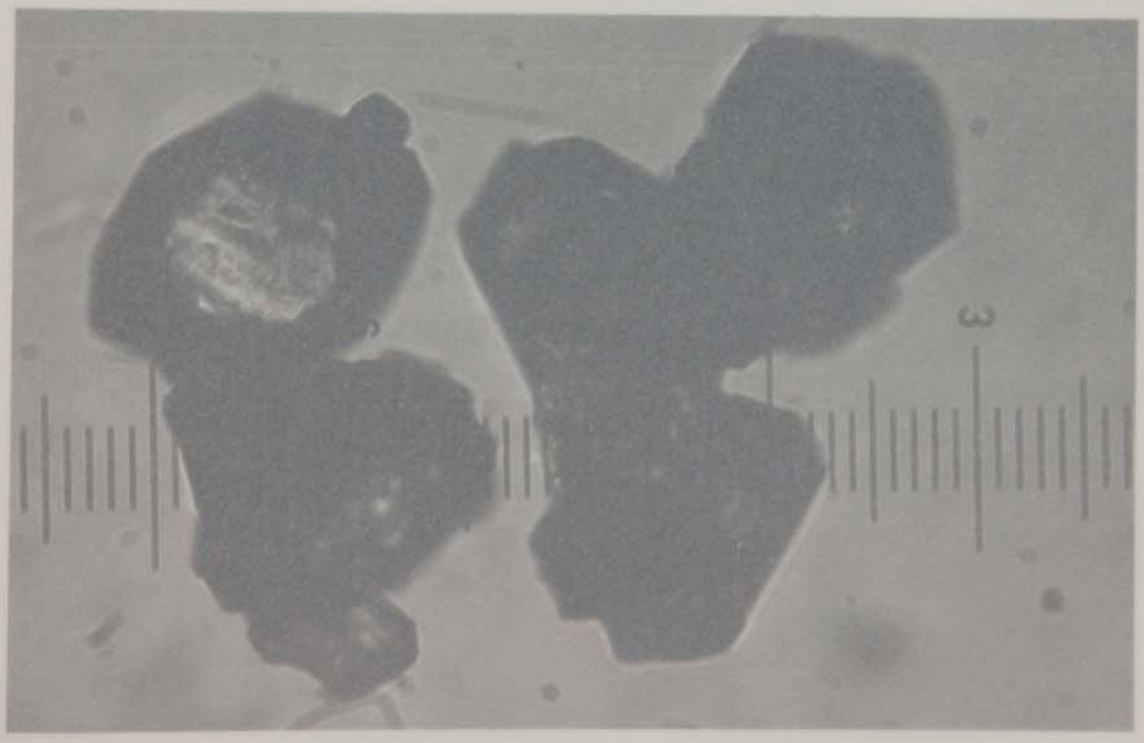

Figure 6.8 - Crystal Agglomerates in a Product from a Series F Experiment in which Product Recovery was Achieved by Methanol Washing and Hot Air Drying (Duration 12675 s) (Scale: 1 Sub-Division of Superimposed Scale = 5.5 μm)


7
2

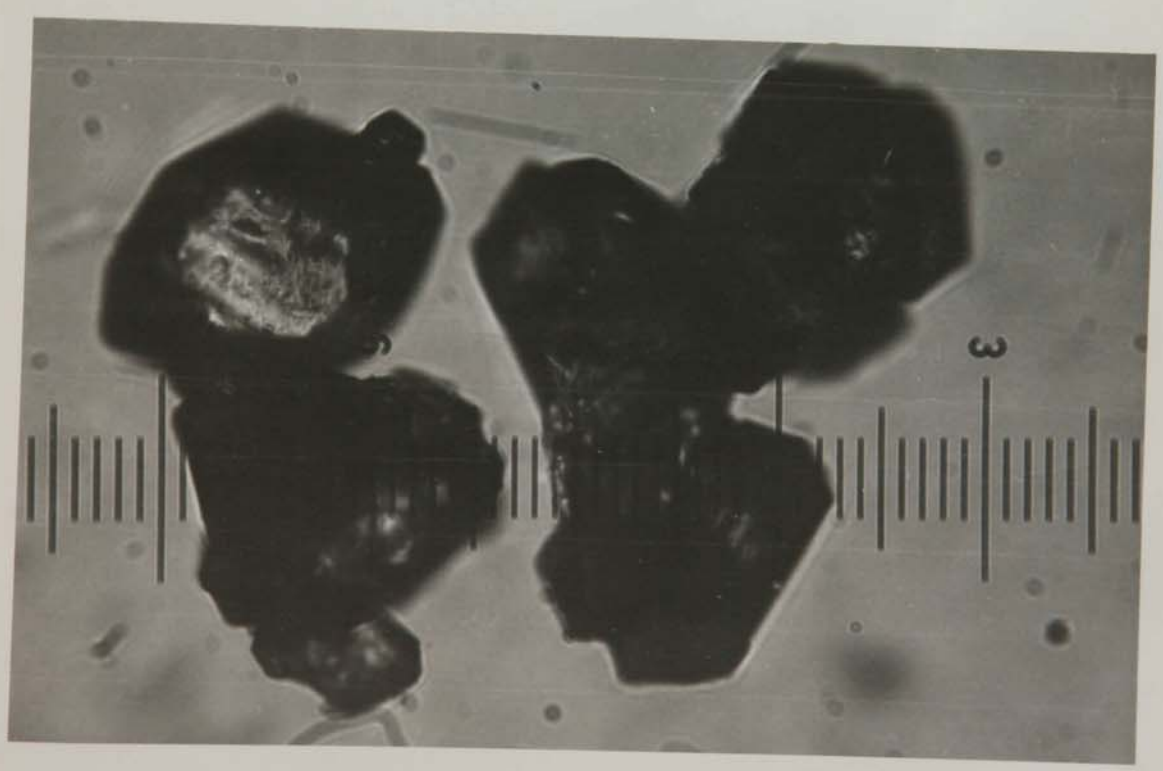
3

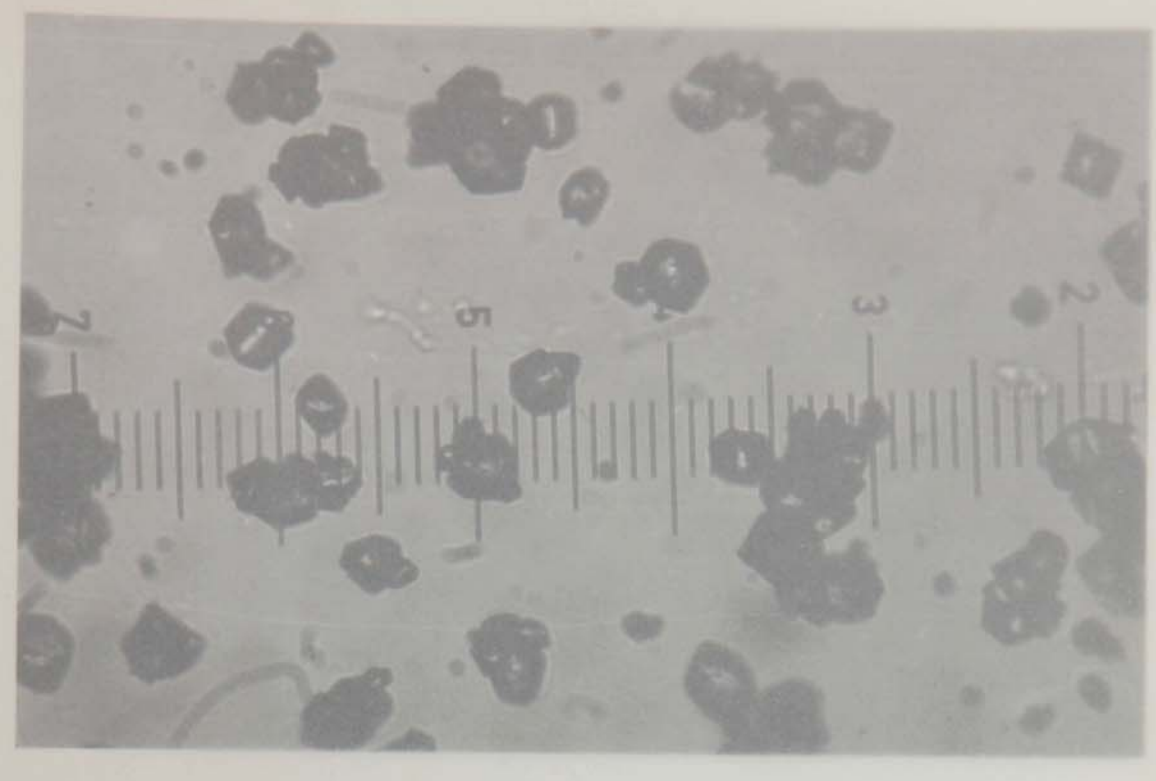

Figure 6.9 - Product from a Short Duration Series G Experiment (Duration 1380 s) (Scale: 1 Sub-Division of Superimposed Scale = 5.5 μm)

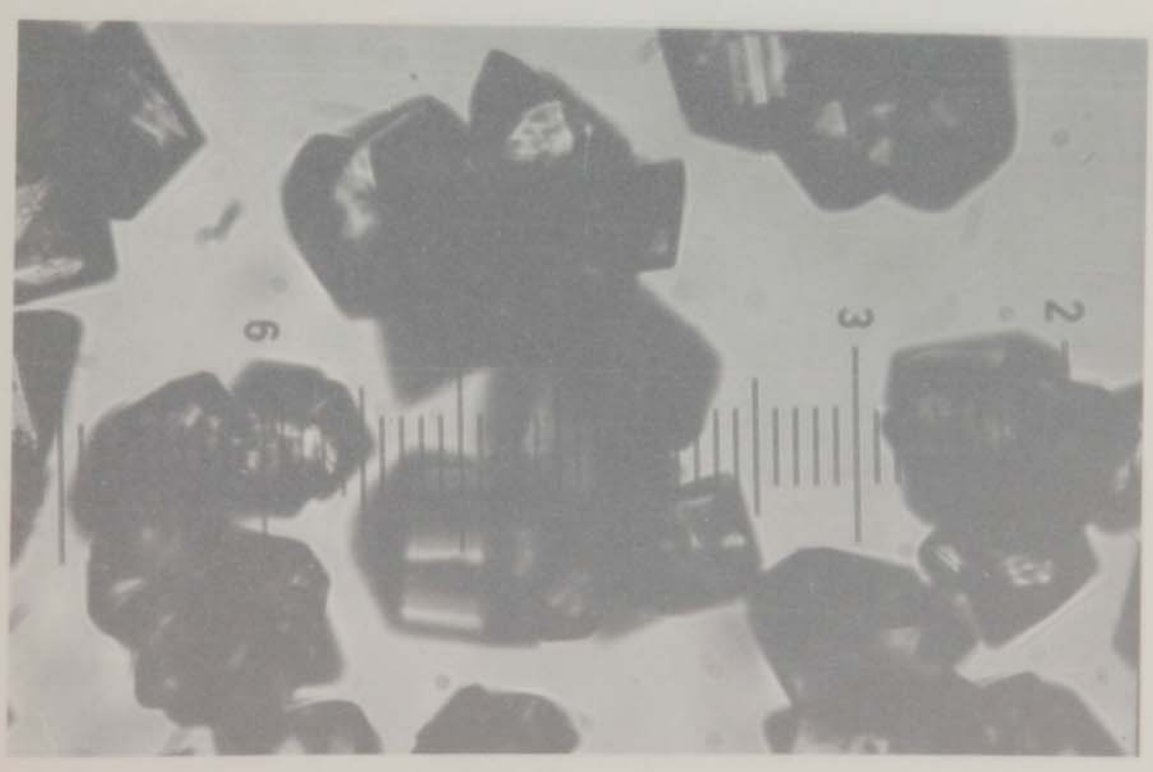

Figure 6.10 - Product from a Long Duration Series G Experiment (Duration 5245 s) (Scale: 1 Sub-Division of Superimposed Scale = 5.5 μm)

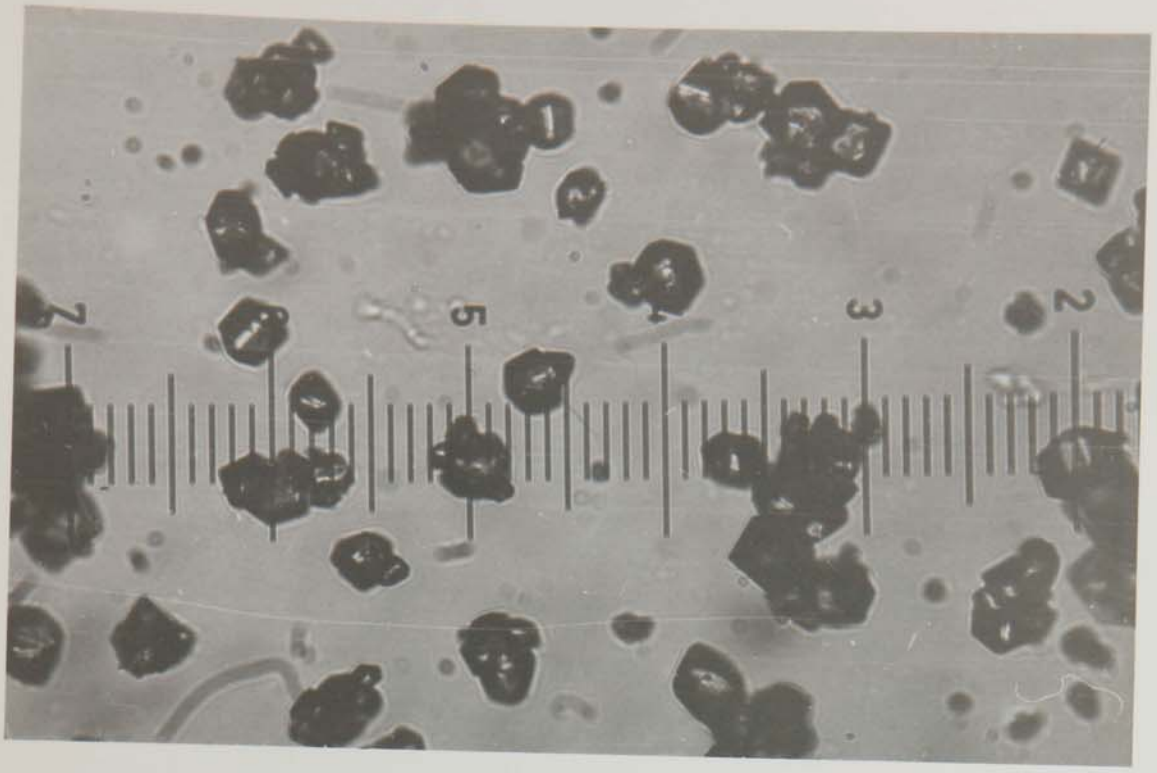
7
5
3
2

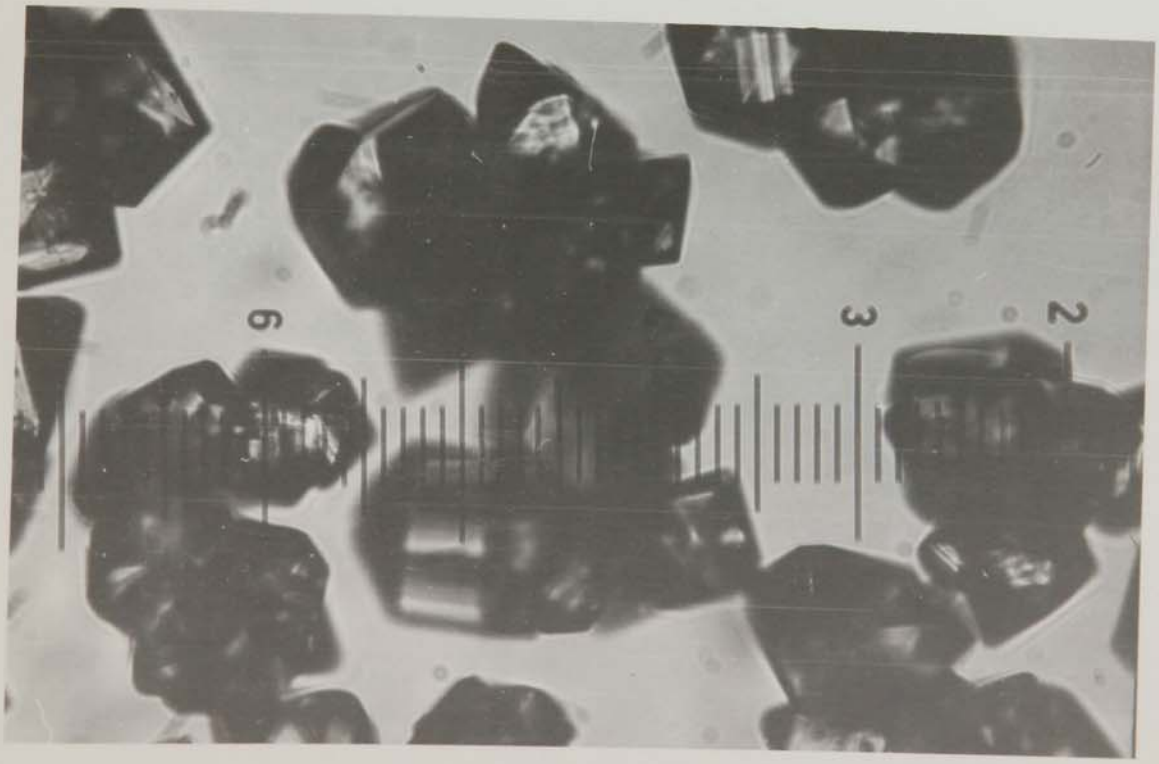
6
3
2

agglomerates in a product from series A is shown in figure 6.5. The product obtained under series D conditions using recrystallised barium chromate is depicted in figure 6.6, while figure 6.7 shows agglomerates in a product from a series E experiment, and figure 6.8 is a photograph of a product from series F, which was recovered by the alternative method of methanol washing and hot air drying. Finally, figures 6.9 and 6.10 show products from series G corresponding to short and long duration experiments, respectively. It can be seen that the shorter duration test product contains fewer agglomerates.

CHAPTER SEVEN

THE SOLUBILITY OF BARIUM CHROMATE

7.0 INTRODUCTION

The solubility of a substance refers to the quantity of the material (solute) which will dissolve in a specified amount of solvent at a specified temperature and pressure, to give a homogeneous mixture or ionic dispersion, which is in equilibrium with the solute. Theoretical calculation of solubility from other physical and chemical properties is often unreliable and experimental measurement is necessary to determine solubility accurately.

7.1 PREVIOUS WORK ON THE SOLUBILITY OF BARIUM CHROMATE

7.1.1 Solubility in Aqueous Systems

Skander (4) has reviewed the published data on the solubility of barium chromate in pure water and in the presence of various ionic and acidic additives. There is little agreement between the results of different studies. Skander's own results on solubility in pure water (4) show that solubility increases with temperature by about 3-4%/K, in agreement with calculations based on the heat of solution (171), but his results are higher by a factor of about 2 than most of those given in the literature. Table 7.1 summarises some of these results.

TABLE 7.1

Solubility of Barium Chromate in Water (4)

Solubility ($x10^6$) ($kmol/m^3$)	Temperature (^oC)	Reference
7.9	0	(179,180)
11.1	10	(179,180)
14.6;30.8	20	(179,180,181)
18.2;50.7	30	(4,179,180)
14.9;74.2	40	(4,182)
92.8	50	(4)
121.1	60	(4)
187.3	70	(4)
240.7	80	(4)
285.0	90	(4)

7.1.2 Solubility in Acidic Media

The solubility of barium chromate is strongly pH dependent (4,5,95,173). Data presented in the International Critical Tables (178) give the solubility of barium chromate in hydrochloric acid and in nitric acid at 291.1 K (18.1°C) and 310.1 K (37.1°C) over a range of pH values from -0.2 to 1.0. Osawa (183) investigated the solubility in acetic acid at 25°C over a pH range of 2.2 to 7. Skander (4) measured solubility in hydrochloric acid at 30, 40, 50, 70 and 90°C. The pH range covered was 0.35 to ∿5.5. Falangas (5) examined the solubility in a variety of media. Table 7.2 summarises the pH and temperature ranges covered. The complete solubility results of Skander and Falangas are tabulated in Appendix 8.

7.1.3 Effect of Complexing Agents

Falangas (5) studied the effect of five specific complexing agents on the solubility of barium chromate, in an attempt to increase barium chromate hold-up in solution. These were ethylenediamine tetra-acetic acid (E.D.T.A.), citric acid, nitrite triacetic acid (N.T.A.), sodium oxalate and tri-sodium ortho-phosphate. The effect of acetic and formic acid was also investigated. It was found that solubility was actually decreased due to the buffering action of the additives. The additives also tended to undergo irreversible reaction and were thought to adversely affect crystal morphology. Therefore their use was not considered

TABLE 7.2

Summary of Solubility Experiments of Falangas (5)

Solvent	pH Range	Temperatures (°C)
Nitric Acid	0.15-6.67	35;52;65
Nitric Acid (Residue Weight Method)	0.05-5.08	35;52;65
Hydrochloric Acid	0.38-6.42	35;52;62;100
Hydrochloric Acid (with 20 kg/m^3 Urea)	0.50-3.80	21;52;65;90

worthwhile.

7.1.4 Equilibria in Acidic Solution

Skander (4) surveyed the published work on the equilibria prevailing in acidic chromate solutions and concluded that the following principal equilibria exist.

$$K_{sp} = [Ba^{2+}][CrO_4^{2-}] \quad \ldots\ldots\ldots\ldots\ldots\ldots \quad (7.1)$$

$$K_1 = [HCrO_4^-][H^+] / [H_2CrO_4] \ldots\ldots\ldots\ldots \quad (7.2)$$

$$K_2 = [CrO_4^{2-}][H^+] / [HCrO_4^-] \ldots\ldots\ldots\ldots \quad (7.3)$$

$$K_3 = [Cr_2O_7^{2-}] / [HCrO_4^-]^2 \quad \ldots\ldots\ldots\ldots \quad (7.4)$$

$$K_4 = [HCr_2O_7^-][H^+] / [H_2Cr_2O_7] \ldots\ldots\ldots\ldots \quad (7.5)$$

$$K_5 = [Cr_2O_7^{2-}][H^+] / [HCr_2O_7^-] \quad \ldots\ldots\ldots\ldots \quad (7.6)$$

Furthermore, in hydrochloric acid the following equilibrium also occurs.

$$K_6 = [CrO_3Cl^-] / [H^+][Cl^-][HCrO_4^-] \ldots \quad (7.7)$$

The overall solubility corresponds to the sum of the concentrations of all the Cr(VI) ionic species in solution. The existence of the chlorochromate equilibrium (equation 7.7), thus indicates an increased solubility in hydrochloric acid. This increase was estimated to be about 20% by Skander (4).

Falangas (5) found that solubility increased further in the presence of urea. The reasons for this were probably twofold. Since urea-water solutions have higher dielectric constants than pure water (184), and because a high dielectric constant facilitates the separation of ions in solution (68, 185), solubility is increased. Moreover, the urea molecule is polar. Thus, its presence aids the solvation of solute ions in solution. The consequent reduction of solvation energy also improves solubility.

7.2 MEASUREMENT OF SOLUBILITY

The methods used for measurement of solubility have been reviewed by Zimmerman (186) and by Kertes et al (187). Two categories of methods exist based on whether or not sampling from the equilibrium system is involved. Those most commonly used with low solubility materials are either electrical methods (188,189), requiring no sampling, or spectrophotometric methods (190), which depend on analysis of samples. Skander (4) and Falangas (5) used sampling from an equilibrium system followed by analysis of the samples by ultraviolet spectrophotometry, in their studies of the solubility of barium chromate. In addition, Falangas (5) used the residue weight method for determining solubility in nitric acid. This method gave rather large errors and very poor reproducibility. Falangas also investigated the technique of atomic absorption spectrometry. The method would have

eliminated possible errors in experimental and theoretical accuracy due to the chromate equilibria but the results of calibration tests lacked linearity and reproducibility.

7.3 SOLUBILITY MEASUREMENTS USING THE BARIUM ION SELECTIVE ELECTRODE

Ion selective potentiometry is of relatively recent origin. The technique has been reviewed by Koryta (191) and by Moody and Thomas (192), and it could be applied to the 'in situ' measurement of solubility of sparingly soluble ionic solutes. In view of the discrepancies in the barium chromate solubility measurements of Skander (4) and Falangas (5), which were probably mainly due to errors associated with sampling, it was decided to use a Philips IS 561 barium ion selective electrode to check solubility 'in situ'.

The solubility apparatus used is shown diagrammatically in figure 7.1 and figure 7.2 shows a photograph of the rig. Barium chromate, hydrochloric acid and urea having specifications described in Chapter 4 were used in these experiments along with appropriate quantities of deionised water. The ion selective electrode whose specifications are listed in Appendix 9 was used in conjunction with a Philips RH 44/2-SD/1, double junction saturated potassium chloride/0.1M ammonium nitrate reference electrode and a Philips PW 9409 digital pH/millivolt meter. Calibration was carried out beforehand in solutions of Analar grade

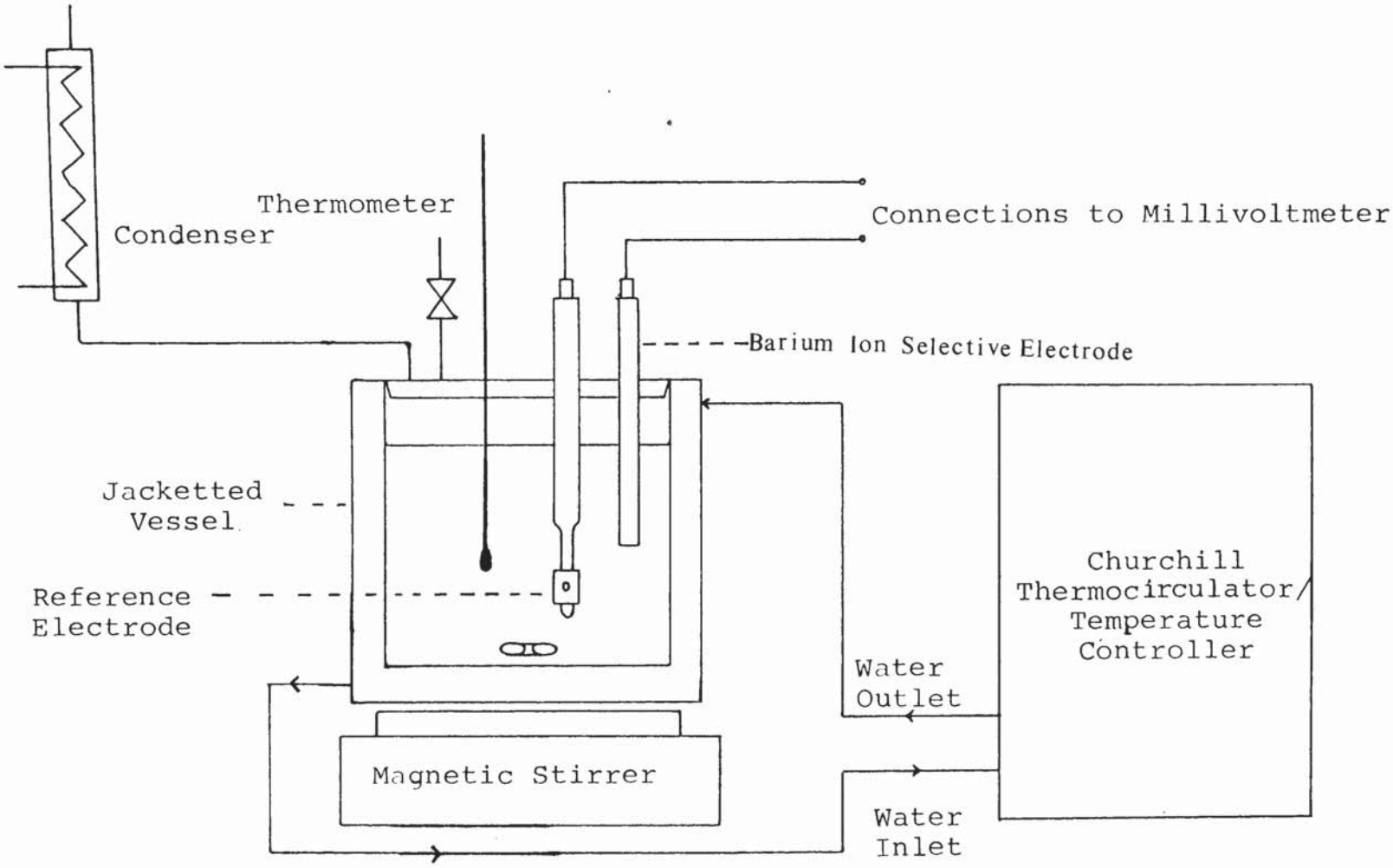

Figure 7.1 Diagrammatic Representation of Solubility Apparatus

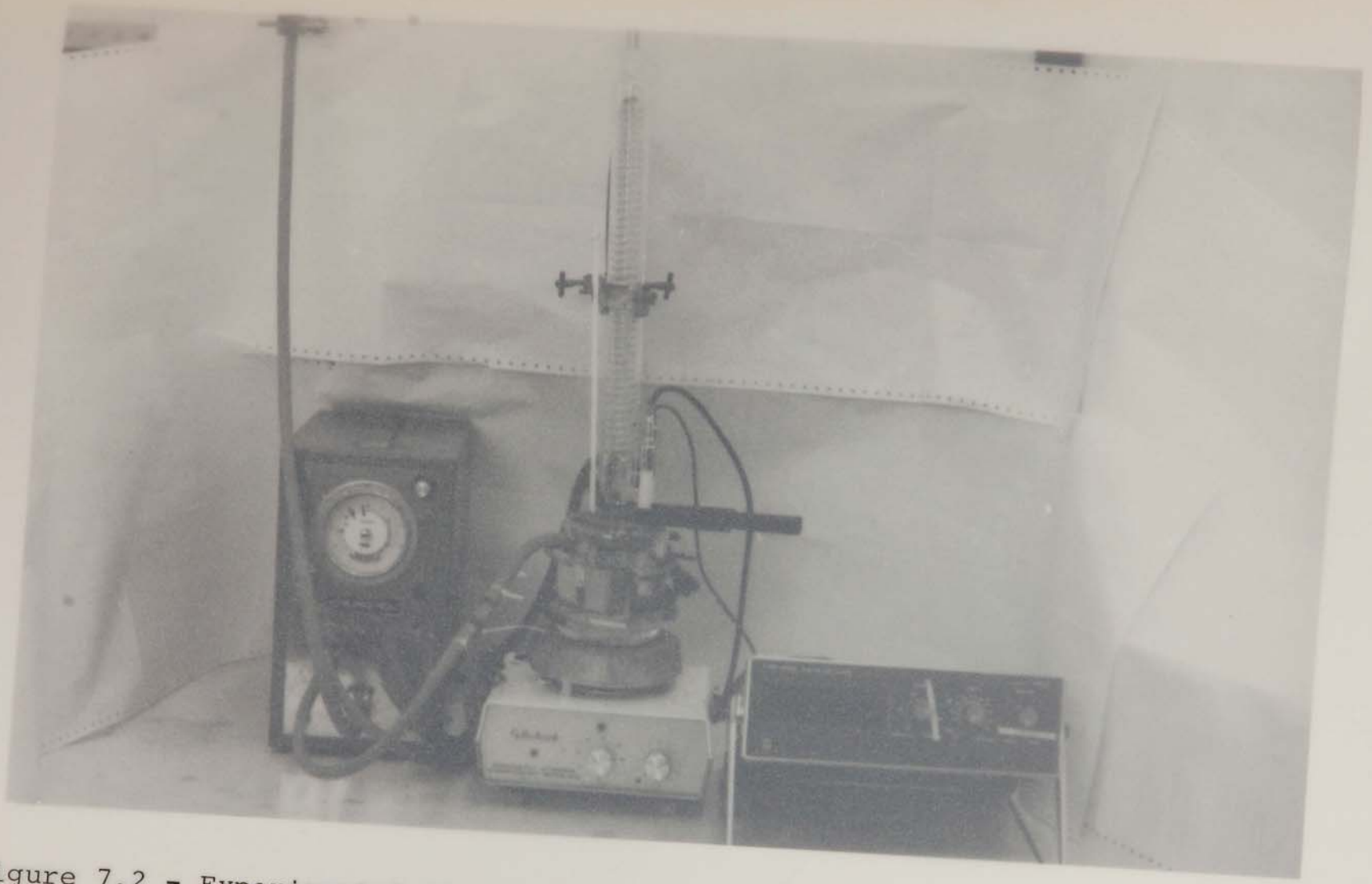

Figure 7.2 - Experimental Rig Used for Solubility Measurement

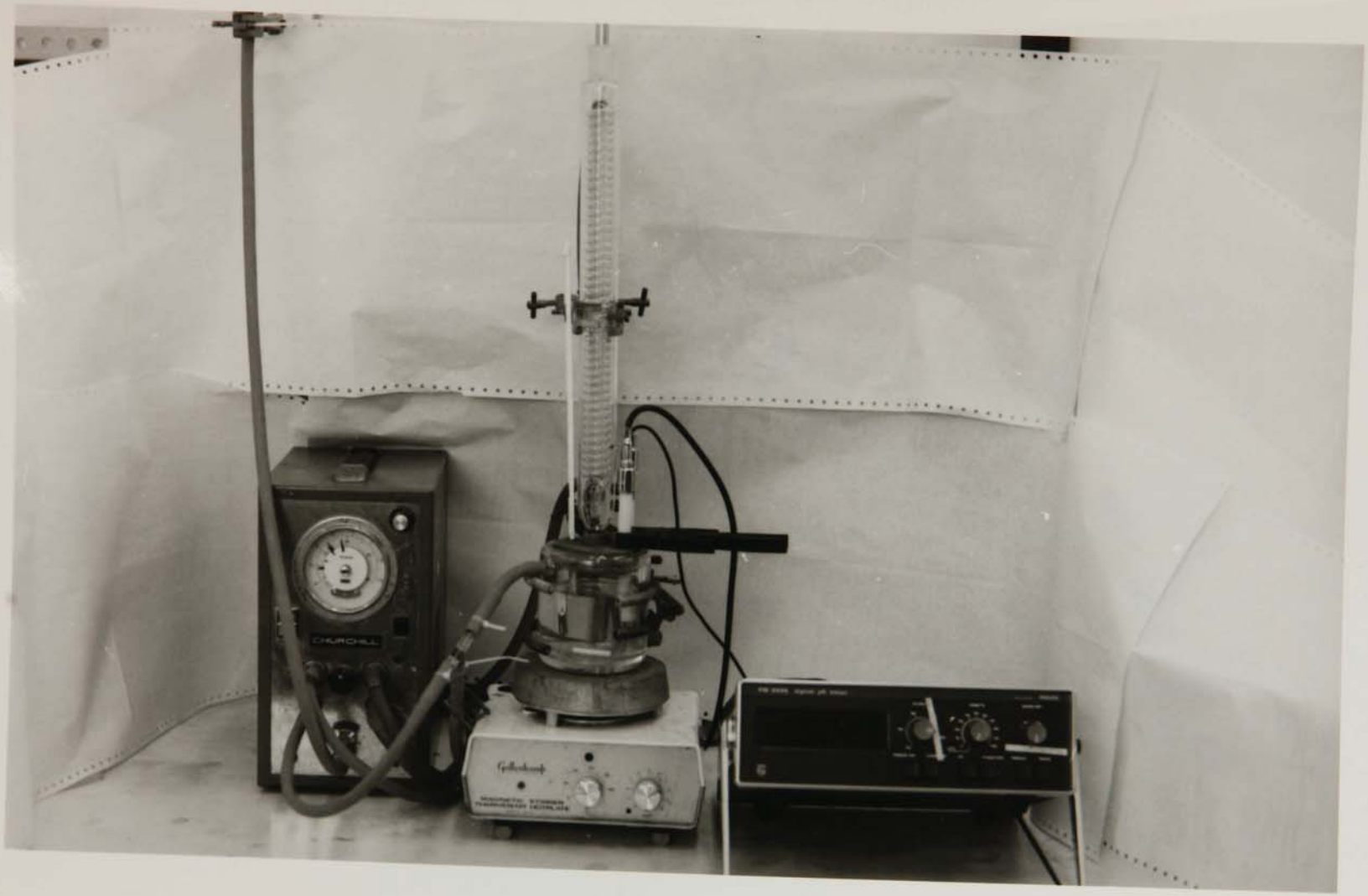

barium chloride, of known barium ion activity, at each experimental temperature. Measurements were made in hydrochloric acid at 20, 30 and 40°C over a range of pH values from 2.0 to 5.7. The effect of 20 kg/m^3 of urea in solution was also examined. The manufacturer's recommended procedure (193) was followed throughout, and an equilibration period of upto six hours was allowed before taking measurements.

There were considerable problems with the barium ion selective electrode. Although used within specified limits, the plastic membrane of the electrode proved to have an extremely short active life in the acidic test solutions. The calibration of the probe drifted markedly with time and showed signs of cycling in some cases. Replacement membranes behaved similarly. Discussions with the probe manufacturers' agents (194) confirmed the sensitivity of the probe to the external conditions, and hence, its unsuitability for use in the system under study. The results obtained by this method are listed in Appendix 10. They show no correlation and because of their wide scatter, comparison with previous solubility measurements was not practicable.

7.4 CORRELATIONS FOR SOLUBILITY

Skander (4) correlated his measurements of the solubility of barium chromate in hydrochloric acid solution by means of a relation based on the

equilibria involved.

$$\text{i.e. } C_e^3 - A_s C_e - B_s = 0 \quad \ldots\ldots\ldots\ldots \quad (7.8)$$

This relation applied to a fixed temperature, and A_s and B_s were complex functions of the seven equilibrium constants (equations 7.1 to 7.7). Skander's results suggested that solubility was proportional to hydrogen ion concentration or activity raised to a small positive power.

$$\text{i.e. } C_e \propto [C_{H^+} \text{ or } a_{H^+}]^{S_3} \quad \ldots\ldots\ldots\ldots \quad (7.9)$$

Furthermore thermodynamic considerations (68,185, 195) indicate that the solubility of a solute is related to temperature by the relation:

$$\left[\frac{\partial(\ln a_e)}{\partial T}\right]_P = -\frac{L_H}{\nu RT^2} \quad \ldots\ldots\ldots\ldots\ldots\ldots \quad (7.10)$$

where, a_e is the equilibrium solute activity; L_H is the relative partial molal heat content of the solute at absolute temperature, T; R is the universal gas constant; and ν is the number of ions in a molecular unit. Integration of equation 7.10, assuming L_H and ν to be constants, yields:

$$\ln a_e = \frac{L_H}{\nu RT} + \ln a_o^* \quad \ldots\ldots\ldots\ldots\ldots\ldots \quad (7.11)$$

where, a_o^* is a constant.

This in turn gives,

$$a_e = a_o^* \exp(L_H/\nu RT) \quad \ldots\ldots\ldots\ldots\ldots\ldots \quad (7.12)$$

It was therefore decided to correlate the solubility data of Skander and Falangas by means of non-linear regression analysis, to fit the semi-empirical equation:

$$C_e = S_1 \cdot \exp(S_2/T) \cdot [C_{H+} \text{ or } a_{H+}]^{S_3} \quad \ldots\ldots (7.13)$$

The optimisation was carried out using a modified version of the direct search algorithm of Nelder and Mead (196-199). The computer program used, has also been applied successfully to a similarly non-linear problem (200), and is listed in Appendix 4. Hydrogen ion concentrations were calculated from pH values using the Debye-Huckel equation (68) to calculate activity coefficients (γ).

$$\text{i.e. } \log_{10}(\gamma) = \frac{-A_o\sqrt{I_c}}{1 + B_o d_o \sqrt{I_c}} \quad \ldots\ldots\ldots\ldots (7.14)$$

$$I_c = \tfrac{1}{2} \sum_i C_i Z_i^2 \quad \ldots\ldots\ldots\ldots (7.15)$$

where, A_o and B_o are constants; I_c is the ionic strength; d_o is the effective ionic radius ($\mathring{A}$); and, C_i is the molar concentration and Z_i is the ionic charge, of the ith ionic species in solution.

The constants A_o and B_o are given by (175)

$$A_o = (2N_a \pi e_o^6)^{0.5} / 2.3026 (10 k_o \varepsilon T)^{1.5} \quad \ldots\ldots\ldots (7.16)$$

$$B_o = (8\pi N_a e_o^2)^{0.5} / (10^3 k_o \varepsilon T)^{0.5} \quad \ldots\ldots\ldots\ldots (7.17)$$

where, N_a is Avogadro's number; k_o is the Boltzmann constant; T is absolute temperature; e_o is the electronic

charge; and, ε is the dielectric constant of the solution.

A_o and B_o were calculated using appropriate values (68,184) for the dielectric constant. In order to avoid the complications of detailed consideration of the diverse chromate equilibria, it was further assumed that all the Cr(VI) ionic species in solution existed either as the univalent form (i.e. $HCrO_4^-$, CrO_3Cl^-) or the divalent form (i.e. CrO_4^{2-}). Since the differences in the derived parameter values for the two cases proved to be negligible, the former assumption was used throughout.

The results obtained are summarised in tables 7.3 and 7.4. The error estimates were based on linearisation of the model (201), in the region about the optimum derived from the Nelder Mead program. Appendix 5 shows the derived correlations in graphical form. The data points used are also shown for comparative purposes. The correlations based on hydrogen ion concentration showed slightly poorer agreement with the data than those based on the activity. As can be seen from the graphs in Appendix 5, the fit to Falangas's data (in all media) was poor due to the wide scatter in the data. In particular, correlation of Falangas's residue weight measurements in nitric acid gave an erroneous inverse relationship for change of solubility with temperature, and correlation of the measurements in hydrochloric acid gave a very small temperature dependence for

TABLE 7.3

Solubility Correlations for Concentration Based Model - $C_e = S_1 \exp(S_2/T)(C_{H^+})^{S_3}$

Description of Data				Optimum Values of Parameters			Percentage Standard Errors		
Source	Acidic Solvent	Number of Data Points	Method	S_1	S_2	S_3	in S_1	in S_2	in S_3
Skander	HCl	74	U.V.S.	362.70	-2487.8	0.7265	±22.75	±2.94	±2.54
Falangas	HCl	37	U.V.S.	0.5208	-354.14	0.8049	±67.36	±59.92	±7.93
Falangas	HCl/Urea	27	U.V.S.	19.41	-1477.2	0.7738	±75.02	±18.78	±6.68
Falangas	HNO_3	91	U.V.S.	2.684×10^7	-6389.6	0.63070	±201.0	±10.35	±6.05
Falangas	HNO_3	49	Residue Weight	0.01632	591.22	0.5819	±96.20	±54.04	±5.68

NOTE: (1) U.V.S. - Ultra Violet Spectrophotometry

(2) Percentage Standard Error = $\frac{\text{Standard Deviation of Parameter}}{\text{Optimum Value of Parameter}} \times 100$

TABLE 7.4

Solubility Correlations for Activity Based Model - $C_e = S_1 \exp(S_2/T)(a_{H^+})^{S_3}$

Description of Data				Optimum Values of Parameters			Percentage Standard Error		
Source	Acidic Solvent	Number of Data Points	Method	S_1	S_2	S_3	in S_1	in S_2	in S_3
Skander	HCl	74	U.V.S.	222.70	-2406.3	0.6975	±21.89	±2.97	±2.51
Falangas	HCl	37	U.V.S.	0.3411	-302.15	0.7709	±65.53	±69.24	±7.86
Falangas	HCl/Urea	27	U.V.S.	12.31	-1412.8	0.7406	±74.71	±19.40	±6.54
Falangas	HNO_3	91	U.V.S.	1.617×10^7	-6289.7	0.6034	±196.1	±10.28	±5.95
Falangas	HNO_3	49	Residue Weight	0.01289	607.34	0.5586	±95.45	±51.94	±5.60

NOTE: (1) U.V.S. - Ultra Violet Spectrophotometry

(2) Percentage Standard Error $= \frac{\text{Standard Deviation of Parameter}}{\text{Optimum Value of Parameter}} \times 100$

the solubility (i.e. <0.5%/K). A better fit was obtained with Skander's data. In all cases there was some evidence of interaction between the parameters S_1 and S_2 during optimisation.

CHAPTER EIGHT

PARTICLE SIZE MEASUREMENT

8.0 INTRODUCTION

Various techniques of particle size measurement exist, whose applicability depend on the size range of the sample to be analysed, the characteristic dimension to be measured, the quantity of sample available, and the desired complexity and cost. The basic physical principles of the diverse methods of particle size analysis have been examined by Hawksley (202,203,204), in a series of detailed reviews, Allen (205,206), and Heywood (207). The main features of the commonly used techniques of size analysis are summarised in table 8.1.

The techniques used in the crystal growth studies were sieve analysis of barium chromate batch crystallisation products and Coulter counter particle size measurement of the -44 μm fines sieve fractions of some of the crystallisation test products. Andreasen sedimentation and Coulter analysis were applied to analyse the metal powders tried out as substrates in epitaxial growth tests. An elutriation technique was also used in an attempt to obtain narrow size fractions of these metal powders. Optical microscopy was employed in a comparative study designed to obtain volume shape factors for mean sieve sizes, to use in converting sieve sizes to equivalent volume dimensions.

TABLE 8.1

Characteristics of Main Methods of Particle Size Measurement (205,206,208)

Technique	Normally Applicable Size Range (μm)	Measured Dimension	Amount of Sample Required	Ease and Cost of Use
Sieving	44 μm to 13 mm	second largest dimension	moderate to large	easy and cheap
Microscopy and Photomicrography	∿1 to 100	projected area diameter	very small	tedious and costly
Sedimentation	>1	Stokes diameter	small	can be slow, but is cheap
Elutriation	>1 to ∿200	Stokes diameter	small to moderate	fairly easy and cheap
Electrical Sensing Zone	1-100 (can be extended to ∿1000)	volume diameter	small	complicated; expensive instrument
Permeametry	>1	specific surface diameter	small	fairly easy and cheap
Light Scattering and Field Scanning	<1 to ∿1000	projected area diameter	small	complicated; very expensive equipment

8.1 SIEVE ANALYSIS

Sieve analysis is a simple, reproducible and inexpensive method of particle size analysis. With the use of strengthened woven wire sieves and special electroformed or micromesh sieves, the range of applicability of the technique can be extended to cover sizes from as small as 5.5 μm to as large as 125 mm (209). The British standard on test sieving (BS 1796 ; 1976) (210) prescribes the method to be followed when conducting a standard sieve analysis.

The guidelines in BS 1796 were followed when sieving the batch crystallisation test products and some of the larger metal powders used as substrates for epitaxial growth. In all analyses a nest of standard sieves conforming to BS 410 (211), and arranged so that the ratio of nominal aperture sizes on consecutive sieves was $2^{\frac{1}{4}}$, was used in conjunction with an Endecott mechanical sieve shaker. The nominal sieve apertures used ranged from 44 to a maximum of 251 μm. The +251 μm sieve fraction, if any, was further analysed using 50 mm diameter hand sieves which also conformed to BS 410, and extended the analysis upto a maximum nominal sieve aperture of 600 μm. The quantity of test sample retained on the 251 μm sieve, and subsequently hand sieved, never exceeded 2% by mass; being usually less than 0.5%. On the other hand, the -44 μm sieve fraction varied from 0.2% by mass, for the product from a test of long duration, to ∿84% for one of extremely short

duration, but was usually less than 10% by mass. The test sample masses also depended on test duration and ranged from 0.2 to 4.9 grammes. Losses during sieving were usually less than 0.5% by mass. Small test samples tended to give higher percentage losses. The largest material loss was ∿0.03 grammes. In an effort to have a reproducible end point, mechanical sieving was done for 45 min. in every case. Any subsequent hand sieving was quickly completed since very small amounts of material were involved. The individual sieve fractions were weighed to the nearest 0.1 mg and this was within the precision of ± 0.1% of sample mass, specified by BS 1796 (210).

8.2 COULTER COUNTER PARTICLE SIZE ANALYSIS (212,213,214)

8.2.1 Principles of Operation

The Coulter counter is an electrical sensing zone method of particle size measurement which determines the number and equivalent volume diameter of particles suspended in an electrolyte solution. Measurement is carried out by forcing the suspension to flow through a small aperture, arranged with an immersed electrode on either side. As each particle passes through the aperture, it causes the resistance between the electrodes to change. This in turn generates a short duration voltage pulse of magnitude proportional to the particle volume. The series of pulses thus produced is then electronically scaled and counted. Electronic arrangements are usually available on

commercial instruments of this type to set lower and/or upper thresholds for the pulses being counted. It is therefore possible to determine a particle size distribution by progressively changing these threshold levels. Allen (215) and Allen and Marshall (214) have carried out a critical study of the Coulter counter and describe important features of the technique such as possible electrochemical changes within the electrolyte, thermal effects, undercounting due to particle coincidence, background noise and response characteristics. The question of an appropriate sampling technique for use with the Coulter counter has been considered by Lines (216). A number of studies have also concentrated on improved methods of stirring for maintaining a uniform suspension during Coulter analysis (217,218). The particular problems of analysing fine metal powders by this method have been reviewed by Chaffin (219) and Ullrich (220).

8.2.2 Experimental Details

A Coulter counter model Z_B (Industrial) was the instrument used. Each -44 μm fines sieve fraction of barium chromate that constituted more than 10% by mass of the overall sample was analysed using the Coulter counter. It was found that Coulter analysis of barium chromate fines that corresponded to less than 10% (by mass) of the total sample did not significantly affect the mean and standard deviation of the overall cumulative particle size distribution. Some of the metal

powders used in the epitaxial growth tests were also analysed. The single threshold technique, giving cumulative percentage oversize distributions, was always applied.

8.2.3 Dispersion Technique

The dispersion technique used for the metal powders was to make up a paste with a known weight of sample and some of the electrolyte, transfer the paste and the rest of a measured volume of electrolyte to the sample beaker, and finally, to disperse the sample using an ultrasonic probe for 30-60 seconds. For barium chromate samples ultrasonic dispersion was omitted due to fear of breaking up the crystals.

8.2.4 Electrolyte Solution

The electrolyte used was developed in consultation with Coulter Electronics Ltd. (221), due to the dense particulate materials used. The optimum composition was found to be 4% (by mass) of sodium chloride (Hopkin and Williams, Analar grade) in 50/50 (vol./vol.) glycerol-distilled water solution, containing 0.5% (by volume) of a solution of the surfactant cetrimide. The surfactant solution consisted of 10% (by mass) of cetrimide in a 50/50 (vol./vol.) ethanol-distilled water solution. The glycerol served to increase the viscosity of the solution thereby facilitating suspension of the sample. Since glycerol also increased the resistivity of the electrolyte, the sodium chloride

concentration had to be increased above the usual 1% (by mass), in order to control the noise generated at high aperture current settings (212) due to thermal effects. It was also found that due to the metal particles in suspension being conducting, a considerable proportion of larger particles were being undersized at higher aperture currents (221). The additive cetrimide overcame this by being adsorbed on the surface of the metal, thereby rendering the particles non-conducting.

8.2.5 Suspension of Sample

The sample was kept in suspension by a small glass two-bladed mechanical stirrer. Suspension of the denser and larger particles was found to be favoured by the use of a round bottomed, 400 ml sample beaker fitted with a single glass baffle (222). It was also found desirable to reposition the aperture tube at right angles to the commonly prescribed position (212), in order that the orifice 'sees' a more representative portion of the solution (219,221,222). Inadequate suspension of the sample was considered to be a potentially greater source of error, due to the failure to count the larger particles, than the conductivity of the particles.

8.2.6 Calibration

Table 8.2 lists the size characteristics of the calibration standards employed with the Coulter counter. Since the recommended practice (212) was to calibrate a

TABLE 8.2

Characteristics of Coulter Counter Calibration Standards (223)

Calibration Material	Singlet Number Median Diameter (μm)	Number Mode (μm)	Weight Peak Split Size (μm)	Number Peak Split Size (μm)
Polyvinyl Toluene Latex	3.08	2.96	3.10	3.08
Barley Smut	4.83	4.90	5.11	5.00
Polystyrene Divinyl Benzene Latex	14.6	14.3	15.3	14.8
Paper Mulberry Pollen	15.6	15.4	15.8	15.6
Ragween Pollen	17.95	-	-	-
Polystyrene Divinyl Benzene Latex	19.5	19.2	20.3	19.8
Paper Bark Birch	27.0	26.5	27.5	27.1
Pecan Pollen	46.5	51.6	47.0	47.3

given orifice tube with a standard having a number median diameter that was between 5 and 20% of the orifice diameter, the following size ranges applied to the 50, 100 and 140 μm orifice tubes respectively: 2.5-10 μm, 5-20 μm, and 7-28 μm. Microscopic examination revealed that the solid calibration standards tended to swell in the electrolyte used. This resulted in calibration errors and a considerable difference in calibration between one standard and another, for the same orifice tube. The emulsion type standard latexes did not change size during calibration and gave much more reliable results. Calibration was carried out at regular intervals during a series of analyses, for each orifice tube and for every fresh batch of electrolyte solution. The calibration tended to change slightly with different batches of electrolyte but did not drift with time.

8.2.7 Errors and Reproducibility

The literature contains considerable references to different types of errors that may occur in Coulter analysis. The effects due to inadequate sample dispersion and poor sampling have been considered by Lloyd et al (224) and Lines (216). Other factors investigated have been coincidence correction (225, 226,227); extrapolation to obtain total sample volume (228,229,230); loss of resolution (231); and, statistical bias in counting (232).

It was standard practice in each analysis performed to carry out a mass balance on the mass of sample taken

against the total sample mass as calculated from the particle counts. When a glycerol free electrolyte was used mass losses as high as 50% were common when analysing metal powders. In some cases mass gains as high as 20% were observed. The main cause of mass loss was inadequate suspension of the sample and addition of glycerol to the electrolyte improved matters. Improper calibration and particle conductivity could also have contributed to the apparent losses (221). The mass gains were mainly caused by overcounting brought about by air bubbles in the suspension and electronic noise at low size settings. Once again calibration could have played some part. Mass balance errors of the same order of magnitude were observed by Coulter Electronics Ltd. (221) on analysing the same metal powders.

Use of the optimum electrolyte composition, adequate sample suspension and careful operating practice enabled the elimination of mass gains and restricted the mass loss to within 10%, although reproducibility of a given sample was within 2%. It is likely that this residual error is due to more fundamental reasons such as: the limit to calibration accuracy, which is $\pm$ 1% (221), and gives a $\pm$ 3% error in mass detected; measurable non-linearity in the response of the instrument at sizes above 20% of the aperture diameter (221), despite the general assumption of linearity in the measuring range of 2 to 40% of aperture diameter (212); and, at least in the case of

the metal powders, a considerable proportion of the sample lying below the lower limit for Coulter analysis, or more significantly, above the upper limit for a particular aperture, since the omission of even a few large particles would have had a marked effect on the mass balance.

8.3 ANDREASEN SEDIMENTATION METHOD

The Andreasen pipette sedimentometer is a homogeneous incremental sedimentation technique for particle size measurement. The method is described in detail by Allen (205) and by Heywood (207). The standard procedure for size analysis is given in BS 3406, Part 2 (233), and this was followed in using the technique for measuring the particle size of some of the metal powders.

Initially water was used as the sedimentation medium but this restricted the measurable range of the denser powders and also gave irreproducible results at larger sizes. A 50/50 (by mass) glycerol-distilled water mixture was found to extend the measuring range of the instrument and reproducibility was within $\pm$ 2% by mass. The experiments were conducted in a 50 litre thermostatted water bath capable of maintaining the temperature to $\pm$ 0.1^{o}C of the set point. The test temperature was 22^{o}C. A sample mass of 10 grammes was used in all cases and this corresponded to a volumetric solids concentration much below the limit of 0.1% specified for free settling (233).

The sources of error in the method are described

by Allen (205). These include: non-isokinetic sampling; disturbances caused by sampling; the region of sample withdrawal not being consistent with theory, inadequate initial sample dispersion, retention of solids in the pipette and the breakdown of laminar flow and/or free settling conditions. However, an investigation by Svarovsky and Allen (234) revealed that relatively large errors arise due to errors in the gravimetric determination of concentrations. The contribution of errors in particle size calculated from Stokes law using experimental measurements, was found to be small.

8.4 SIZE CLASSIFICATION BY ELUTRIATION

In order to overcome the problems of excessive bed expansion and particle elutriation in the fluidised bed crystallisers used for epitaxial growth experiments (Chapter 5), attempts were made to obtain narrow sized cuts from the metal powders, particularly tungsten. The method used was a water elutriation column of 40 mm diameter based on a fluidised bed type classifier developed by I.C.I. Ltd. (235), for somewhat larger particles. Difficulties arose because of the wide size distribution of the feed material coupled with its extremely fine size. Maintaining water flow rates at the desired low value of around 3×10^{-3} to 6×10^{-3} m^3/h (5 to 10 cm^3/min) for long periods of time proved difficult. Recovery of dry fractions was also a problem and material losses of 30% were common. The fractions collected were found to be no narrower than

that of the starting materials. The method was therefore abandoned.

8.5 VOLUME SHAPE FACTORS FOR SIEVE ANALYSIS

Since an appropriate dimension to use for characterising crystal populations from the point of view of crystal growth studies is the equivalent spherical volume diameter, it was necessary to determine shape factors to convert sieve sizes to equivalent volume diameters. This conversion was also required in order to combine a sieve analysis with the Coulter analysis of the sub-sieve sized fines.

8.5.1 Previous Comparative Studies

Many comparative studies have been reported. Chaffin (219) and Ullrich (220) compared the Coulter counter and micromesh or woven wire sieves when used to analyse fine metal powders. Their results indicated close agreement between the two techniques with sieve sizes being slightly larger, but no conversion factors were calculated. King and Burrus (236) found that in the range of overlap, micro sieves gave larger sizes than the Coulter counter. Grimes (237) found that generally consistent results were obtained with sieving and the Coulter counter for size analyses of lubricant grade molysulphide. Mistler et al (238) compared the use of different types of sieves (woven wire and precision etched round and square hole types) with the Coulter counter, for a variety of materials differing in shape

from angular alumina to spherical glass beads, and in density from 2500 to 6600 kg/m^3. Their results indicated that, in general equivalent volume (Coulter) diameters of the angular materials were much smaller than the corresponding sieve sizes, while those of the spherical materials closely matched their mean sieve sizes. Mullin and Ang (239) and Rosen and Hulburt (240) compared the results of sieving and Coulter analysis of crystalline samples of nickel ammonium sulphate hexahydrate and potassium sulphate respectively. Both these studies claimed that the average equivalent spherical volume diameter of particles in a sieve cut could be greater than the average sieve aperture. Specific conversion factors, based on the median sizes, on a size basis and on a mass basis, were calculated for each sieve fraction. These had values between 1.0 and 1.3. These results are in direct contradiction to most other comparative studies (219,220,236,237,238). In particular, subsequent work by Shah (241) on nickel ammonium sulphate hexahydrate yielded average mass mean Coulter sizes smaller than the corresponding mean sieve sizes. The crystals analysed by Mullin and Ang and by Rosen and Hulburt probably had comparatively large aspect ratios (240), and thus tended to have somewhat larger equivalent volume diameters than less elongated materials. However, Shah (244) has suggested that the discrepancy could be due to differences in the regularity of shape and the state of agglomeration of the crystals.

8.5.2 Experimental Work

The British standard on test sieving (210) and Garside et al (242) have stressed the desirability of using shape factors specifically determined for the test material. It was decided to employ the simple microscopic method described by Harris (243) to establish volume shape factors for different sieve fractions of barium chromate produced by batch crystallisation.

The method made use of a rectangular piece of double sided sticky tape mounted on a glass slide. The slide was then stuck onto the bottom of a sieve with the sides of the piece of tape parallel to the wire mesh. A sample of material retained by the next lowest sieve was then dusted over the region of the sticky tape. This generally resulted in one particle per aperture being retained by the adhesive film on the sticky tape. After careful removal of the slide, the number of particles, n_p was counted under a microscope. Since the particles were arranged in a regular grid counting was comparatively easy. The mass of the particles, m_p was determined by weighing the slide before and after dusting on the sample. Then, knowing the density of the material, ρ and the average sieve size, d it was possible to calculate the shape factor, f from,

$$\frac{m_p}{n_p \rho} = f\, d^3 \qquad \ldots\ldots\ldots\ldots\ldots\ldots\ldots\ldots \quad (8.1)$$

It can also be shown that the ratio (R_D) of mean equivalent volume diameter to mean sieve size is given by:

$$R_D = \left(\frac{6f}{\pi}\right)^{1/3} \quad \ldots\ldots\ldots\ldots\ldots\ldots\ldots \quad (8.2)$$

8.5.3 Results

Table 8.3 gives a summary of the particle counts done for each sieve fraction and the shape factors derived. Graph 8.1 shows the values of the ratio R_D at different mean sieve sizes. For the range of sieve sizes considered the results are adequately represented by a single value of R_D.

$$\text{i.e. } R_D = 0.8749 \pm 0.0403 \quad \ldots\ldots\ldots\ldots\ldots \quad (8.3)$$

The calculations in Appendix 7 indicate that this value lies within the range expected from consideration of an ideal crystal. Moreover, Falangas (5) has reported the value of the ratio between volume diameter and Stokes diameter for barium chromate crystals, and if a value of 0.94 (210) is assumed for the Stokes diameter/sieve diameter ratio, Falangas's results yield a value of 0.871 ± 0.041 for R_D, which is in excellent agreement with equation 8.3.

The experimental value (equation 8.3) was used to convert sieve sizes to equivalent volume diameters and to combine sieve and Coulter counter size analyses.

TABLE 8.3

Summary of Particle Counting Experiments for Estimating Shape Factors

Sieve Fraction (μm)	Mean Sieve Size (μm)	Number of Counts (-)	Ratio of Equivalent Volume Diameter to Mean Sieve Size (R_D) (-)	Volume Shape Factor (f) (-)	Mean Equivalent Volume Diameter (μm)
+ 44/-53	48.5	20	0.9052 ± 0.0467	0.3912 ± 0.0585	43.90
+ 53/-63	58.0	20	0.8504 ± 0.0319	0.3233 ± 0.0365	49.32
+ 63/-75	69.0	20	0.8926 ± 0.0290	0.3735 ± 0.0369	61.59
+ 75/-90	82.5	20	0.8560 ± 0.0313	0.3296 ± 0.0352	70.62
+ 90/-105	97.5	20	0.8849 ± 0.0370	0.3647 ± 0.0470	86.28
+105/-125	115.0	20	0.8765 ± 0.0345	0.3541 ± 0.0419	100.80
+125/-150	137.5	20	0.8651 ± 0.0435	0.3414 ± 0.0524	118.95
+150/-180	165.0	20	0.8653 ± 0.0337	0.3407 ± 0.0403	142.77
+180/-210	195.0	5	0.8737 ± 0.0334	0.3505 ± 0.0404	170.38
+210/-251	230.5	5	0.8670 ± 0.0648	0.3459 ± 0.0820	199.84
+251/-295	273.0	4	0.9048 ± 0.0403	0.3895 ± 0.0527	247.00

GRAPH 8.1 Graph of Ratio of Volume Diameter to Mean Sieve Diameter Against Mean Sieve Diameter

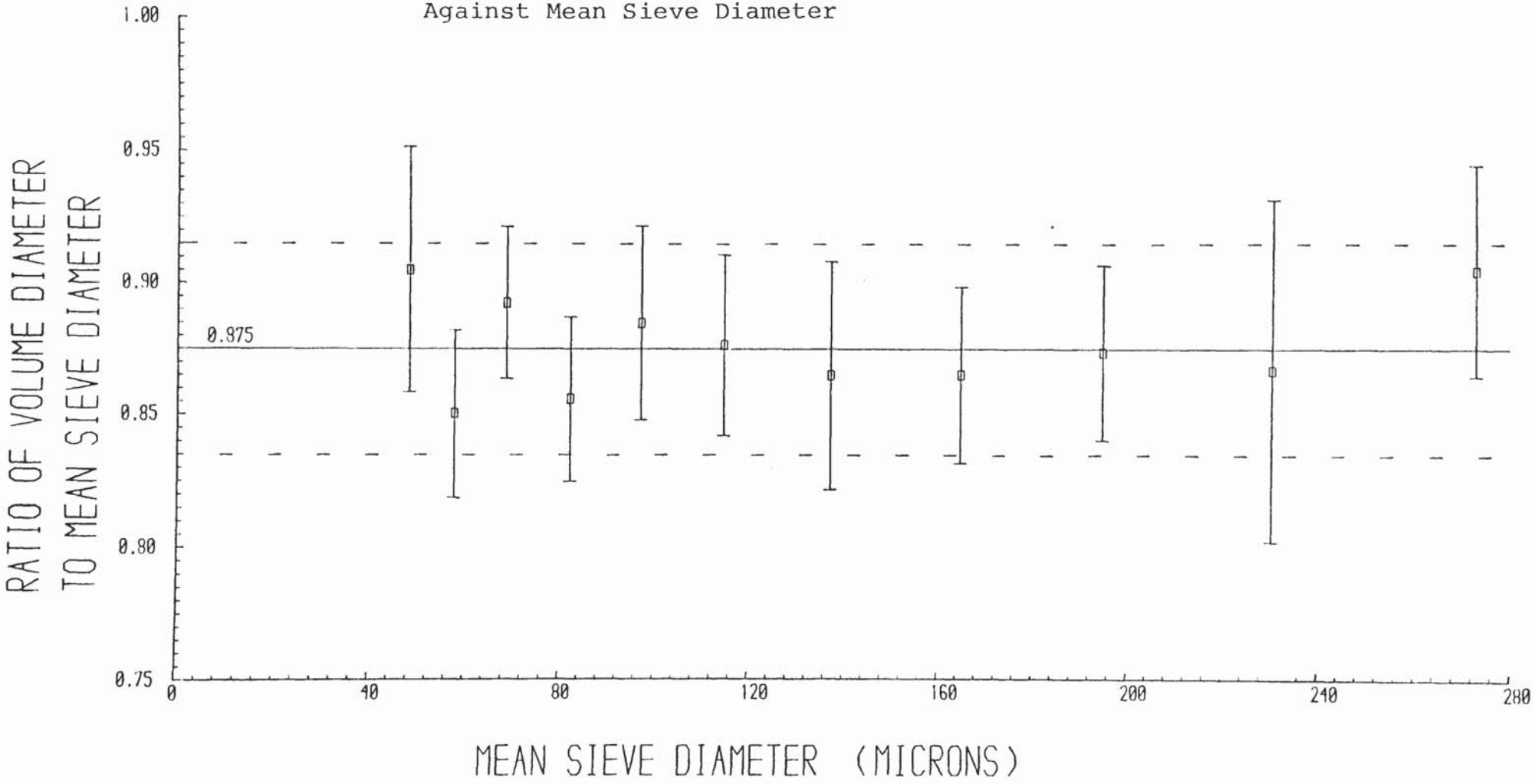

CHAPTER NINE

MODELLING BATCH CRYSTALLISATION OF BARIUM CHROMATE

9.0 INTRODUCTION

Laboratory scale batch crystallisation is in principle a simple method of determining crystal growth rates over wide ranges of supersaturation. However, the analysis of such experimental data is often a complex problem. The advent of population balance theory, originally developed for the analytical description of continuous crystallisers (244), has been a key factor in the successful modelling of batch crystallisation processes as well. Solution of the population balance, together with mass balance and moment equations enables the evaluation of crystal size distributions as functions of time and size for various operational modes (53-55, 244-247). The general population balance equation takes the form (246):

$$\frac{\partial n}{\partial t} + \frac{\partial (Gn)}{\partial L} = B - D \quad \ldots\ldots\ldots\ldots\ldots \quad (9.1)$$

where, G is the linear growth rate; B is the crystal birth rate; D is the crystal loss rate; L is the crystal size; and n is the population density function.

9.1 EMPIRICAL EXPRESSIONS FOR NUCLEATION RATE AND GROWTH RATE

9.1.1 Nucleation Rate

The numerical nucleation rate, B_N is conventionally expressed as an empirical power law type function of supersaturation driving force, S.

$$\text{i.e.} \quad B_N = \left[\frac{dN}{dt}\right]_{L=O} = k_N S^b \quad \ldots\ldots\ldots\ldots\ldots\ldots \quad (9.2)$$

In this expression k_N and b are constants. The nucleation rate constant k_N is dependent on operating conditions and, where relevant, may be expanded to include power law terms for stirrer speed, crystal suspension density and specific energy input (53).

9.1.2 Growth Rate

The overall linear growth rate is commonly expressed as:

$$G = \frac{dL}{dt} = k_L S^g \quad \ldots\ldots\ldots\ldots\ldots\ldots\ldots\ldots \quad (9.3)$$

where, k_L and g are constants. The growth rate constant, k_L depends on factors such as crystal size, temperature, impurities and system hydrodynamics (53).

For systems in which the growth rate is size dependent, two different types of growth models can be used (53,54,248); namely, a Bransom power law type relation (249),

$$\text{i.e.} \quad G = k_L L^{\alpha} S^g \quad \ldots\ldots\ldots\ldots\ldots\ldots\ldots\ldots \quad (9.4)$$

or, a simple linear size dependent model (56,248) similar to that developed for continuous crystallisers by Abegg et al (58).

$$\text{i.e.} \quad G = k_L(1 + \beta L)S^g \quad \ldots\ldots\ldots\ldots\ldots\ldots \quad (9.5)$$

9.2 MEAN LINEAR GROWTH RATE

The linear growth rate, G can be related to the growth rate per unit surface area, R_G. For a crystal population consisting of monosized particles, each of mass, m and size, L:

$$m = f_v L^3 \rho \quad \ldots\ldots\ldots\ldots\ldots\ldots \quad (9.6)$$

where, f_v is the volume shape factor and ρ is the crystal density.

Differentiation of equation 9.6 gives,

$$\frac{dm}{dt} = f_v \rho (3L^2) \frac{dL}{dt} \quad \ldots\ldots\ldots\ldots\ldots\ldots \quad (9.7)$$

If the surface shape factor for the crystals is f_s, the crystal surface area, A is given by,

$$A = f_s L^2 \quad \ldots\ldots\ldots\ldots\ldots\ldots \quad (9.8)$$

Also, by definition (245),

$$R_G = \frac{1}{A} \frac{dm}{dt} \quad \ldots\ldots\ldots\ldots\ldots\ldots \quad (9.9)$$

Combining equations, 9.7, 9.8 and 9.9 gives,

$$R_G = \left[\frac{3 f_v \rho}{f_s} \right] \cdot \frac{dL}{dt} = \left[\frac{3 f_v \rho}{f_s} \right] G \quad \ldots\ldots\ldots \quad (9.10)$$

Furthermore, for a polydisperse crystal population a mean linear growth rate, $\bar{G}$ can be defined, as proposed by van Oosterhout and van Rosmalen (250) and applied by van Rosmalen et al (251).

$$\text{i.e.} \quad \bar{G} = \frac{1}{A} \cdot \frac{dv_t}{dt} = \sum_j \left[G_j \left(\frac{A_j}{A} \right) \right] \quad \ldots\ldots \quad (9.11)$$

where, G_j is the growth rate of each individual crystal face, j; A_j is the total surface area of all crystal faces of type, j; A is the overall crystal surface area; and v_t is the overall volume of the crystal population at time, t.

The mean linear growth rate, $\bar{G}$ is simply related to the growth rate per unit surface area, R_G

$$\text{i.e.} \quad R_G = \frac{1}{A} \cdot \frac{dm_t}{dt} = \frac{\rho}{A} \frac{dv_t}{dt} = \rho \bar{G} \quad \ldots\ldots \quad (9.12)$$

9.3 MODEL FOR LIMITED NUCLEATION FOLLOWED BY GROWTH

This model is applied to the case when nucleation is restricted to an initial 'burst' at the start of batch crystallisation. It has been used to analyse the experimental data for the batch crystallisation of barium chromate.

9.3.1 Assumptions

1. Nucleation only occurs during a short period at the commencement of batch crystallisation, and takes place at effectively zero size.
2. Growth rate is independent of size but can be expressed as a function of driving force

and process conditions.

3. Agglomeration and attrition are disregarded.

4. Volume shape factor (f_v), surface area shape factor (f_s), crystal density (ρ), and system volume (V) are constants.

9.3.2 Model

A solute mass balance for the batch crystalliser gives:

$$C_t = (m_o - m_t)/(MV) \quad \ldots\ldots\ldots\ldots\ldots\ldots \quad (9.13)$$

where, C_t is the solute concentration at time t; m_o is the initial mass of solute taken; m_t is the crystal mass at time t; M is the molecular weight of the solute; and V is the system volume.

Furthermore, an instantaneous solute balance at time t yields:

$$R_G A + R_N = - VM\frac{dC_t}{dt} \quad \ldots\ldots\ldots\ldots\ldots\ldots \quad (9.14)$$

where, R_N is the mass nucleation rate; R_G is the crystal growth rate per unit surface area; and, A is the crystal surface area at time, t.

When nucleation is restricted to an initial 'burst' of short duration (245), the mass nucleation rate after this initial period will be negligible. Moreover, if it is considered that nucleation takes place at effectively zero size (53,252,253), this assumption is reinforced since mass nucleation rate

would then be negligible.

Thus, $R_G = -\frac{VM}{A}\frac{dC_t}{dt}$ ..... (9.15)

and from equation 9.13,

$$R_G = \frac{1}{A}\frac{dm_t}{dt} \quad \text{..... (9.16)}$$

A Bransom power law type (249) empirical relation is used to represent growth rate per unit surface area, R_G (8,9,53,54,56,248,249).

i.e. $R_G = k_G S^g$ ..... (9.17)

The growth rate constant k_G is dependent on process conditions and may, for example, be expressed as a power law function of hydrogen ion activity, a_{H^+}, stirrer speed, w, and crystal size, L. Furthermore, temperature dependence of growth rate can be accommodated by including an Arrhenius type activation energy term in k_G (9). Thus,

$$k_G = k_1 (a_{H^+})^{k_2} (L)^{k_3} (w)^{k_5} \exp(-E/RT) \quad \text{..... (9.18)}$$

Hence,

$$R_G = k_1 (a_{H^+})^{k_2} (L)^{k_3} (S)^{k_4} (w)^{k_5} \exp(-E/RT) \quad \text{. (9.19)}$$

where, k_1, k_2, k_3, k_4 and k_5 are constants; E is the activation energy for growth; and, R is the universal gas constant.

For size independent growth, equation 9.19 reduces to,

$$R_G = k_1(a_{H^+})^{k_2}(S)^{k_4}(w)^{k_5}\exp(-E/RT) \quad \ldots\ldots \quad (9.20)$$

and, in addition, for isothermal operation at a fixed stirrer speed,

$$R_G = k_1(a_{H^+})^{k_2}(S)^{k_4} \quad \ldots\ldots\ldots\ldots\ldots\ldots \quad (9.21)$$

Furthermore, as explained previously in section 9.2, R_G can be related to the mean linear growth rate, $\bar{G}$.

9.4 MODEL FOR CONCURRENT NUCLEATION AND GROWTH

A model was also derived for the case involving concurrent continuous nucleation and growth during batch crystallisation. This model was based on that originally presented by Bransom and Dunning (252), and was applicable when both nucleation and growth were independent of crystal size. Details of the model are presented in Appendix 12. Since it was considered that nucleation in the barium chromate batch crystallisation experiments was restricted to an initial 'burst' only, this model was not applied to the analysis of these experimental results.

9.5 AGGLOMERATION IN BATCH CRYSTALLISATION

9.5.1 General Considerations

The principles involved in agglomerate formation were first elucidated by von Smoluchowski (3,254,255) who described two different types of agglomeration; namely perikinetic agglomeration, in which particle movement is caused by Brownian motion, and orthokinetic

agglomeration, which occurs in agitated systems.

Microscopic observation of crystal products from the barium chromate batch crystallisation experiments described in Chapter 6, revealed the existence of considerable numbers of agglomerates. A simple agglomeration model for batch crystallisation was therefore formulated and is presented below. It must be noted, however, that this model is capable of further extension and its verification ideally requires data from a series of experiments designed specifically for that purpose.

9.5.2 Assumptions for Agglomeration Model

The following assumptions are made in deriving the agglomeration model.

1. The growth rate is independent of crystal size.
2. Crystal nucleation occurs at effectively zero size.
3. Of all the other processes that may account for crystal birth and loss, only agglomeration is considered. Processes such as attrition and classification are disregarded.
4. The size of agglomerating crystals is characterised by a characteristic length, L which is conserved during agglomeration. This approach has been used in a number of investigations (241,253,256). The alternative assumption that mass is conserved during agglomeration has also been adopted in

some studies (247,257,258). However, this approach leads to a complex equation which cannot be easily solved (241,247).

5. The agglomeration rate constant is independent of agglomerate size. Most studies of agglomeration during crystallisation have made this assumption (3,241,253). However, for orthokinetic agglomeration, the rate constant has been found to be approximately proportional to agglomerate volume (257). Stirrer speed (257), temperature (258) and supersaturation (259) have also been found to affect the rate constant. Moreover, more complex functional forms for the rate constant can, if necessary, be borrowed from mathematical studies of coagulating aerosols (260).

6. Agglomeration is considered to occur solely as a result of two-particle collisions.

9.5.3 Agglomeration Model

The model developed here for agglomeration during batch crystallisation is an extension of the model developed by Liao and Hulburt (253) for a continuous, MSMPR type crystalliser, and applied to the continuous crystallisation of nickel ammonium sulphate by Shah (241).

The general population balance represented by equation 9.1 is taken as the basis for the model. Application of assumptions 1, 2 and 3 (listed in

section 9.5.2) to the population balance, yields:

$$G \frac{\partial n}{\partial L} + \frac{\partial n}{\partial t} = B - D \quad \ldots\ldots\ldots\ldots\ldots\ldots \quad (9.22)$$

If collisions between particles of size ℓ and $L-\ell$ are considered, on the basis of the assumptions made, the birth rate of particles of size L is (253):

$$B = (0.5\lambda) \int_0^L n(L-\ell)_t n(\ell)_t d\ell \quad \ldots\ldots\ldots\ldots \quad (9.23)$$

where, $n(L-\ell)_t$ and $n(\ell)_t$ are the population density functions at time, t; λ is the collision frequency factor; and the multiplication factor of 0.5 compensates for repetitive counting in the integration.

The loss of particles of size **L** due to the agglomeration is given by (253),

$$D = \lambda n(L)_t \int_0^\infty n(\ell)_t d\ell \quad \ldots\ldots\ldots\ldots\ldots\ldots \quad (9.24)$$

The crystal population at time, t may be defined as,

$$P_t = \int_0^\infty n(\ell)_t d\ell \quad \ldots\ldots\ldots\ldots\ldots\ldots\ldots \quad (9.25)$$

$$\therefore \quad D = \lambda n(L)_t P_t \quad \ldots\ldots\ldots\ldots\ldots\ldots\ldots \quad (9.26)$$

Substituting for B and D in the population balance (equation 9.22) gives,

$$G \frac{\partial n}{\partial L} + \frac{\partial n}{\partial t} = \lambda \left[0.5 \int_0^L n(L-\ell)_t n(\ell)_t d\ell - n(L)_t P_t \right] \quad (9.27)$$

Equation 9.27 can be integrated over all possible values of crystal size, L to obtain the zeroth moment equation.

$$G \int_0^\infty dn(L)_t + \int_0^\infty \frac{\partial n(L)_t}{\partial t}\, dL = \lambda \int_0^\infty \left[0.5 \int_0^L n(L-\ell)_t n(\ell)_t d\ell - n(L)_t P_t \right] dL \quad \ldots (9.28)$$

The right hand side of equation 9.28 can be solved by relaxing the upper limit of the inner integral to infinity and changing variables (247). This results in the relation,

$$-Gn(O)_t + \frac{\partial P_t}{\partial t} = \lambda \left[0.5P_t^2 - P_t^2 \right] \quad \ldots\ldots\ldots\ldots (9.29)$$

Since, by definition, the nucleation rate, B_N is given by,

$$Gn(O)_t = B_N \,, \quad \ldots\ldots\ldots\ldots\ldots\ldots (9.30)$$

equation 9.29 simplifies further to,

$$-B_N + \frac{dP_t}{dt} = -\frac{\lambda}{2} P_t^2 \quad \ldots\ldots\ldots\ldots\ldots\ldots (9.31)$$

$$\text{i.e.} \quad \frac{dP_t}{dt} = -\frac{\lambda}{2} P_t^2 + B_N \quad \ldots\ldots\ldots\ldots\ldots\ldots (9.32)$$

If nucleation is considered to occur only for short but finite time interval of duration, t_o, equation 9.32 is reduced to,

$$\frac{dP_t}{dt} = -\frac{\lambda}{2} P_t^2 \,, \quad \ldots\ldots\ldots\ldots\ldots\ldots (9.33)$$

for times t greater than t_o.

On integration this leads to,

$$\int_{P_o}^{P_t} dP_t/P_t^2 = (-\lambda/2) \int_{t_o}^{t} dt \quad \ldots\ldots\ldots\ldots\ldots\ldots (9.34)$$

$$\text{i.e.} \quad P_t = \frac{1}{(\lambda/2)(t-t_o) + (1/P_o)} \quad \ldots\ldots\ldots\ldots \quad (9.35)$$

For the case when t_o is zero this relation tends to that obtained by von Smoluchowski (254,255).

$$\text{i.e.} \quad P_t = \frac{P_o}{1 + (\lambda P_o/2)t} \quad \ldots\ldots\ldots\ldots\ldots\ldots \quad (9.36)$$

The coagulation time, T^*, defined by von Smoluchowski (254) as the time required to halve the initial population, is then given by:

$$T^* = 2/\lambda P_o \quad \ldots\ldots\ldots\ldots\ldots\ldots\ldots \quad (9.37)$$

For the case when nucleation rate is constant, either only for $t < t_o$ or for all t, equation 9.32 can be written as:

$$\frac{dP_t}{dt} = (-\frac{\lambda}{2})(P_t^2 - u^2) \quad \ldots\ldots\ldots\ldots\ldots\ldots \quad (9.38)$$

$$\text{where,} \quad u^2 = 2B_N/\lambda \quad \ldots\ldots\ldots\ldots\ldots\ldots\ldots\ldots \quad (9.39)$$

Equation 9.38 can be integrated to give,

$$P_t = u(1 + e^{-\lambda u t})/(1 - e^{-\lambda u t}) \quad \ldots\ldots\ldots\ldots \quad (9.40)$$

Provided the functional form of nucleation rate is known or assumed, equation 9.32 can be integrated either analytically or numerically to obtain relations, similar to those denoted by equations 9.35, 9.36 and 9.40, for crystal population as a function of time.

CHAPTER TEN

ANALYSIS OF BATCH CRYSTALLISATION EXPERIMENTS

10.0 INTRODUCTION

The procedures employed in the analysis of experimental data collected from the barium chromate batch crystallisation experiments described in Chapter 6, are detailed in this chapter. The results obtained by the application of these techniques are also presented and discussed.

10.1 CRYSTAL SIZE DISTRIBUTION DATA

As described in Chapter 8, all crystal products were size analysed, by a combination of methods. This size distribution data was used to derive mean product crystal size, crystal surface area and crystal population for each experiment.

The raw experimental size distribution data was converted from sieve diameters to equivalent spherical volume diameters using the appropriate shape factor, the determination of which was explained in Chapter 8. The data was then fitted to a cumulative normal distribution on a mass basis by means of the Gauss-Newton non-linear optimisation algorithm (201). The fitting procedure yielded the mean (μ_m) and the standard deviation (σ_m) of the distribution.

$$\text{i.e.} \quad m_L = \frac{1}{\sigma_m \sqrt{2\pi}} \int_L^{\infty} \exp\left[-(L-\mu_m)^2/2\sigma_m^2\right] dL \qquad (10.1)$$

where, m_L is the mass fraction of particles in the product having diameters greater than L. The degree of fit was usually good and graphs 10.1 and 10.2 reveal this graphically for a short duration experiment and a longer duration experiment, respectively. The fitted distribution, characterised by μ_m and σ_m was subsequently used to calculate crystal surface area and crystal population. First, however, the overall product mass was corrected on the basis that the fitted distribution applied only to the size range from 0 to $L_{t(max)}$, where $L_{t(max)}$ was the diameter of the largest crystals present in the product recovered at time, t. This correction was usually very small and amounted to less than 0.1%, based on the original mass.

$$\text{i.e.} \qquad m_t = \frac{m_t^*}{\sigma_m\sqrt{2\pi}} \int_0^{L_{t(max)}} \exp\left[-(\ell-\mu_m)^2/2\sigma_m^2\right] d\ell \qquad \text{..... (10.2)}$$

The crystal population, P_t is given by:

$$P_t = \frac{6m_t}{\pi\rho\sigma_m\sqrt{2\pi}} \int_0^{L_{t(max)}} (1/\ell^3)\exp\left[-(\ell-\mu_m)^2/2\sigma_m^2\right] d\ell \qquad \text{..... (10.3)}$$

where, ρ is the crystal density.

Furthermore, crystal surface area is given by:

$$A = \frac{6m_t}{\phi\rho\sigma_m\sqrt{2\pi}} \int_0^{L_{t(max)}} (1/\ell)\exp\left[-(\ell-\mu_m)^2/2\sigma_m^2\right] d\ell \qquad \text{..... (10.4)}$$

where, ϕ is the sphericity of the crystals. The integrals in equations 10.2, 10.3 and 10.4 were evaluated numerically.

GRAPH 10.1 Cumulative Crystal Size Distribution on a Mass Basis for a Product from a Short Duration Experiment (Series E, Duration 1470s)

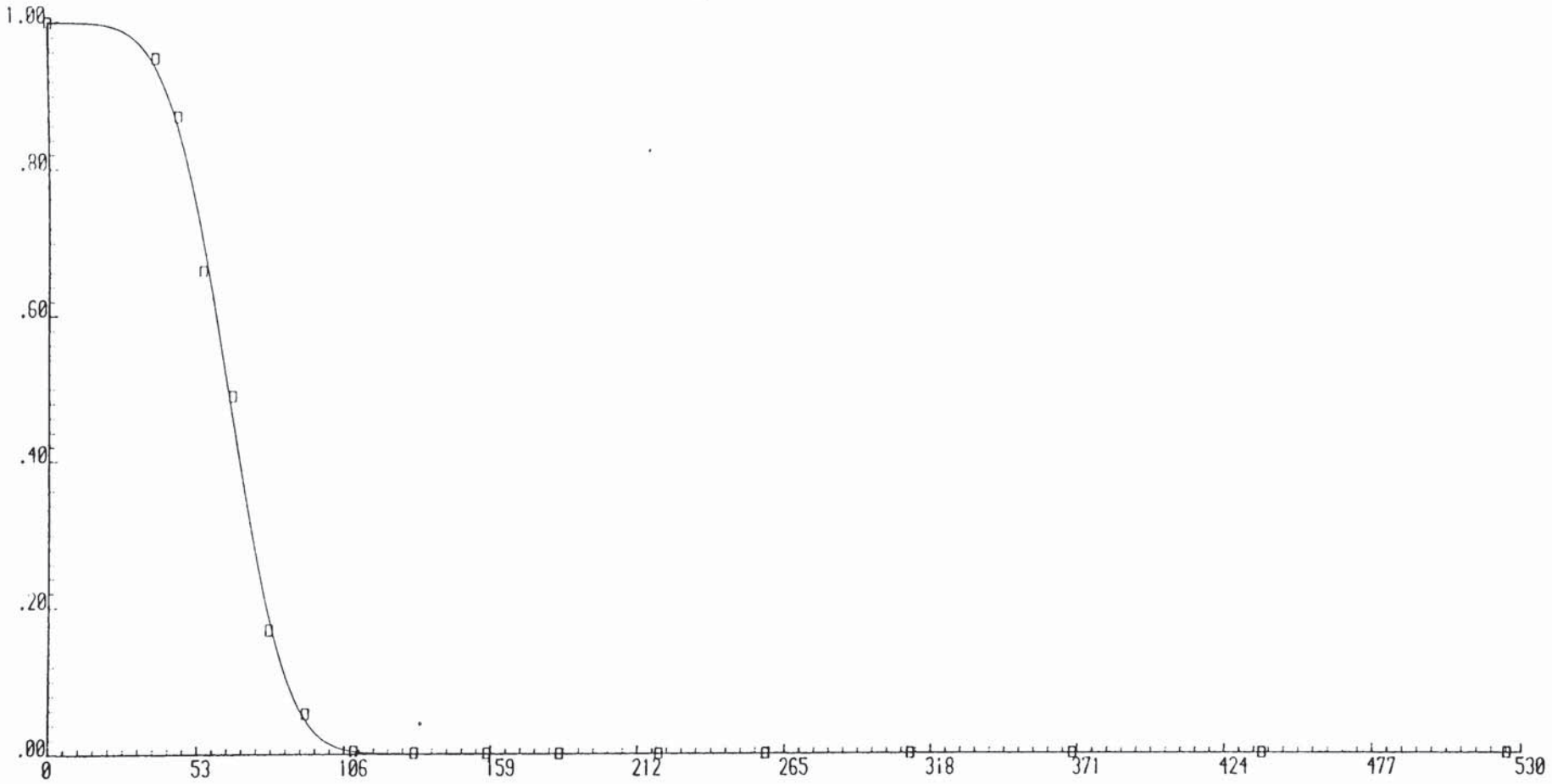

GRAPH 10.2 Cumulative Crystal Size Distribution on a Mass Basis for a Product from a Long Duration Experiment (Series F, Duration 12320s)

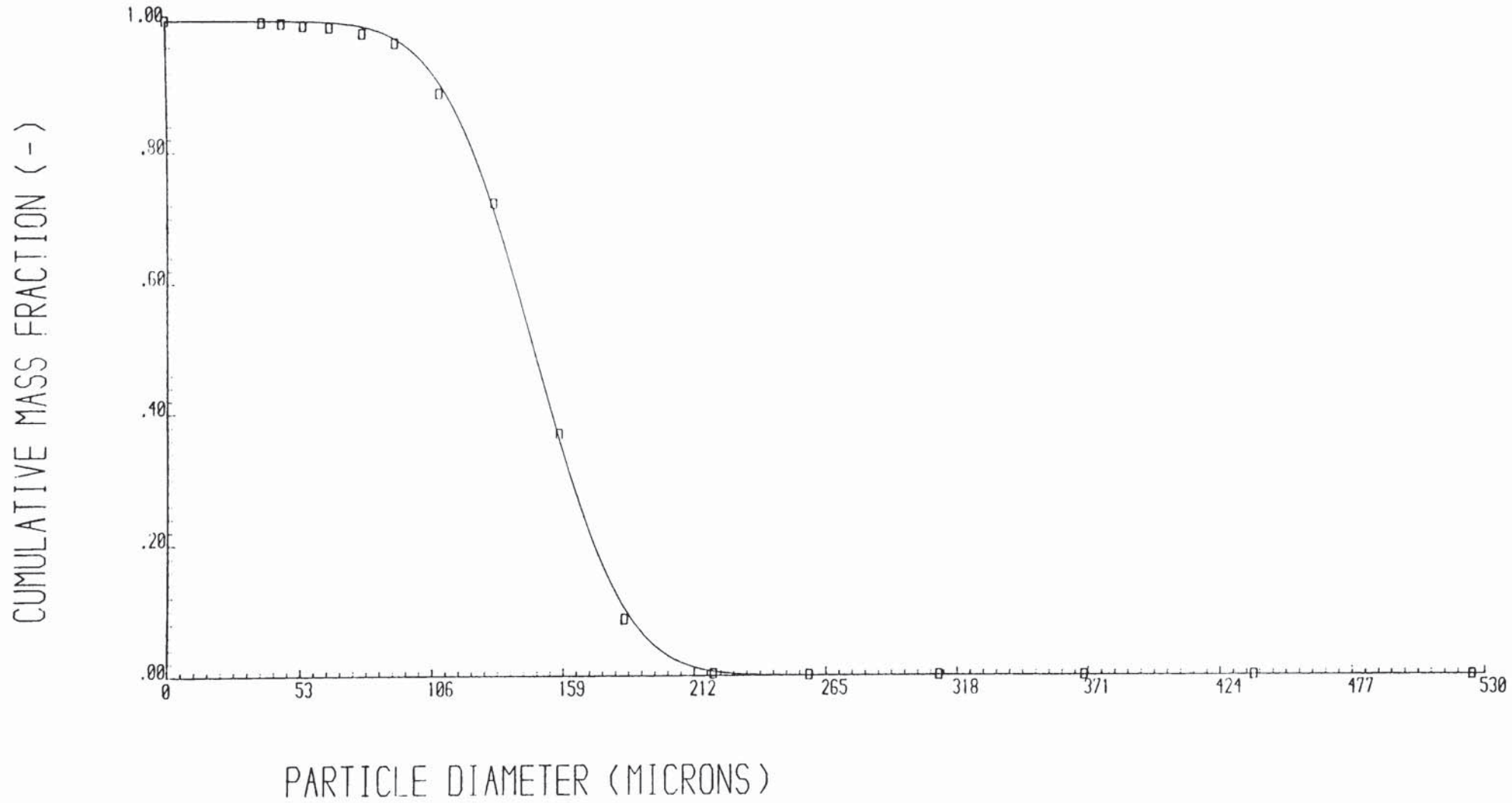

The whole of the fitting process and ensuing calculations were carried out by means of a computer program named GRAPHICS, which was specifically written for this purpose, and produced graphical as well as numerical output. This program was written in Fortran IV and was run on a Harris 500 computer. It is presented in Appendix 13. Numerical results from the crystal product size distributions are included with the experimental data for the different series, in Appendix 2.

10.2 CRYSTAL MASS - TIME DATA

Determination of the masses of the crystal products, obtained from the individual runs in each series of batch crystallisation experiments, provided a measure of the change in crystal mass with time. For each series of experiments, this crystal mass-time data was fitted to two consecutive straight lines by means of linear regression. To maintain consistency, the corrected crystal mass m_t was used in these calculations. A computer program named MASFITL was written in Fortran IV to perform these calculations, and provide the results in graphical form. This program is listed in Appendix 14. The graphical results are presented in graphs 10.3, 10.4, 10.5, 10.6 and 10.7. Details of the slopes and intercepts of the fitted lines are shown in table 10.1.

GRAPH 10.3 Graph of Crystal Mass Against Time for Experimental Series A

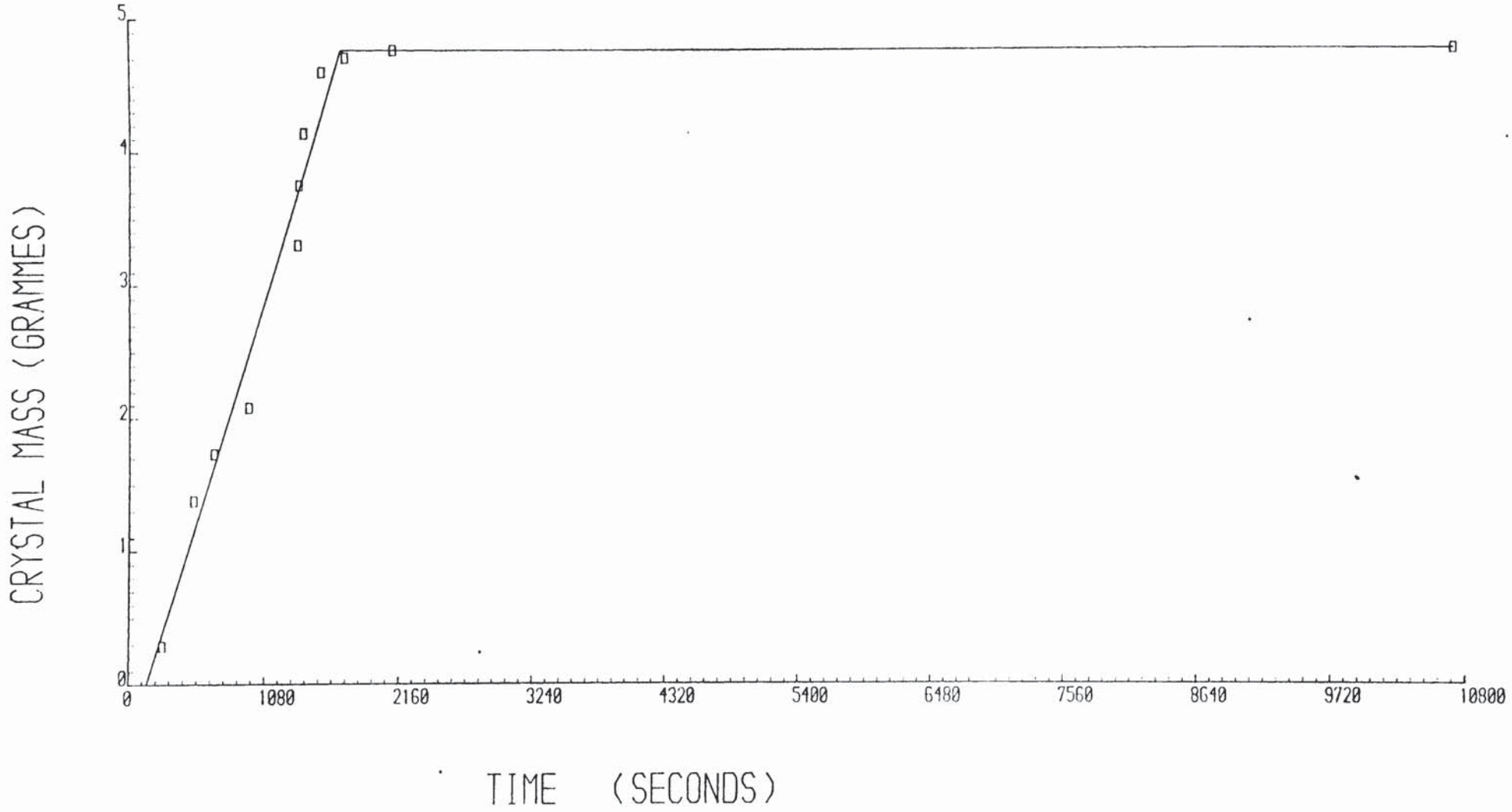

GRAPH 10.4 Graph of Crystal Mass Against Time for Experimental Series D

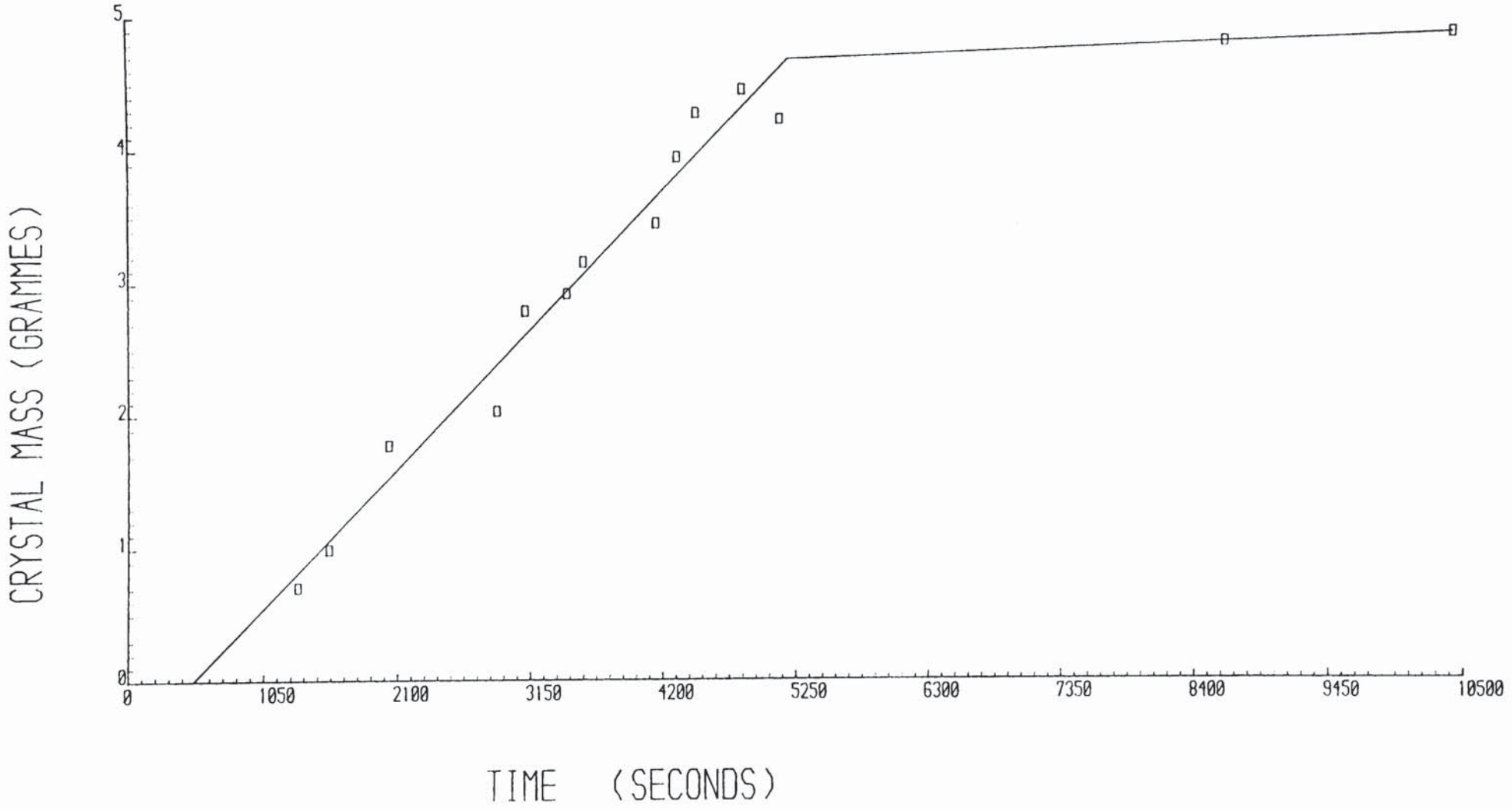

GRAPH 10.5 Graph of Crystal Mass Against Time for Experimental Series E

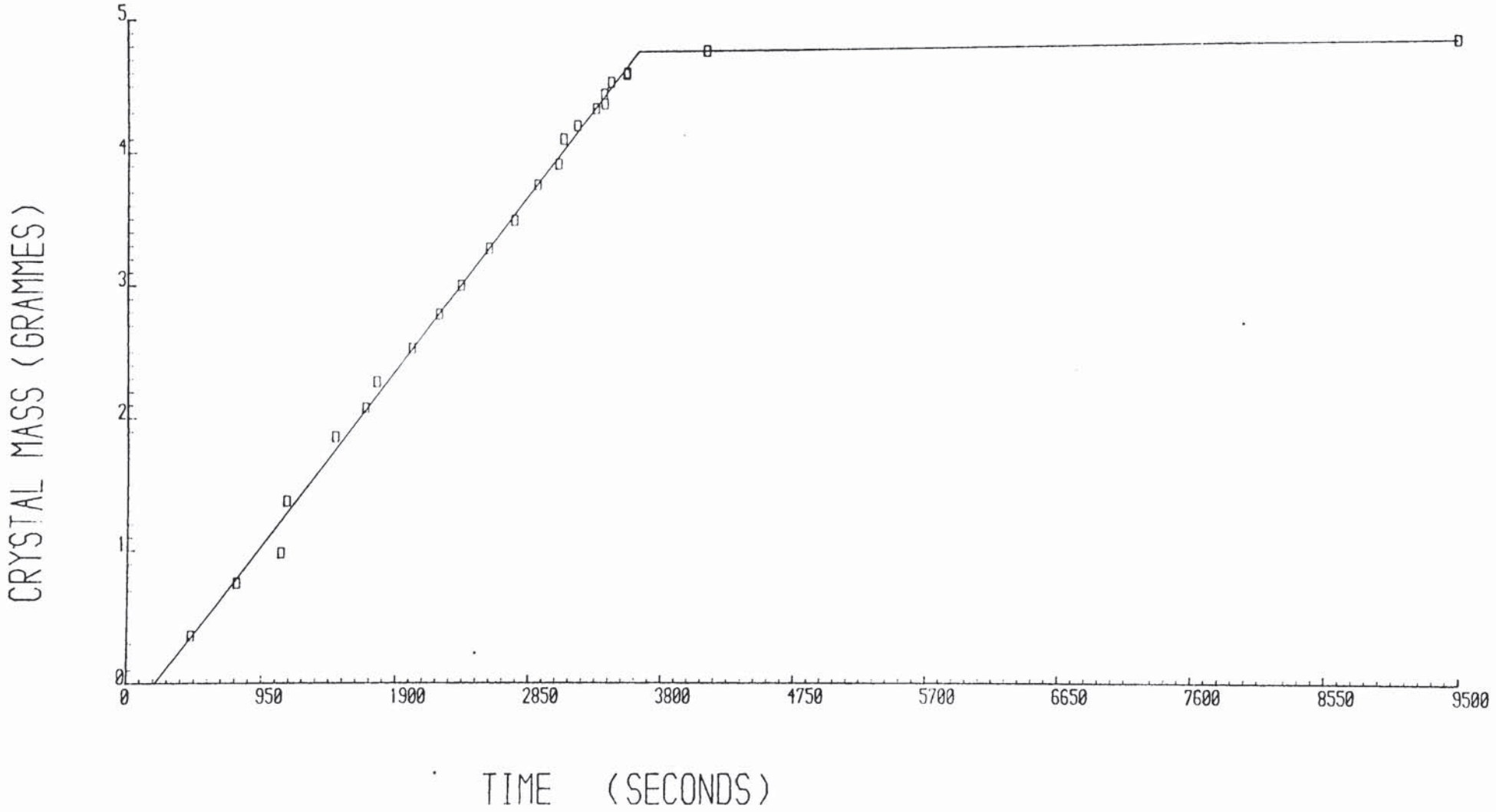

GRAPH 10.6 Graph of Crystal Mass Against Time for Experimental Series F

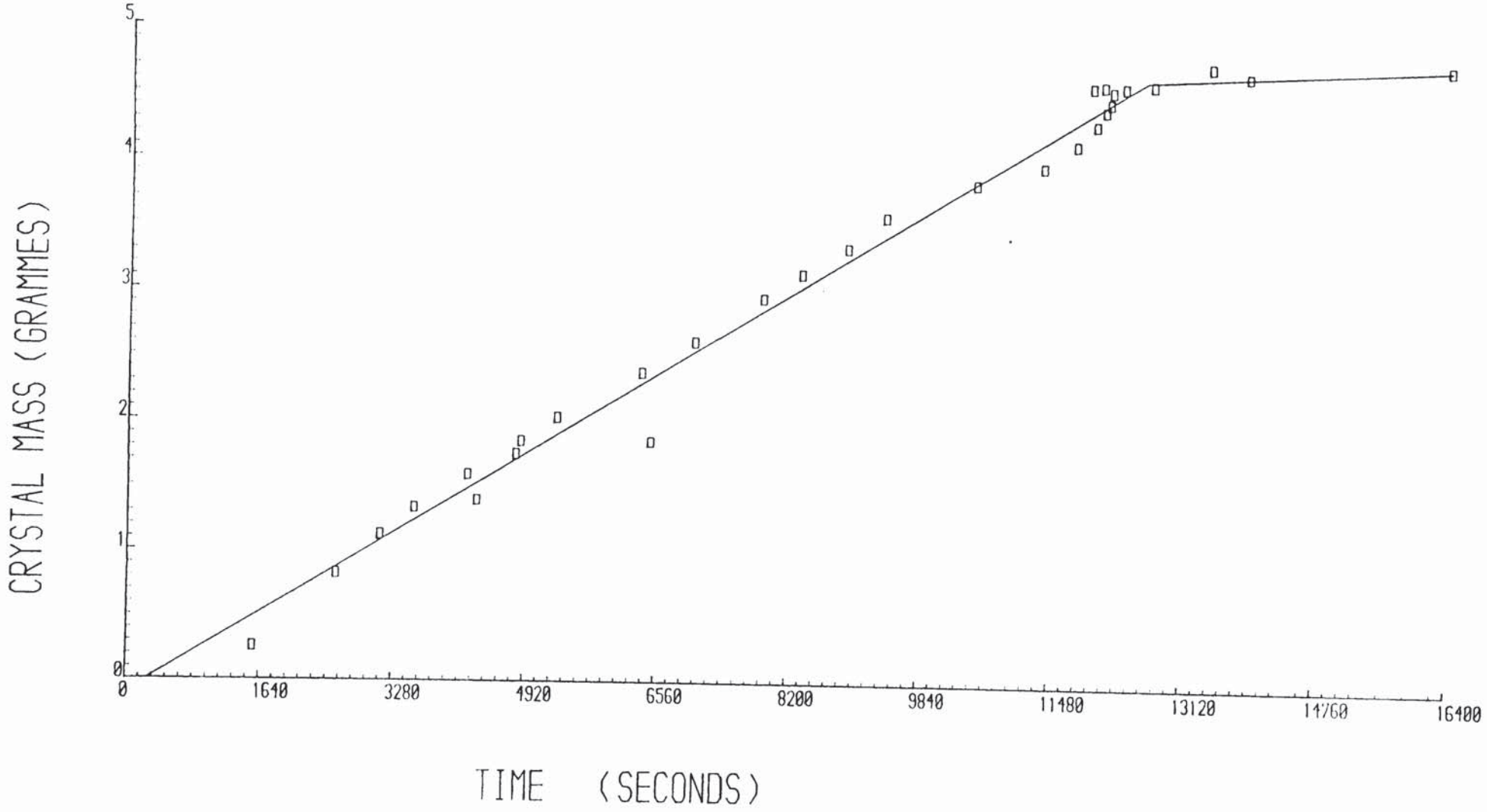

GRAPH 10.7 Graph of Crystal Mass Against Time for Experimental Series G

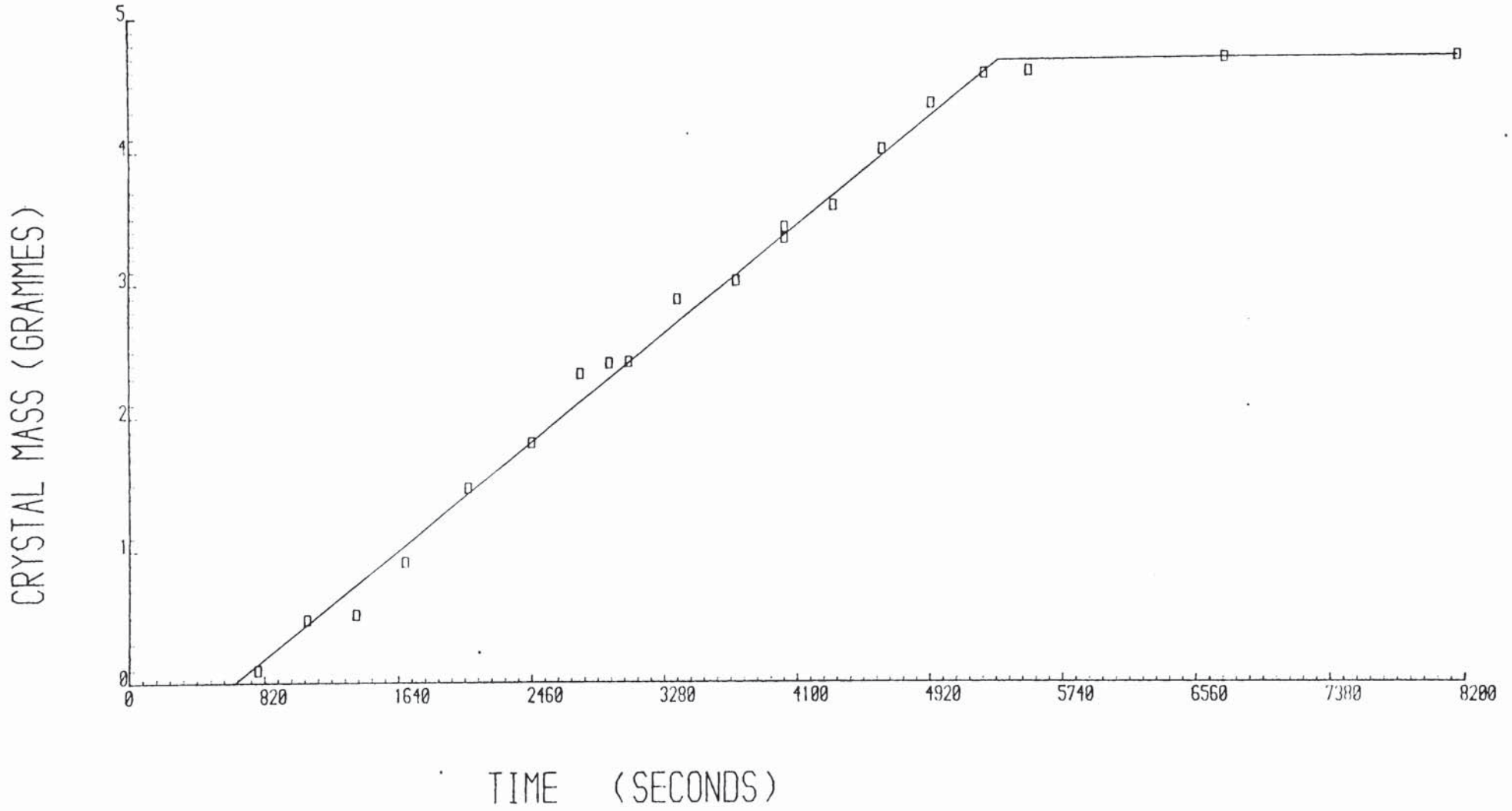

TABLE 10.1

Details of Straight Lines Fitted to Crystal Mass - Time Data

Experimental Series	Time (θ) at Intersection of Lines (s)	Straight Line for $t \leq \theta$			Straight Line for $t > \theta$			'Induction Time' (s)
		Slope ($\times 10^6$) (kg/s)	Intercept ($\times 10^4$) (kg)	Correlation Coefficient (-)	Slope ($\times 10^9$) (kg/s)	Intercept ($\times 10^3$) (kg)	Correlation Coefficient (-)	
A	1704	3.064	-4.391	0.985	0.189	4.778	1.000	143.3
D	5192	1.003	-5.042	0.984	3.367	4.528	1.000	502.7
E	3632	1.397	-2.831	0.999	1.681	4.731	1.000	202.6
F	12592	0.378	-0.970	0.994	3.177	4.260	1.000	256.6
G	5331	1.002	-6.362	0.996	0.875	4.659	1.000	634.9

10.3 DISCUSSION OF CRYSTAL MASS - TIME RELATIONS

The empirical relations fitted to the crystal mass-time data display several significant features. Firstly, the straight line fitted to the initial part of the data in each series, does not pass through the origin of the plot. Moreover, an adequate fit cannot be obtained if the fitted line is forced to pass through the origin. It is possible that this feature is due to inaccurate determination of the instant of initial nucleation, which corresponds to zero time. However, in order to explain the observed characteristic of the first crystal mass line of each series, it is necessary to presume that the onset of nucleation had been erroneously anticipated before it actually occurred. Although a delay in detecting nucleation is physically possible, the converse is unlikely, and so this explanation appears improbable. The more likely explanation is that the intercept, made by the first crystal mass line of each series, on the time axis is a real effect and corresponds to an 'induction period' during which nucleation predominates and crystal growth is negligible or non-existant. Induction periods of this type have been observed, during precipitation by direct mixing of aqueous solutions of appropriate reagents, for barium chromate (120,122,124,126) and for a large number of other sparingly and moderately soluble salts (124-126, 261-266). Induction periods have also been observed for precipitation of barium chromate from homogeneous

solution (124).

The second noteworthy aspect of the crystal mass-time plots is that there is a sharp change of slope from the first fitted straight line to the second, which applies to relatively longer times, in each experimental series. As can be seen from table 10.1, the change of slope is greater than tenfold for all cases. This would indicate that crystal growth rate has declined to a very low value. All the data sets have few data points corresponding to longer times, and hence in each case, the second crystal mass line has usually been fitted to only two data points, which is the reason for the unit correlation coefficients given in table 10.1 for these lines. Furthermore, this would mean that the calculated slopes and intercepts for these lines are subject to considerable uncertainty. Therefore, it is likely that in this region crystal growth rate has actually dropped to a negligible level.

It has been shown in Chapter 9 (section 9.3.2), that crystal mass at any time (m_t) may be related to the solute concentration (C_t):

i.e. $$C_t = (m_o - m_t)/VM \quad \ldots\ldots\ldots\ldots\ldots\ldots \quad (10.5)$$

The solute concentration at the point of intersection of the fitted straight lines has been calculated in this manner, and the results for each series are tabulated in table 10.2, which also includes the corresponding solubility values, calculated by means

TABLE 10.2

Details of Solute Concentration and Solubility at Intersection of Crystal Mass Lines

Experimental Series	Crystal Mass Corresponding to Intersection of Fitted Straight Lines ($m_i \times 10^3$) (kg)	Crystal Mass Corresponding to Longest Experiment in Series ($m_\infty \times 10^3$) (kg)	Solute Concentration ($\times 10^3$) (kmol/m^3)		Equilibrium Solubility Corresponding to the Point of Intersection ($\times 10^4$) (kmol/m^3)	
			Calculated from m_i	Calculated from m_∞	From Falangas's Data	From Skander's Data
A	4.7808	4.7978	0.798	0.736	1.493	2.918
D	4.7032	4.8799	1.081	0.437	0.635	1.204
E	4.7917	4.8900	0.759	0.401	0.777	1.578
F	4.6596	4.7800	1.241	0.803	0.530	1.017
G	4.7059	4.7307	1.071	0.982	0.349	0.687

of the empirical relations developed in Chapter 7. In every case, it is apparent that the solute concentration from the point of intersection of the fitted lines to the final data point, is greater than the corresponding equilibrium solubility. It is possible that this difference is at least partly due to the fact that solubility of barium chromate shows a tendency to level off at pH values greater than about 4.5. This has been reported by both Skander (4) and Falangas (5), and thus, the empirical relations of Chapter 7 would have tended to underestimate solubility at these longer times, for which pH was greater than 4.5. However, it is also possible that, when crystal growth rate drops to a negligible level, the system exists in a metastable state with solute concentrations somewhat greater than at equilibrium being maintained.

For each experimental series, the fitted straight line corresponding to the leading part of the data was used to calculate solute concentrations by means of equation 10.5. The corresponding values for crystal growth rate per unit surface area (R_G) were also calculated using this straight line and the equation presented in Chapter 9 (section 9.3.2).

i.e. $$R_G = \frac{1}{A}\frac{dm_t}{dt} \quad \ldots\ldots\ldots\ldots\ldots\ldots\ldots \quad (10.6)$$

Values of R_G for the different experimental series are included in Appendix 2 with the other data.

10.4 pH - TIME DATA AND SOLUBILITY

The method of precipitation from homogeneous solution employed in the batch crystallisation experiments made use of a controlled change in pH to cause a controlled change in solubility, with system temperature held constant. Therefore, the solubility depended solely on pH and provided pH was known at any time, solubility could be determined using the empirical relations presented in Chapter 7.

i.e. $$C_e = S_1 \exp(S_2/T) \, (a_{H^+})^{S_3} \quad \ldots\ldots\ldots\ldots \quad (10.7)$$

where, by definition:

$$pH = -\log_{10}(a_{H^+}) \quad \ldots\ldots\ldots\ldots\ldots\ldots \quad (10.8)$$

During each experiment, pH was measured at regular intervals. Thus, for a given experimental series a considerable number of pH-time data points were available. This data was fitted to an empirical function of time. The function used was,

$$pH_t = x_5 \int_{-\infty}^{t} \exp\left[-(\theta - x_2)^2 / 2x_3^2 \right] d\theta + x_4 t + x_1 \quad \ldots \quad (10.9)$$

where, pH_t is the pH value at time t and x_1, x_2, x_3, x_4 and x_5 are empirical constants. The fitting procedure used was a comprehensive quasi-Newton algorithm for non-linear optimisation (267). All the calculations were carried out by means of a computer program, named PHFIT, which was written in Fortran IV for this purpose, and run on a Harris 500 computer. This program produced graphical results showing the

experimental data points and the fitted curve. These results are presented in graphs 10.8, 10.9, 10.10, 10.11 and 10.12, for the five experimental series. Values of the empirical constants are given in table 10.3. The program PHFIT is listed in Appendix 15.

The fitted relations for pH were used to calculate hydrogen ion activity, and thereby determine equilibrium solubility, by means of equation 10.7, for each batch crystallisation experiment. The values of the constants S_1, S_2 and S_3 in equation 10.7 have been presented previously in table 7.4 of Chapter 7. The solubility values calculated in this manner and the solute concentrations calculated using equation 10.5, were then used to calculate the supersaturation, ΔC_t, based on concentrations.

i.e. $\Delta C_t = C_t - C_e$ ..... (10.10)

10.5 DRIVING FORCE FOR CRYSTAL GROWTH

10.5.1 General Considerations

Many different empirical expressions for driving force have been used in the analysis of crystallisation experiments. The concept of a fundamental driving force for crystal growth proposed by Mullin and co-workers (74-77), has been detailed in Chapter 2. When crystallisation of an ionic solid takes place under conditions in which equivalent stoichiometric concentrations of cation and anion are present in solution, the fundamental driving force is

GRAPH 10.8 Empirical pH-Time Relation for Experimental Series A

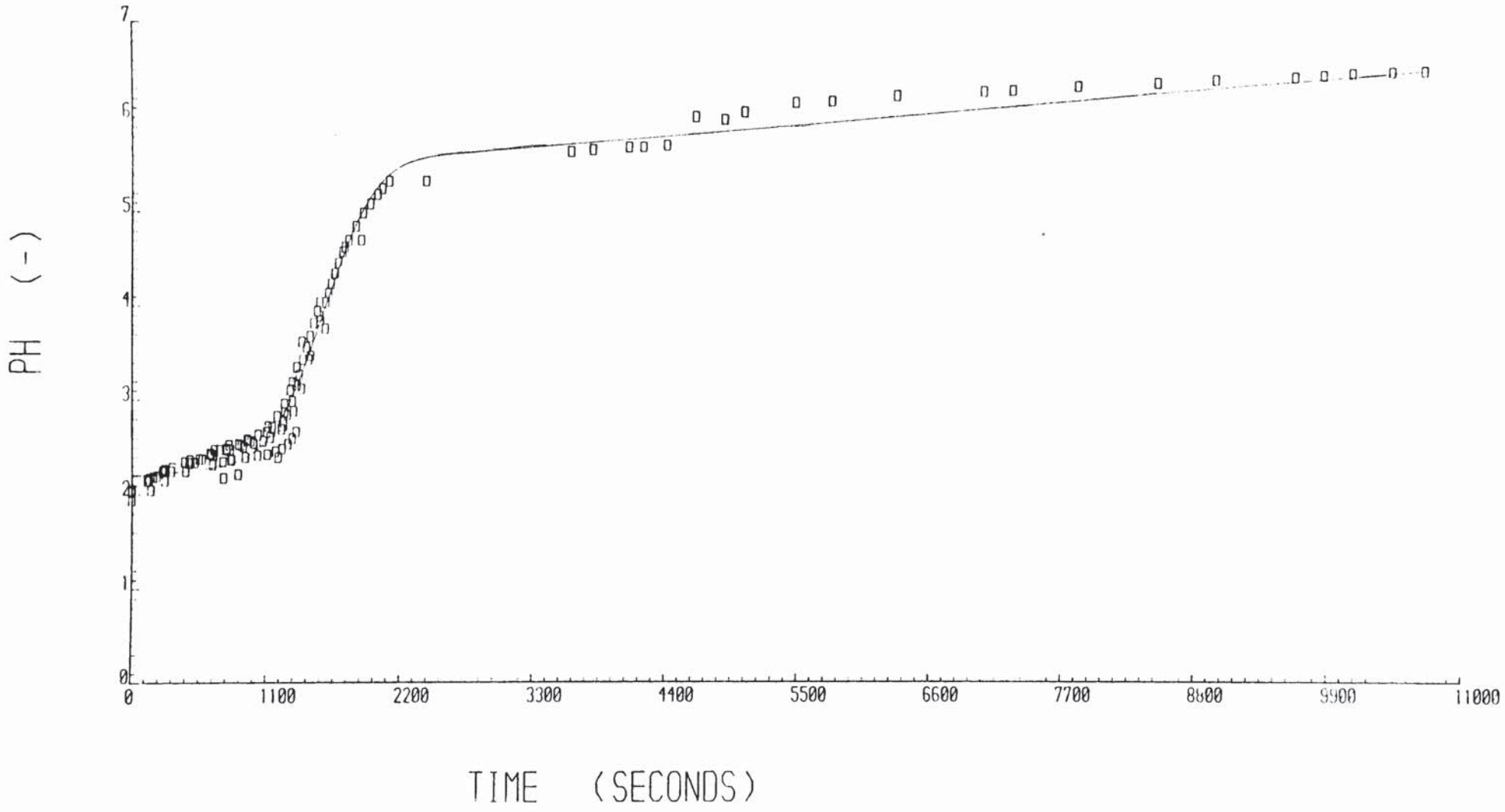

GRAPH 10.9 Empirical pH-Time Relation for Experimental Series D

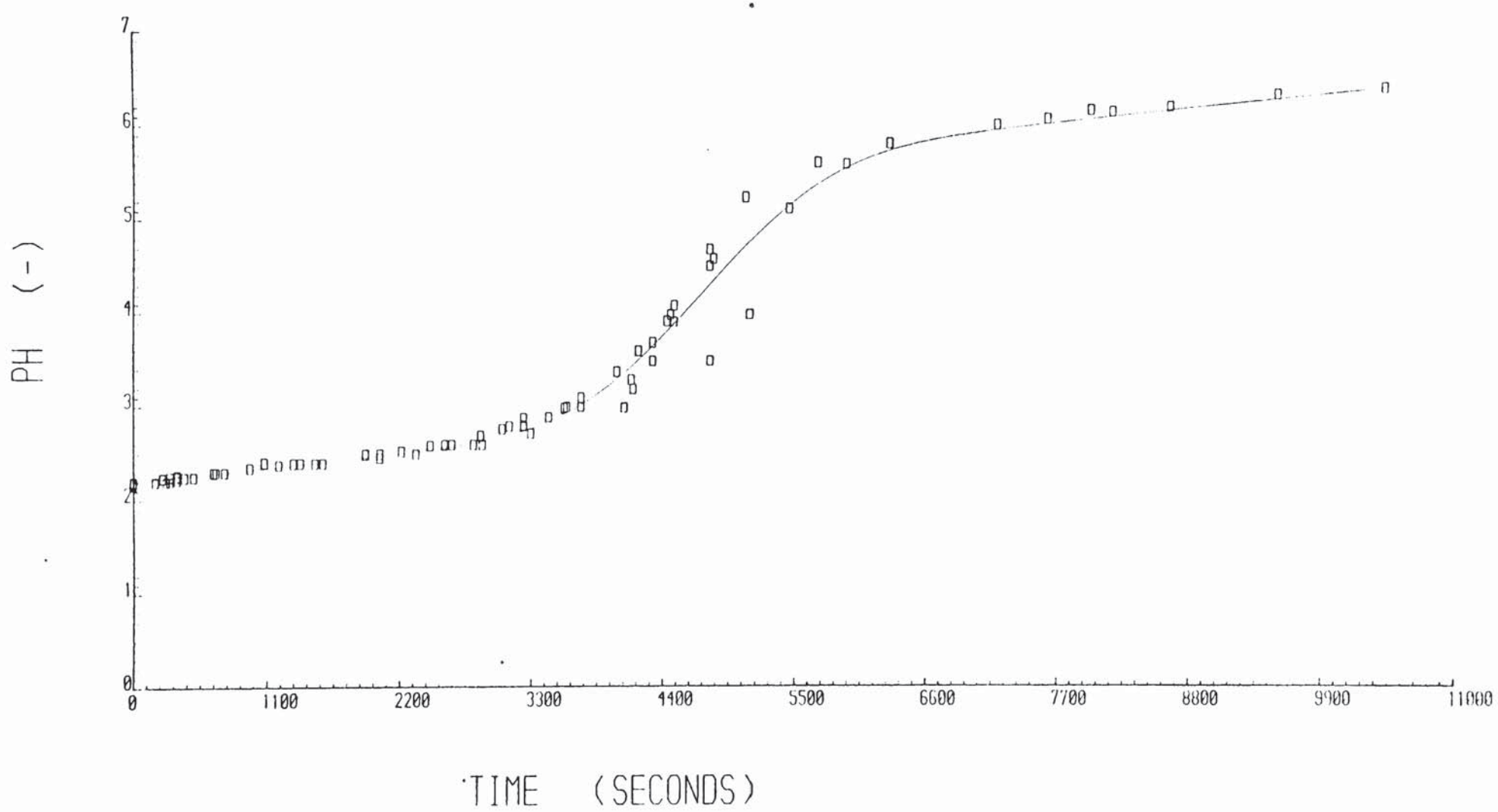

GRAPH 10.10 Empirical pH-Time Relation for Experimental Series E

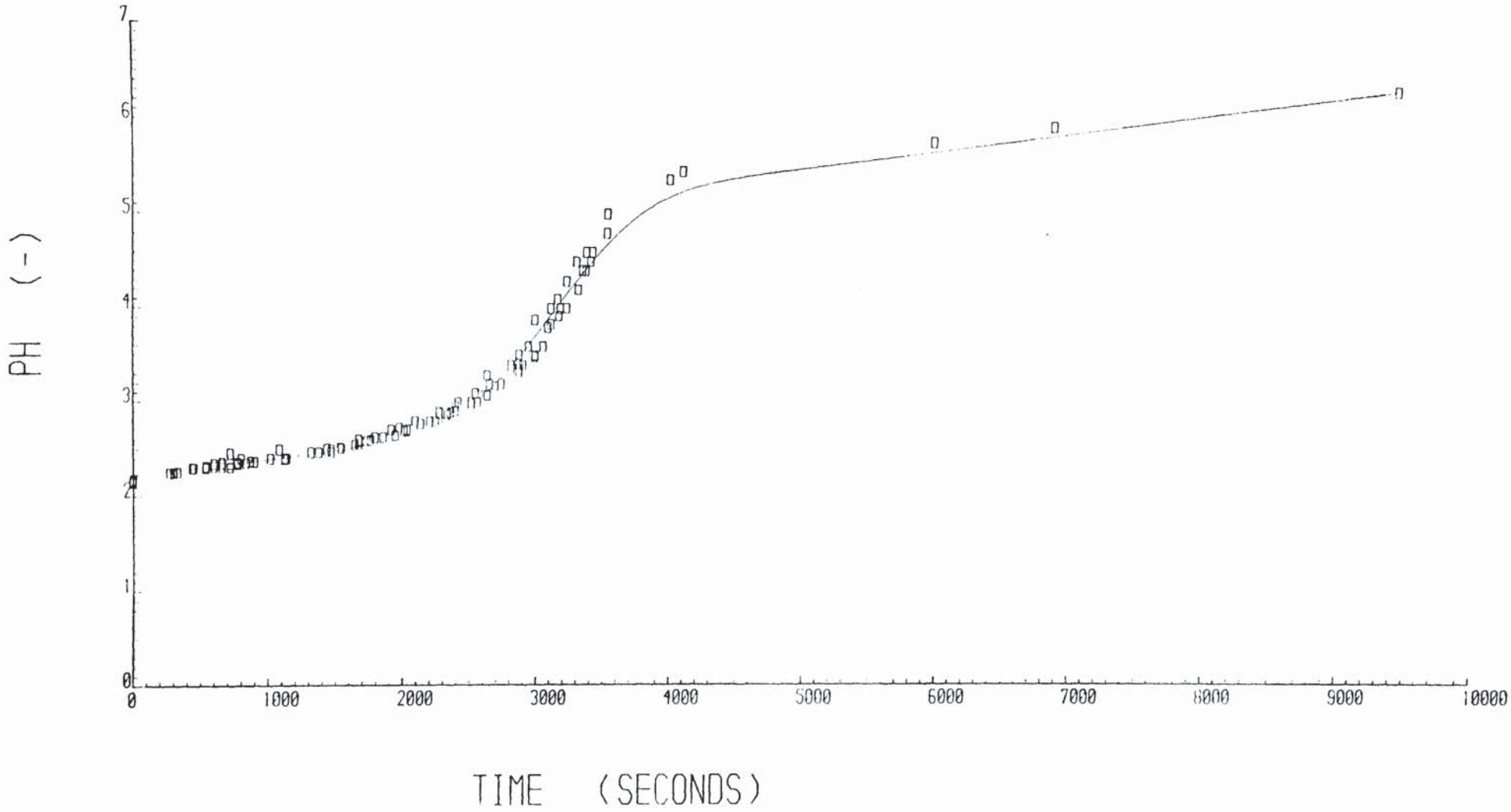

GRAPH 10.11 Empirical pH-Time Relation for Experimental Series F

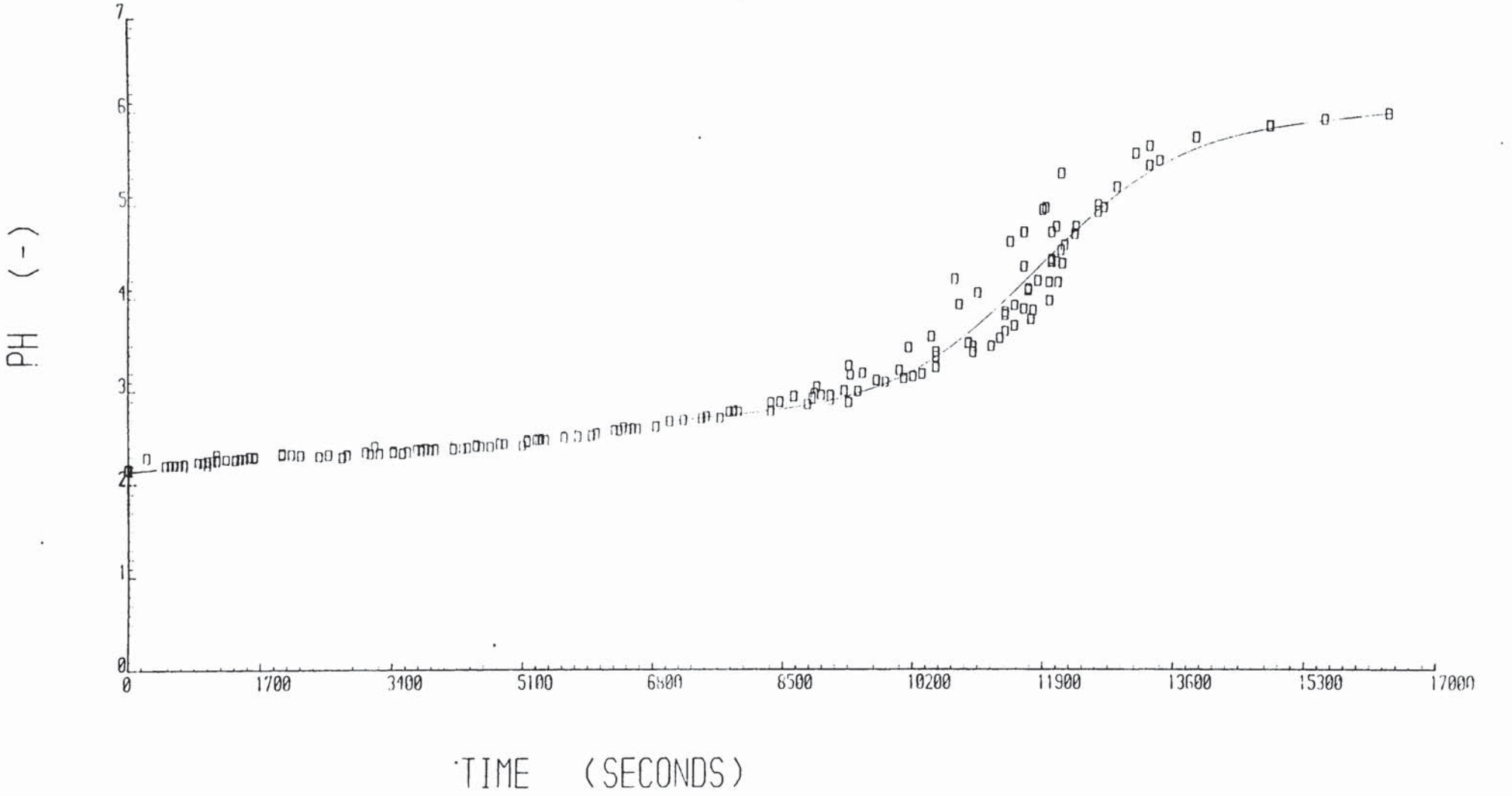

GRAPH 10.12 Empirical pH-Time Relation for Experimental Series G

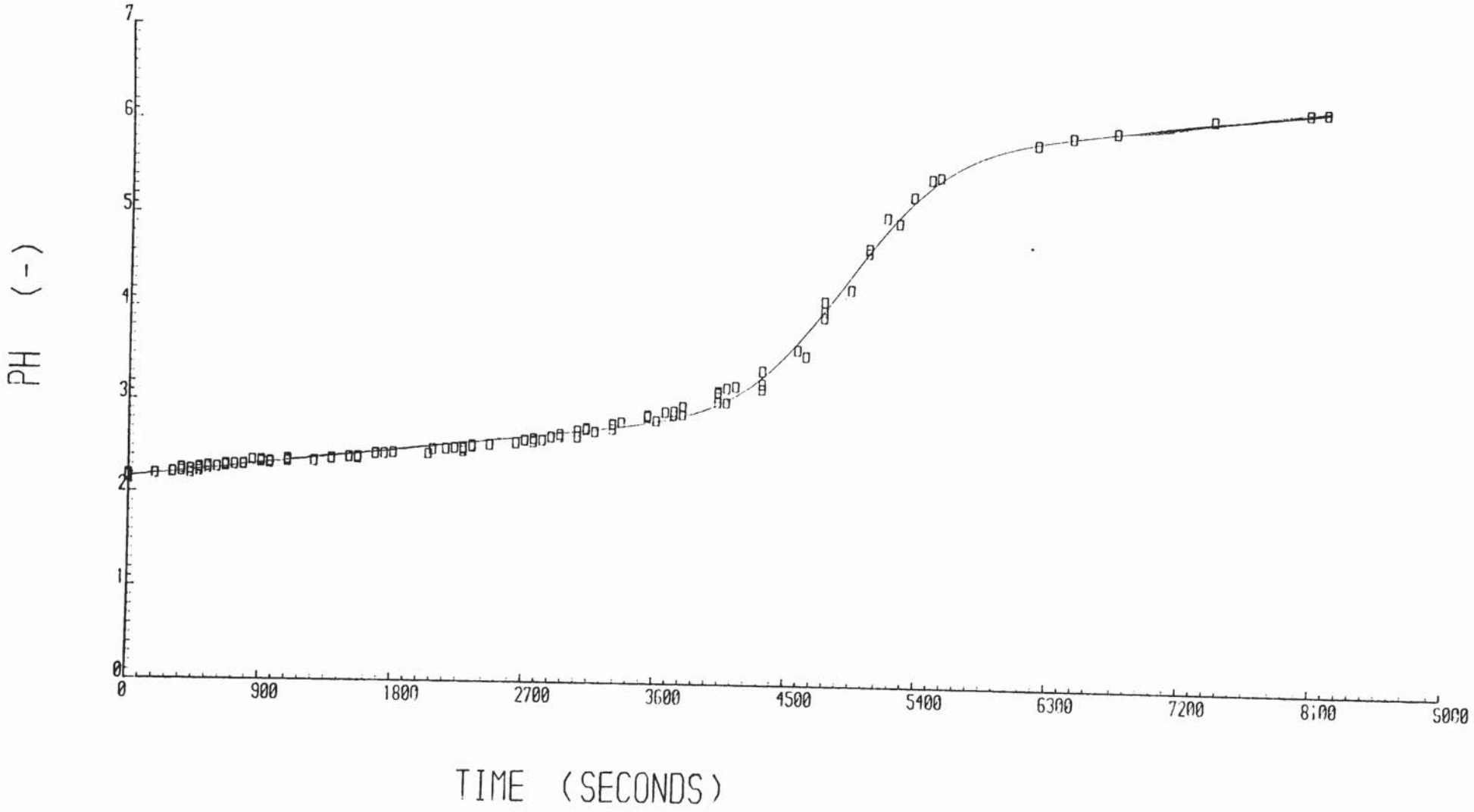

TABLE 10.3

Values of Constants for Empirical pH-Time Relations

Experimental Series	Number of Data Points	x_1 (-)	x_2 (s)	x_3 (s)	$x_4 (x10^4)$ (1/s)	$x_5 (x10^3)$ (1/s)
A	149	2.2084	1577.48	340.22	1.0721	3.6859
D	89	2.2098	4742.68	868.72	1.3145	1.2941
E	138	2.2265	3137.31	549.75	1.7297	1.7298
F	202	2.1393	11829.80	1360.10	0.7947	0.7506
G	129	2.1634	4882.94	541.96	1.7890	1.9336

conventionally defined as demonstrated in Chapter 2.

i.e. $$S = \frac{\phi^*}{RT} = \nu \ln(a/a_e) \quad \ldots\ldots\ldots\ldots\ldots\ldots \quad (10.11)$$

where, $$a = \gamma C_t \quad \ldots\ldots\ldots\ldots\ldots\ldots\ldots\ldots \quad (10.12)$$

and, $$a_e = \gamma_e C_e \quad \ldots\ldots\ldots\ldots\ldots\ldots\ldots\ldots \quad (10.13)$$

Under these conditions, empirical expressions for driving force such as supersaturation, supersaturation ratio and relative supersaturation are distinctly defined, whether in terms of activities or concentrations.

However, when crystallisation takes place from a solution in which the cations and anions are not present in equivalent stoichiometric concentrations, quantities such as supersaturation, supersaturation ratio and relative supersaturation, cannot be clearly defined. Furthermore, the dimensionless driving force for crystal growth is then defined by:

$$S = \frac{\phi^*}{RT} = \ln \left[\frac{a_+^{\nu+} \; a_-^{\nu-}}{a_{+e}^{\nu+e} \; a_{-e}^{\nu-e}} \right] \quad \ldots\ldots\ldots\ldots \quad (10.14)$$

where, a_+ is the activity of the cation; a_- is the activity of the anion; ν_+ is the number of cations obtained per molecular unit; ν_- is the number of anions obtained per molecular unit; and, the subscript 'e' applies to equilibrium saturation conditions. The following relations also apply.

$$a_+ = \gamma_+ C_+ \quad \ldots\ldots\ldots\ldots\ldots\ldots\ldots \quad (10.15)$$

$$a_- = \gamma_- C_- \quad \ldots\ldots\ldots\ldots\ldots\ldots\ldots \quad (10.16)$$

$$\nu = \nu_+ + \nu_- \quad \ldots\ldots\ldots\ldots\ldots\ldots\ldots \quad (10.17)$$

where, γ_+ is the activity coefficient of the cation; γ_- is the activity coefficient of the anion; C_+ is the concentration of the cation; C_- is the concentration of the anion; and, ν is the number of ions obtained per molecular unit.

10.5.2 Ionic Concentrations in Acidic Barium Chromate Solutions

In the batch crystallisation experiments, solutions of barium chromate in hydrochloric acid underwent gradual neutralisation. The equilibria that prevail in these solutions have been described in Chapter 7 and are represented by equations 7.1, 7.2, 7.3, 7.4, 7.5, 7.6 and 7.7. An important consequence of these ionic equilibria is that at any time during crystallisation, the concentrations of barium and chromate ions in solution are non-stoichiometric. If the equilibrium constants are known, it is possible to calculate the activities and concentrations of all the ionic species in solution at a given pH (i.e. hydrogen ion activity) and total barium chromate concentration. The method of calculation and relevant equations have been set down in Appendix 18. If it is further assumed that the same ionic equilibria prevail in supersaturated as well as in saturated solution, all the ionic activities required to calculate the driving force for crystal growth can be obtained in this way.

The equilibrium constants required for this purpose have been estimated from values quoted in the literature, on the assumption that an Arrhenius type temperature dependence is applicable. These values are tabulated in table 10.4.

10.5.3 Expressions for Driving Force

The equilibrium calculations described in the preceding section permitted a number of different expressions for driving force to be calculated from the experimental data. Since, a number of different chromium species exist in solution, several different variants on the fundamental driving force, as expressed by equation 10.14, were examined. These are listed in table 10.5. In addition, a number of other empirical expressions for driving force, used in previous studies of crystal growth, were examined. These are tabulated in table 10.6. Of these latter expressions, those numbered from 1 to 4 were alternatively defined in terms of activities, as opposed to concentrations, and these relations were also investigated.

10.5.4 Choice of Driving Force

The general effect of the equilibria existing in acidic solutions of barium chromate is that there is an increase in the chromate ion concentration from low pH values to high. Since solution pH increases in the course of a batch crystallisation,

TABLE 10.4

Values of Equilibrium Constants Used to Calculate Driving Force

Equilibrium Constant	Units	Estimates of Equilibrium Constants		References on which Estimates are Based and Comments
		At 90°C	At 100°C	
K_1	$kmol/m^3$	0.559	0.460	(110, 268-273)
K_2	$kmol/m^3$	1.639×10^{-7}	1.547×10^{-7}	(4, 110, 274-283)
K_3	$m^3/kmol$	19.81	18.26	(4, 283-287)
K_4	$kmol/m^3$	13	12	(110); due to insufficient data, a temperature dependence similar to that of K_3 has been assumed
K_5	$kmol/m^3$	0.07	0.06	(110,270,271); due to insufficient data, a temperature dependence similar to that of K_3 has been assumed
K_6	$(m^3/kmol)^2$	60.00	65.78	(268, 270, 273, 288)

TABLE 10.5

Expressions for Driving Force Based on Fundamental Driving Force

Expressions for Driving Force (S)	Comments
$\ln\left[\frac{a_+^{\nu_+} \cdot a_-^{\nu_-}}{a_{+e}^{\nu_{+e}} \cdot a_{-e}^{\nu_{-e}}}\right]$	Only the activity of the chromate ion from among the different Cr(VI) species is considered.
$\ln\left[\frac{a_+^{\nu_+} \cdot \prod_i^{\text{all Cr species}} (a_{-i}^{\nu_{-i}})}{a_{+e}^{\nu_{+e}} \cdot \prod_i^{\text{all Cr species}} (a_{-ei}^{\nu_{-ei}})}\right]$	The activities of all the Cr(VI) species in solution are considered.
$\ln\left[\frac{a_+^{\nu_+} \cdot \prod_i^{\text{anions}} (a_{-i}^{\nu_{-i}})}{a_{+e}^{\nu_{+e}} \cdot \prod_i^{\text{anions}} (a_{-ei}^{\nu_{-ei}})}\right]$	The activities of all the Cr(VI) anions in solution are considered.
$\ln\left[\frac{a_+ \cdot a_-}{a_{+e} \cdot a_{-e}}\right]$	The activities of barium and chromate ions, with unit values for the ν terms, are considered.
$\ln\left[\frac{C_+ \; C_-}{C_{+e} \; C_{-e}}\right]$	This is a similar expression to that immediately preceding, but is based on concentrations.

TABLE 10.6

Empirical Expressions for Driving Force

No.	Empirical Expression for Driving Force, S	References in which Empirical Expression was Used
1	$S = \Delta C = C_+ - C_{+e} = C_t - C_e$	(8,48,120,122,123,131,133,136,245,261,264, 265,289-292,295,296)
2	$S = (C_+C_-)^{\frac{1}{2}} - (C_{+e}C_{-e})^{\frac{1}{2}}$	(8,292-295,298).
3	$S = (C_+-C_{+e})(C_--C_{-e})$	(8,292)
4	$S = (C_+C_-) - (C_{+e}C_{-e})$	(134,135,295,298,299)
5	S is given by the solution to: $(C_+-S)(C_--S) = C_{+e}C_{-e}$	(292,296)
6	$S = (a_+a_- - a_{+e}a_{-e})/a_{+e}a_{-e}$	(297,298)

chromate ion concentration increases as well. During the initial stages when pH is below 2.5, chromate ion concentration is very low. This effect was found to predominate in all the expressions for driving force involving anions. The driving force as expressed by these relations showed an increasing trend with decreasing crystal growth rate per unit surface area (R_G, equation 10.6), for all the experimental series. Clearly this was physically impossible.

One possible reason for these anomalous results was that the values of the equilibrium constants tabulated in table 10.4 were inaccurate. A heuristic approach was adopted to investigate this aspect, and combinations of values of the equilibrium constants, both larger and smaller, by a factor of ten, than those given in table 10.4, were used to recalculate the different expressions for driving force. The same anomalous trend with growth rate per unit surface area, was observed for each such combination of values of the equilibrium constants.

The abnormal results obtained for these various expressions of driving force, and especially those expressions based on fundamental thermodynamic considerations, may be due to a number of factors. These are:

1. The use of the same expression to calculate activity coefficients, on a molar basis, in both saturated and supersaturated solution. Sohnel et al (75) have shown that for some

soluble substances, mean molal activity coefficient is a continuous function at and beyond the saturation point upto low supersaturations. However, barium chromate in acidic solution is a considerably more complex system.

2. The equilibria involved may be different in supersaturated solutions in which crystal growth is taking place, than in saturated solutions. Moreover, different values of the equilibrium constants may apply to these two cases. Significantly, Christoffersen et al (78) have concurred that the difficulty in obtaining accurate values of fundamental driving force is primarily a problem of obtaining accurate experimental data for relevant equilibrium constants.

3. The ionic activities and concentrations involved are small, and of the order of 10^{-3} kmol/m^3 or less. Thus, those expressions for driving force listed in table 10.5 in particular, will be subject to arithmetic instability and consequent error, caused by division of small numbers.

4. Anomalous values for many of the empirical expressions for driving force would indicate that these were unsuitable for use in investigating batchwise precipitation from homogeneous solution of barium chromate.

Of all the expressions for driving force, the first empirical relation in table 10.6 was the only one that yielded values of driving force that showed a consistent trend with values of growth rate per unit surface area (R_G) for each experimental series.

i.e. $S = \Delta C_t = C_+ - C_{+e} = C_t - C_e$ ..... (10.18)

This expression for driving force, based on the concentrations of the barium ion at supersaturation and at equilibrium saturation, was therefore used in the analysis of the barium chromate batch crystallisation experiments.

10.5.5 Calculation of Supersaturation Driving Force

The driving force expressed by equation 10.18 was calculated by means of equation 10.5 which, together with the fitted crystal mass lines, yielded the solute concentration (C_t), and by equation 10.7 which gave the equilibrium concentration (C_e). The empirical constants, S_1, S_2 and S_3 in equation 10.7 have been independently estimated from the solubility data of Skander (4) and Falangas (5), in Chapter 7. Thus, for each data point, two different values of the driving force were calculated. However, Skander's solubility measurements were made in the absence of urea, while crystallisation occurred with urea present in solution. Hence, it was decided that, the driving force calculated using values for S_1, S_2, and S_3 derived from Falangas's solubility

measurements made in the presence of urea, was more appropriate for modelling crystal growth rate. Nevertheless it has been noted in Chapter 7 that Falangas's solubility measurements overall were less consistent than those of Skander. Calculated values of driving force are presented in Appendix 2 along with the other data for each series of experiments.

10.6 CRYSTAL POPULATION - TIME DATA

The crystal population data derived from crystal size distributions, in the manner described previously in section 10.1, have been plotted against time for each experimental series, in graphs 10.13, 10.14, 10.15, 10.16 and 10.17. These graphs show the average population and also the results of fitting the simple agglomeration model presented in Chapter 9, to this data.

The agglomeration model yielded the following final equation.

$$P_t = 1/\left[(\lambda/2)(t-t_o) + (1/P_o) \right] \quad \ldots\ldots\ldots \quad (10.19)$$

where, the model parameters λ, t_o and P_o are the agglomeration rate constant, the duration of the initial 'burst' of nucleation, and the population after the initial 'burst' of nucleation, respectively. Furthermore the coagulation time, T* was given by:

$$T^* = 2/\lambda P_o \quad \ldots\ldots\ldots\ldots\ldots\ldots\ldots\ldots \quad (10.20)$$

GRAPH 10.13 Graph of Crystal Population Against Time for Experimental Series A

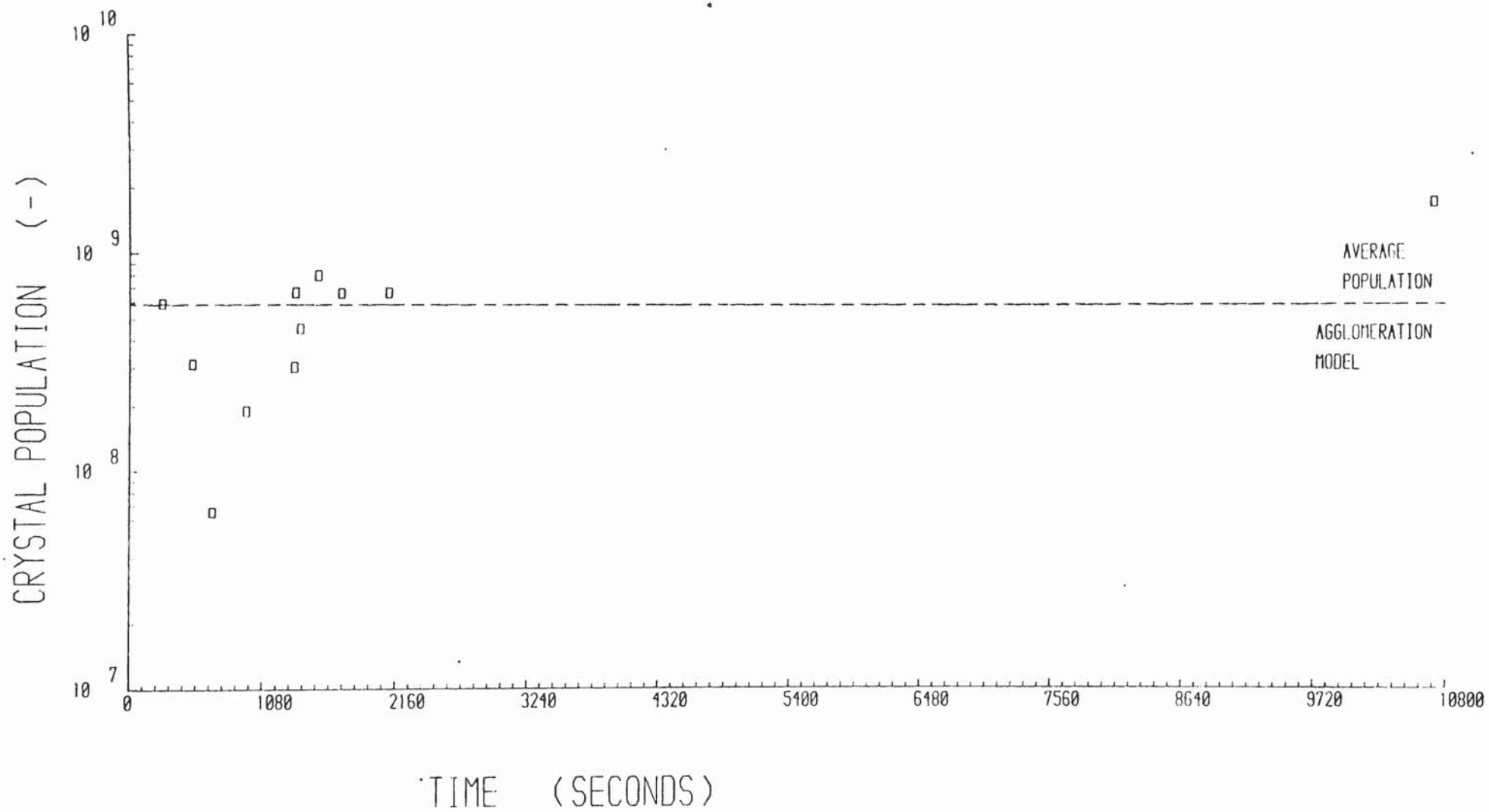

GRAPH 10.14 Graph of Crystal Population Against Time for Experimental Series D (points marked with an asterix have been excluded when fitting agglomeration model)

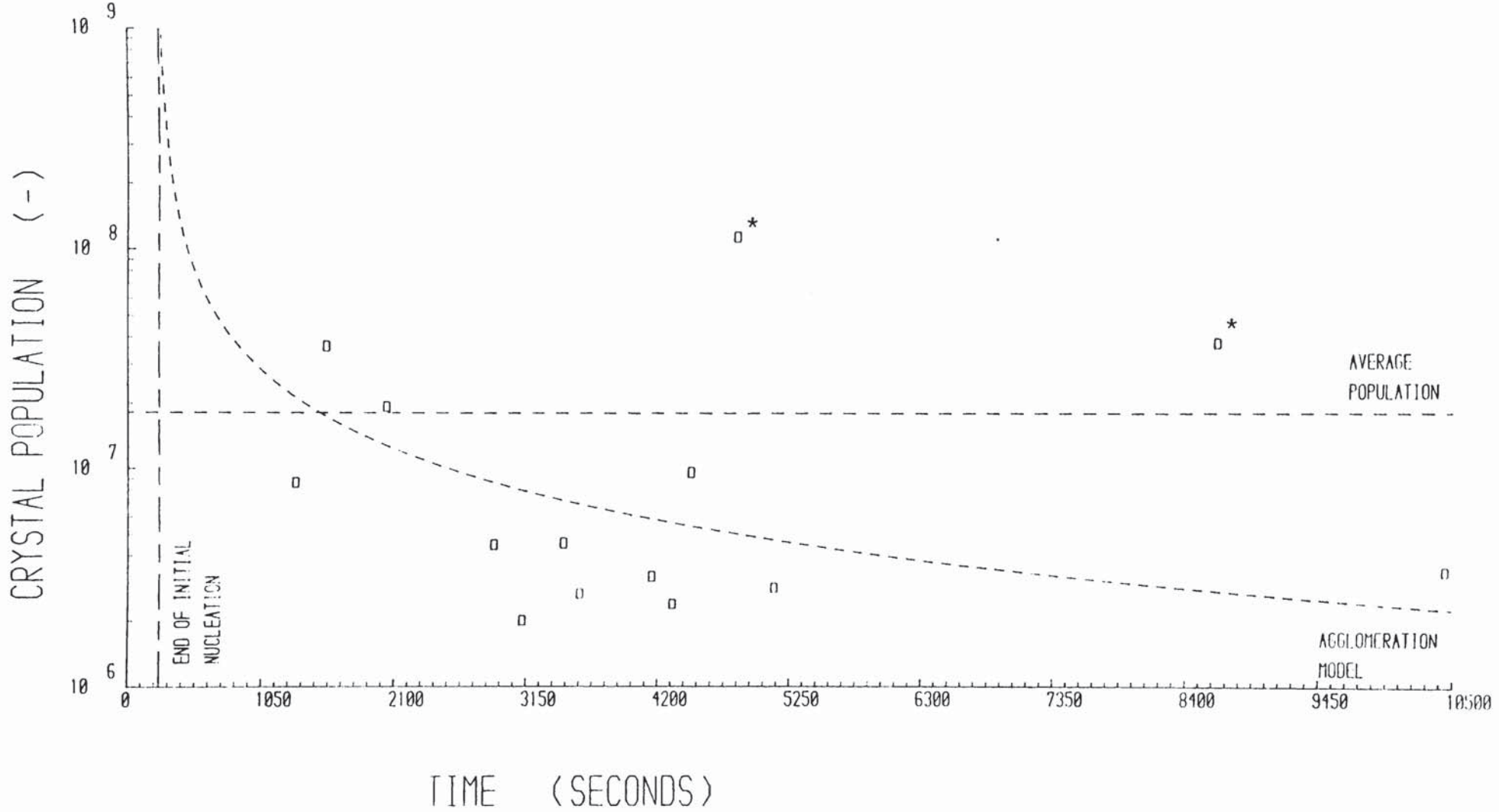

GRAPH 10.15 Graph of Crystal Population Against Time for Experimental Series E

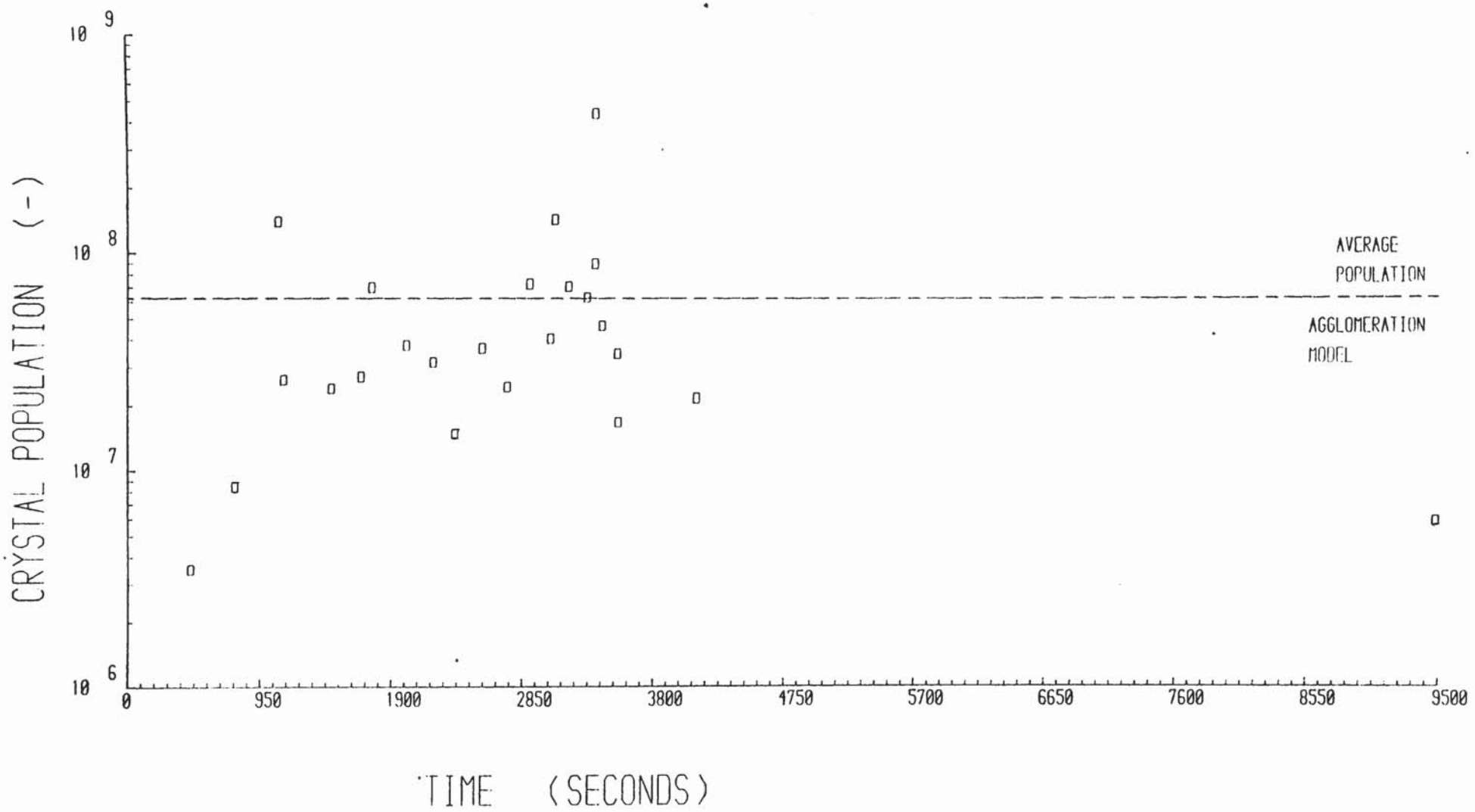

GRAPH 10.16 Graph of Crystal Population Against Time for Experimental Series F

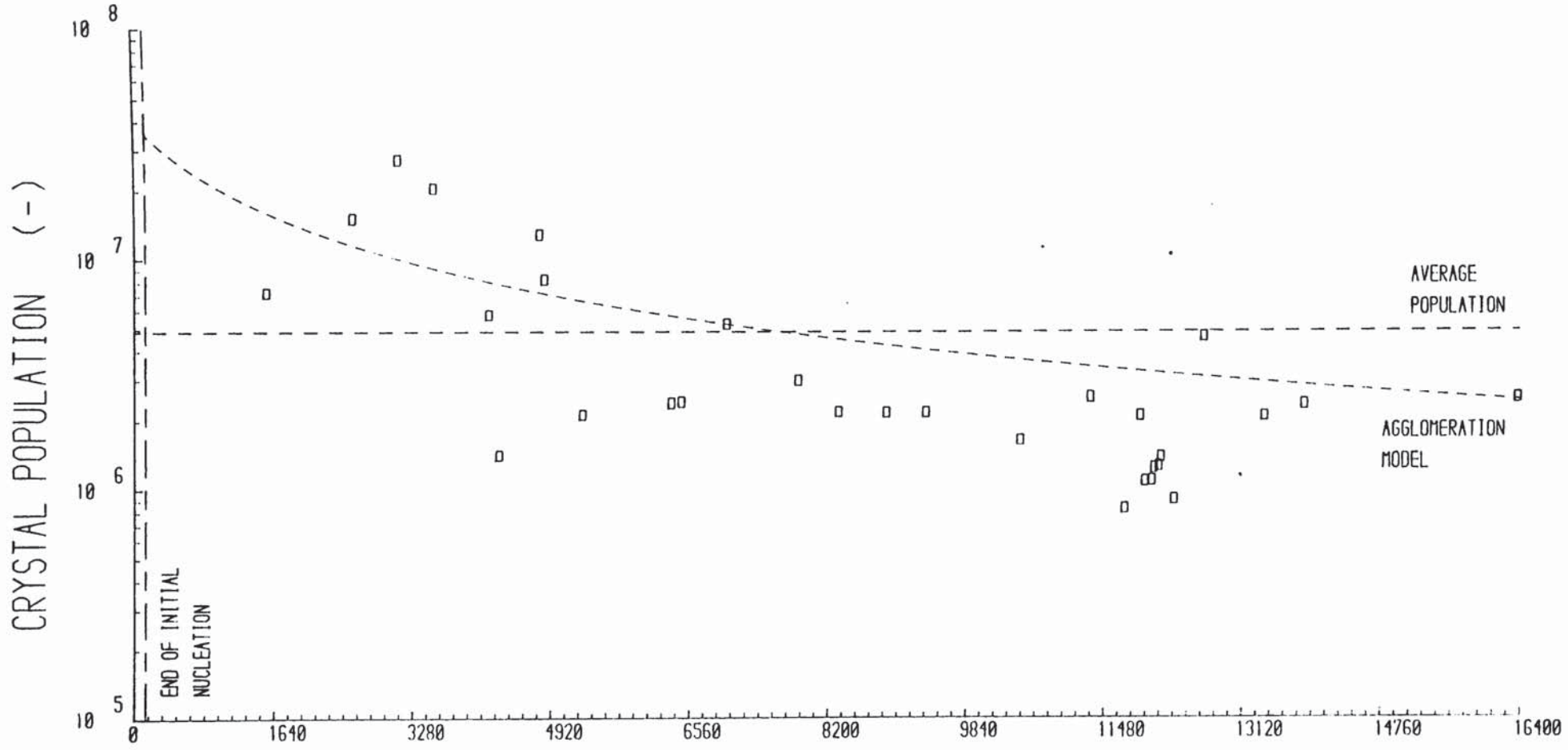

GRAPH 10.17 Graph of Crystal Population Against Time for Experimental Series G

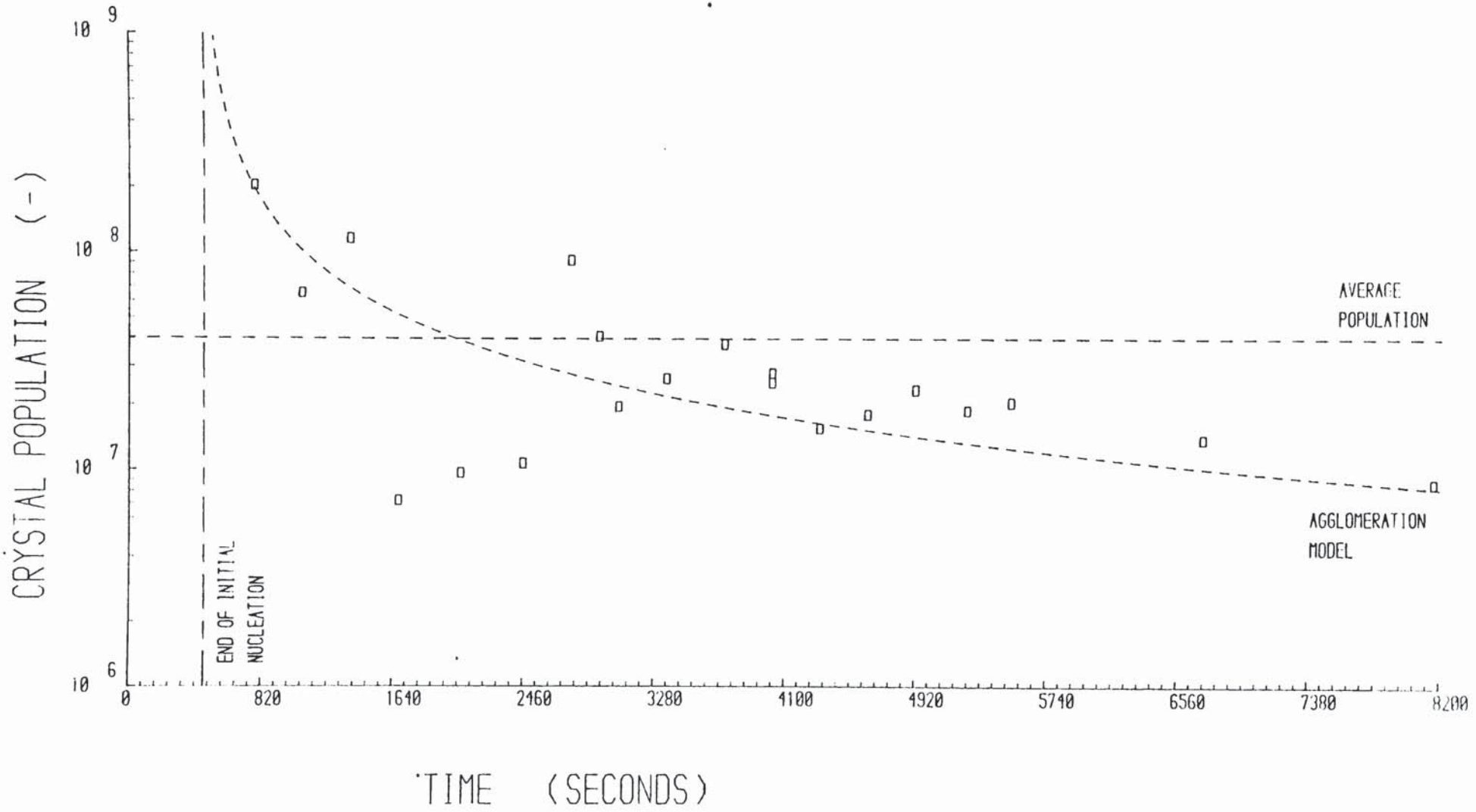

This model was fitted to the population data using the same comprehensive quasi-Newton algorithm for non-linear optimisation (267), which was employed in fitting an empirical curve to the pH-time data (in section 10.4). However, in this case scaling of model parameters and objective function was utilised to facilitate the optimisation process. Optimisation was carried out by means of a computer program named AGLOM, which was written in Fortran IV for this purpose, and run on a Harris 500 computer. The program AGLOM is listed in Appendix 17. Graphs 10.13 to 10.17 are the graphical results produced by this program. The values obtained for the model parameters are presented in table 10.7. It can be seen from this table, and from graphs 10.13 and 10.15, that for experimental series A and E, the agglomeration model degenerates to the trivial case corresponding to the average population.

10.7 DISCUSSION OF CRYSTAL POPULATION-TIME DATA

10.7.1 The Experimental Data

The crystal population data for all the experimental series show a wide scatter. Probable reasons for this are twofold. The population data were derived from fitted cumulative normal crystal size distributions and hence are necessarily less accurate than if crystal numbers were determined directly by an 'in situ' particle counting technique. The scatter also reflects the variability in experimental conditions

TABLE 10.7

Results from Fitting Crystal Population-Time Data to Agglomeration Model

Experimental Series	Average Population (-)	Population After Initial 'Burst' of Nucleation (P_o) (-)	Duration of Initial 'Burst' of Nucleation (t_o) (s)	Agglomeration Rate Constant (λ) (1/s)	Coagulation Time (T*) (s)
A	5.841×10^{8}	5.841×10^{8}	0.0	0.000	0.0
D	1.816×10^{7}	4.885×10^{9}	245.7	8.696×10^{-11}	4.7
E	6.233×10^{7}	6.233×10^{7}	0.0	0.000	0.0
F	4.875×10^{6}	3.514×10^{7}	129.8	4.730×10^{-11}	1203.4
G	4.031×10^{7}	1.065×10^{10}	463.9	3.146×10^{-11}	6.0

between individual batch crystallisation experiments, particularly the state of the solution when nucleation occurred.

10.7.2 The Type of Nucleation

In most precipitations, heterogeneous nucleation occurs at low supersaturations. However, when supersaturation is sufficiently high, homogeneous nucleation occurs and increases rapidly thereafter with increasing supersaturation. Heterogeneous nucleation has been found to predominate at low supersaturations, during precipitation of many different sparingly soluble salts by direct mixing of appropriate reagents (123-126,300). In particular, this has been observed in the precipitation of barium chromate, both by direct mixing of reagents (123,126), and by precipitation from homogeneous solution employing urea hydrolysis (124). Walton (129) and Packter et al (300) have suggested that heterogeneous nucleation takes place onto microscopic particles of foreign matter present in most solutions. The number of such heteronuclei normally present in aqueous solution is considered to be between 10^9 and 10^{11} per dm^3 (129). Thus, it is likely that precipitation processes yielding fewer particles in the product than this, have undergone heterogeneous nucleation. In this respect, it is therefore significant that for each series of batch crystallisations the average population is below 10^9. Furthermore, Packter and Alleem (123) have found that at pH values

below 5, heterogeneous nucleation predominated in barium chromate precipitation, with crystal numbers being generally of the order of 10^{13} per dm^3. It should be noted that pH was well below 2.5 when nucleation commenced in the present batch crystallisation experiments, and exceeded 5 only towards the end of long duration experiments. Moreover, the technique of precipitation from homogeneous solution produces a gradual build-up of supersaturation, and so, it is unlikely that levels of supersaturation high enough to cause homogeneous nucleation would have occurred in these experiments.

10.7.3 The Agglomeration Phenomenon

The graphs of crystal population against time (graphs 10.13 to 10.17) provide an indication that crystal numbers tend to decrease at longer times. The photographs of crystal products presented in Chapter 6, reveal that agglomeration does occur, and that there are more agglomerates present in the products from long duration experiments than in those from short period experiments.

The simple agglomeration model could not be fitted to the data from experimental series A and E (see graphs 10.13 and 10.15, respectively). These series of experiments were carried out at $100^{\circ}C$. A rough fit of the model was obtained for the other experimental series, but the scatter of the experimental data does prevent any firm conclusions being

drawn. However, the results presented in table 10.7 indicate that the agglomeration rate constant was of the order of 10^{-11} 1/s, and the duration of nucleation was of the order of hundreds of seconds, comparable in magnitude to the 'induction times' derived from the empirical crystal mass lines and presented in table 10.1.

Microscopic observation of crystal products provided an indication that agglomeration was perhaps of greater significance in longer duration experiments. However, it would be expected that the opposite effect of crystal breakage would also be prominent in such experiments, thereby tending to retard agglomeration. Firm conclusions on the relative importance of phenomena such as nucleation, agglomeration and crystal breakage during the course of a batch crystallisation would require 'in situ' monitoring of crystal numbers, in specific size ranges over a wide band.

10.7.4 The Assumptions on Nucleation and Agglomeration

Crystal growth of barium chromate, during batch crystallisation by precipitation from homogeneous solution, has been modelled in ensuing sections of this chapter on the assumptions that nucleation is limited to an initial 'burst' of short duration, and that the effect of secondary growth phenomena (3) are not separately considered.

Graph 10.15 for experimental series E, and, to

a lesser extent graph 10.13 for series A, provide some evidence for an increase in crystal numbers during the early stages of the batch process. Nevertheless, there appears to be no firm evidence for a continuing increase in population during the whole of the process in any series. Thus, given the poor quality of the population data, as well as the existence of 'induction periods' (as discussed in section 10.3), the conclusion that nucleation is restricted to a finite initial period, is considered reasonable.

Some agglomeration does occur in the course of the crystallisation. However, as indicated previously, separate consideration of this effect requires direct experimental monitoring of crystal numbers. Furthermore, there was some evidence that agglomeration became prominent principally at longer times. Thus, this and other secondary growth phenomena, such as Ostwald ripening, have not been separately considered in the analysis of crystal growth which follows. Therefore, the term for crystal growth rate will include any contributions from these forms of secondary growth. However, Ostwald ripening has been shown to be a slow process for sparingly soluble salts (3), and is unlikely to have made a major contribution to the growth rate.

10.8 MODELLING CRYSTAL GROWTH RATE

10.8.1 Computational Aspects

The empirical, power law type model for crystal growth rate, which was presented in Chapter 9 (section 9.3), was fitted to the results from each experimental series, using the same comprehensive quasi-Newton non-linear optimisation algorithm (267) that was used to fit an empirical curve to the pH-time data, and to fit an agglomeration model to the crystal population-time data. This algorithm takes the form of a library routine named E04KBF, from the program library of the Numerical Algorithms Group (NAG) (301), which was incorporated into a program written in Fortran IV to carry out the optimisation. This program is called TOTE, and is listed in Appendix 16. The program was run on a Harris 500 computer.

The optimisation program TOTE incorporated a number of additional features to facilitate the fitting process and to permit appropriate selection of model parameters. The objective function for optimisation was formulated as a least squares function (201) in crystal growth rate per unit surface area, and the optimisation procedure was streamlined by scaling this objective function as well as the model parameters. The NAG library routine E04KBF had provision for setting bounds on the model parameters and also permitted imposition of constant values on one or more of the parameters. The choice of variables to be included in the power law model for growth rate per

unit surface area, was made by setting appropriate optional flags during compilation of the program TOTE. These options are explained by comment statements in the program listing given in Appendix 16.

10.8.2 Preliminary Modelling

Since the five independent series of experiments were each carried out at a constant stirrer speed and a constant temperature, the variables initially considered in the power law model were crystal size, hydrogen ion activity and supersaturation driving force. In the notation used in Chapter 9, growth rate per unit surface area was thus given by,

$$R_G = k_1(a_{H^+})^{k_2}(L)^{k_3}(\Delta C_t)^{k_4} \quad \ldots\ldots\ldots\ldots \quad (10.21)$$

In this model, the characteristic size, L, was taken to be the mass mean equivalent volume diameter of the crystal population. The experimental data from each series was separately fitted to this model, and the model parameters k_1, k_2, k_3 and k_4 were derived from the optimisation process. The optimum values of the model parameters are presented in table 10.8. The mean square about the regression ($\bar{y}$), which is tabulated in table 10.8, is defined by,

$$\bar{y} = \sum_{p=1}^{i} \frac{(R_{G(\text{calculated})} - R_{G(\text{experimental})})^2}{(i - 1 - j)} \quad \ldots\ldots\ldots\ldots\ldots\ldots \quad (10.22)$$

TABLE 10.8

Preliminary Results of Modelling Crystal Growth Rate

Experimental Series	Optimum Values of Model Parameters in Equation 10.21				Mean Squares About Regression ($\times 10^{11}$)
	$k_1(\times 10^2)$	$k_2(\times 10^1)$	$k_3(\times 10^5)$	k_4	
A	7.049	-4.776	0.859	1.996	13.297
D	2.913	-4.270	0.723	1.980	1.864
E	5.792	-3.870	0.992	1.999	1.792
F	0.577	-5.590	0.993	1.999	0.187
G	2.523	-4.128	1.122	2.012	1.269

where, i is the number of data points; j is the number of parameters in the model; $R_{G(calculated)}$ is the growth rate per unit surface area calculated from the model; and, $R_{G(experimental)}$ is the experimental growth rate per unit surface area.

10.8.3 Main Modelling

As can be seen from table 10.8, preliminary modelling of crystal growth rate per unit surface area revealed that the exponent for crystal size (k_3), had a very low optimum value for each experimental series. In addition, the exponent for driving force (k_4), had an optimum value which was close to 2 for each series. Therefore, it was decided to refine the modelling process by removing the crystal size term in the power law model and setting the exponent of driving force to 2. This yielded the modified model:

$$R_G = k_1 (a_{H^+})^{k_2} (\Delta C_t)^{k_4} \quad \ldots\ldots\ldots\ldots\ldots\ldots \quad (10.23)$$

with the proviso that $k_4=2$. The experimental data sets were reanalysed on this basis and yielded results which are presented in table 10.9.

As can be seen from table 6.1 of Chapter 6, the only difference in the experimental conditions of series D and G is the stirrer speed. Thus, the data from these two series were combined and fitted to a power law type model expanded to include the effect of stirrer speed, w.

TABLE 10.9

Main Results of Modelling Crystal Growth Rate (Using Falangas's (5) Solubility Data)

Experimental Series	Optimum Values of Model Parameters in Equations 10.23 and 10.24				Mean Squares About Regression ($\times 10^{11}$)
	$k_1 (\times 10^2)$	$k_2 (\times 10^1)$	k_4 (fixed)	$k_5 (\times 10^6)$	
A	7.190	-4.785	2.00	-	7.989
D	3.191	-4.291	2.00	-	1.459
E	5.798	-3.874	2.00	-	1.568
F	0.578	-5.593	2.00	-	0.170
G	2.397	-4.124	2.00	-	1.076
D+G	2.297	-4.443	2.00	9.97	2.821

i.e. $R_G = k_1(a_{H^+})^{k2}(\Delta C_t)^{k4}(w)^{k5}$ ..... (10.24)

These results are also included in table 10.9. The results of optimisation are presented graphically in graphs 10.18 to 10.23. These graphs have been produced by the optimisation program TOTE. The results given in table 10.9 were obtained using driving force values calculated using Falangas's (5) solubility data, in the manner described previously in section 10.5.5. Driving force has also been calculated on the basis of Skander's (4) solubility data. These alternative values for driving force were similarly used in fitting the power law models represented by equations 10.23 and 10.24. The results thus obtained are presented in table 10.10.

10.8.4 Mean Linear Growth Rate

The mean linear growth rate, $\bar{G}$ was defined in Chapter 9 (section 9.2), and was expressed in terms of the growth rate per unit surface area.

i.e. $\bar{G} = R_G/\rho$ ..... (10.25)

Since the crystal density ρ is effectively a constant, expressing the empirical models for crystal growth rate in terms of the mean linear growth rate would only result in changes to those optimum values of the model parameter k_1, presented in tables 10.9 and 10.10. The optimum values for k_1 would then be divided by the density of barium chromate (i.e. 4500 kg/m^3).

GRAPH 10.18 Results of fitting Empirical Model for Crystal Growth Rate to Experimental Series A

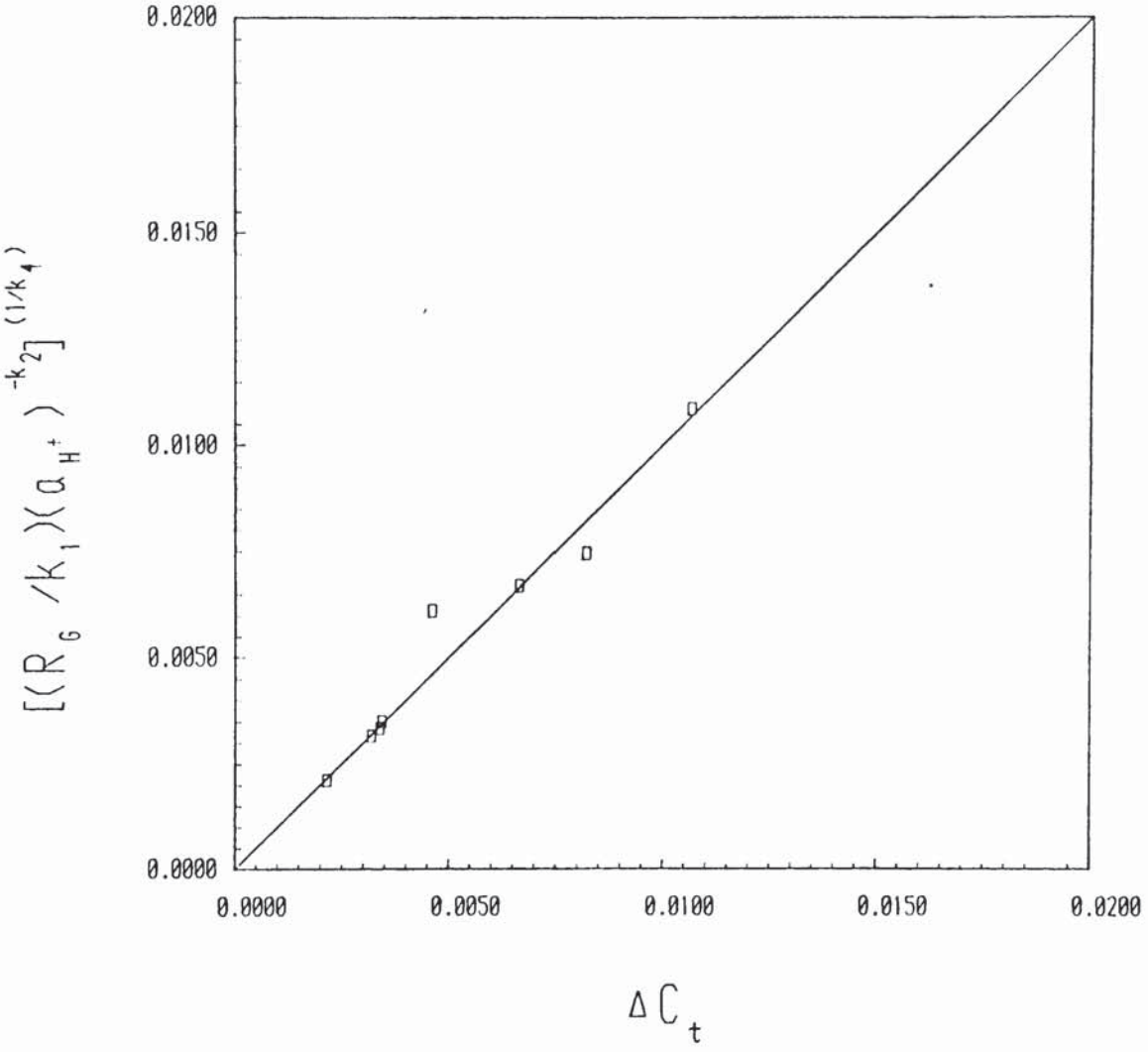

GRAPH 10.19 Results of Fitting Empirical Model for Crystal Growth Rate to Experimental Series D

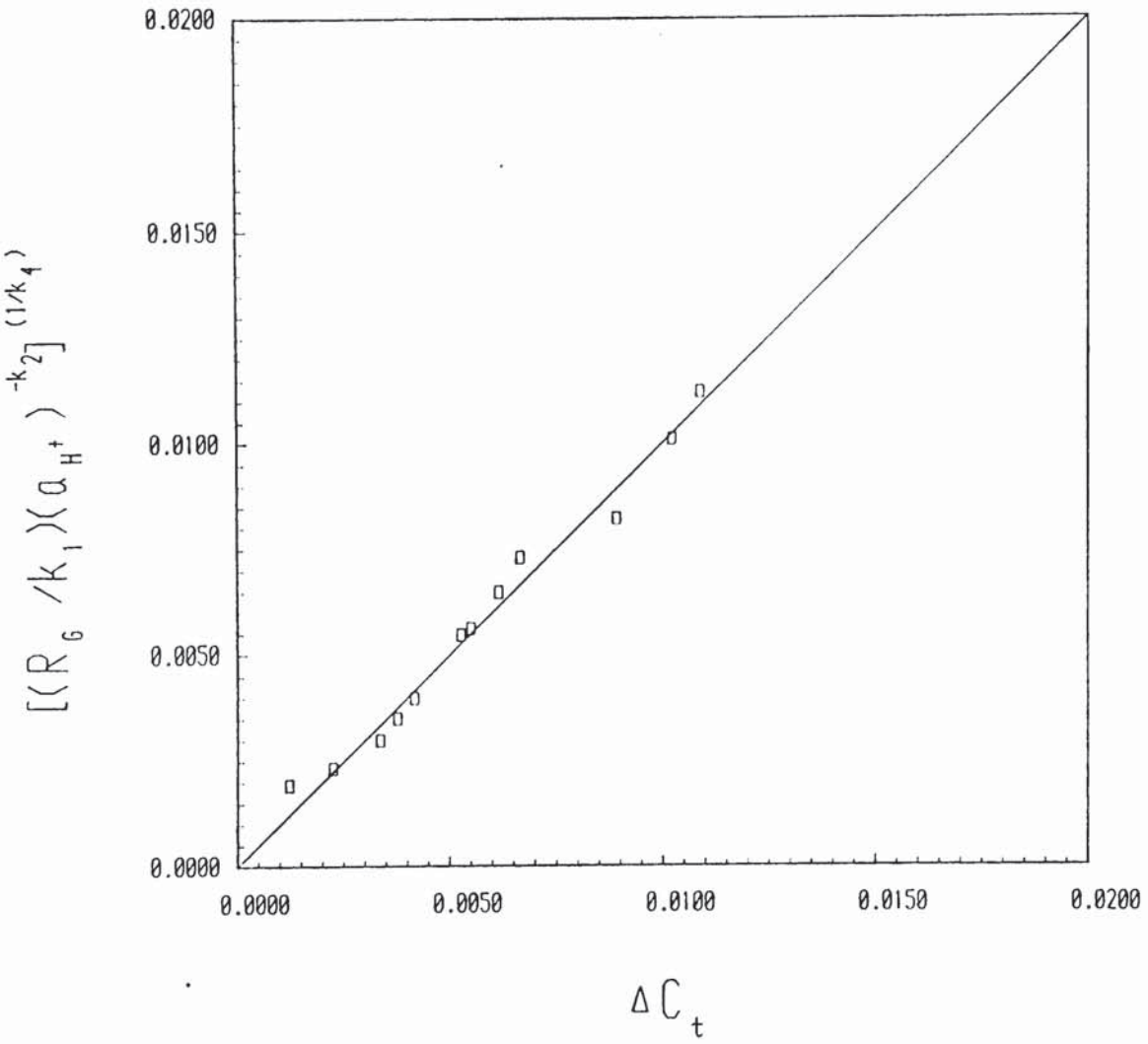

GRAPH 10.20 Results of Fitting Empirical Model for Crystal Growth Rate to Experimental Series E

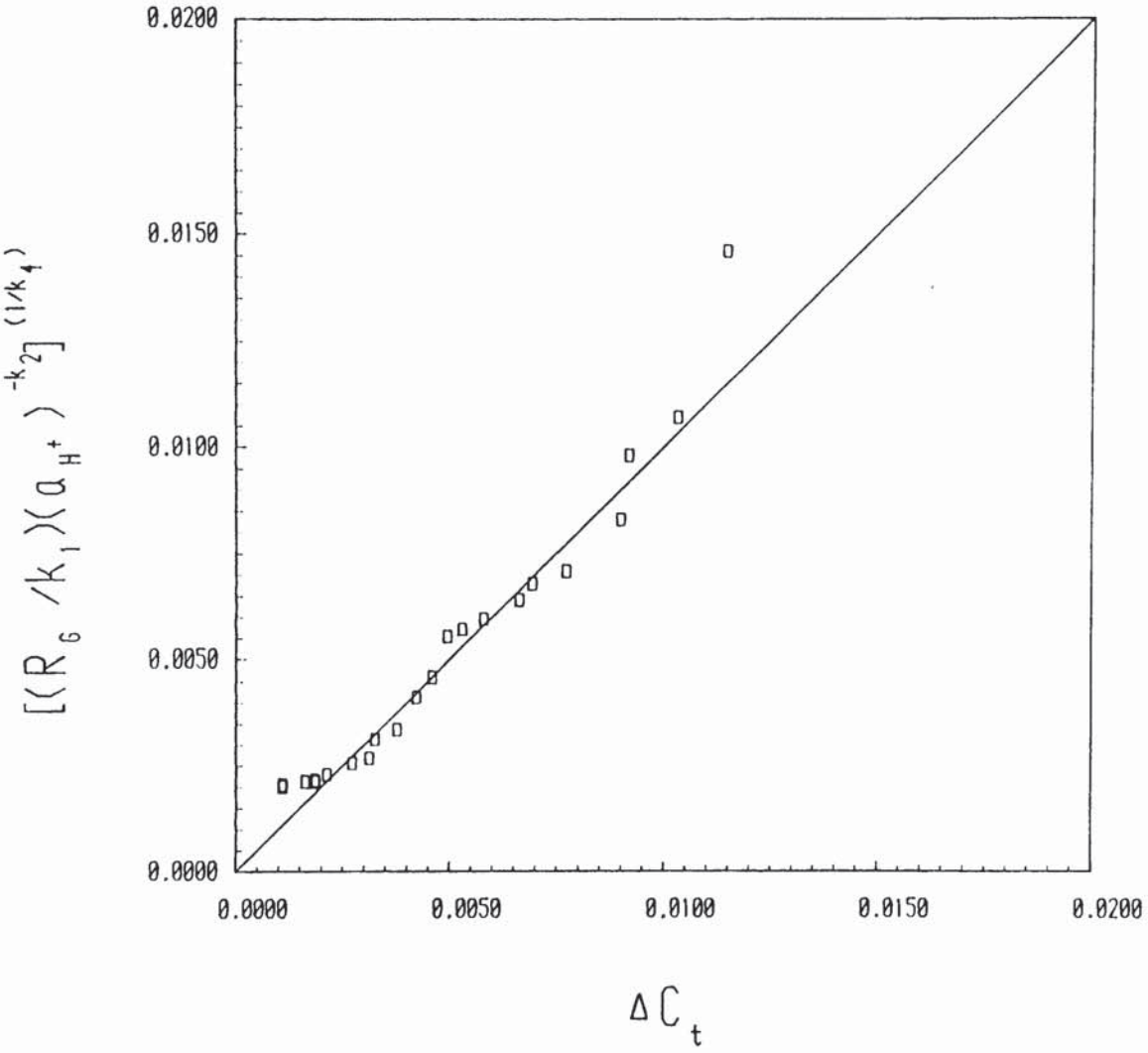

GRAPH 10.21 Results of Fitting Empirical Model for Crystal Growth Rate to Experimental Series F

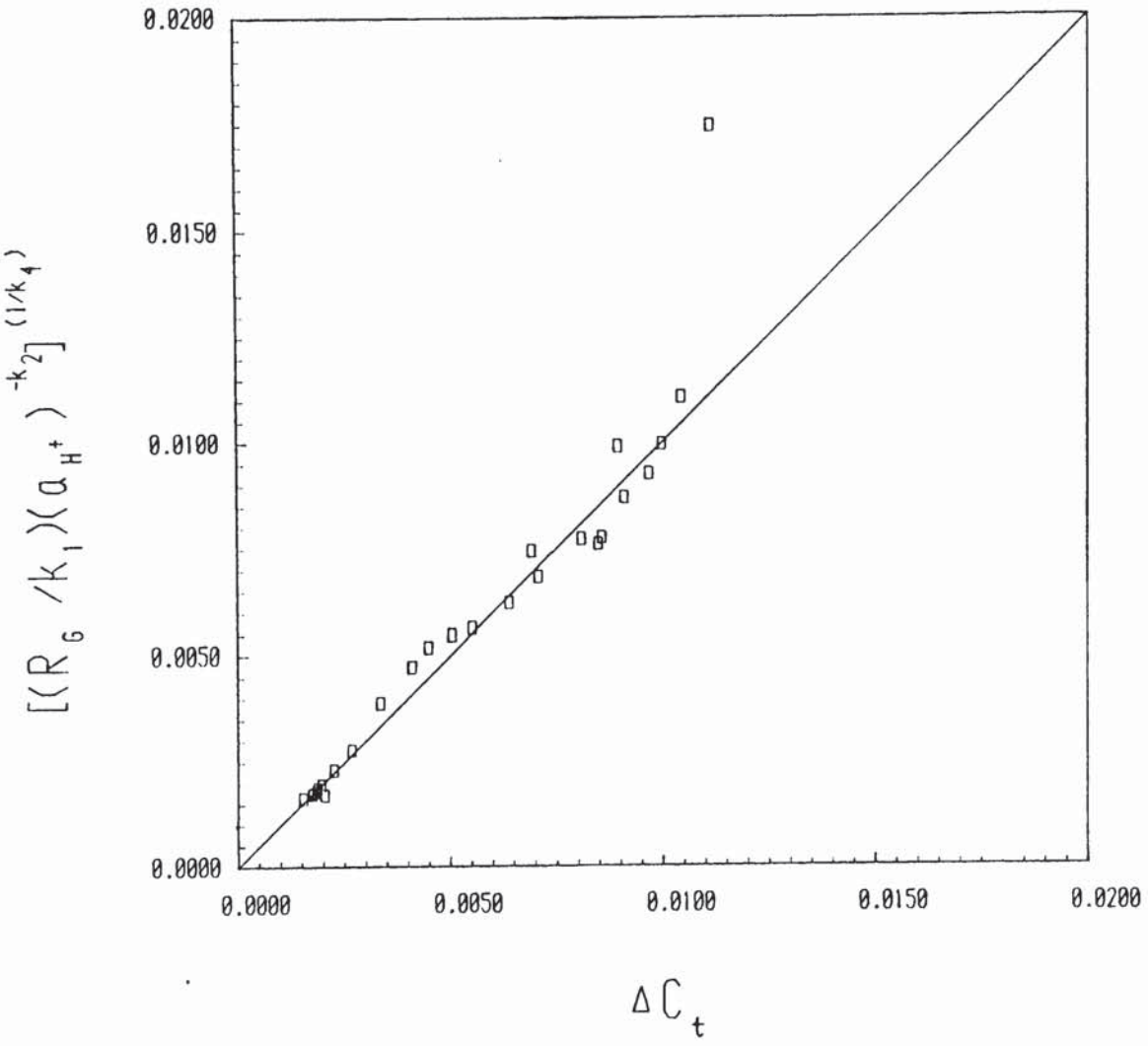

GRAPH 10.22 Results of Fitting Empirical Model for Crystal Growth Rate to Experimental Series G

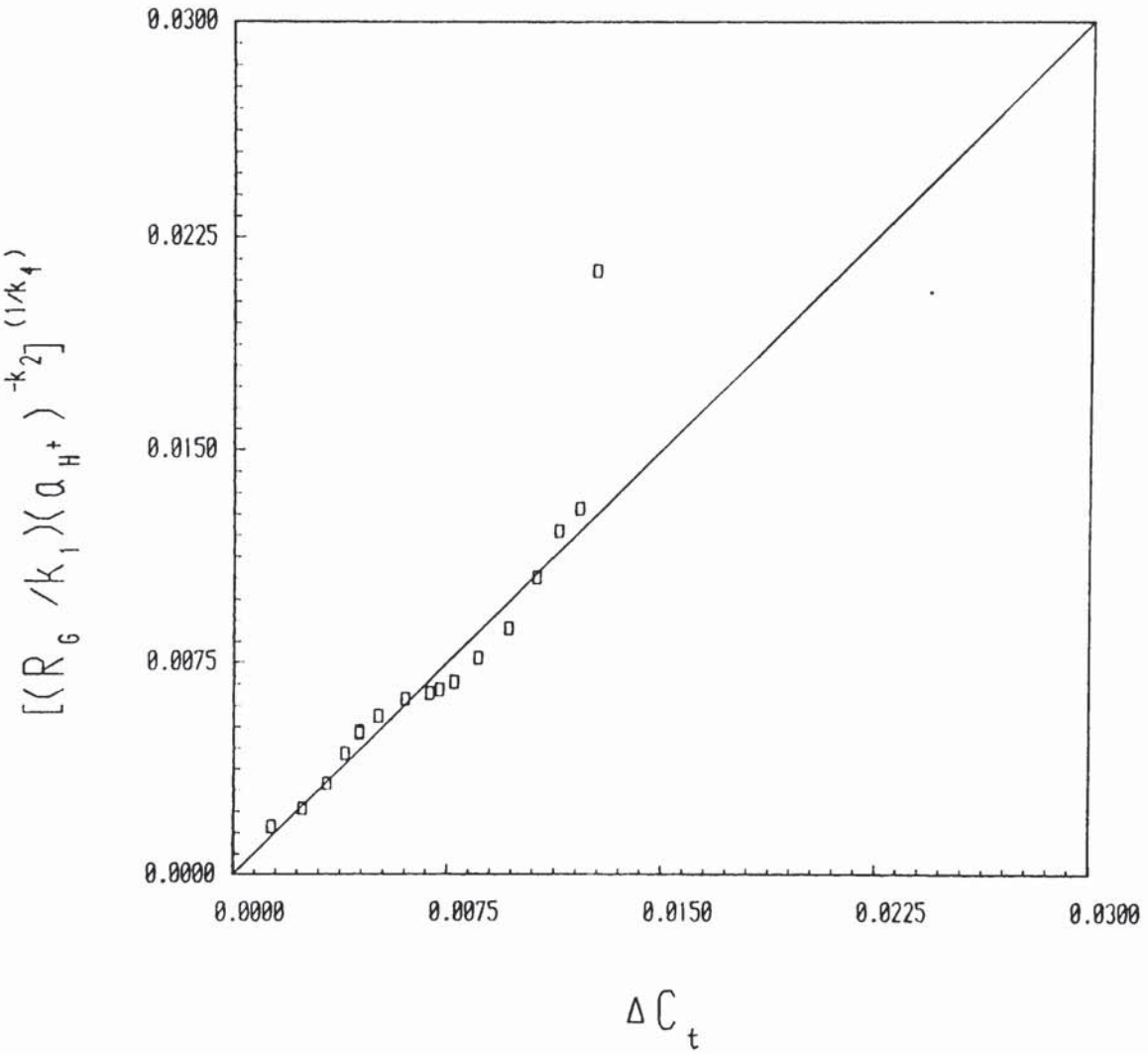

GRAPH 10.23 Results of Fitting Empirical Model for Crystal Growth Rate to Experimental Series D and G in Combination

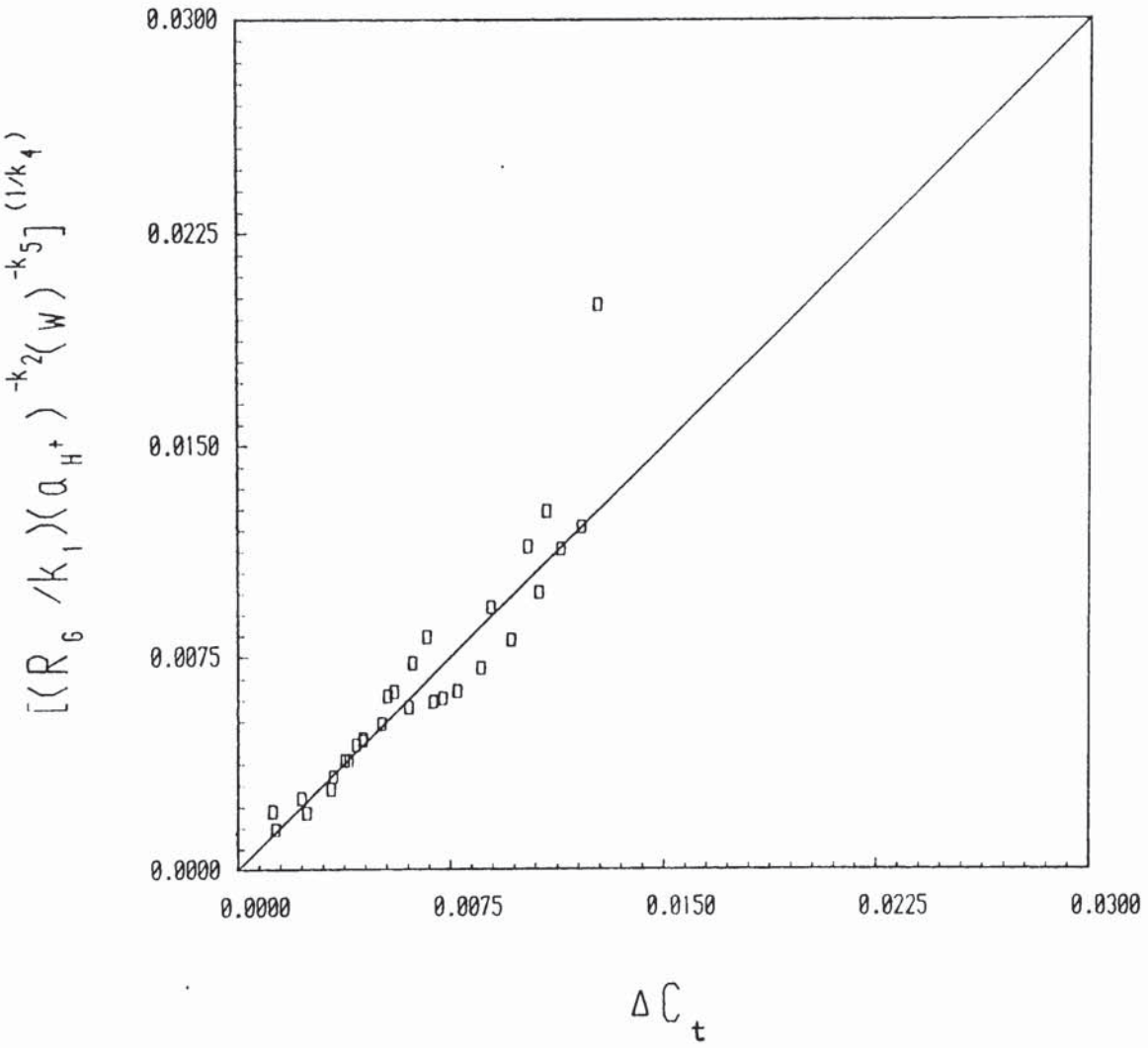

TABLE 10.10

Results of Modelling Crystal Growth Rate Using Skander's (4) Solubility Data

Experimental Series	Optimum Values of Model Parameters in Equations 10.23 and 10.24				Mean Squares About Regression ($x10^{11}$)
	$k_1 (x10^1)$	$k_2 (x10^1)$	k_4 (fixed)	$k_5 (x10^7)$	
A	3.464	-3.450	2.00	-	23.664
D	0.790	-3.469	2.00	-	1.861
E	2.647	-2.460	2.00	-	2.127
F	0.142	-4.831	2.00	-	0.203
G	0.489	-3.573	2.00	-	1.067
D+G	0.502	-3.787	2.00	9.99	3.178

These altered values for k_1 are given in table 10.11.

10.8.5 Estimation of Activation Energies for Crystal Growth

The temperature dependence of crystal growth has been found to be given by an Arrhenius type relation in many cases (9). Application of such an expression to the present analysis leads to an expansion of the model parameter k_1, which may then be represented by,

$$k_1 = A_a \exp(-E/RT) \quad \ldots\ldots\ldots\ldots\ldots\ldots \quad (10.26)$$

where, A_a is a constant pre-exponential factor; E is the activation energy for crystal growth; R is the universal gas constant; and, T is the absolute temperature.

Since the batch crystallisation experiments were carried out at two different temperatures (i.e. $90^{\circ}C$ and $100^{\circ}C$), the relevant optimum values of the parameter k_1 can be used to estimate the activation energy.

$$\text{i.e.} \qquad E = \frac{R \ln(k_{1(1)}/k_{1(2)})}{(\frac{1}{T_2} - \frac{1}{T_1})} \quad \ldots\ldots\ldots \quad (10.27)$$

where, $k_{1(1)}$ and $k_{1(2)}$ are the optimum values of the model parameter k_1 at temperatures T_1 and T_2 respectively, with $T_1 > T_2$. Values obtained for activation energy are tabulated in table 10.12. In calculating activation energy, the values of k_1 corresponding to an operating temperature of $90^{\circ}C$ and an initial urea mass of 20 g, were taken to be the optimum values obtained by fitting the combined experimental results of series D and G,

TABLE 10.11

Optimum Values of Model Parameter k_1

Experimental Series	Optimum Values of Model Parameter k_1			
	Driving Force Based on Falangas's Solubility		Driving Force Based on Skander's Solubility	
	Model Based on R_G	Model Based on $\bar{G}$	Model Based on R_G	Model Based on $\bar{G}$
A	7.190×10^{-2}	1.598×10^{-5}	3.464×10^{-1}	7.698×10^{-5}
D	3.191×10^{-2}	0.709×10^{-5}	0.790×10^{-1}	1.756×10^{-5}
E	5.798×10^{-2}	1.288×10^{-5}	2.647×10^{-1}	5.882×10^{-5}
F	0.578×10^{-2}	0.128×10^{-5}	0.142×10^{-1}	0.316×10^{-5}
G	2.397×10^{-2}	0.533×10^{-5}	0.489×10^{-1}	1.087×10^{-5}
D+G	2.297×10^{-2}	0.510×10^{-5}	0.502×10^{-1}	1.116×10^{-5}

TABLE 10.12

Activation Energies for Crystal Growth

Initial Mass of Urea Used in Batch Crystallisation (g)	Activation Energies (kJ/mol)	
	Driving Force Based on Falangas's Solubilities	Driving Force Based on Skander's Solubilities
20	128.5	217.4
10	259.6	329.3

to the empirical model given by equation 10.24. Also, values of k_1 corresponding to an operating temperature of 100°C and an initial urea mass of either 10 or 20 g, were taken to be the optimum values obtained by separately fitting the results of each of the other experimental series, to the empirical model given by equation 10.23. Activation energy was found to be dependent on the initial mass of urea.

10.9 DISCUSSION OF RESULTS OF MODELLING CRYSTAL GROWTH RATE

10.9.1 The Optimisation Technique

The desirable attributes of a non-linear optimisation method are rapid convergence to a solution at which the gradient vector of the model parameters has a very low value and the Hessian matrix is positive definite; and, provision for overcoming the problems of premature convergence (267,301-303). Murray (303) has pointed out that second derivative and quasi-Newton methods are more likely to satisfy these requirements than gradient, conjugate direction or direct search methods.

The quasi-Newton algorithm of Gill and Murray (267) which was used to fit empirical models to crystal growth rate (and also used for other fitting procedures, as described earlier), had several specific advantages that recommended its use in preference to a second derivative method. The algorithm employed a positive definite approximation to the second derivative Hessian

matrix (301), thus requiring only the first derivatives of the objective function relative to the model parameters, to be supplied. Hence, the problem that besets second derivative methods, of computational accuracy affecting the Hessian matrix and rendering it singular close to the minimum, was circumvented. Furthermore, the NAG library routine which incorporated this algorithm had provision for a local search to be carried out if premature convergence, as in the case of a saddle point, occurred (301). This helped overcome the problem of false convergence. Moreover, the routine was structured so that scaling of model parameters and objective function was facilitated. In all cases scaling was carried out so that the scaled values of the model parameters and the objective function were of the same order of magnitude at the minimum. This modification helped to reduce the problem of convergence to an incorrect solution. In general quasi-Newton methods are susceptible to premature convergence (302), and therefore, the optimisation routine had incorporated in it multiple stopping criteria designed to surmount these difficulties (301).

When used for modelling crystal growth rate, the quasi-Newton algorithm proved very robust. Provided suitable scaling had been applied and a practical starting point chosen, the method invariably converged rapidly to a unique solution from a number of different starting points.

10.9.2 Results Using Different Driving Force Values

Driving force was calculated on the basis of two different solubility correlations derived from the solubility data of Falangas (5) and Skander (4) respectively. Results of modelling crystal growth rate using these different estimates for driving force were presented in tables 10.9 and 10.10. It can be seen from these tabulations that in general a better fit, as measured by the mean square about regression, was obtained when driving force was based on Falangas's data. For experimental series G alone, the mean square about regression was approximately the same for each case. Furthermore, Falangas's solubility data (5) were obtained in acidic solutions containing urea, and this resembled more closely the conditions prevailing during crystallisation, than did the experimental conditions under which Skander's solubility data (4) were derived. Therefore, it was concluded that, modelling growth rate on the basis of driving force values calculated using a solubility correlation based on Falangas's data, was more appropriate and resulted in a significantly better fit.

10.9.3 Graphical Results

Results of modelling crystal growth rate were presented graphically for each experimental series, in graphs 10.18 to 10.22. These graphs correspond to the optimum model parameter values presented in

table 10.9. The graphs reveal several important features. Graphs 10.20, 10.21 and 10.22, for experimental series E, F and G respectively, show that the initial data point, at the highest supersaturation (ΔC_t) in each of the experimental series, does not fit the empirical growth rate model. In carrying out the optimisation these abnormal data points were excluded. The anomalies are almost certainly due to nucleation still taking place at the times corresponding to these data points. Therefore, growth rate derived on the assumption that nucleation rate was negligible would tend to yield too high a value, which in turn would result in an overestimate of the combination of variables plotted on the y-axis of each of the graphs. This is bourne out by the position of these initial data points on the relevant graphs.

A further feature, shown by graphs 10.19 and 10.20, for experimental series D and E respectively, is that there is a slight tendency of the data points to diverge from the model at low supersaturations. This was probably due to the greater uncertainty in the supersaturation when both solute concentration (C_t) and solubility (C_e) took on low values. In addition, as pointed out in section 10.3, the empirical relations for solubility tend to underestimate solubility at pH values above about 4.5. The divergent data points at low supersaturations corresponded to pH values greater than 4.5, and hence this could also have been a factor.

In general, all the graphs revealed that the modelling process had produced a reasonable fit for each series. The observed deviations of the data points from the models are considered to be mainly due to the errors caused by experimental conditions not being identical for each batch crystallisation experiment in a given series.

10.9.4 The Effect of Hydrogen Ion Activity

The empirical models used for crystal growth rate each included a power law term for hydrogen ion activity. Fitting the different sets of experimental data to these models, consistently yielded a negative, fractional value for the exponent (k_2) of the hydrogen ion activity term. Optimum values for the exponent k_2 lay in the range -0.56 to -0.39. The significance of this negative exponent is that at higher hydrogen ion activities (and hence, concentrations), growth rate per unit surface area (R_G), and mean linear growth rate ($\bar{G}$), is reduced. This effect can be explained in terms of a surface reaction, or surface integration, controlled process for crystal growth. At high hydrogen ion activities there would be an increased adsorption of hydroxonium ions (H_3O^+), or hydrated hydroxonium ions, at active sites on the growing crystal-solution interface. This would hinder the surface integration process and thereby cause a reduction in growth rate. In general, the effects of impurity ions on crystal habit and growth

rate in many different systems, have been explained in terms of this type of adsorption mechanism (304). In particular, the effect of pH on crystal growth has been similarly attributed to the adsorption of hydrated hydrogen ionic species, in experimental investigations of crystal habit modification and single crystal growth, by Davey and Mullin (70) and by Pazourek (69).

The range of optimum values obtained for the exponent k_2, though narrow, is probably a real effect since different urea contents and temperatures would be expected to affect the hydrogen ion activity. However, it was not considered feasible to quantitatively account for these effects.

10.9.5 The Effect of Supersaturation

The empirical models for crystal growth rate included a power law term for supersaturation. Preliminary modelling of the individual data sets resulted in values for the exponent (k_4) of the supersaturation term, which were all close to 2. These results were given in table 10.8. Subsequent modelling carried out with this exponent set to a fixed value of 2, yielded the results presented in table 10.9. Comparison of the mean squares about regression for each experimental series, in these two tables, reveal that setting k_4 to 2 actually reduces the mean squares for series A, D and E, while only a slight increase in mean squares occurs for

series F and G. It was therefore concluded that a supersaturation dependence of order 2 for crystal growth rate, provided an adequate fit.

This type of supersaturation dependence is termed a parabolic rate law. Nielsen (305) has shown that at low supersaturations, such as those that prevailed in this study, a parabolic rate law is indicative of a surface integration controlled process, with the rate determining step involving the transfer of growth units from the solution, or from an adsorption layer, to the growth step or to a growth site on a step. Parabolic rate laws have been observed for many sparingly soluble substances at low supersaturations (8,305). Alkaline earth sulphates (131,133,261,290,291), calcium phosphates (136), lead sulphate (261), calcium oxalate (296) and silver chloride (292), have all been found to exhibit a parabolic supersaturation dependence of growth rate. In particular, the precipitation of barium chromate from both acidic and neutral solutions, with either slow or rapid development of supersaturation, has been found to be represented by this form of parabolic growth rate law (120,122,123). The current results for the growth rate of barium chromate are thus in good agreement with the results of previous investigations and are indicative of a surface controlled growth process.

10.9.6 The Effect of Stirrer Speed

An empirical model for crystal growth rate, which included a power law term for stirrer speed (in r.p.m.), was fitted to the combined data from experimental series D and G, which differed in their experimental conditions only in the stirrer speed used. The optimum value for the exponent (k_5) of the stirrer speed term was found to be less than 10^{-5} (see table 10.9). Hence, it appears that crystal growth rate is effectively independent of stirrer speed. A bulk diffusion controlled growth process would have shown a definite stirrer speed effect (9,14,306). Thus, this result is further evidence that the crystal growth of barium chromate is a surface integration controlled process, unaffected by crystal-solution relative velocity.

10.9.7 The Effect of Crystal Size

Preliminary modelling of crystal growth rate was done using a model which included a power law term for crystal size, with the mass mean equivalent volume diameter chosen as the characteristic dimension of the crystal populations. The optimum value for the exponent (k_3) of the crystal size term was approximately 10^{-5} for each experimental series, thereby indicating that crystal size had no effect on growth rate. Therefore, the crystal size term was dropped from the empirical models in subsequent analyses.

The mass mean equivalent volume diameter has

been commonly employed to characterise crystal size (5,59,239-241,245). However, it has been pointed out that the mean equivalent volume diameter on a number basis is a more logical and sounder basis for characterising crystal size distributions, provided a direct particle counting technique is employed to determine the distributions (307). Nevertheless, it was considered unlikely that use of mean equivalent volume diameters on a mass basis, would have masked an existing size dependence of growth rate.

The observed size independence of crystal growth rate has a further significance in that, if a secondary growth process such as agglomeration or ripening (3) had made a significant contribution to overall growth, it would have been expected that this would have manifested itself in some form of size effect on growth rate. The absence of such an effect indicates that such secondary growth processes are probably not of critical importance in the analysis of crystal growth rate.

10.9.8 Activation Energy and the Rate Determining Step

Estimates for the activation energy for crystal growth were obtained from the optimum values of the growth rate model parameter, k_1. These estimates have been presented in table 10.12. The activation energy appears to be relatively high, being greater than 100 kJ/mol, and is markedly dependent upon the

quantity of urea used to carry out the process of precipitation from homogeneous solution, with activation energy approximately halved by a doubling of the mass of urea initially taken.

Values of activation energy for surface controlled growth processes have been found to be usually in excess of 40 kJ/mol (8,9,132,135,261,296,299,308), while activation energies of diffusion processes normally lie in the range 10 to 20 kJ/mol (308). Therefore, the calculated activation energies constitute additional evidence that crystal growth of barium chromate is surface integration controlled.

The activation energies for crystal growth of a number of sparingly soluble sulphates have been found to be related to the degree of hydration of the cation of the salt, with the salt having the least cation hydration showing the lowest activation energy (261). This has been explained on the basis that the rate determining process is the dehydration of the cation, with the rate of the corresponding process for the anion being much larger, and hence not rate determining (261,305). Reich and Kahlweit (309) have presented a theoretical model for crystal growth from aqueous solution, on the assumption that dehydration of cations at kink sites on the crystal surface is the rate determining step. The theory was found to satisfactorily account for growth rate at low super-saturations, of thallium bromide (310), the alkaline earth oxalates (310) and calcium sulphate (295). It

is significant that, at low supersaturations, this theory yields a parabolic supersaturation dependence for growth rate, with supersaturation expressed in terms of concentrations of the cation. This is in accord with the current results obtained for crystallisation of barium chromate. Furthermore, the effect of urea concentration on the activation energy can be explained on the basis of cation dehydration. An increased urea concentration gives the solution a higher dielectric constant. This in turn reduces the solvation energy and hence facilitates the dissolution of ionic solids, but it also means that the energy barrier for the reverse process of ion dehydration is reduced as well. Thus, if cation dehydration was the rate determining step, the result would be a decrease in the activation energy for crystal growth when a higher urea content was used. However, the effect of urea content is not a direct one, because the dielectric constant for the bulk solution is not applicable in the immediate vicinity of the ions, where the intense electric field is believed to cause dielectric saturation, so that the effective dielectric constant is reduced (185). Therefore, the approximate halving of activation energy, from 259.6 kJ/mol to 128.5 kJ/mol, when the initial mass of urea taken was doubled from 10 to 20 grammes, is entirely fortuitous.

Eigen and Maas (311) have used a sound absorption relaxation method to examine the kinetics of substitution of water molecules in the primary

hydration shell of alkali metal and alkaline earth ions, including the barium ion. The rate constant for the barium ion was reported as 7.2×10^8 1/s at $20^{\circ}C$ (311). Nielsen (305) has suggested a method for calculating the activation energy for the removal of a water molecule from the inner hydration sphere of a cation, by using this information. If it is assumed that the rate constant for removal of a water molecule can be represented by the Eyring equation (312) for a unimolecular reaction rate constant, it follows that:

$$k_w = (k_o T/h) \exp(-E_H/RT) \quad \ldots\ldots\ldots\ldots\ldots \quad (10.28)$$

where, k_w is the rate constant for removal of a water molecule from the inner hydration sphere; E_H is the molar activation energy for this process; h is Planck's constant; k_o is the Boltzmann constant; R is the universal gas constant; and, T is the absolute temperature. Equation 10.28 can be rearranged to give:

$$E_H = RT \ln(k_o T/hk_w) \quad \ldots\ldots\ldots\ldots\ldots\ldots \quad (10.29)$$

The rate constant given by Eigen and Maas (311) for the barium ion can be used to estimate E_H. The results are activation energy values of 28.8 and 27.9 kJ/mol at temperatures of $100^{\circ}C$ and $90^{\circ}C$ respectively. Now, the number of water molecules constituting the primary hydration sphere of an ion is termed its hydration number. Unfortunately, different methods of determining hydration number yield different results (185,313). For the barium ion, theoretical

and experimental investigations have produced values of hydration number from as low as 4 to as high as 11 (314-319). However, the results of Padova (315) and the discontinuous model for hydration of monoatomic ions, of Muirhead-Gould and Laidler (316), indicate that the barium ion probably has an octahedral primary hydration shell. Thus, if a value of 28.5 kJ/mol is taken for the activation energy to remove one molecule of water from the inner hydration shell, and it is assumed that removal of each water molecule in turn entails an energy barrier of similar magnitude, the activation energy for removal of the primary hydration shell of the barium ion would work out to 228 kJ/mol. This value is of the same order of magnitude as those obtained for the activation energy for crystal growth. Therefore, it is likely that cation dehydration is indeed the rate determining step in the crystal growth of barium chromate under the experimental conditions employed.

However, it should be noted that the estimate of 228 kJ/mol for primary hydration shell dehydration energy, involved a number of assumptions. The rate constant for removal of a water molecule was taken to be adequately represented by the rate constant for substitution of one molecule in the inner hydration shell, at 20°C. These two processes do not strictly correspond, and moreover, the operating temperatures were 90°C and 100°C rather than 20°C. In addition, removal of a water molecule in turn from the hydration

shell would probably alter the energy barrier for removing remaining molecules. Thus, this calculated energy for primary dehydration only provides an order of magnitude comparison with the activation energy for crystal growth.

10.10 ANALYSIS OF EXPERIMENTAL DATA OF FALANGAS

10.10.1 Selection of Data

The batch crystallisation experiments carried out by Falangas (5), by the technique of precipitation from homogeneous solution, employed similar conditions to those used in this investigation. However, in the majority of Falangas's experiments, the progress of desupersaturation was followed by sampling the solution. Due to problems with precipitation of barium chromate during the sampling process, Falangas (5) reported that this technique gave rise to considerable error. The alternative 'freezing' method used by Falangas (5) was to carry out a series of experiments, all under the same conditions but having progressively longer durations. These experiments were carried out at 100^{o}C, with an initial hydrochloric acid strength of 0.06M, and an initial mass of urea of 20 grammes. Stirrer speeds of 200, 400 and 800 r.p.m. were employed. Different initial masses of barium chromate of 2, 3, 4, 5 and 10 grammes were used. However, the 5g case was taken to represent standard conditions, and the experiments with different initial masses of barium chromate were assumed to follow the

same desupersaturation curve. This assumption is a weak one, and Falangas's (5) claim that, for example, the 10g case is identical to the 5g case with 5g of crystals present in solution is clearly incorrect, since the effects of differing acidity and urea content, on solubility and supersaturation have been disregarded. In addition, the real and the postulated case would have shown quite different initial nucleation behaviour.

It was decided to reanalyse Falangas's (5) data using the methods employed in the current study, but in view of the shortcomings detailed above, only the data obtained by the 'freezing' method, with an initial mass of barium chromate of 5 grammes, was considered in order to permit relevant comparison with the results presented earlier in this chapter. Falangas (5) has not reported the experimental system volumes, and product crystal surface areas, nor presented all the size distributions. Therefore, a nominal system volume of 1 dm^3 was assumed, and crystal surface areas were derived from reported values of mass mean equivalent volume diameters, subject to certain assumptions. These assumptions, the manner of deriving surface areas, and the collected data of Falangas (5) that were taken for analysis, are presented in Appendix 3.

10.10.2 Analysis of Data

Falangas's experimental crystal mass-time data was fitted empirically to a pair of straight lines by

the technique described in section 10.2. The graphical results of this fitting procedure are presented in graph 10.24 along with the experimental data points. The fitted straight line relations were,

$$m_t = 1.711 \times 10^{-5} t - 9.474 \times 10^{-4}, \text{ for } t < 346.1 \quad \ldots\ldots\ldots\ldots\ldots\ldots \quad (10.30.1)$$

and,

$$m_t = 7.164 \times 10^{-8} t + 4.949 \times 10^{-3}, \text{ for } t > 346.1 \quad \ldots\ldots\ldots\ldots\ldots\ldots \quad (10.30.2)$$

where, the time t is expressed in seconds; and, the crystal mass m_t is expressed in kilogrammes. The correlation coefficients for these two regression lines were found to be 0.982 and 0.996, respectively. These empirical relations were employed in calculating crystal growth rate per unit surface area and supersaturation, by means of equation 10.6 and equations 10.5 and 10.7, respectively. The values obtained are tabulated in Appendix 3.

The main part of the experimental data given in Appendix 3 correspond to a stirrer speed of 800 r.p.m. In addition three data points correspond to 200 r.p.m. and four to 400 r.p.m. The empirical power law type models for crystal growth rate presented in Chapter 9, were fitted separately to the 800 r.p.m. data and to the combined data at all speeds. As indicated by the second of the fitted crystal mass lines, supersaturation and growth rate had decreased to a negligible level at times greater than 346.1 s.

GRAPH 10.24 Graph of Crystal Mass Against Time for Falangas's Experiments

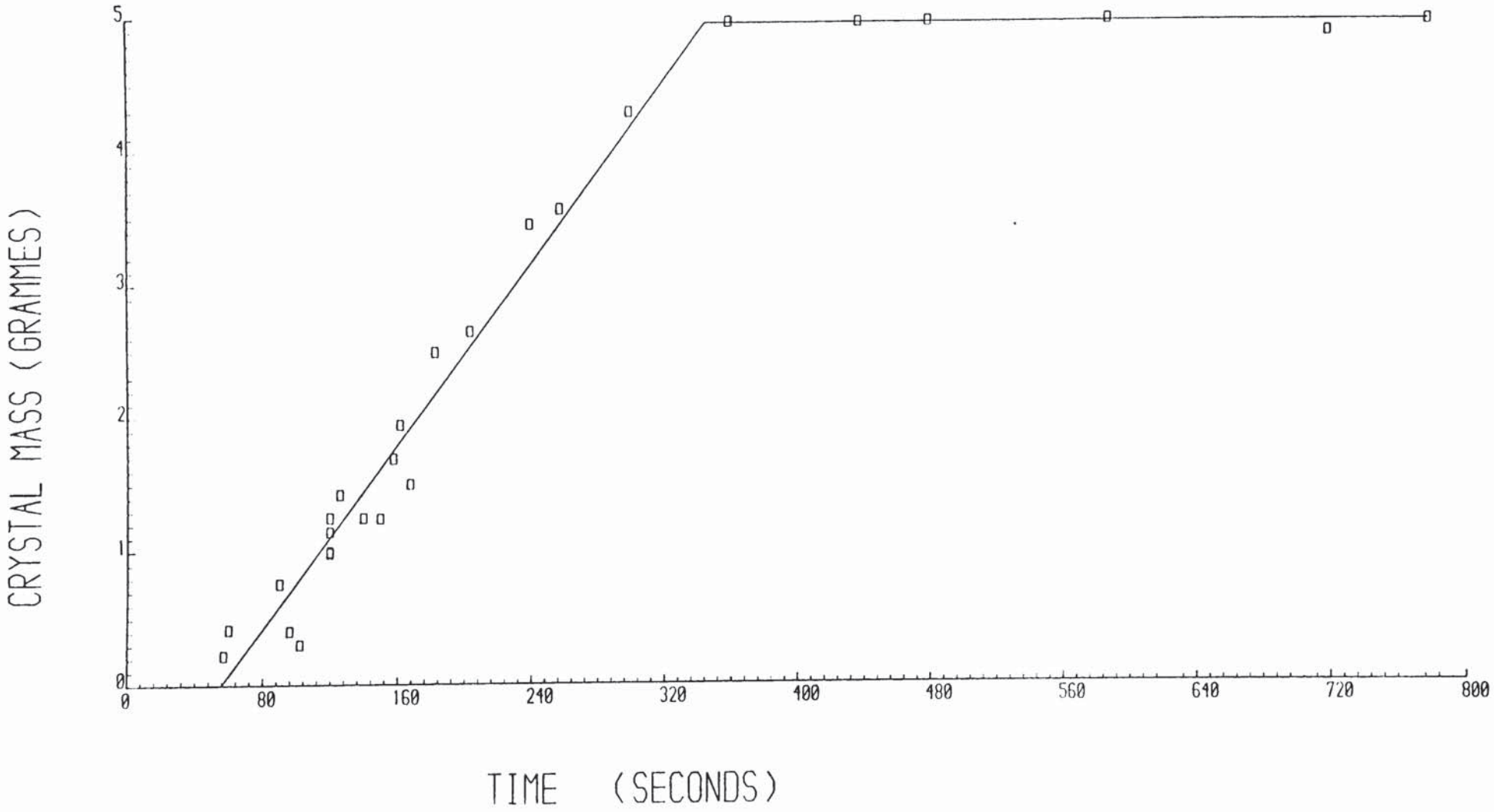

Thus, the data points corresponding to these longer duration experiments were disregarded in the modelling, just as similar data points from the five experimental series of the current investigation, were omitted. Furthermore, the data of the four shortest duration experiments (each lasting for less than 110 s) carried out at 800 r.p.m., were omitted on the grounds that nucleation was still taking place at these short times. For the modelling process, the exponent, k_4, for driving force was set to 2 and a size independent model was chosen in accordance with the approach adopted in section 10.8.3. The computations were carried out by the program TOTE, which has been described in section 10.8.1 and listed in Appendix 16.

The results of this optimisation are presented in table 10.13. Graphs 10.25 and 10.26 depict these results in graphical form.

10.10.3 Discussion of Results

The results, presented in table 10.13 and as graphs 10.25 and 10.26, reveal that the fit of Falangas's data to the models was poorer than for experimental series A,D,E,F and G. The data points in graphs 10.25 and 10.26 show a greater scatter and the mean squares about regression are greater by approximately tenfold. However, it is significant that the numerical results obtained are comparable with those presented in section 10.8. In particular, these features are:

TABLE 10.13

Results of Modelling Crystal Growth Rate for Falangas's Batch Crystallisation Experiments

Experimental Data	Optimum Values of Model Parameters in Equations 10.23 and 10.24					Mean Squares About Regression ($\times 10^{10}$)
	$k_1 (\times 10^2)$	$k_2 (\times 10^1)$	k_3	k_4	$k_5 (\times 10^9)$	
Experiments at 800 r.p.m.	4.082	-5.126	-	2.00	-	1.978
Experiments at all Speeds	1.692	-6.860	-	2.00	9.97	8.498

GRAPH 10.25 Results of Fitting Empirical Model for Crystal Growth Rate to Falangas's Experiments at a Stirrer Speed of 800 r.p.m.

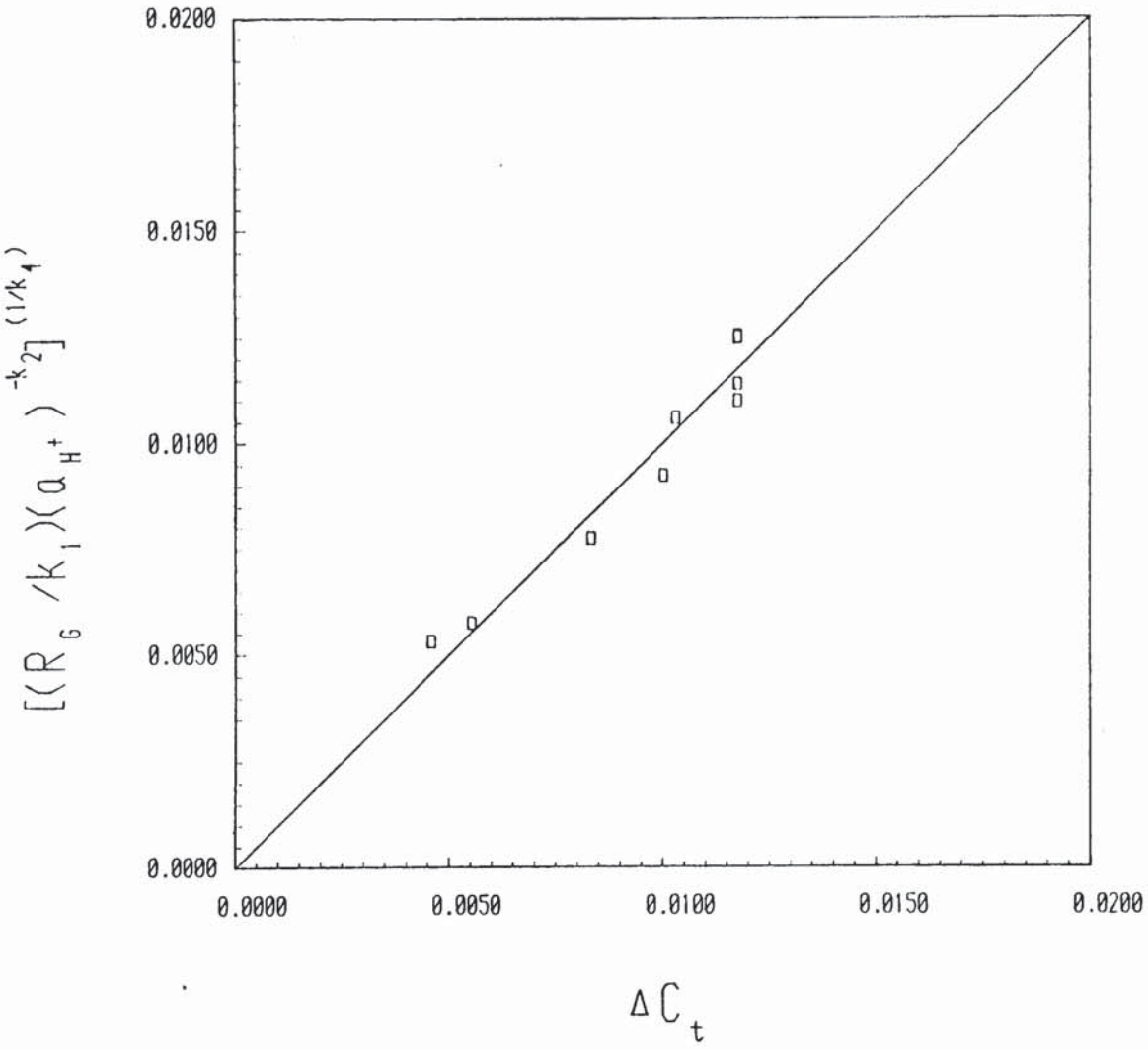

GRAPH 10.26 Results of Fitting Empirical Model for Crystal Growth Rate to Falangas's Experiments at all Stirrer Speeds

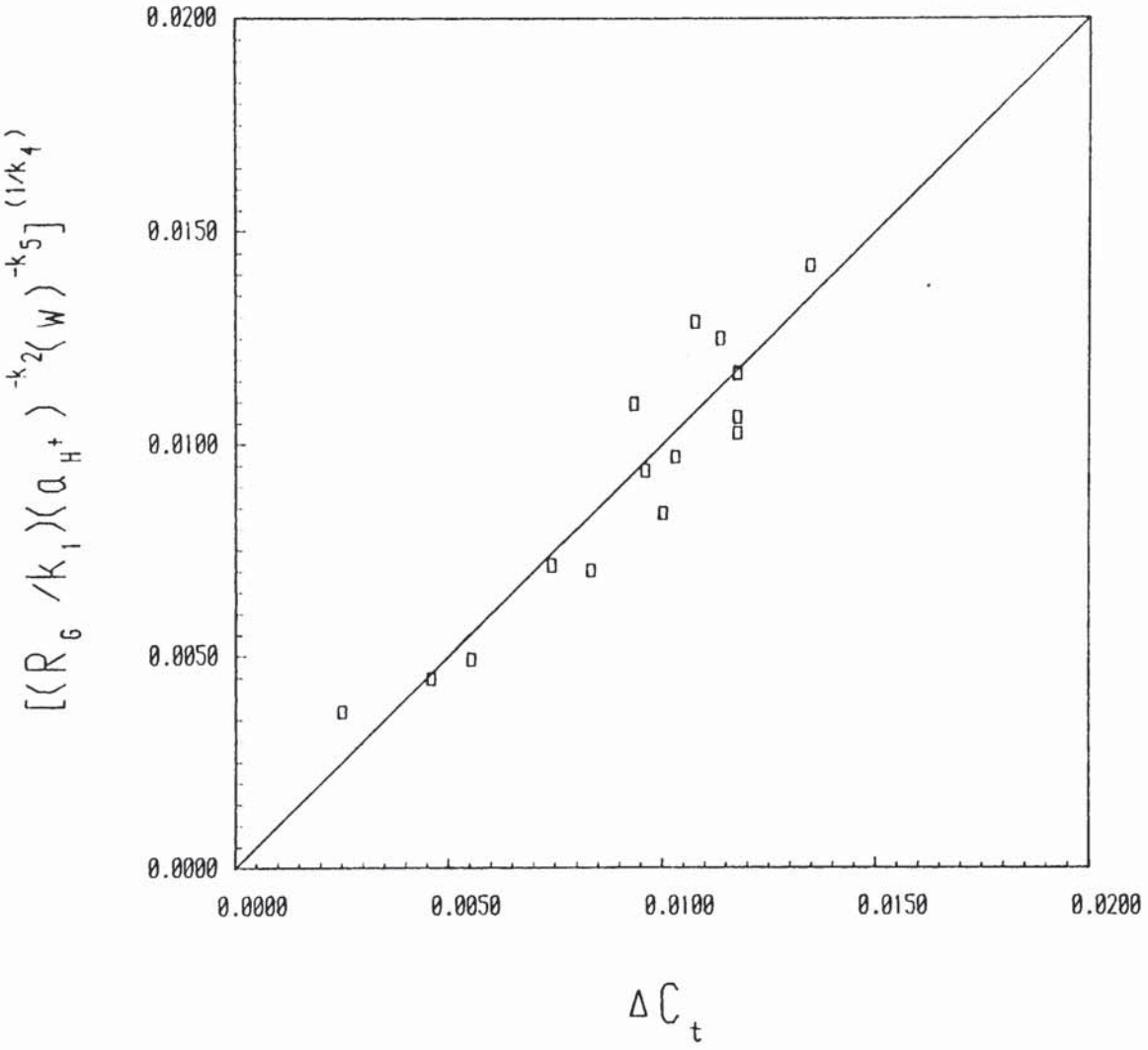

1. A size independent model with a parabolic supersaturation dependence is adequate for modelling the data.

2. The exponent for the hydrogen ion activity term is negative and of similar magnitude to the results for experimental series A,D,E,F and G.

3. Growth rate is found to be effectively independent of stirrer speed, since the exponent for the stirrer speed term takes on an optimum value of less than 10^{-8}.

The final model presented by Falangas (5) was:

$$\frac{dL}{dt} = 2.1 \times 10^{-3}(L)^{-1.5}(pH)^{0.03}(w)^{1.2}(S)^{0.83} \quad \ldots\ldots\ldots\ldots\ldots\ldots \quad (10.31)$$

Moreover, the fit of this model to experimental data was very poor, with the percentage difference between calculated and experimental values of linear growth rate exceeding 10% and ranging upto 100% for the majority of the data.

Falangas chose to express the effect of acidity in his model in terms of pH instead of the activity or concentration. Furthermore, the equipment used to measure pH was less accurate than that used in the current study, being graduated only to 0.1 of a pH unit, and not having satisfactory temperature compensation. It is likely that these factors accounted for the negligible dependence of acidity on growth rate found by Falangas (5). In particular, expressing

acidity in terms of pH would have tended to cause a masking effect.

The approximately linear dependence on stirrer speed described by Falangas (5) conflicts with the independence of stirrer speed obtained in the present analysis. Falangas has reported that settling of crystals was a major problem at the low speeds of 200 and 400 r.p.m. This could have caused a spurious dependence on stirrer speed.

Falangas (5) presented a model for crystal growth termed the 'stationary particle model'. This model was formulated to account for the observed negative size dependence of growth rate. However, in developing the model, the following arbitrary, unsupported relation was assumed in order to remove the effect of nucleation.

$$\text{i.e.} \quad \frac{\partial L}{\partial t} + \frac{L}{3P_t}\frac{\partial P_t}{\partial t} = P_t^{p-1}\frac{\partial L}{\partial t} \quad \ldots\ldots\ldots\ldots\ldots \quad (10.32)$$

Consequently, it was deduced by Falangas that the model was applicable irrespective of nucleation. Thus, data points corresponding to conditions under which significant nucleation was still occurring, were included in the modelling process. Concentration of such data at a particular speed would also have caused an erroneous dependence of growth rate on stirrer speed.

The negative size dependence claimed by Falangas, leads to the conclusion that smaller crystals grow faster than larger ones, which is incompatible with the established evidence of the Gibbs-Kelvin

equation (3,13), according to which larger particles would grow at the expense of smaller ones which would tend to dissolve. Furthermore, a negative size dependence would reveal itself in the crystal size distributions after nucleation had stopped, because the fines 'tail' would tend to disappear from succeeding distributions. Re-analysis of some of Falangas's product samples on the Coulter counter model Z_B, revealed the existence of significant fines fractions. The apparent lack of fines on initial analysis was probably due to an arbitrary detection limit being set on the Coulter counter model A, which was used by Falangas (5). Therefore, it was concluded that the size independent growth rate model fitted in the current analysis was more valid than a negative size dependence.

Falangas (5) reported a near linear dependence of growth rate on driving force, with driving force expressed as the relative supersaturation of barium ions.

i.e. $S = (C_+ - C_{+e})/C_{+e}$ ..... (10.33)

This was explained by Falangas (5) by asserting that this expression for driving force was a good approximation to the fundamental driving force, at low supersaturations. However, this assertion was based on the assumptions that activity coefficients were unity and chromate ion concentration at any pH was a simple power law function of barium ion concentration.

i.e. $C_- = k\, C_+^{\alpha}$ ..... (10.34)

The complex chromium equilibria that prevail in acidic barium chromate solutions have been described in Chapter 7, and consequently, it has been shown in section 10.5 that the expression for fundamental driving force is a complicated one, affected by all the ionic species in solution, and requiring the use of activities in its computation (as was done in Appendix 18). Therefore, the assumptions of Falangas (5) appear to be inappropriate. It is concluded that a parabolic dependence of growth rate, on supersaturation expressed in terms of barium ion concentrations, is a more reasonable basis in the absence of sufficiently accurate information to calculate the fundamental driving force.

Finally, it is concluded that the experimental data of Falangas (5) are adequately described by the same model fitted to the data obtained in the current investigation. Thus, it is not necessary to invoke the unrealistic 'stationary particle model' to explain Falangas's results.

10.11 USE OF RECRYSTALLISED BARIUM CHROMATE

The batch crystallisation experiments carried out using recrystallised barium chromate have been reported in Chapter 6, and the results obtained are tabulated in Appendix 2. In table 10.14, the final mean crystal diameters and populations for these

TABLE 10.14

Comparison of Experiments Using Recrystallised Barium Chromate with Those Using Laboratory Reagent (L.R.) Grade Barium Chromate

Experimental Series	Crystal Populations (-)		Mass Mean Equivalent Volume Diameter (μm)	
	Recrystallised Barium Chromate	L.R. Grade Barium Chromate	Recrystallised Barium Chromate	L.R. Grade Barium Chromate
A	1.259×10^{9}	6.663×10^{8}	66.31	72.01
D	2.035×10^{6}	3.396×10^{6}	111.13	113.49
E	9.799×10^{6}	5.832×10^{6}	99.21	94.66
F	1.679×10^{6}	2.491×10^{6}	141.00	107.20
G	2.867×10^{6}	8.736×10^{6}	96.33	75.13

experiments, have been compared with corresponding values for experiments of similar duration, where laboratory reagent grade barium chromate was used.

The recrystallised barium chromate was considered to contain less impurities than the laboratory reagent grade material. The effect of impurities on crystallisation has often been found to be an increase in nucleation and a decrease in crystal growth (42). Even if growth rate was unaffected by impurities, a reduction in nucleation rate when recrystallised barium chromate was used, would manifest itself in lower final populations, and consequently, larger mean product sizes. It can be seen from table 10.14 that this is indeed the case for series E, F and G. However, the converse is observed for series A and D. Thus, the effect, if any, of impurities is unclear and further investigation is required before any firm conclusions can be drawn.

CHAPTER ELEVEN

CONCLUSIONS AND SUGGESTIONS FOR FURTHER WORK

11.0 INTRODUCTION

The conclusions deduced from the experimental work on batch crystallisation of barium chromate, by the technique of precipitation from homogeneous solution, are summarised in this chapter. In addition, probable reasons for the failure to achieve epitaxial growth of barium chromate on particulate metal substrates, in the epitaxial growth experiments, are detailed. Finally, some suggestions for further work are presented.

11.1 CONCLUSIONS FROM BATCH CRYSTALLISATION EXPERIMENTS

11.1.1 Main Conclusions

Batch crystallisation of barium chromate was found to be adequately represented by an empirical power law type model of the form:

$$R_G = k_1 (a_{H^+})^{k_2} (\Delta C_t)^{k_4} \quad \ldots\ldots\ldots\ldots \quad (11.1)$$

The parameter k_4 took on a value of 2 for all experimental conditions. The parameters k_1 and k_2 depended on experimental conditions, particularly temperature and urea content. Values for k_1 varied from 0.6×10^{-2} to 7.2×10^{-2}, when growth rate per unit surface area (R_G) was expressed in kg/m^2s, and both hydrogen ion activity (a_{H^+}) and driving force (ΔC_t) were expressed in $kmol/m^3$. The corresponding values for k_2 ranged from -0.56 to -0.39. These results were presented

in Chapter 10.

Crystal growth of barium chromate was established as being a surface reaction, or surface integration, controlled process, with the probable rate determining step being the removal of the primary hydration shell of the barium ion prior to surface incorporation (section 10.9.8). Evidence for this was:

1. The parabolic dependence of growth rate on driving force, which was expressed in terms of concentrations of the barium ion (section 10.9.5). This was in accord with the theory of Reich and Kahlweit (309), for crystal growth at low supersaturations, when cation dehydration was the rate determining step.

2. The activation energy for crystal growth was very high (>100 kJ/mol) and depended markedly on urea content. This dependence was explicable on the basis of a cation dehydration rate determining step (section 10.9.8). In addition, the energy barrier for removing the inner hydration shell of the barium ion was estimated to be of the same order of magnitude as the activation energy for crystal growth.

3. Crystal growth rate was found to be independent of stirrer speed, and hence independent of crystal-solution relative velocity (section 10.9.6). A bulk diffusion controlled process would have given rise to a stirrer speed dependence.

4. Crystal growth rate was found to decrease with increasing hydrogen ion activity (section 10.9.4). A surface integration controlled process would have been retarded in this manner at higher hydrogen ion activities, by greater adsorption of hydroxonium ions at active growth sites on the crystal-solution interface.

11.1.2 Subsidiary Conclusions

A number of subsidiary conclusions were drawn in relation to the batch crystallisation experiments, and some supplementary models and techniques were developed. These were:

1. The crystal growth rate of barium chromate was shown to be independent of crystal size, when the characteristic dimension of the crystal populations was taken to be the mass mean equivalent volume diameter (section 10.9.7).

2. The empirical model for crystal growth rate, represented above by equation 11.1, was found to be also applicable to the batch crystallisation experiments carried out by Falangas (5) under comparable conditions (section 10.10).

3. Nucleation appeared to be restricted to an initial 'burst' lasting for a short period of time. The 'induction periods', discussed in section 10.3, and the results of fitting a simple agglomeration model to the crystal population data

(section 10.7.4), indicated that the duration of this initial 'burst' was probably of the order of a few hundred seconds.

4. Some agglomeration occurred during crystal growth, but since growth rate was found to be independent of crystal size (section 10.9.7), it was concluded that secondary growth processes, such as agglomeration and Ostwald ripening, did not make a significant contribution to overall crystal growth.

5. A simple agglomeration model, which was an extension of that developed by Liao and Hulburt (253) for continuous crystallisers, was derived (section 9.5). Attempts to fit crystal population-time data to this model were relatively unsuccessful due to the poor quality of the data available.

6. A model for concurrent, size independent nucleation and growth during batch crystallisation was developed (Appendix 12), by an approach similar to that employed by Bransom and Dunning (252). Since nucleation was restricted to an initial 'burst' this model was not applied.

7. The experimental solubility data of Skander (4) and Falangas (5), for barium chromate in various acidic media (hydrochloric acid, hydrochloric acid/urea, nitric acid) were fitted to a semi-empirical model of the form:

$$C_e = S_1 \exp(S_2/T) \cdot (a_{H^+})^{S_3} \quad \ldots\ldots\ldots \quad (11.2)$$

Values of the model parameters S_1, S_2 and S_3 have been presented in Chapter 7. This solubility model was fitted by means of the Nelder-Mead direct search optimisation algorithm (197). The computer program written for this purpose successfully employed the modifications to the algorithm proposed by Schnabel (198) and by Parkinson and Hutchinson (199).

8. In order to combine crystal size data from the Coulter counter with those from sieve analysis, a volume shape factor was derived from experiments employing a microscopic counting technique first used by Harris (243) (section 8.5). For barium chromate crystal products, the ratio of equivalent volume diameter to mean sieve size, for sieve fractions upto 295 μm, was found to have a constant value of 0.875.

9. A technique was developed for Coulter counter size analysis of high density fine particulate materials (such as barium chromate, and fine powders of high density metals). The technique has been described in detail in section 8.2, and involved development of a glycerol based high viscosity electrolyte, refinement of the sample dispersion method, improvement of sample suspension characteristics, and suppression of particle conductivity effects.

11.2 CONCLUSIONS FROM EPITAXIAL GROWTH EXPERIMENTS

Attempts to achieve epitaxial growth of barium chromate on substrates consisting of fine, polydisperse metal particles proved to be unsuccessful. Probable reasons for this were:

1. Under the experimental conditions that prevailed, the degree of lattice match between the tested substrates and the intended overgrowth, was probably not sufficiently close, particularly in corresponding mutually perpendicular directions.

2. The vigorous conditions of agitation required to keep the dense metal particles suspended, combined with the agitation caused by the continual generation of carbon dioxide because of urea hydrolysis, hindered epitaxy.

3. The carbon dioxide bubbles that were continually generated acted as nucleation sites (10), for the heterogeneous nucleation of barium chromate in the bulk of the solution rather than on the substrate particles.

4. Adsorption of hydroxonium ions and impurities present in the laboratory reagent grade barium chromate (as well as possibly carbon dioxide) on the metal particles, rendered them poorly wetted by the solution (124), thus preventing epitaxial nucleation.

11.3 SUGGESTIONS FOR FURTHER WORK

11.3.1 Crystallisation of Barium Chromate

The approach adopted for the analysis of barium chromate batch crystallisation in this investigation has been largely empirically based. It would be desirable in any further work to establish a more fundamental basis of analysis. For this purpose, use of the thermodynamic driving force approach of Mullin and co-workers (74-77) is recommended. However, exact determination of this fundamental driving force requires more accurate information than is presently available. Further experimental work suggested in this respect are as follows:

1. More accurate determination of the solubility of barium chromate in acidic solutions containing urea is required, particularly at high temperatures. Since urea hydrolyses rapidly at high temperatures, it is envisaged that establishing a true equilibrium would be difficult. It is suggested that this impediment may be circumvented by measurements at moderate temperatures (urea hydrolysis rate is negligible at temperatures below $\sim 70^{\circ}C$), combined with a reliable technique for extrapolation of the results to higher temperatures.

2. A comprehensive investigation of the equilibria prevailing in acidic barium chromate solutions at high temperatures is necessary. Values of relevant equilibrium constants at temperatures

above 90°C should be derived. It is also desirable to obtain information on the differences, if any, between the ionic compositions, and the activity coefficients of the ionic species, in super-saturated and saturated solutions of barium chromate in hydrochloric acid. It is envisaged that an investigation of these aspects would be largely carried out by spectrophotometric methods (190).

3. An 'in situ' method for following solute concentration would be a desirable adjunct in monitoring the progress of crystallisation, as well as in solubility measurements and studies of ionic equilibria. A barium ion selective electrode would appear to be ideal for this purpose, but as reported in Chapter 7, the electrodes presently available are not sufficiently robust to withstand prevailing operating conditions. Therefore, it is suggested that development of an electrode insensitive to, high temperature, agitation of the solution, and solids content of the solution, would be a helpful subsidiary aspect of any further experimental work on solubilities and ionic equilibria.

Some evidence for the occurrence of agglomeration was detected in the batch crystallisation experiments of the current investigation. It is suggested that this phenomenon is examined in depth by means of an

appropriate programme of experiments. Skander (4) reported considerable practical difficulties in using a continuous MSMPR type crystalliser for precipitation of barium chromate from homogeneous solution. Hence, it is recommended that a batch process be employed for these further studies. Since the crystal growth of barium chromate has been shown to be independent of size (section 10.9.7), it is proposed that the model for concurrent size independent nucleation and growth presented in Appendix 12, is combined with the simple agglomeration model derived in section 9.5, to provide a suitable basis for analysis of the results from such experiments. It is considered that extension of this combined model, to include other effects such as crystal breakage, would be a feasible proposition.

An alternative to the supposition that nucleation was limited to an initial 'burst', has been the postulate that the particle generative effects of primary nucleation and crystal breakage, are always balanced by the particle destructive effects of agglomeration. Therefore, an experimental study of the phenomenon of agglomeration, as that suggested above, should also be directed towards determining the relative importance of the processes of nucleation, agglomeration and breakage. It is likely that this would require 'in situ' monitoring of crystal numbers, in specific size ranges over a considerable band. In this respect, it is important that a direct particle counting technique be employed rather than one which

infers particle numbers from measured mass based size distributions (307). It is suggested that the new, microprocessor controlled, multi-channel Coulter counter model ZM (320), would be suitable for this purpose. However, it would be necessary to develop an adequate experimental technique involving, adaptation of the instrument to 'in situ' operation, proving its applicability under operating conditions of high temperature and considerable suspended solids, and ensuring representative sampling in the course of size analysis.

Preliminary experiments with recrystallised barium chromate indicated a possible impurity effect, although these results were unclear (section 10.11). It is therefore suggested that more extensive experimentation is carried out with a view to establishing the influence of impurities present in laboratory reagent grade barium chromate, on nucleation and growth. A secondary aim would be to identify the active impurities and characterize their mode of action, since this would help to clarify the effect, if any, of these impurities in preventing epitaxial growth.

11.3.2 Epitaxial Growth

It was evident from the current investigation that the conditions required for precipitation of barium chromate from homogeneous solution, were not conducive to the epitaxial growth of barium chromate on substrates of fine metal particles. It is therefore suggested

that any further studies are carried out by the experimental technique used by Miller and Benge (1,165,321), in the original experiments on the formulation of igniferous compositions and pyrotechnic time delay fuses. This method employed direct mixing of dilute solutions of appropriate soluble salts, into a ballast solution in which the potential substrate was kept suspended by means of a flat, single blade paddle stirrer (321). Precipitations were carried out at high temperatures above $90^{o}C$ and the nominal scale of operation was 10 dm^3 (165,321). There was some evidence that true epitaxy did not occur under these conditions, but that precipitation took place in sufficiently massive form to physically incorporate the suspended solids in a crystalline matrix (1,321). Further experimental work should concentrate on resolving this question, in order to determine whether true epitaxy is indeed necessary or desirable from the point of view of time delay fuse compositions. It is further suggested that the suitability of less dense materials, such as boron and titanium, for use as the fuel component of delay fuse compositions be examined, since this would ease the problem of uniform suspension of these 'substrate' particles.

APPENDIX 1

NOMENCLATURE USED IN THE THESIS

A compilation of all the symbols used in the main text and appendices of this thesis is given below, along with a brief description of the meaning of each symbol. The unit or units commonly used for each symbol are presented in parentheses under its description. S.I. units are used in most cases, except where other units are used by convention.

SYMBOL	DESCRIPTION
A, A_B, $A_{x,t}$	surface area of a crystal face, a single crystal, a whole crystal population, or a fluidised bed of crystals (m^2)
A_a	pre-exponential factor in Arrhenius type temperature dependence (equation 10.26) (-)
A_j	surface area of all crystal faces of type j in a given population (m^2)
A_o	constant in Debye-Huckel equation (equation 7.14) (various units)
A_s	empirical parameter in equation 7.8 ($(kmol/m^3)^2$)
A_1, A_2	constants in equation A6.5 (various units)
a	solute activity in solution ($kmol/m^3$; kg/kg; kmol/kg)
a_b	cross sectional area of fluidised bed (m^2)
a_e	equilibrium solute activity in solution ($kmol/m^3$; kg/kg; kmol/kg)

SYMBOL	DESCRIPTION
a_{H^+}	hydrogen ion activity (kmol/m^3)
a_n	surface area occupied by a single nucleus (m^2)
a_o	lattice parameter (Å)
a_o^*	constant in equations 7.11 and 7.12 (kmol/m^3)
a_+	molar activity of cation (kmol/m^3)
a_-	molar activity of anion (kmol/m^3)
Δa	supersaturation based on activities (i.e. $\Delta a = a - a_e$) (kmol/m^3; kg/kg; kmol/kg)
B	crystal birth rate (1/s)
B_N	numerical nucleation rate (1/s)
B_o	constant in Debye-Huckel equation (equation 7.14) (various units)
B_s	empirical parameter in equation 7.8 ((kmol/m^3)^3)
b	constant index (equation 9.2) (-)
b_o	lattice parameter (Å)
$C_{B,t}$	solute concentration at time t in whole of fluidised bed (kmol/m^3)
C_e	equilibrium solubility of solute (kmol/m^3)
C_{H^+}	hydrogen ion concentration (kmol/m^3)
$C_{H_o^+}$	initial hydrogen ion concentration (kmol/m^3)
$C_{H,t}$	solute concentration at time t, on exit from fluidised bed (kmol/m^3)

SYMBOL	DESCRIPTION
C_i	concentration of i th ionic species ($kmol/m^3$)
C_o'	constant in modified Debye-Huckel equation (equation A10.1) (various units)
$C_{o,t}$	solute concentration at time t, on entry to fluidised bed ($kmol/m^3$)
C_t, C	solute concentration at time t ($kmol/m^3$)
C_u	urea concentration ($kmol/m^3$)
C_{u_o}	initial urea concentration ($kmol/m^3$)
$C_{x,t}$	solute concentration at time t, in element of fluidised bed ($kmol/m^3$)
C_+	molar concentration of cation ($kmol/m^3$)
C_-	molar concentration of anion ($kmol/m^3$)
ΔC	supersaturation based on concentrations (i.e. $\Delta C = C_t - C_e$) ($kmol/m^3$; kg/kg; kmol/kg)
c_o	lattice parameter (Å)
D	crystal loss rate (1/s)
D_v	diffusivity of solute molecules in solution (m^2/s)
d	average sieve size (m; μm)
d_{crit}	critical diameter of nucleus, in primary homogeneous nucleation (m; Å)
d_o	effective ionic radius (Å)
d_s	equivalent spherical surface area diameter (m; μm; Å)
d_v	equivalent spherical volume diameter (m; μm; Å)

SYMBOL	DESCRIPTION
E	activation energy for crystal growth (kJ/kmol; kJ/mol)
E_H	activation energy for cation dehydration (kJ/kmol; kJ/mol)
E_1, E_2	moduli of elasticity of overgrowth in mutually perpendicular directions (N/m^2)
e	subscript used to denote equilibrium conditions (-)
e_o	electronic charge (C)
F_G	function representing linear growth rate (equation A12.2) (m/s)
F_N	function representing numerical nucleation rate (equation A12.1) (1/s)
F_1, F_2	dimensionless constants in equation 2.9 (-)
f	shape factor defined by equation 8.1 (-)
$f_G(S)$	function of driving force (equation A12.2) (various units)
$f_N(S)$	function of driving force (equation A12.1) (various units)
f_s	surface shape factor (-)
f_v	volume shape factor (-)
G	linear growth rate (m/s)
$\bar{G}$	mean linear growth rate (m/s)
$\Delta G_{crit.}$	critical free energy for homogeneous nucleation (kJ/kmol)

SYMBOL	DESCRIPTION
$\Delta G^*_{crit.}$	critical free energy for heterogeneous nucleation (kJ/kmol)
g	constant index (equations 9.3 and 9.17) (-)
H	height of fluidised bed (m)
h	height of a growth step or Planck's constant (m; μm; Å or Js)
$h_G(pH,T)$	function of pH and temperature (equation A12.2) (various units)
$h_N(pH,T)$	function of pH and temperature (equation A12.1) (various units)
I	integral defined by equation A12.17 (m^3)
I_c	ionic strength of electrolyte solution ($kmol/m^3$)
i	dummy index or number of data points (-)
j	dummy index or number of model parameters (-)
K	empirical constant in equation 2.19 ($kg/s\ m^{0.5}\ Hz^{1.2}$)
K_H	constant in expression for rate of steady state homogeneous nucleation (equation 2.2) (1/s)
K_M	empirical mass transfer coefficient for crystal growth (equation 2.8) ($kg/s\ m^2$; $kmol/s\ m^2$; etc)
K_{sp}	solubility product of barium chromate ($(kmol/m^3)^2$)
$K_1, K_2, K_3, K_4,$ K_5, K_6	equilibrium constants for Cr(VI) equilibria in solution (various units)

SYMBOL	DESCRIPTION
k	empirical constant in equations 10.34 and A6.10 (various units)
k_G	empirical constant in expression for crystal growth rate per unit surface area (equation 9.17) (various units)
k_L	empirical constant in expression for linear crystal growth rate (equation 9.3) (various units)
k_N	empirical constant in expression for numerical nucleation rate (equation 9.2) (1/s)
k_o	Boltzmann constant (J/K)
k_u	rate constant for urea hydrolysis (1/s)
k_w	rate constant for removal of a water molecule from inner hydration sphere of a cation (1/s)
k_1, k_2, k_3, k_4, k_5	empirical constants in expression for crystal growth rate per unit surface area (equation 9.19) (various units)
L	characteristic linear dimension of a crystal (usually equivalent volume diameter) (m; μm)
L_H	relative partial molal heat content of solute (kJ/kmol)
L_t, L_θ, L_ζ	final diameter of particles nucleated at times t, θ and ζ, respectively (m, μm)

SYMBOL	DESCRIPTION
$L_{t(max)}$	diameter of largest crystals present in population at time t (m; μm)
$L_{\infty(max)}$	diameter of largest crystals present in the final product (m; μm)
ℓ	dummy particle size variable (m)
M	molecular weight of solute (-)
m	mass of a single particle (kg)
m_L	mass fraction of crystal population having diameters greater than L (-)
m_o	initial mass of solute taken or initial mass of fluidised bed material (kg)
m_p	mass of particles in a given sample (kg)
m_t	corrected mass of crystal population at time, t (kg)
m_t^*	mass of crystal population at time, t (kg)
m_∞	final product crystal mass (kg)
m_1, m_2	constant indices (equation 2.9) (-)
N_a	Avogadro's number (1/kmol)
N(L,t)	total number of crystals in population at time t, having a size greater than L (-)
n, n(L,t), $n(L)_t$	population density function at time t (1/s m)
n_i	number of particles in i th size range (1/m; 1/μm)

SYMBOL	DESCRIPTION
$n(L,\infty)$	final product population density (1/s m)
n_p	number of particles in sample (-)
n_x	number of particles in element of fluidised bed (-)
P_o	crystal population after initial burst of nucleation (-)
P_t	crystal population at time t (-)
p	dummy index or constant index (equations 2.5 and 10.32) (-)
p_o	parameter defined by equation A6.28 (m^3/s)
pH_t	value of pH at time t (-)
R	universal gas constant (kJ/kmol K)
R_D	ratio of mean equivalent volume diameter to mean sieve diameter (-)
Re	Reynolds number ($Re=\rho LU/\mu$) (-)
R_G	growth rate per unit surface area (kg/m^2s)
R_H	rate of steady state homogeneous nucleation (1/s)
R_M	crystal growth rate (kg/s; kmol/s)
R_N	primary mass nucleation rate (kg/s)
$r_{i,o}$	initial radius of particles in i th size range (m; μm)
$r_{i,t}$	radius of particles in i th size range at time t (m; μm)
$\bar{r}_o$	number mass mean radius (m; μm)

SYMBOL	DESCRIPTION
$\bar{r}_{s,o}$	initial number surface mean radius of substrate particles (m; μm)
$\bar{r}_{s,t}$	number surface mean radius of substrate particles at time t (m; μm)
S	driving force ($kmol/m^3$; kg/kg; kmol/kg; etc)
$S_{B,t}$	relative supersaturation (based on concentrations) at time t, in whole of fluidised bed (-)
Sc	Schmidt number ($Sc=\mu/\rho_{sol.}.D_v$) (-)
$S_{c,rel.}$	relative supersaturation based on concentrations (-)
$S_{H,t}$	relative supersaturation (based on concentrations) at time t, on exit from fluidised bed (-)
Sh	Sherwood number ($Sh=k_L L/D_v$) (-)
S_o	initial relative supersaturation (based on concentrations) in reservoir of fluidised bed crystalliser (-)
$S_{o,t}$	relative supersaturation (based on concentrations) at time t, on entry to fluidised bed (-)
S_r	supersaturation ratio based on activities (-)
$S_{rel.}$	relative supersaturation based on activities (-)
S_t	relative supersaturation (based on concentrations) at time t, in reservoir of fluidised bed crystalliser (-)
$S_{x,t}$	relative supersaturation (based on concentrations) at time t, in element of fluidised bed (-)

SYMBOL	DESCRIPTION
S_1, S_2, S_3	empirical constants in solubility correlation (equation 7.13) (various units)
T	absolute temperature (K)
T'	parameter defined by equation A6.21 (-)
T*	coagulation time (equation 9.37) (s)
T_o	parameter defined by equation A6.18 (1/m)
t	time (denotes variable at time t, when used as a subscript) (s)
t_o	duration of period of nucleation (s)
U	velocity of crystal relative to solution (m/s)
U_1	parameter defined by equation A18.12 (m^3/kmol)
U_2	parameter defined by equation A18.13 (-)
u	parameter defined by equation 9.39 (1/s)
V	system volume (m^3)
V_R	volume of reservoir in fluidised bed crystalliser (m^3)
v_L	superficial liquid velocity through fluidised bed (m/s)
$v_L(O)$	initial value of v_L (m/s)
v_t	overall volume of crystal population at time t (m^3)
w	stirrer speed (r.p.m.)
x	dummy variable for height of fluidised bed (m)

SYMBOL	DESCRIPTION
$x_1, x_2, x_3,$ x_4, x_5	empirical constants in pH-time correlation (equation 10.9) (various units)
$\bar{y}$	mean square about regression (equation 10.22) $((kg/m^2s)^2)$
z_i	ionic charge of i th ionic species in solution (-)
α	constant index (equations 9.4 and 10.34) (-)
α_o	relevant lattice spacing of overgrowth (m; μm; Å)
α_o^*	parameter defined by equation A6.29 (m)
β	constant in equation 9.5 (-)
γ	activity coefficient of solute (-)
γ_e	activity coefficient of solute in equilibrium solution (-)
γ_+	activity coefficient of cation (-)
γ_-	activity coefficient of anion (-)
δ	critical lattice misfit for epitaxy (m; μm; Å)
θ	dummy time variable (denotes variable at time θ, when used as a subscript) (s)
Λ	parameter defined by equation A6.26 (various units)
λ	agglomeration rate constant (1/s)
μ	dynamic viscosity of solution (kg/m s)
μ_m	mean of cumulative normal distribution fitted to crystal size distribution data (μm)

SYMBOL	DESCRIPTION
ν	number of ions in a molecular unit (-)
ν_+	number of cations obtained from a molecular unit (-)
ν_-	number of anions obtained from a molecular unit (-)
ξ	activity coefficient ratio (-)
ξ_o	effective value for the number of particles formed per molecule of solute (-)
ρ	density of nucleus or crystalline solid (kg/m^3)
ρ_b	density of solids in fluidised bed (kg/m^3)
$\rho_{sol.}$	density of solution (kg/m^3)
σ_m	standard deviation of cumulative normal distribution fitted to crystal size distribution data (μm)
σ_o	relevant lattice spacing of overgrowth (m; μm; $\mathring{A}$)
σ_s	surface energy of nucleus (kJ/m^2)
ζ	dummy time variable (denotes variable at time ζ, when used as a subscript) (s)
ζ_c	concentration ratio (-)
ϕ	sphericity of a crystal in crystal population (-)
ϕ^*	molar growth affinity (kJ/kmol)

SYMBOL	DESCRIPTION
ψ	stirrer speed or stirrer speed ratio (r.p.m.; -)
Ω	proportionality factor in equation 2.4 (-)

APPENDIX 2

EXPERIMENTAL RESULTS FROM BATCH CRYSTALLISATION EXPERIMENTS

The experimental results from the five main series of batch crystallisation experiments are tabulated here in tables A2.1, A2.2, A2.3, A2.4 and A2.5. The experimental results from the experiments carried out using recrystallised barium chromate are listed in table A2.6. These tables have been computer generated and hence the symbol E denotes exponents to the base ten. The symbols used as headings for the tabulated numbers have been explained in Appendix 1, and are the same as those used in the main text. The driving force, ΔC bears the subscript F or S. Subscript F denotes driving force calculated using the empirical relation for solubility derived from Falangas's (5) solubility measurements in the presence of urea. Subscript S denotes driving force calculated using the empirical relation for solubility derived from Skander's (4) solubility measurements. These empirical relations were developed in Chapter 7. Each individual data set in these tables constitutes a separate batch crystallisation experiment. The general experimental conditions for the five main experimental series have been presented in table 6.1 of Chapter 6.

TABLE A2.1

Experimental Results from Series A

t (s)	m_t (g)	μ_m (μm)	σ_m (μm)	V (dm^3)	a_{H^+} ($kmol/m^3$)	A (m^2)	P_t (-)	ΔC_F ($kmol/m^3$)	ΔC_S ($kmol/m^3$)	R_G (kg/m^2s)
266.0	0.2886	20.67	8.66	1.084	5.793E-03	3.075E-02	5.897E+08	1.069E-02	7.163E-03	9.963E-05
514.0	1.3806	43.06	14.39	1.084	5.416E-03	6.333E-02	3.112E+08	8.224E-03	4.839E-03	4.839E-05
678.0	1.7373	41.35	11.02	1.084	5.082E-03	7.590E-02	6.497E+07	6.664E-03	3.411E-03	4.037E-05
955.0	2.0890	49.83	15.20	1.084	3.832E-03	7.937E-02	1.904E+08	4.626E-03	1.899E-03	3.860E-05
1347.0	3.3152	57.92	18.12	1.084	7.316E-04	1.097E-01	3.035E+08	3.449E-03	2.492E-03	2.793E-05
1358.0	3.7622	66.32	23.18	1.084	6.769E-04	1.157E-01	6.677E+08	3.401E-03	2.490E-03	2.648E-05
1398.0	4.1551	73.38	24.37	1.084	5.036E-04	1.122E-01	4.532E+08	3.201E-03	2.447E-03	2.731E-05
1545.0	4.6139	66.99	23.38	1.084	1.492E-04	1.404E-01	8.004E+08	2.158E-03	1.814E-03	2.183E-05
1735.0	4.7226	65.58	22.11	1.084	2.974E-05	1.437E-01	6.605E+08	6.741E-04	5.532E-04	1.315E-08
2122.0	4.7816	72.01	24.65	1.084	3.916E-06	1.339E-01	6.663E+08	7.677E-04	7.357E-04	1.412E-08
10710.0	4.7978	66.00	25.94	1.084	3.162E-07	1.606E-01	1.717E+09	7.319E-04	7.259E-04	1.176E-08

TABLE A2.2

Experimental Results from Series D

t (s)	m_t (g)	μ_m (μm)	σ_m (μm)	V (dm^3)	a_{H^+} ($kmol/m^3$)	A (m^2)	P_t (-)	ΔC_F ($kmol/m^3$)	ΔC_S ($kmol/m^3$)	R_G (kg/m^2s)
1320.0	0.7100	53.34	13.28	1.084	4.136E-03	2.366E-02	8.684E+06	1.091E-02	8.819E-03	4.239E-05
1565.0	0.9997	65.60	18.89	1.084	3.838E-03	2.823E-02	3.657E+07	1.025E-02	8.249E-03	3.553E-05
2040.0	1.7898	80.44	21.21	1.084	3.307E-03	4.011E-02	1.939E+07	8.937E-03	7.114E-03	2.501E-05
2895.0	2.0499	82.50	18.80	1.084	2.304E-03	4.347E-02	4.476E+06	6.673E-03	5.212E-03	2.308E-05
3120.0	2.8100	93.92	18.23	1.084	1.964E-03	5.131E-02	2.001E+06	6.163E-03	4.840E-03	1.955E-05
3450.0	2.9400	86.61	19.20	1.084	1.393E-03	5.913E-02	4.582E+06	5.516E-03	4.445E-03	1.696E-05
3580.0	3.1800	95.56	19.93	1.084	1.161E-03	5.751E-02	2.666E+06	5.284E-03	4.328E-03	1.744E-05
4155.0	3.4700	92.93	19.49	1.084	3.478E-04	6.457E-02	3.217E+06	4.178E-03	3.729E-03	1.553E-05
4320.0	3.9699	99.47	19.28	1.084	2.185E-04	6.843E-02	2.383E+06	3.776E-03	3.442E-03	1.466E-05
4470.0	4.2999	98.43	23.31	1.084	1.383E-04	7.691E-02	9.702E+06	3.369E-03	3.119E-03	1.304E-05
4830.0	4.4781	109.30	32.49	1.084	4.301E-05	7.702E-02	1.163E+08	2.256E-03	2.137E-03	1.302E-05
5130.0	4.2500	98.11	19.61	1.084	1.667E-05	7.450E-02	2.842E+06	1.234E-03	1.170E-03	1.346E-05
8640.0	4.8193	116.63	31.28	1.084	6.865E-07	7.489E-02	3.810E+07	6.511E-04	6.431E-04	4.496E-07
10440.0	4.8799	113.49	24.63	1.084	3.981E-07	7.468E-02	3.396E+06	4.326E-04	4.271E-04	4.509E-07

TABLE A2.3

Experimental Results from Series E

t (s)	m_t (g)	μ_m (μm)	σ_m (μm)	V (dm^3)	a_{H+} ($kmol/m^3$)	A (m^2)	P_t (-)	ΔC_F ($kmol/m^3$)	ΔC_S ($kmol/m^3$)	R_G (kg/m^2 s)
450.0	0.3600	43.36	9.68	1.083	4.962E-03	1.448E-02	3.504E+06	1.149E-02	8.280E-03	9.649E-05
770.0	0.7600	52.43	12.87	1.084	4.368E-03	2.569E-02	8.506E+06	1.034E-02	7.376E-03	5.438E-05
1085.0	0.9883	68.16	23.20	1.083	3.851E-03	2.911E-02	1.410E+08	9.189E-03	6.454E-03	4.799E-05
1125.0	1.3799	61.69	16.50	1.086	3.790E-03	4.047E-02	2.633E+07	9.002E-03	6.294E-03	3.452E-05
1470.0	1.8699	63.96	16.56	1.084	3.284E-03	5.245E-02	2.399E+07	7.724E-03	5.249E-03	2.664E-05
1685.0	2.0898	68.46	17.94	1.082	2.966E-03	5.493E-02	2.727E+07	6.942E-03	4.620E-03	2.543E-05
1765.0	2.2895	69.87	19.94	1.084	2.839E-03	6.053E-02	7.041E+07	6.635E-03	4.375E-03	2.308E-05
2017.0	2.5398	70.17	18.69	1.084	2.372E-03	6.541E-02	3.784E+07	5.805E-03	3.787E-03	2.136E-05
2210.0	2.7998	77.23	20.33	1.082	1.914E-03	6.532E-02	3.173E+07	5.304E-03	3.541E-03	2.139E-05
2365.0	3.0199	85.07	21.08	1.084	1.492E-03	6.306E-02	1.480E+07	4.957E-03	3.451E-03	2.216E-05
2565.0	3.2998	77.26	20.31	1.082	9.437E-04	7.693E-02	3.683E+07	4.598E-03	3.472E-03	1.816E-05
2745.0	3.5098	81.84	20.80	1.082	5.395E-04	7.660E-02	2.439E+07	4.224E-03	3.435E-03	1.824E-05
2910.0	3.7794	76.32	21.07	1.084	2.888E-04	9.046E-02	7.287E+07	3.767E-03	3.239E-03	1.544E-05
3060.0	3.9397	86.96	23.06	1.083	1.533E-04	8.180E-02	4.060E+07	3.257E-03	2.906E-03	1.708E-05

TABLE A2.3 (continued)

Experimental Results from Series E

t (s)	m_t (g)	μ_m (μm)	σ_m (μm)	V (dm^3)	a_{H+} ($kmol/m^3$)	A (m^2)	P_t (-)	ΔC_F ($kmol/m^3$)	ΔC_S ($kmol/m^3$)	R_G (kg/m^2 s)
3095.0	4.1288	72.92	21.20	1.084	1.316E-04	1.053E-01	1.438E+08	3.120E-03	2.802E-03	1.327E-05
3193.0	4.2294	78.31	21.40	1.084	8.574E-05	9.837E-02	7.075E+07	2.723E-03	2.482E-03	1.420E-05
3327.0	4.3595	80.64	21.83	1.083	4.835E-05	9.819E-02	6.311E+07	2.137E-03	1.971E-03	1.423E-05
3385.0	4.4693	78.82	21.94	1.083	3.817E-05	1.039E-01	9.009E+07	1.870E-03	1.728E-03	1.345E-05
3390.0	4.3929	88.84	30.09	1.084	3.742E-05	9.934E-02	4.426E+08	1.845E-03	1.704E-03	1.406E-05
3435.0	4.5596	85.70	22.67	1.085	3.138E-05	9.599E-02	4.659E+07	1.632E-03	1.507E-03	1.455E-05
3545.0	4.6197	90.38	23.43	1.085	2.103E-05	9.174E-02	3.463E+07	1.106E-03	1.010E-03	1.523E-05
3550.0	4.6298	93.75	22.96	1.082	2.068E-05	8.750E-02	1.675E+07	1.085E-03	9.900E-04	1.597E-05
4120.0	4.7999	88.44	21.89	1.084	5.823E-06	9.638E-02	2.169E+07	6.918E-04	6.503E-04	1.744E-07
9480.0	4.8900	94.66	20.83	1.082	5.623E-07	8.990E-02	5.832E+06	3.948E-04	3.860E-04	1.870E-07

TABLE A2.4

Experimental Results from Series F

t (s)	m_t (g)	μ_m (μm)	σ_m (μm)	V (dm^3)	a_{H^+} ($kmol/m^3$)	A (m^2)	P_t (-)	ΔC_F ($kmol/m^3$)	ΔC_S ($kmol/m^3$)	R_G (kg/m^2s)
1560.0	0.2600	40.06	10.24	1.082	5.454E-03	1.160E-02	7.225E+06	1.115E-02	8.679E-03	3.257E-05
2580.0	0.8299	57.50	15.14	1.080	4.526E-03	2.600E-02	1.524E+07	1.046E-02	8.249E-03	1.453E-05
3120.0	1.1298	68.11	18.92	1.083	4.100E-03	3.036E-02	2.744E+07	9.996E-03	7.918E-03	1.244E-05
3540.0	1.3399	72.11	19.33	1.080	3.796E-03	3.365E-02	2.055E+07	9.693E-03	7.710E-03	1.123E-05
4200.0	1.6000	79.25	18.87	1.082	3.365E-03	3.558E-02	5.779E+06	9.105E-03	7.262E-03	1.062E-05
4320.0	1.4000	89.31	18.62	1.086	3.292E-03	2.709E-02	1.410E+06	8.952E-03	7.134E-03	1.394E-05
4800.0	1.7599	74.42	18.74	1.081	3.015E-03	4.215E-02	1.294E+07	8.578E-03	6.855E-03	8.962E-06
4860.0	1.8600	75.30	18.11	1.084	2.982E-03	4.361E-02	8.230E+06	8.490E-03	6.779E-03	8.662E-06
5310.0	2.0400	87.43	18.12	1.082	2.746E-03	4.029E-02	2.126E+06	8.092E-03	6.465E-03	9.376E-06
6360.0	2.3900	89.05	18.51	1.080	2.266E-03	4.636E-02	2.396E+06	7.086E-03	5.640E-03	8.148E-06
6480.0	1.8600	83.69	17.77	1.084	2.216E-03	3.849E-02	2.425E+06	6.929E-03	5.503E-03	9.815E-06
7020.0	2.6300	88.42	20.30	1.082	2.006E-03	5.209E-02	5.277E+06	6.396E-03	5.055E-03	7.252E-06
7860.0	2.9700	88.39	18.29	1.082	1.704E-03	5.802E-02	2.987E+06	5.525E-03	4.312E-03	6.511E-06
8340.0	3.1600	93.53	17.66	1.080	1.530E-03	5.779E-02	2.187E+06	5.049E-03	3.914E-03	6.537E-06
8910.0	3.3599	98.41	19.48	1.082	1.294E-03	5.867E-02	2.175E+06	4.491E-03	3.469E-03	6.439E-06

TABLE A2.4 (continued)

Experimental Results from Series F

t (s)	m_t (g)	μ_m (μm)	σ_m (μm)	V (dm^3)	a_{H+} ($kmol/m^3$)	A (m^2)	P_t (-)	ΔC_F ($kmol/m^3$)	ΔC_S ($kmol/m^3$)	R_G (kg/m^2s)
9380.0	3.6000	98.04	18.59	1.082	1.056E-03	6.283E-02	2.178E+06	4.099E-03	3.197E-03	6.012E-06
10500.0	3.8599	122.36	25.41	1.082	4.040E-04	5.449E-02	1.641E+06	3.354E-03	2.860E-03	6.933E-06
11330.0	3.9998	133.57	29.78	1.084	1.116E-04	5.221E-02	2.541E+06	2.678E-03	2.460E-03	7.235E-06
11735.0	4.1699	144.64	27.82	1.082	5.245E-05	4.940E-02	8.286E+05	2.253E-03	2.118E-03	7.648E-06
11920.0	4.6100	107.69	20.40	1.083	3.684E-05	7.325E-02	2.111E+06	2.035E-03	1.928E-03	5.157E-06
11975.0	4.3198	139.77	28.07	1.086	3.317E-05	5.319E-02	1.088E+06	1.963E-03	1.863E-03	7.103E-06
12060.0	4.6198	149.92	30.84	1.083	2.824E-05	5.317E-02	1.098E+06	1.865E-03	1.775E-03	7.105E-06
12085.0	4.4299	137.27	27.92	1.083	2.694E-05	5.561E-02	1.243E+06	1.835E-03	1.747E-03	6.793E-06
12140.0	4.4899	137.51	28.03	1.085	2.430E-05	5.628E-02	1.268E+06	1.763E-03	1.681E-03	6.713E-06
12165.0	4.5799	141.15	29.42	1.084	2.319E-05	5.607E-02	1.386E+06	1.734E-03	1.654E-03	6.737E-06
12320.0	4.6098	147.41	28.82	1.084	1.746E-05	5.367E-02	9.073E+05	1.538E-03	1.472E-03	7.039E-06
12675.0	4.6296	163.39	38.73	1.084	9.508E-06	4.990E-02	4.630E+06	1.182E-03	1.137E-03	6.367E-07
13390.0	4.7697	136.24	29.42	1.083	3.624E-06	6.077E-02	2.093E+06	1.125E-03	1.101E-03	5.228E-07
13860.0	4.6999	113.79	23.52	1.084	2.364E-06	7.130E-02	2.361E+06	1.076E-03	1.058E-03	4.456E-07
16380.0	4.7800	107.20	21.45	1.082	1.002E-06	7.670E-02	2.491E+06	7.936E-04	7.834E-04	4.142E-07

TABLE A2.5

Experimental Results from Series G

t (s)	m_t (g)	μ_m (μm)	σ_m (μm)	V (dm^3)	a_{H+} ($kmol/m^3$)	A (m^2)	P_t (-)	ΔC_F ($kmol/m^3$)	ΔC_S ($kmol/m^3$)	R_G (kg/m^2 s)
780.0	2.4276	21.68	9.24	1.086	4.978E-03	1.032E-02	2.042E+08	1.270E-02	1.036E-02	9.710E-05
1080.0	3.3681	33.89	10.09	1.081	4.399E-03	2.665E-02	6.553E+07	1.211E-02	9.944E-03	3.760E-05
1380.0	0.1004	35.02	11.22	1.082	3.888E-03	2.880E-02	1.169E+08	1.140E-02	9.384E-03	3.479E-05
1680.0	0.4826	43.69	9.20	1.084	3.436E-03	3.651E-02	7.248E+06	1.063E-02	8.767E-03	2.745E-05
2070.0	0.5227	52.20	11.90	1.082	2.926E-03	4.968E-02	9.773E+06	9.656E-03	7.964E-03	2.017E-05
2460.0	0.9220	53.09	11.97	1.084	2.492E-03	6.010E-02	1.082E+07	8.583E-03	7.051E-03	1.667E-05
2760.0	4.3872	60.17	17.25	1.084	2.202E-03	7.216E-02	9.314E+07	7.748E-03	6.328E-03	1.389E-05
2940.0	4.0453	57.58	15.06	1.084	2.043E-03	7.581E-02	4.133E+07	7.237E-03	5.881E-03	1.322E-05
3060.0	3.6186	55.83	13.40	1.084	1.942E-03	7.707E-02	1.971E+07	6.894E-03	5.579E-03	1.300E-05
3360.0	3.4554	66.82	16.87	1.085	1.694E-03	7.766E-02	2.656E+07	6.028E-03	4.819E-03	1.290E-05
3720.0	3.0514	63.16	16.28	1.083	1.347E-03	8.657E-02	3.820E+07	5.077E-03	4.029E-03	1.158E-05
4020.0	2.9101	63.63	15.78	1.085	9.359E-04	9.402E-02	2.803E+07	4.414E-03	3.578E-03	1.066E-05
4020.0	2.4385	67.65	16.76	1.084	9.359E-04	9.071E-02	2.537E+07	4.420E-03	3.583E-03	1.105E-05
4320.0	2.3478	66.43	15.49	1.081	4.690E-04	9.563E-02	1.562E+07	3.913E-03	3.370E-03	1.048E-05

TABLE A2.5 (continued)

Experimental Results from Series G

t (s)	m_t (g)	μm (μm)	σ_m (μm)	V (dm^3)	a_{H+} ($kmol/m^3$)	A (m^2)	P_t (-)	ΔC_F ($kmol/m^3$)	ΔC_S ($kmol/m^3$)	R_G (kg/m^2 s)
4620.0	1.8271	66.23	15.51	1.084	1.534E-04	1.073E-01	1.818E+07	3.289E-03	3.022E-03	9.339E-06
4920.0	1.4825	68.26	16.41	1.085	3.728E-05	1.135E-01	2.352E+07	2.436E-03	2.328E-03	8.832E-06
5245.0	4.6085	69.11	16.18	1.085	8.582E-06	1.172E-01	1.888E+07	1.339E-03	1.297E-03	8.553E-06
5520.0	4.6278	70.00	16.60	1.084	3.446E-06	1.164E-01	2.062E+07	1.042E-03	1.019E-03	7.517E-08
6720.0	4.7181	70.65	15.98	1.085	1.020E-06	1.167E-01	1.387E+07	1.016E-03	1.006E-03	7.500E-08
8160.0	4.7307	75.13	16.15	1.083	5.623E-07	1.092E-01	8.736E+06	9.756E-04	9.687E-04	8.011E-08

TABLE A2.6

Experimental Results from Experiments with Recrystallised Barium Chromate

Main series having same experimental conditions	Duration (s)	m_t (g)	μ_m (μm)	σ_m (μm)	A (m^2)	P_t (-)
A	2122.0	4.8796	66.31	24.60	1.561E-01	1.259E+09
D	10440.0	4.9238	111.13	20.91	9.576E-02	2.035E+06
E	9480.0	4.9238	99.21	23.26	8.765E-02	9.799E+06
F	15600.0	4.8942	141.00	29.87	6.010E-02	1.679E+06
G	8160.0	5.0574	96.33	15.43	8.873E-02	2.867E+06

APPENDIX 3

DATA FROM FALANGAS'S 'FREEZING' EXPERIMENTS

The data presented here correspond to the experiments carried out by Falangas (5) by the 'freezing' method using an initial mass of barium chromate of 5 grammes. Stirrer speeds used were 200, 400 and 800 r.p.m. The initial mass of urea taken was 20 grammes. Initial hydrochloric acid strength was 0.06 M and operating temperature was 100°C. A nominal system volume of 1 dm^3 was assumed for all the experiments.

Since only the mass mean equivalent volume diameters of the crystal populations were presented by Falangas (5), crystal surface areas were derived from this data in the manner described below.

For a single crystal, the sphericity (ϕ) can be related to the volume diameter (d_v) and surface area diameter (d_s).

i.e. $$\phi = (d_v/d_s)^2 \quad \ldots\ldots\ldots\ldots\ldots\ldots\ldots \quad (A3.1)$$

A similar relation is assumed to apply to a whole crystal population; and so,

$$d_s^2 = d_v^2/\phi \quad \ldots\ldots\ldots\ldots\ldots\ldots\ldots \quad (A3.2)$$

where, for the population, d_s is the number mean surface area diameter and d_v is the number mean volume diameter.

Now, Falangas's experiments were of short duration, the majority being less than 300 seconds, and the mass

mean volume diameters reported by Falangas were in the main less than 20 μm. If it is assumed that at these small sizes the mass mean volume diameter is a reasonable approximation to the number mean volume diameter, the population (P_t) at any time can be related to the crystal mass (m_t)

$$\text{i.e.} \quad P_t \frac{\pi}{6} L^3 \rho \approx P_t \frac{\pi}{6} d_v^3 \rho = m_t \quad \ldots\ldots\ldots\ldots \quad (A3.3)$$

where, L is the mass mean volume diameter and ρ is the crystal density.

Also, crystal surface area is given by,

$$A = P_t \pi d_s^2 \quad \ldots\ldots\ldots\ldots\ldots\ldots \quad (A3.4)$$

Substituting in equation A3.4 for P_t, using equation A3.3, gives:

$$A = \frac{6 m_t d_s^2}{\rho L^3} \quad \ldots\ldots\ldots\ldots\ldots\ldots \quad (A3.5)$$

Substituting in equation A3.5 for d_s, using equation A3.2 and noting that $d_v \approx L$, yields:

$$A = \frac{6 m_t}{\rho \phi L} \quad \ldots\ldots\ldots\ldots\ldots\ldots \quad (A3.6)$$

It should be noted that equation A3.6 gives an underestimate for crystal surface area because in reality $L > d_v$. This in turn means that growth rate per unit surface area (R_G), calculated using these surface areas, will be overestimated because,

$$R_G = \frac{1}{A} \frac{dm_t}{dt} \quad \ldots\ldots\ldots\ldots\ldots\ldots \quad (A3.7)$$

as presented in Chapter 9.

The collected data of Falangas are listed in table A3.1. Crystal surface areas are tabulated along with values of R_G, calculated using the equations presented above, and also the corresponding mass mean volume diameters. A value of 0.811 was used for crystal sphericity (see Appendix 7) in the surface area calculations. Supersaturation (ΔC) was calculated using the empirical correlation for solubility derived in Chapter 7 from Falangas's own solubility data. Table A3.1 has been computer generated and hence the symbol E denotes exponents to the base ten. The symbols used as headings for the tabulations have been explained in Appendix 1. Each individual data set in table A3.1 corresponds to a separate batch crystallisation experiment.

TABLE A3.1

Experimental Results from Falangas's Batch Crystallisation Experiments

t (s)	m_t (g)	L (μm)	a_{H^+} (kmol/m^3)	A (m^2)	ΔC (kmol/m^3)	R_G (kg/m^2s)	w (r.p.m.)
57.0	0.2246	8.60	3.631E-03	4.294E-02	1.528E-02	3.984E-04	800.0
60.0	0.4222	8.10	3.631E-03	8.569E-02	1.508E-02	1.996E-04	800.0
90.0	0.7632	13.00	3.162E-03	9.652E-02	1.347E-02	1.773E-04	200.0
96.0	0.4054	7.90	3.162E-03	8.437E-02	1.307E-02	2.028E-04	800.0
102.0	0.3027	11.20	3.162E-03	4.443E-02	1.266E-02	3.850E-04	800.0
120.0	1.1507	11.90	2.818E-03	1.590E-01	1.177E-02	1.076E-04	800.0
120.0	1.2571	12.10	2.818E-03	1.708E-01	1.177E-02	1.002E-04	800.0
120.0	1.0025	12.55	2.818E-03	1.313E-01	1.177E-02	1.303E-04	800.0
120.0	0.9895	12.30	2.818E-03	1.323E-01	1.177E-02	1.294E-04	800.0
126.0	1.4328	20.50	2.818E-03	1.149E-01	1.136E-02	1.489E-04	400.0
140.0	1.2565	21.00	2.455E-03	9.837E-02	1.077E-02	1.739E-04	400.0
150.0	1.2515	12.60	2.239E-03	1.633E-01	1.031E-02	1.048E-04	800.0
158.0	1.6992	13.80	1.995E-03	2.024E-01	1.002E-02	8.451E-05	800.0

TABLE A3.1 (Continued)

Experimental Results from Falangas's Batch Crystallisation Experiments

t (s)	m_t (g)	L (μm)	a_{H^+} (kmol/m^3)	A (m^2)	ΔC (kmol/m^3)	R_G (kg/m^2s)	w (r.p.m.)
162.0	1.9527	19.00	2.138E-03	1.690E-01	9.599E-03	1.013E-04	200.0
168.0	1.5095	21.00	1.995E-03	1.182E-01	9.341E-03	1.448E-04	400.0
183.0	2.5065	14.30	1.995E-03	2.882E-01	8.328E-03	5.937E-05	800.0
204.0	2.6635	19.00	1.514E-03	2.305E-01	7.426E-03	7.423E-05	200.0
240.0	3.4720	15.20	1.047E-03	3.755E-01	5.538E-03	4.556E-05	800.0
258.0	3.5845	15.10	8.318E-04	3.903E-01	4.594E-03	4.384E-05	800.0
300.0	4.3115	24.00	3.162E-04	2.953E-01	2.504E-03	5.792E-05	400.0
360.0	4.9835	14.45	1.000E-04	5.670E-01	0.000E+00	1.264E-07	800.0
438.0	4.9795	18.50	3.162E-05	4.425E-01	0.000E+00	1.619E-07	800.0
480.0	4.9835	17.90	1.995E-05	4.577E-01	0.000E+00	1.565E-07	800.0
588.0	4.9905	17.80	1.000E-05	4.609E-01	0.000E+00	1.554E-07	800.0
720.0	4.8907	18.83	5.012E-06	4.270E-01	0.000E+00	1.678E-07	800.0
780.0	4.9768	18.89	3.162E-06	4.331E-01	0.000E+00	1.654E-07	800.0

APPENDIX 4

LISTING OF DIRECT SEARCH OPTIMISATION PROGRAM USED TO CORRELATE SOLUBILITY DATA

The computer program written to correlate the solubility data of Skander (4) and Falangas (5), by means of the direct search non-linear optimisation algorithm of Nelder and Mead (197), is listed in this appendix. The improvements suggested by the work of Schnabel (198) and by Parkinson and Hutchinson (199) have been allowed for in writing and running this program. The program is named SOLPROG and was written in a version of Fortran IV (i.e. extended Fortran) suitable for an ICL 1904S computer. Extensive comment statements in the body of the listing clarify the function of the various program segments.

```
C*********************************************************************
C     PROGRAM TO FIT EXPERIMENTAL DATA FOR THE SOLUBILITY OF  **
C     BARIUM CHROMATE IN ACIDIC SOLUTION, TO A SEMI-EMPIRICAL **
C     MODEL, BY MEANS OF THE NELDER-MEAD, DIRECT SEARCH,      **
C     NONLINEAR OPTIMISATION ALGORITHM                        **
C*********************************************************************
C
C
C     MAIN SEGMENT
C     ************
C
C
      TRACE 0
C
C
      MASTER CONNELMEAD
C
C
C     TYPE SPECIFICATION STATEMENTS
C
      REAL C(100), T(100), R(100)
      REAL S, TOLFM, TOLCR, ALPHA, BETA, GAMMA, RED, CAR
      REAL X(4),P(3),V(3,4),VIH(3),VTOP(3),VLOW(3),Q(3),VR(3),VE(3)
      REAL VC(3), U(3), W(4), FFF, TTT, SUM, PM, PR, PE, PC
      REAL Y(3), TOLTOL, TOLRES, TAB
      REAL A1(21), B1(21), T1(21), D1, FRAC
C
      INTEGER N, K, NS, IH, IL, LC, ITEM, K1, I, J, IMOD
C
C     INPUT FLAG FOR CHOOSING BETWEEN THE HYDROGEN ION ACTIVITY
C     MODEL AND THE HYDROGEN ION CONCENTRATION MODEL
C
      READ(1,5) IMOD
    5 FORMAT(1I0)
C
C     INPUT STOPPING TOLERANCE FOR MAXIMUM RANGE OF
C     OBJECTIVE FUNCTION VALUES IN THE SIMPLEX
C
      READ(1,10) TOLTOL
   10 FORMAT(G20.5)
C
C     INPUT TOLERANCE CRITERION FOR RESTARTING SEARCH
C
      READ(1,10) TOLRES
C
C     INPUT STOPPING TOLERANCE FOR STANDARD DEVIATION OF
C     OBJECTIVE FUNCTION VALUES IN THE SIMPLEX; STOPPING
C     TOLERANCE FOR THE PENALTY FUNCTION; STEP LENGTH OF
C     THE INITIAL SIMPLEX; REFLECTION, CONTRACTION AND
C     EXPANSION PARAMETERS; REDUCTION FACTOR FOR PENALTY
C     FUNCTION; AND, MULTIPLICATION FACTOR FOR PENALTY
C     FUNCTION
C
      READ(1,20) TOLFM, TOLCR, S, ALPHA, BETA, GAMMA, RED, CAR
   20 FORMAT(2G10.5,6G7.5)
C
C     INPUT NUMBER OF PARAMETERS, NUMBER OF DATA POINTS
C     AND NUMBER OF PENALTY FUNCTION CONSTRAINT FACTORS
```

```
C
      READ(1,40) N, K, LC
   40 FORMAT(3(2X,I3))
C
C     INPUT INITIAL VALUES OF THE PARAMETERS
C
      READ(1,60) (X(I), I = 1, N)
   60 FORMAT(10G7.5)
C
C     INPUT SCALE FACTORS FOR THE PARAMETERS
C
      READ(1,60) (U(I), I = 1, N)
C
C     INPUT FACTORS FOR THE PENALTY FUNCTION CONSTRAINTS
C
      READ(1,60) (W(I), I = 1, LC)
C
      K1=21-K
C
C     CALL SUBROUTINE TO INPUT EXPERIMENTAL DATA
C
      CALL DATAIN(K,C(K1),T(K1),R(K1))
C
C     TEST THE MODEL FLAG TO DETERMINE WHETHER THE EXTRA DATA,
C     REQUIRED BY THE HYDROGEN ION CONCENTRATION MODEL, SHOULD
C     BE READ IN
C
      IF(IMOD.GT.0)  GO  TO  100
C
C     READ IN THE EXTRA DATA AND PARAMETERS REQUIRED BY THE
C     HYDROGEN ION CONCENTRATION MODEL
C
      DO 80 I = 1, 21
      READ(1,70) A1(I), B1(I), T1(I)
   70 FORMAT(3F0.0)
   80 CONTINUE
C
      READ(1,90) D1, FRAC
   90 FORMAT(2F0.0)
C
C     INITIALISE VARIABLES AND FLAGS
C
  100 INDEX=0
      ITEM=0
      TAB=0.
      NS=N+1
C
C     CALL SUBROUTINE TO PRINT OUT CONTROL VARIABLES AND
C     PARAMETERS FOR THE OPTIMISATION AND THE
C     EXPERIMENTAL DATA
C
      CALL PARAMETERS(N,NS,K,C(K1),T(K1),TOLFM,TOLCR,S,ALPHA,BETA,GAMMA,
     1X,U,W,LC,RED,CAR,TOLTOL,TOLRES,R(K1))
C
C     CALL SUBROUTINE TO CONVERT PH VALUES TO HYDROGEN
C     ION CONCENTRATION VALUES
C
      IF(IMOD.LT.0)
```

```
     1CALL GEMMA(K,R(K1),A1(1),B1(1),T1(1),D1,FRAC,T(K1),C(K1))
C
C     CALL SUBROUTINE TO SET UP INITIAL SIMPLEX
C
  110 CALL POSIT(N,NS,S,X,V)
C
C     COMPUTE VALUES OF THE OBJECTIVE FUNCTION
C     FOR ALL POINTS OF THE SIMPLEX
C
      DO 120 I = 1, NS
C
C     CALL SUBROUTINE TO TRANSFER THE VECTOR REPRESENTING ONE
C     POINT OF THE SIMPLEX TO AN INTERMEDIATE ARRAY
C
      CALL TRANS(N,NS,I,V,Q)
C
C     CALL SUBROUTINE TO CHECK THE BOUND OF THE SECOND
C     MODEL PARAMETER, FOR EACH POINT OF THE SIMPLEX
C
      CALL BOUND(Q,U,N)
C
C     CALL SUBROUTINE TO CALCULATE THE OBJECTIVE FUNCTION
C
      CALL FUNCT(Q,K,C(K1),T(K1),P(I),CAR,U,W,N,LC,R(K1))
C
  120 CONTINUE
C
C     CALL SUBROUTINE TO CALCULATE THE MEAN OBJECTIVE FUNCTION
C     FOR THE SIMPLEX, AND ITS STANDARD DEVIATION
C
      CALL MEAN(N,NS,P,PM,TTT)
C
C     CALL SUBROUTINE TO PRINT OUT THE SIMPLEX AND ASSOCIATED
C     FUNCTION VALUES AT ANY SPECIFIED ITERATION DURING THE
C     OPTIMISATION
C
  140 CALL PRINT(INDEX,N,NS,V,CAR,TTT)
C
C
C     INCREMENT ITERATION NUMBER
C
      INDEX=INDEX+1
C
C     CALL SUBROUTINE TO FIND THE MINIMUM AND THE MAXIMUM
C     VALUES OF THE OBJECTIVE FUNCTION AT POINTS OF THE
C     CURRENT SIMPLEX
C
      CALL MINIMAX(NS,P,IH,IL)
C
C     CALL SUBROUTINE TO TRANSFER THE VECTOR REPRESENTING THE
C     POINT OF THE SIMPLEX HAVING THE LARGEST VALUE OF THE
C     OBJECTIVE FUNCTION, TO AN INTERMEDIATE ARRAY
C
      CALL TRANS(N,NS,IH,V,VTOP)
C
C     CALL SUBROUTINE TO TRANSFER THE VECTOR REPRESENTING THE
C     POINT OF THE SIMPLEX HAVING THE SMALLEST VALUE OF THE
C     OBJECTIVE FUNCTION, TO AN INTERMEDIATE ARRAY
```

```
C
      CALL TRANS(N,NS,IL,V,VLOW)
C
C     CALL SUBROUTINE TO CALCULATE THE CENTROID OF
C     THE CURRENT SIMPLEX
C
      CALL CENT(N,NS,V,IH,VIH)
C
C     CALL SUBROUTINE TO CARRY OUT REFLECTION STEP
C     OF THE SEARCH ALGORITHM
C
      CALL REFLECT(N,VTOP,VR,VIH,ALPHA)
C
C     CALL SUBROUTINE TO CHECK THE BOUND OF THE SECOND
C     MODEL PARAMETER, FOR THE REFLECTED POINT
C
      CALL BOUND(VR,U,N)
C
C     CALL SUBROUTINE TO CALCULATE THE OBJECTIVE FUNCTION
C     FOR THE REFLECTED POINT
C
      CALL FUNCT(VR,K,C(K1),T(K1),PR,CAR,U,W,N,LC,R(K1))
C
C     TEST OBJECTIVE FUNCTION VALUES TO EITHER, TRANSFER CONTROL
C     TO TEST WHETHER REFLECTED POINT SHOULD BE RETAINED OR
C     DISCARDED, OR TO CARRY OUT EXPANSION
C
      IF(PR.GT.P(IL)) GO TO 200
C
C     CALL SUBROUTINE TO CARRY OUT EXPANSION STEP
C     OF THE SEARCH ALGORITHM
C
      CALL EXPAND(N,VR,VE,VIH,GAMMA)
C
C     CALL SUBROUTINE TO CHECK THE BOUND OF THE SECOND
C     MODEL PARAMETER, FOR THE EXPANDED POINT
C
      CALL BOUND(VE,U,N)
C
C     CALL SUBROUTINE TO CALCULATE THE OBJECTIVE
C     FUNCTION FOR THE EXPANDED POINT
C
      CALL FUNCT(VE,K,C(K1),T(K1),PE,CAR,U,W,N,LC,R(K1))
C
C     TEST OBJECTIVE FUNCTION VALUES TO REPLACE THE POINT
C     OF THE SIMPLEX, HAVING THE LARGEST VALUE OF THE
C     OBJECTIVE FUNCTION, WITH EITHER THE EXPANDED POINT
C     OR THE REFLECTED POINT
C
      IF(PE.LT.P(IL)) GO TO 180
C
C     CALL SUBROUTINE TO REPLACE THE POINT OF THE SIMPLEX,
C     HAVING THE LARGEST VALUE OF THE OBJECTIVE FUNCTION,
C     WITH THE REFLECTED POINT
C
  160 CALL REPLACE(N,NS,IH,VR,V)
C
      P(IH)=PR
```

```
C
      GO TO 400
C
C     CALL SUBROUTINE TO REPLACE THE POINT OF THE SIMPLEX,
C     HAVING THE LARGEST VALUE OF THE OBJECTIVE FUNCTION,
C     WITH THE EXPANDED POINT
C
  180 CALL REPLACE(N,NS,IH,VE,V)
C
      P(IH)=PE
C
      GO TO 400
C
C     TEST OBJECTIVE FUNCTION VALUES TO EITHER RETAIN REFLECTED
C     POINT, OR TO DISCARD IT AND PROCEED TO THE CONTRACTION
C     STEP OF THE SEARCH ALGORITHM
C
  200 DO 220 I = 1, NS
C
      IF(I.EQ.IH) GO TO 220
C
      IF(PR.LE.P(I)) GO TO 160
C
  220 CONTINUE
C
      IF(PR.GT.P(IH)) GO TO 240
C
C     CALL SUBROUTINE TO REPLACE THE POINT OF THE SIMPLEX,
C     HAVING THE LARGEST VALUE OF THE OBJECTIVE FUNCTION,
C     WITH THE REFLECTED POINT
C
      CALL REPLACE(N,NS,IH,VR,V)
C
      P(IH)=PR
C
C     CALL SUBROUTINE TO TRANSFER THE VECTOR REPRESENTING THE
C     POINT OF THE SIMPLEX HAVING THE LARGEST VALUE OF THE
C     OBJECTIVE FUNCTION, TO AN INTERMEDIATE ARRAY
C
      CALL TRANS(N,NS,IH,V,VTOP)
C
C     CALL SUBROUTINE TO CARRY OUT THE CONTRACTION
C     STEP OF THE SEARCH ALGORITHM
C
  240 CALL CONTRACT(N,VTOP,VC,VIH,BETA)
C
C     CALL SUBROUTINE TO CHECK THE BOUND OF THE SECOND
C     MODEL PARAMETER, FOR THE CONTRACTED POINT
C
      CALL BOUND(VC,U,N)
C
C     CALL SUBROUTINE TO CALCULATE THE OBJECTIVE FUNCTION
C     FOR THE CONTRACTED POINT
C
      CALL FUNCT(VC,K,C(K1),T(K1),PC,CAR,U,W,N,LC,R(K1))
C
C     TEST OBJECTIVE FUNCTION VALUES TO EITHER RETAIN CONTRACTED
C     POINT, OR TO SET UP A NEW, SMALLER, SIMPLEX
```

```
C
      IF(PC.GT.P(IH)) GO TO 260
C
C     CALL SUBROUTINE TO REPLACE THE POINT OF THE SIMPLEX,
C     HAVING THE LARGEST VALUE OF THE OBJECTIVE FUNCTION,
C     WITH THE CONTRACTED POINT
C
      CALL REPLACE(N,NS,IH,VC,V)
C
      P(IH)=PC
C
      GO TO 400
C
C     CONSTRUCT NEW, SMALLER, SIMPLEX
C
  260 DO 300 I = 1, NS
C
      IF(I.EQ.IL) GO TO 300
C
      DO 280 J = 1, N
      V(J,I)=0.5*(V(J,I)+V(J,IL))
  280 CONTINUE
C
  300 CONTINUE
C
C     COMPUTE VALUES OF THE OBJECTIVE FUNCTION
C     FOR ALL POINTS OF THE SIMPLEX
C
      DO 320 I = 1, NS
C       .
C     CALL SUBROUTINE TO TRANSFER THE VECTOR REPRESENTING ONE
C     POINT OF THE SIMPLEX TO AN INTERMEDIATE ARRAY
C
      CALL TRANS(N,NS,I,V,Q)
C
C     CALL SUBROUTINE TO CHECK THE BOUND OF THE SECOND
C     MODEL PARAMETER, FOR EACH POINT OF THE SIMPLEX
C
      CALL BOUND(Q,U,N)
C
C     CALL SUBROUTINE TO CALCULATE THE OBJECTIVE FUNCTION
C
      CALL FUNCT(Q,K,C(K1),T(K1),P(I),CAR,U,W,N,LC,R(K1))
  320 CONTINUE
C
C     CALL SUBROUTINE TO CALCULATE THE MEAN OBJECTIVE FUNCTION
C     FOR THE SIMPLEX, AND ITS STANDARD DEVIATION
C
  400 CALL MEAN(N,NS,P,PM,TTT)
C
C     CALL SUBROUTINE TO CHECK FOR FALSE CONVERGENCE
C     AND, IF SO, TO RESTART THE SEARCH
C
      CALL RESTART(TAB,TTT,ITEM,TOLRES,V,N,NS,X,S,&110)
C
C     TEST THE TOLERANCE CRITERION FOR THE STANDARD
C     DEVIATION OF THE MEAN OBJECTIVE FUNCTION
C
```

```
      IF(PM.GE.TOLFM) GO TO 140
C
C     CALL SUBROUTINE TO FIND THE MINIMUM AND THE MAXIMUM
C     VALUES OF THE OBJECTIVE FUNCTION AT POINTS OF THE
C     CURRENT SIMPLEX
C
      CALL MINIMAX(NS,P,IH,IL)
C
C     TEST THE RANGE TOLERANCE CRITERION FOR THE VALUES OF
C     THE OBJECTIVE FUNCTION, AT THE POINTS OF THE SIMPLEX
C
      IF(ABS(P(IH)-P(IL)).GE.TOLTOL) GO TO 140
C
C     TEST THE TOLERANCE FOR THE PENALTY FUNCTION
C     MULTIPLICATION FACTOR
C
      IF(CAR.LT.TOLCR) GO TO 420
C
C     REDUCE THE PENALTY FUNCTION MULTIPLICATION FACTOR
C
      CAR=CAR/RED
C
      GO TO 140
C
C     CARRY OUT FINAL TEST ON PENALTY FUNCTION MULTIPLICATION
C     FACTOR, AND SET IT TO ZERO
C
  420 IF(.NOT.CAR.GT.0.) GO TO 440
C
      CAR=0.
C
      GO TO 140
C
C     PRINT OUT HEADING FOR RESULTS OF OPTIMISATION
C
  440 WRITE(2,460)
  460 FORMAT(1H0//20X,7HRESULTS,//10X,27(1H*))
C
C     PRINT OUT NUMBER OF CYCLES AND VALUE OF PENALTY FUNCTION
C
      WRITE(2,480) INDEX, CAR
  480 FORMAT(1H0//10X,27HPOSITION MATRIX AT CYCLE : ,I4,10X,19HCARROLL C
     1ONSTANT : ,G10.5)
C
C     PRINT OUT FINAL SEARCH SIMPLEX
C
      DO 520 I = 1, N
      WRITE(2,500) (V(I,J), J = 1, NS)
  500 FORMAT(1H0//5X,10(F9.4,2X))
  520 CONTINUE
C
C     COMPUTE MEAN VALUES OF OPTIMISED MODEL PARAMETERS
C     FROM FINAL SIMPLEX
C
      DO 560 I = 1, N
C
      SUM=0.
C
```

```
      DO 540 J = 1, NS
      SUM=SUM+V(I,J)
  540 CONTINUE
C
      Y(I)=SUM/FLOAT(NS)
      X(I)=SUM*U(I)/FLOAT(NS)
C
  560 CONTINUE
C
C     PRINT OUT MEAN VALUES OF OPTIMISED MODEL PARAMETERS
C
      WRITE(2,580)
  580 FORMAT(1H0//15X,8HVARIABLE,20X,5HVALUE)
C
      DO 620 I = 1, N
      WRITE(2,600) I, X(I)
  600 FORMAT(1H0//17X,I4,22X,F12.5)
  620 CONTINUE
C
C     CALCULATE FINAL VALUE OF MEAN OBJECTIVE FUNCTION
C
      CALL FUNCT(Y,K,C(K1),T(K1),FFF,CAR,U,W,N,LC,R(K1))
C
C     PRINT OUT  FINAL VALUE OF MEAN OBJECTIVE FUNCTION
C
      WRITE(2,640) FFF
  640 FORMAT(1H0//17X,21HOBJECTIVE FUNCTION = ,F15.6)
C
C     CALCULATE THE STANDARD ERROR OF THE FIT
C
      FFF=SQRT(FFF/FLOAT(K))
C
C     PRINT OUT THE STANDARD ERROR OF THE FIT
C
      WRITE(2,660) FFF
  660 FORMAT(1H0//17X,15HR.M.S. ERROR : ,F15.6)
C
      STOP
C
      END
C
C
C
C     THE SUBROUTINE 'DATAIN' READS IN THE SETS OF EXPERIMENTAL
C     DATA, CONSISTING OF SOLUBILITY, SOLUTION PH AND TEMPERATURE
C     ************************************************************
C
      SUBROUTINE DATAIN(K,C,T,R)
C
      REAL C(K), T(K), R(K)
C
      INTEGER K, I
C
      DO 40 I = 1, K
C
      READ(1,20) C(I), R(I), T(I)
   20 FORMAT(3G20.5)
C
```

```
   40 CONTINUE
C
      RETURN
C
      END
C
C
C
C     THE SUBROUTINE 'PARAMETERS' PRINTS OUT THE VALUES OF ALL
C     THE CONTROL VARIABLES AND PARAMETERS FOR THE OPTIMISATION
C     PROCESS, AND THE EXPERIMENTAL DATA POINTS
C     ********************************************************
C
      SUBROUTINE PARAMETERS(N,NS,K,C,T,TOLFM,TOLCR,S,ALPHA,BETA,GAMMA,X,
     1U,W,LC,RED,CAR,TOLTOL,TOLRES,R)
C
      REAL C(K),T(K),TOLFM,TOLCR,S,ALPHA,BETA,GAMMA,X(N),U(N),W(LC),RED
      REAL R(K), TOLTOL, TOLRES
C
      INTEGER N, NS, K, LC, I
C
      WRITE(2,20)
   20 FORMAT(1H0//25X,15HTEST PARAMETERS//20X,25(1H*))
C
      WRITE(2,40) N, NS, LC, K
   40 FORMAT(1H0//10X,22HNUMBER OF VARIABLES : ,I3//10X,30HNUMBER OF POI
     1NTS IN SIMPLEX : ,I3//10X,24HNUMBER OF CONSTRAINTS : ,I3//10X,24HN
     2UMBER OF DATA POINTS : ,I3)
C
      WRITE(2,60)
   60 FORMAT(1H0//30X,12HDATA  POINTS//20X,1HC,30X,1HT)
C
      DO 100 I = 1, K
      WRITE(2,80) C(I), R(I), T(I)
   80 FORMAT(1H0//16X,F11.5,20X,F11.5,20X,F11.5)
  100 CONTINUE
C
      WRITE(2,120) ALPHA, BETA, GAMMA, S, TOLFM, TOLTOL, TOLCR, RED, CAR
  120 FORMAT(1H0//10X,17HSEARCH PARAMETERS//10X,8HALPHA : ,F9.4//10X,7HB
     1ETA : ,F10.4//10X,8HGAMMA : ,F9.4//10X,33HSTEP LENGTH OF INITIAL S
     2IMPLEX : ,F10.4//10X,32HOBJECTIVE FUNCTION TOLERANCES : ,G20.5,2X,
     33HAND,2X,G20.5//10X,29HPENALTY FUNCTION TOLERANCE : ,G20.5//10X,19
     4HREDUCTION FACTOR : ,F9.4//10X,19HCARROLL CONSTANT : ,F9.4)
C
      WRITE(2,130) TOLRES
  130 FORMAT(1H0//10X,20HRESTART TOLERANCE : ,G20.5)
C
      WRITE(2,140)
  140 FORMAT(1H0//10X,30HINITIAL ESTIMATES OF VARIABLES//10X,8HVARIABLE,
     110X,12HSCALED VALUE)
C
      DO 180 I = 1, N
      WRITE(2,160) I, X(I)
  160 FORMAT(1H0/14X,I3,11X,F10.4)
  180 CONTINUE
C
      WRITE(2,200)
  200 FORMAT(1H0//10X,13HSCALE FACTORS//10X,8HVARIABLE,10X,6HFACTOR)
```

```
C
      DO 240 I = 1, N
      WRITE(2,220) I, U(I)
  220 FORMAT(1H0/10X,I3,10X,G20.5)
  240 CONTINUE
C
      WRITE(2,260)
  260 FORMAT(1H0//10X,24HPENALTY FUNCTION FACTORS//10X,8HVARIABLE,10X,6H
     1FACTOR)
C
      DO 300 I = 1, LC
      WRITE(2,280) I, W(I)
  280 FORMAT(1H0/10X,I3,10X,G20.5)
  300 CONTINUE
C
      RETURN
C
      END
C
C
C
C     THE SUBROUTINE 'POSIT' SETS UP THE INITIAL SIMPLEX AT THE
C     START OF THE SEARCH METHOD, AND WHEN THE SEARCH IS
C     RESTARTED AFTER CHECKING FOR FALSE CONVERGENCE
C     ***********************************************************
C
      SUBROUTINE POSIT(N,NS,S,X,V)
C
      REAL X(N), V(N,NS), S
C
      INTEGER M, N, NS, L
C
      DO 20 M = 1, N
      V(M,1)=X(M)
   20 CONTINUE
C
      DO 60 L = 2, NS
C
      DO 40 M = 1, N
C
      V(M,L)=X(M)+S
C
      IF(.NOT.M.EQ.L-1)  V(M,L)=X(M)
C
   40 CONTINUE
C
   60 CONTINUE
C
      RETURN
C
      END
C
C
C
C     THE SUBROUTINE 'BOUND' CHECKS THE PRESET BOUND ON THE
C     SECOND MODEL PARAMETER AND RESETS ITS VALUE IF THE
C     BOUND HAS BEEN EXCEEDED
C     ***********************************************************
```

```
C
      SUBROUTINE BOUND(Q,U,N)
C
      REAL Q(N), U(N)
C
      INTEGER N
C
      IF(Q(2)*U(2).GT.0.0)  Q(2)=0.0
C
      RETURN
C
      END
C
C
C
C     THE SUBROUTINE 'TRANS' TRANSFERS A VECTOR REPRESENTING
C     ONE OF THE POINTS OF THE SEARCH SIMPLEX TO A HOLDING
C     ARRAY TO FACILITATE ITS PROCESSING BY OTHER SUBROUTINES
C     ************************************************************
C
      SUBROUTINE TRANS (N,NS,IND,V,R)
C
      REAL V(N,NS),R(N)
C
      INTEGER N,NS,IND, I
C
      DO 20 I = 1, N
      R(I)=V(I,IND)
   20 CONTINUE
C
      RETURN
C
      END
C
C
C
C     THE SUBROUTINE 'FUNCT' CALCULATES THE VALUE OF THE
C     OBJECTIVE FUNCTION AT ANY SUPPLIED POINT OF THE
C     SIMPLEX. A LEAST SQUARES OBJECTIVE FUNCTION WAS
C     USED HERE, WITH THE SOLUBILITY BEING REPRESENTED
C     BY A MODEL CONSISTING OF A POWER LAW TERM IN
C     HYDROGEN ION ACTIVITY AND AN ARRHENIUS TYPE
C     TEMPERATURE DEPENDENCE TERM
C     ************************************************
C
      SUBROUTINE FUNCT(Q,K,C,T,P,CAR,U,W,N,LC,R)
C
      REAL Q(N), C(K), T(K), P, CAR, U(N), W(LC), R(K)
      REAL A, B, D, G, F, S, Z, SUM
C
      INTEGER K, I, N, LC
C
      A=Q(1)*U(1)
      B=Q(2)*U(2)
      D=Q(3)*U(3)
C
      SUM=0.0
C
```


```
      DO 60 I = 1, K
C
      G=1.0/(273.0+T(I))
      F=A*EXP(B*G)
      S=EXP10(-1.0*R(I))
C
      IF(D.GE.0.0)  Z=S**D
C
      IF(D.LT.0.0)  Z=1.0/(S**(ABS(D)))
C
      SUM=SUM+((C(I)-(Z*F))**2.0)
C
   60 CONTINUE
C
      P=SUM
C
      RETURN
C
      END
C
C
C
C     THE SUBROUTINE 'PRINT' PRINTS OUT THE SIMPLEX AT A
C     PARTICULAR ITERATION. THE NUMBER OF CYCLES, THE
C     PENALTY FUNCTION AND THE MEAN OBJECTIVE FUNCTION
C     ARE ALSO PRINTED OUT
C     ***************************************************
C
      SUBROUTINE PRINT(INDEX,N,NS,V,CAR,TTT)
C
      REAL V(N,NS), CAR, TTT
C
      INTEGER INDEX, N, NS, L, I
C
      IF(INDEX.GT.1) GO TO 100
C
      WRITE(2,40) INDEX, CAR
   40 FORMAT(1H0//10X,27HPOSITION MATRIX AT CYCLE : ,I4,10X,19HCARROLL C
     1ONSTANT : ,G10.5)
C
      DO 80 I = 1, N
      WRITE(2,60) (V(I,J), J = 1, NS)
   60 FORMAT(1H0//5X,10(F9.4,2X))
   80 CONTINUE
C
      WRITE(2,90) TTT
   90 FORMAT(1H0,10X,26HMEAN OBJECTIVE FUNCTION = ,F15.6)
C
      GO TO 200
C
  100 DO 120 L = 1000, 10000, 2000
      IF(INDEX.EQ.L) GO TO 140
  120 CONTINUE
C
      GO TO 200
C
  140 WRITE(2,40) INDEX,CAR
C
```

```
      DO 160 I = 1, N
      WRITE(2,60) (V(I,J), J = 1, NS)
  160 CONTINUE
C
      WRITE(2,90) TTT
C
  200 RETURN
C
      END
C
C
C
C     THE SUBROUTINE 'MINIMAX' IDENTIFIES THE MINIMUM AND
C     THE MAXIMUM VALUES OF THE OBJECTIVE FUNCTION AT THE
C     POINTS OF THE SIMPLEX
C     ****************************************************
C
      SUBROUTINE MINIMAX(NS,F,IH,IL)
C
      REAL F(NS)
C
      INTEGER NS, IH, IL, M
C
      IH=1
      IL=1
C
      DO 20 M = 2, NS
C
      IF(F(M).GE.F(IL)) GO TO 20
C
      IL=M
C
   20 CONTINUE
C
      DO 40 M = 2, NS
C
      IF(F(M).LE.F(IH)) GO TO 40
C
      IH=M
C
   40 CONTINUE
C
      RETURN
C
      END
C
C
C
C     THE SUBROUTINE 'CENT' CALCULATES THE VECTOR OF THE
C     CENTROID OF THE CURRENT SIMPLEX
C     ****************************************************
C
      SUBROUTINE CENT(N,NS,V,IH,VIH)
C
      REAL SUM, V(N,NS), VIH(N)
C
      INTEGER N, NS, IH, M, L
C
```

```
      DO 20 M = 1, N
C
      SUM=0.
C
      DO 10 L = 1, NS
C
      IF(L.EQ.IH) GO TO 10
C
      SUM=SUM+V(M,L)
C
   10 CONTINUE
C
      VIH(M)=SUM/FLOAT(N)
C
   20 CONTINUE
C
      RETURN
C
      END
C
C
C
C     THE SUBROUTINE 'REFLECT' CARRIES OUT THE REFLECTION STEP
C     OF THE SEARCH ALGORITHM. THE POINT OF THE SIMPLEX
C     CORRESPONDING TO THE LARGEST VALUE OF THE OBJECTIVE
C     FUNCTION, IS REFLECTED WITH RESPECT TO THE CENTROID OF
C     THE SIMPLEX
C     ***********************************************************
C
      SUBROUTINE REFLECT(N,VTOP,VR,VIH,ALPHA)
C
      REAL VTOP(N),VR(N),VIH(N),ALPHA
C
      INTEGER N, I
C
      DO 20 I = 1, N
      VR(I)=VIH(I)+ALPHA*(VIH(I)-VTOP(I))
   20 CONTINUE
C
      RETURN
C
      END
C
C
C
C     THE SUBROUTINE 'EXPAND' CARRIES OUT THE EXPANSION STEP
C     OF THE SEARCH ALGORITHM. THE REFLECTED POINT IS EXPANDED
C     ALONG THE DIRECTION IN WHICH REFLECTION WAS ORIGINALLY
C     CARRIED OUT
C     ***********************************************************
C
      SUBROUTINE EXPAND(N,VR,VE,VIH,GAMMA)
C
      REAL VR(N),VE(N),VIH(N),GAMMA
C
      INTEGER N, I
C
      DO 20 I = 1, N
```

```
      VE(I)=VIH(I)+GAMMA*(VR(I)-VIH(I))
   20 CONTINUE
C
      RETURN
C
      END
C
C
C
C     THE SUBROUTINE 'REPLACE' REPLACES ONE SPECIFIED COLUMN
C     OF THE MATRIX REPRESENTING THE SIMPLEX, WITH A SUPPLIED
C     VECTOR, WHICH REPRESENTS A NEW POINT TO BE INCLUDED IN
C     THE SIMPLEX
C     ******************************************************
C
      SUBROUTINE REPLACE(N,NS,IND,R,V)
C
      REAL R(N), V(N,NS)
C
      INTEGER N, NS, I, IND
C
      DO 20 I = 1, N
      V(I,IND)=R(I)
   20 CONTINUE
C
      RETURN
C
      END
C
C
C
C     THE SUBROUTINE 'CONTRACT' CARRIES OUT THE CONTRACTION STEP
C     OF THE SEARCH ALGORITHM. THE POINT OF THE SIMPLEX
C     CORRESPONDING TO THE LARGEST VALUE OF THE OBJECTIVE
C     FUNCTION IS CONTRACTED WITH RESPECT TO THE CENTROID OF
C     THE SIMPLEX
C     ************************************************************
C
      SUBROUTINE CONTRACT(N,VTOP,VC,VIH,BETA)
C
      REAL VTOP(N),VC(N),VIH(N),BETA
C
      INTEGER N, I
C
      DO 20 I = 1, N
      VC(I)=VIH(I)+BETA*(VTOP(I)-VIH(I))
   20 CONTINUE
C
      RETURN
C
      END
C
C
C
C     THE SUBROUTINE 'MEAN' CALCULATES THE MEAN VALUE OF
C     THE OBJECTIVE FUNCTION, FOR THE CURRENT SIMPLEX,
C     AND THE STANDARD DEVIATION OF THE OBJECTIVE FUNCTION
C     ****************************************************
```

```
C
      SUBROUTINE MEAN(N,NS,F,FM,T)
C
      REAL F(NS), FM, T, SUM
C
      INTEGER NS, N, I
C
      SUM=0.
C
      DO 20 I = 1, NS
      SUM=SUM+F(I)
   20 CONTINUE
C
      T=SUM/FLOAT(NS)
      SUM=0.
C
      DO 40 I = 1, NS
      SUM=SUM+((F(I)-T)**2)
   40 CONTINUE
C
      FM=SUM/FLOAT(N)
C
      RETURN
C
      END
C
C
C
C     THE SUBROUTINE 'RESTART' CHECKS FOR FALSE CONVERGENCE
C     ACCORDING TO A SIMPLE RESTART TOLERANCE CRITERION
C     APPLIED TO THE MEAN OBJECTIVE FUNCTION OF THE SIMPLEX.
C     IF A RESTART IS FOUND TO BE NECESSARY, THE STEP LENGTH
C     FOR THE NEW STARTING SIMPLEX IS ALSO SET
C     ********************************************************
C
      SUBROUTINE RESTART(TAB,TTT,ITEM,TOLRES,V,N,NS,X,S,*)
C
      REAL TAB,SUM,S,TTT,TOLRES,V(N,NS),X(N)
C
      INTEGER ITEM,N,NS,I
C
      IF(ABS(TAB-TTT).GT.TOLRES) GO TO 60
C
      ITEM=ITEM+1
C
      IF(ITEM.LT.10) GO TO 60
C
      DO 40 I = 1, N
C
      SUM=0.
C
      DO 20 J = 1, NS
      SUM=SUM+V(I,J)
   20 CONTINUE
C
      X(I)=(SUM/FLOAT(NS))
C
   40 CONTINUE
```

```
C
      ITEM=0
      TAB=0.
      S=0.005
C
      RETURN 1
C
   60 TAB=TTT
C
      S=0.1
C
      RETURN
C
      END
C
C
C
C     THE SUBROUTINE 'GEMMA' CONVERTS THE EXPERIMENTAL PH
C     VALUES TO HYDROGEN ION CONCENTRATION VALUES.THE
C     ACTIVITY COEFFICIENTS ARE CALCULATED BY MEANS OF
C     THE DEBYE-HUCKEL EQUATION.THE CONSTANTS REQUIRED BY
C     THIS EQUATION ARE CALCULATED BY INTERPOLATION FROM
C     SUPPLIED DATA, AT THE OPERATING TEMPERATURE.THE
C     SUPPLIED DATA TAKES INTO ACCOUNT THE EFFECT OF
C     UREA, IF ANY IS PRESENT, ON THE DIELECTRIC CONSTANT
C     OF THE MEDIUM, AND HENCE ON THE CONSTANTS. THE
C     INTERPOLATION IS CARRIED OUT USING THE ROUTINE
C     'E01ADF' FROM THE NAG LIBRARY. FURTHERMORE, IT IS
C     ASSUMED THAT ALL THE CR(VI) SPECIES PRESENT IN
C     SOLUTION ARE IN EITHER THE MONOVALENT STATE OR THE
C     DIVALENT STATE
C     ***************************************************
C
      SUBROUTINE GEMMA(K,R,A1,B1,T1,D1,F,T,C)
C
      REAL A1(21), B1(21), T1(21), W1(21), W2(21)
      REAL D1, F, R(K), T(K), C(K)
      REAL A, B, X1, X2, Y, H
C
      INTEGER K, I
C
      DO 60 I = 1, K
C
      CALL E01ADF(20,T(I),T1,A1,W1,W2,21,A)
      CALL E01ADF(20,T(I),T1,B1,W1,W2,21,B)
C
      H=1.0
C
   20 Y=H
C
      X=EXP10(-1.0*R(I))
      X1=(X/Y)+(4.0-F)*C(I)
      X2=SQRT(X1)
C
      H=-1.0*A*X2/(1.0+(D1*B*X2))
      H=EXP10(H)
C
      IF(ABS(Y-H).LT.1.0E-05)  GO  TO  40
```

```
C
      GO  TO  20
C
   40 R(I)=X/H
C
   60 CONTINUE
C
      RETURN
C
      END
C
C
C
      FINISH
C
C
C     END OF PROGRAM
C     **************
```

APPENDIX 5

CORRELATIONS FOR BARIUM CHROMATE SOLUBILITY - GRAPHICAL RESULTS

The graphs in this appendix represent the correlations derived from the solubility data of Skander (4) and Falangas (5). Graphs A5.1 to A5.5 are for the correlations based on hydrogen ion concentrations (i.e. pC_H values). Graphs A5.6 to A5.10 are based on hydrogen ion activities (i.e. pH values).

GRAPH A5. 1 SOLUBILITY IN HYDROCHLORIC ACID

(SKANDER'S DATA) .

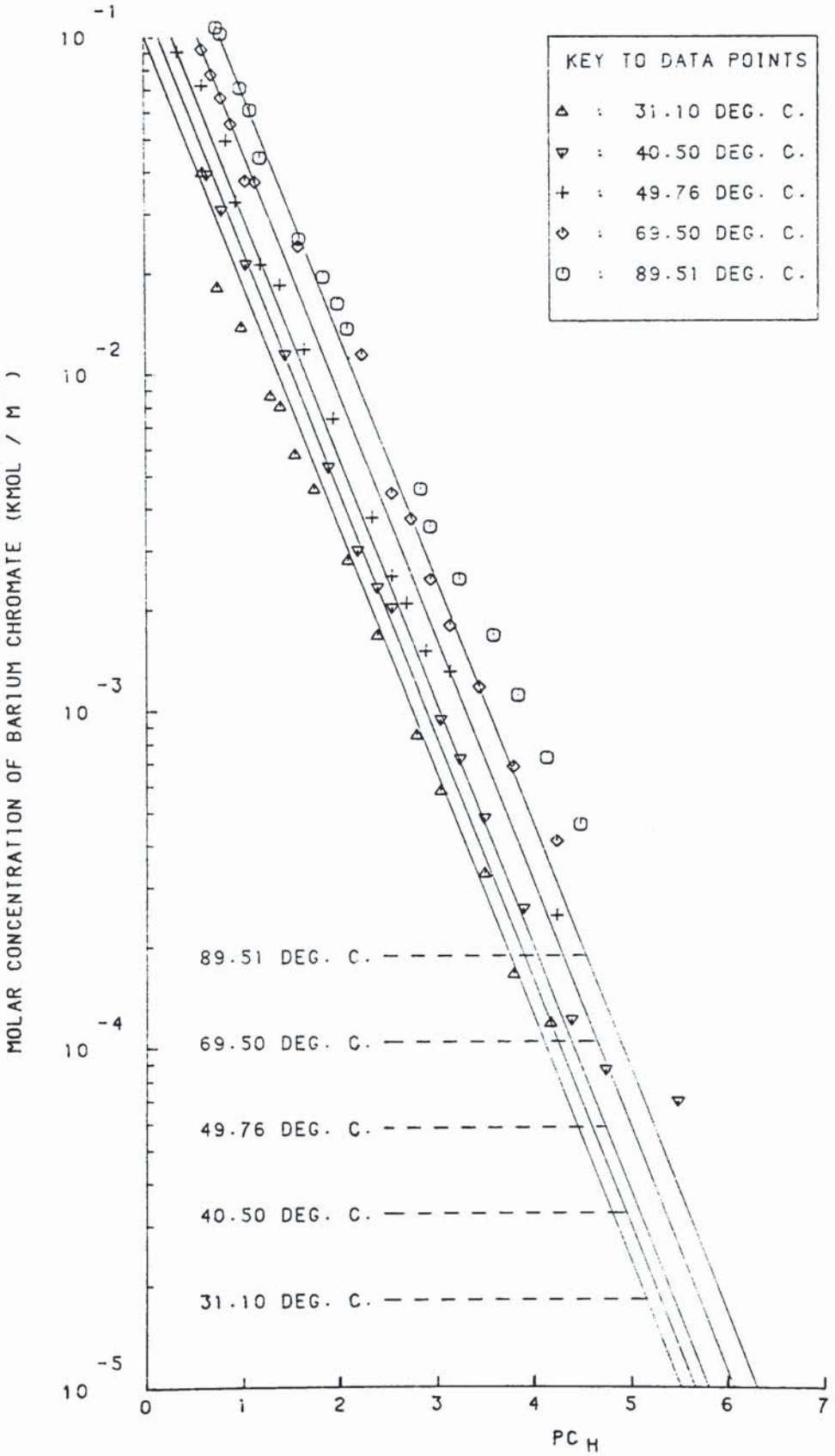

GRAPH A5. 2 SOLUBILITY IN HYDROCHLORIC ACID

(FALANGAS'S DATA)

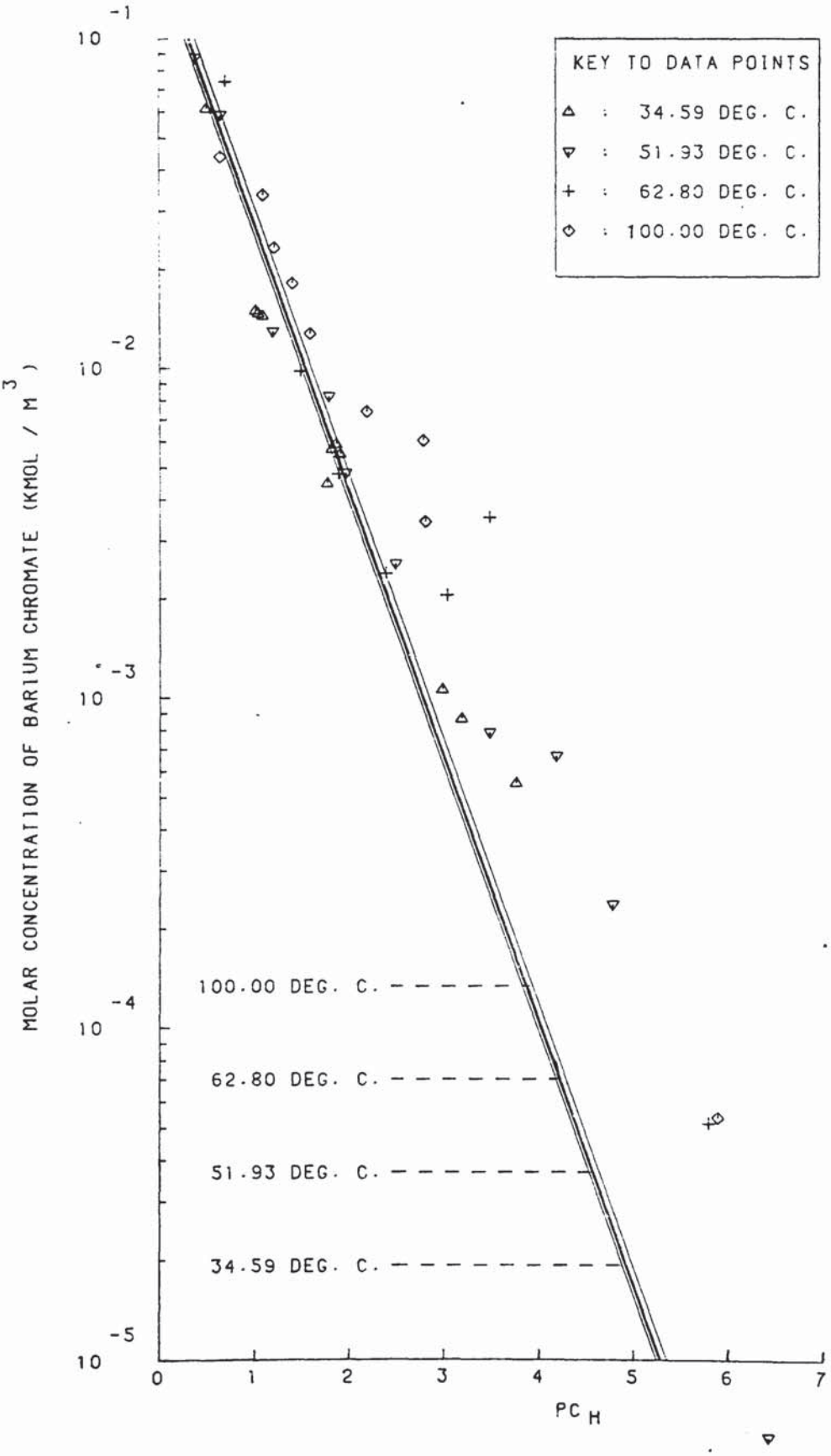

GRAPH AS. 3 SOLUBILITY IN HYDROCHLORIC ACID / UREA

(FALANGAS'S DATA)

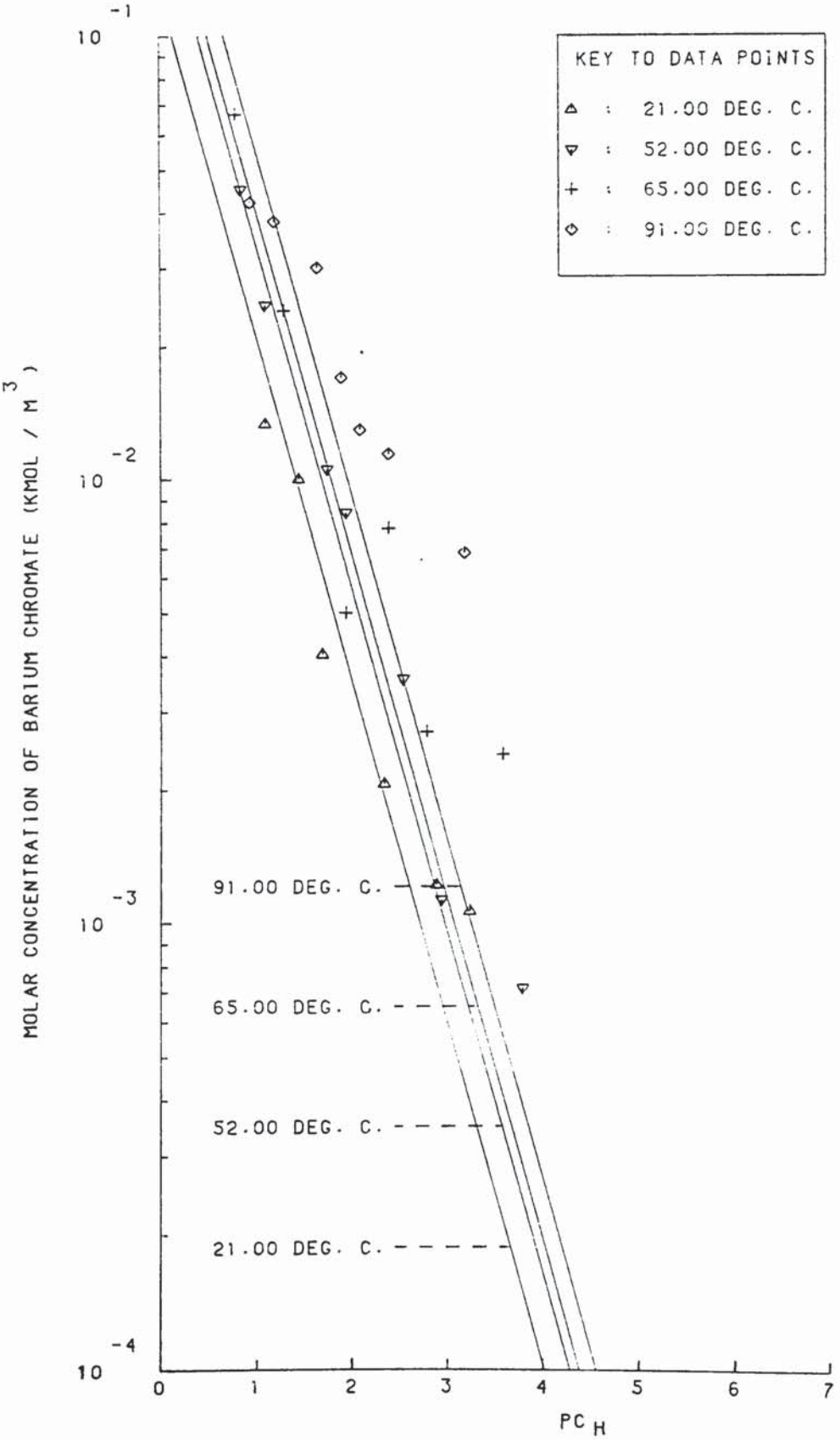

GRAPH A5. 4 SOLUBILITY IN NITRIC ACID

(FALANGAS'S DATA)

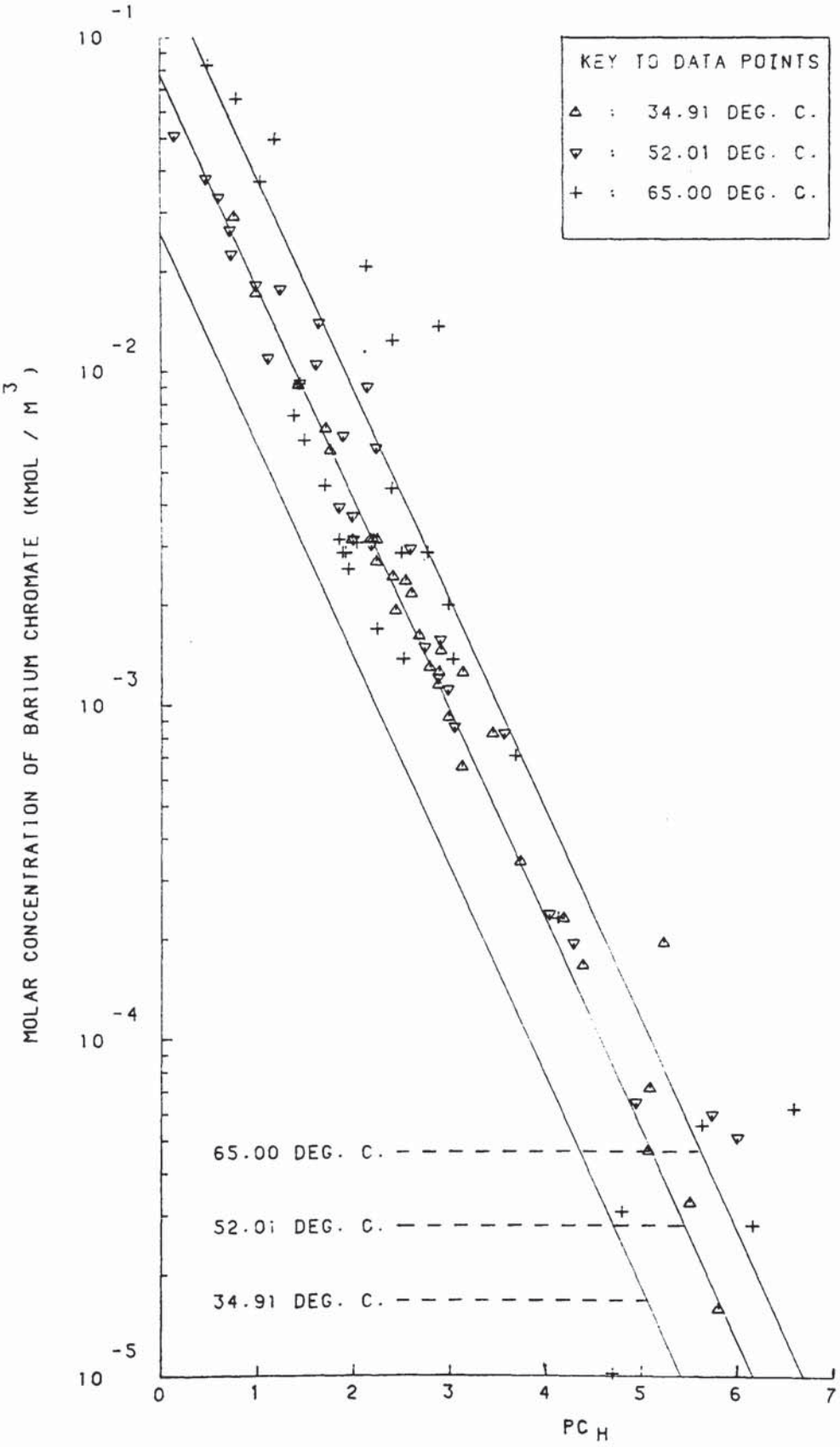

GRAPH A5. 5 SOLUBILITY IN NITRIC ACID

(FALANGAS'S RESIDUE WEIGHT DATA)

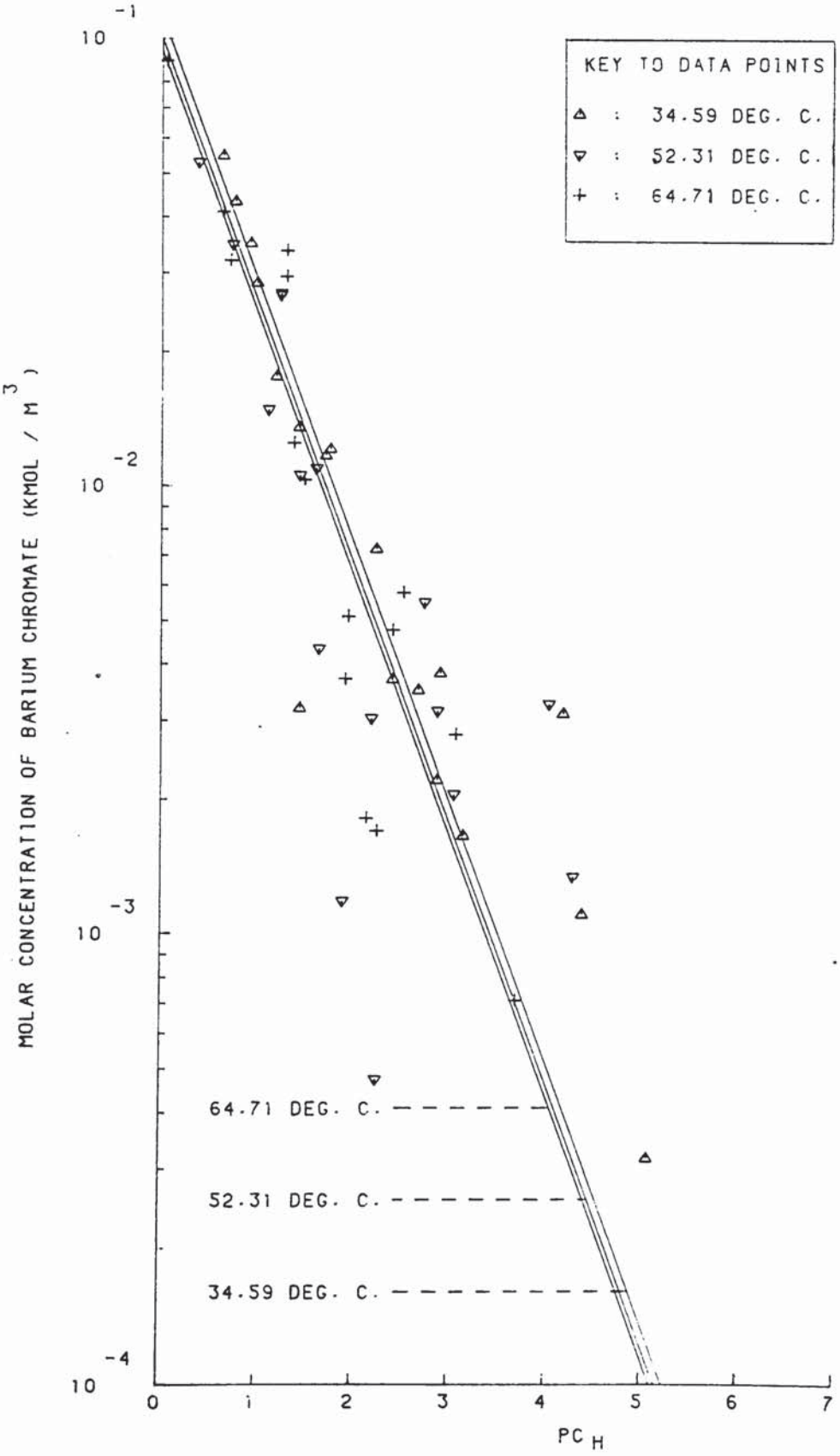

GRAPH AS. 6 SOLUBILITY IN HYDROCHLORIC ACID

(SKANDER'S DATA)

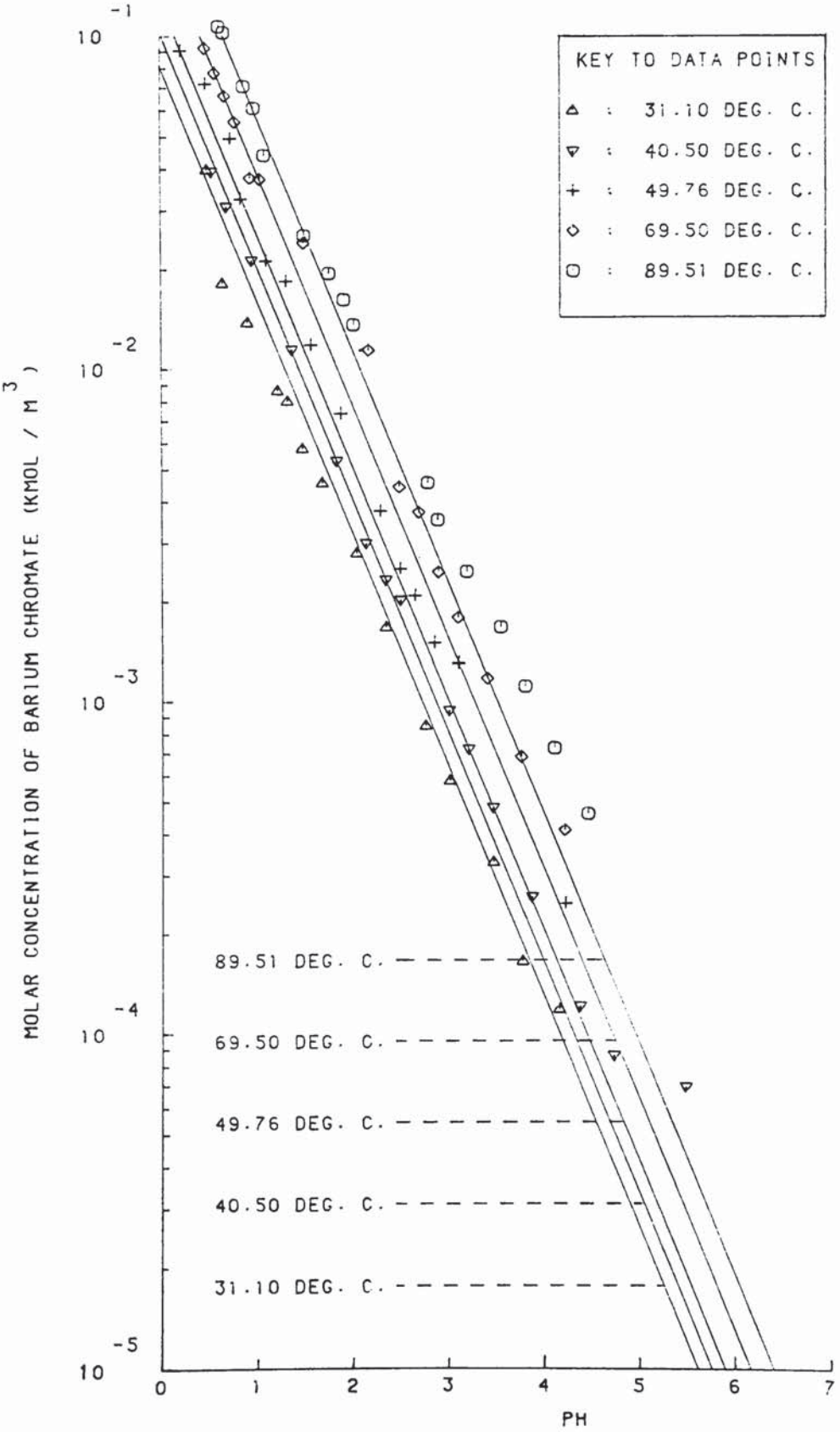

GRAPH A5. 7 SOLUBILITY IN HYDROCHLORIC ACID

(FALANGAS'S DATA)

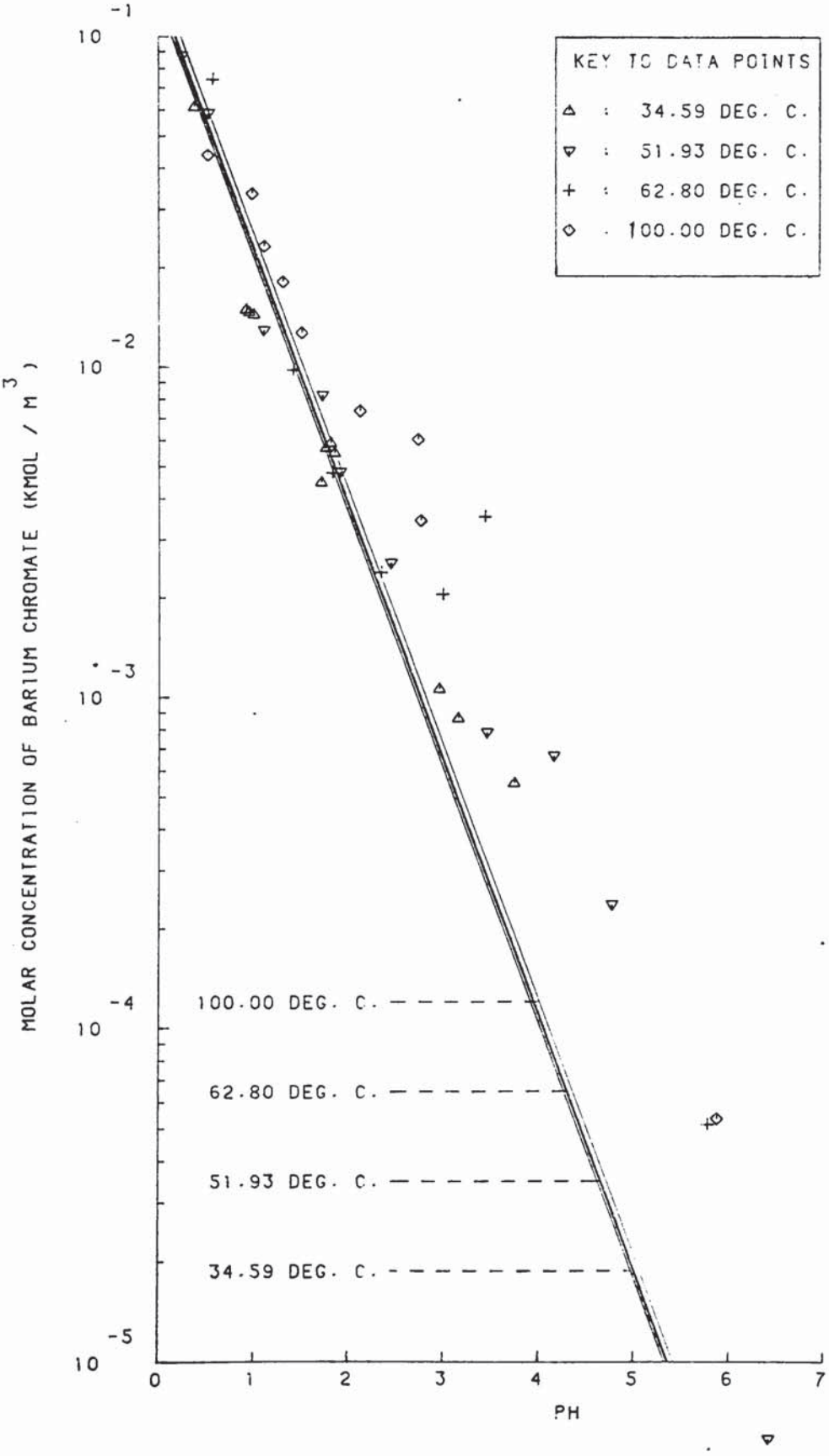

GRAPH A5. 8 SOLUBILITY IN HYDROCHLORIC ACID / UREA

(FALANGAS'S DATA)

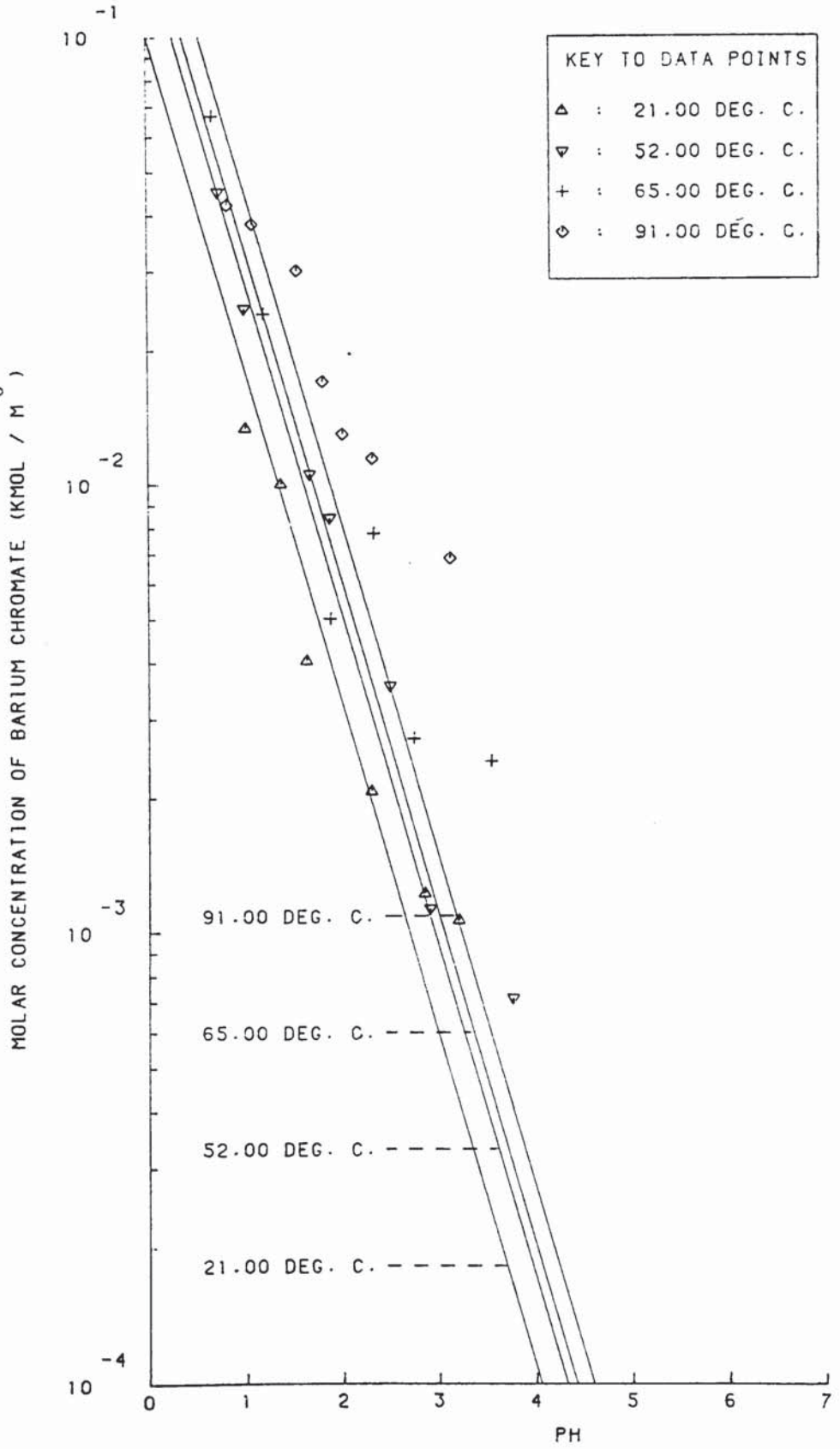

GRAPH A5. 9 SOLUBILITY IN NITRIC ACID

(FALANGAS'S DATA)

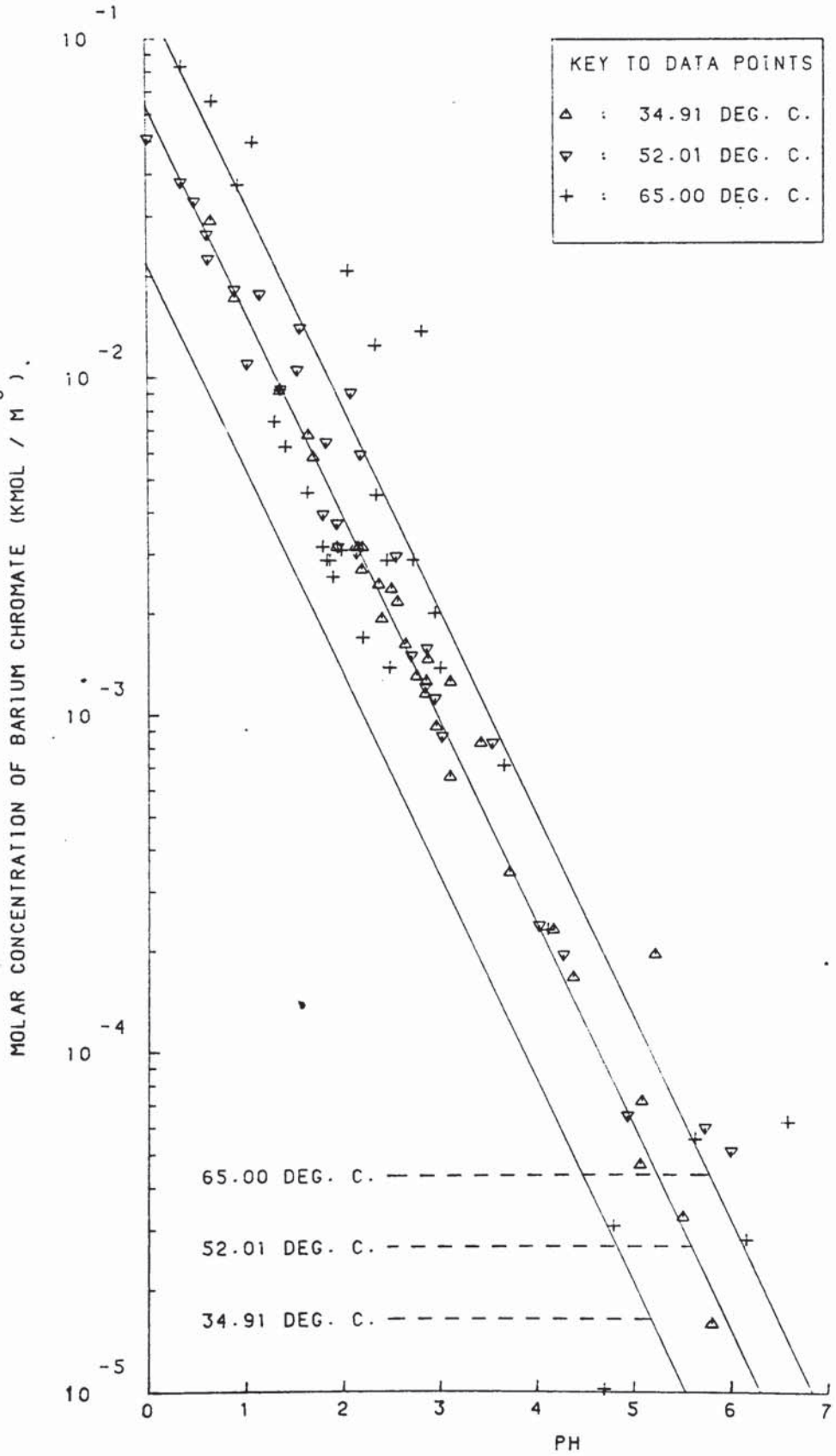

GRAPH A5.10 SOLUBILITY IN NITRIC ACID

(FALANGAS'S RESIDUE WEIGHT DATA)

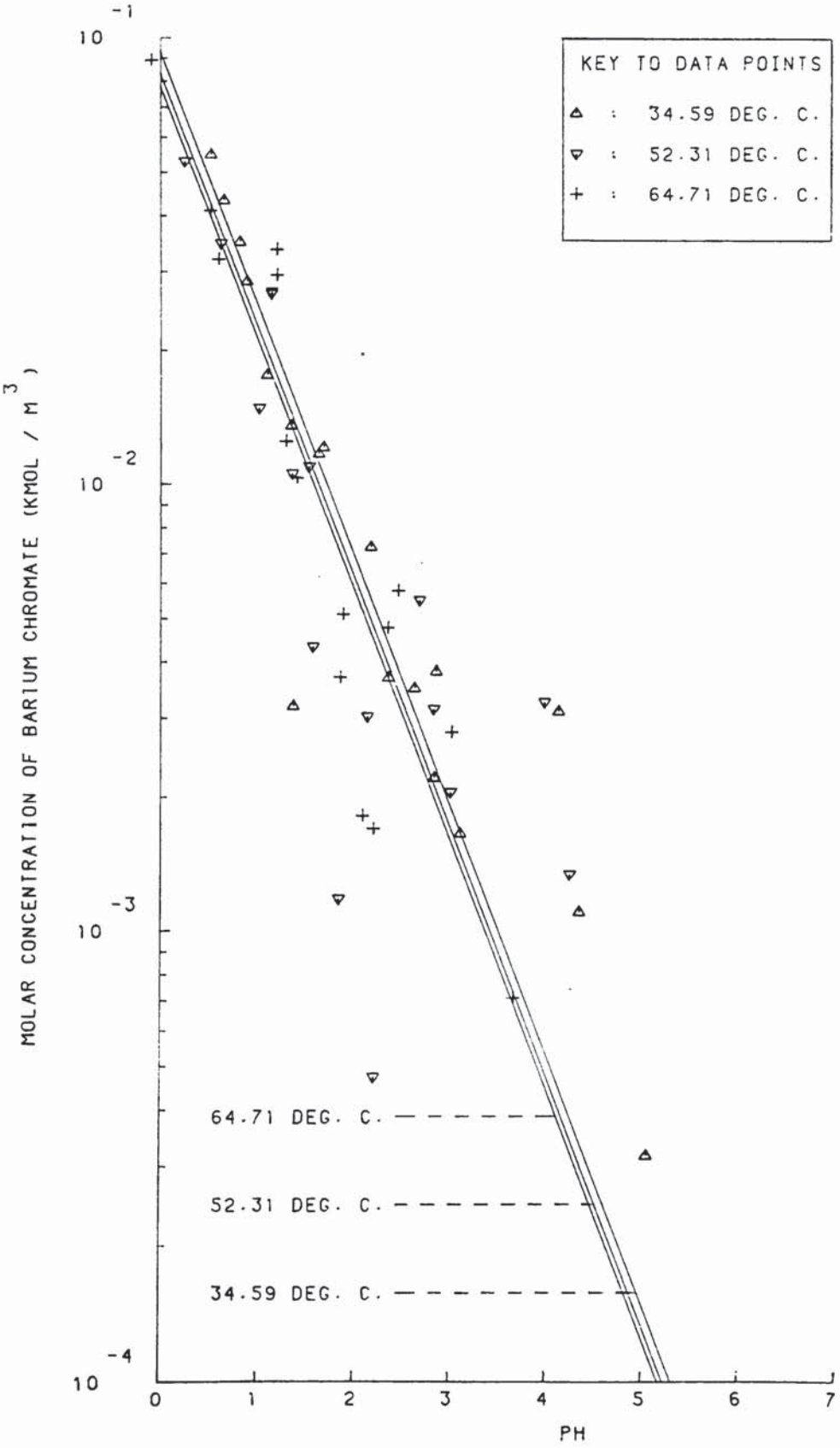

APPENDIX 6

MATHEMATICAL MODEL FOR BATCH FLUIDISED BED CRYSTALLISER

A6.0 INTRODUCTION

This model applies to a fluidised bed crystalliser rig in which supersaturation is generated in a reservoir. The solution is then circulated through a fluidised bed, in which crystal growth occurs thereby removing the supersaturation, before being returned to the reservoir. The model equates the rates of generation and removal of supersaturation on the basis of certain assumptions concerning the hydrolysis of urea and the hydrodynamics of the bed.

A6.1 HYDROLYSIS OF UREA

Urea hydrolysis can be considered to be a pseudo first order process (103):

$$\text{i.e.} \quad \frac{dC_u}{dt} = -k_u . C_u \quad \ldots\ldots\ldots\ldots\ldots\ldots\ldots \quad (A6.1)$$

where, C_u is the (molar) concentration of urea at time, t; and, k_u is the first order rate constant. k_u is a function of pH and temperature, but at a constant temperature and above a pH of unity, k_u is essentially constant (103).

Integration of equation (A6.1) gives:

$$C_u = C_{u_o} . e^{-k_u t} \quad \ldots\ldots\ldots\ldots\ldots\ldots \quad (A6.2)$$

where C_{u_o} is the initial urea concentration.

Since one mole of urea neutralises two moles of monobasic acid on hydrolysis and since the system can be assumed to be of constant volume,

$$C_{H^+} = C_{H_o^+} - 2(C_{u_o} - C_u) \quad \text{..... (A6.3)}$$

and $$C_{H^+} = C_{H_o^+} - 2C_{u_o}(1 - e^{-k_u t}) \quad \text{..... (A6.4)}$$

where $C_{H_o^+}$ is the initial hydrogen ion concentration and C_{H^+} is the corresponding value at time, t.

The solubility of barium chromate has been found to vary with acid strength according to a relation of the form (322),

$$C_{e,t} = A_2(C_{H^+})^{A_1} \quad \text{..... (A6.5)}$$

where A_1 and A_2 are constants and $C_{e,t}$ is the solubility at time, t.

$$\therefore C_{e,t} = A_2[C_{H_o^+} - 2C_{u_o}(1 - e^{-k_u t})]^{A_1} \quad \text{..... (A6.6)}$$

If the relative supersaturation, S_t, in the reservoir is assumed to be constant,

$$C_t = (1 + S_t)\, C_{e,t} \quad \text{..... (A6.7)}$$

where C_t is the concentration of barium chromate at time, t.

$$\therefore C_t = (1 + S_t) \cdot A_2[C_{H_o^+} - 2C_{u_o}(1 - e^{-k_u t})]^{A_1} \quad \text{(A6.8)}$$

$$\therefore \frac{dCt}{dt} = -2C_{u_o} k_u A_1 A_2 e^{-k_u t}(1+S_t) \left[C_{H_o^+} - 2C_{u_o}(1-e^{-k_u t}) \right]^{(A_1-1)} \quad \text{..... (A6.9)}$$

A6.2 MODEL OF FLUIDISED BED

The following assumptions are made:

1. Ideal mixing of the particles in the bed occurs with no classification and both bed voidage and particle surface area per unit bed volume are constant throughout the bed.

2. At any given time, the solubility of barium chromate in the bed is the same for all points.

3. No nucleation occurs in the reservoir. Heterogeneous nucleation and growth occurs in the bed.

4. No pH change occurs within the bed.

5. The growth rate of barium chromate is given by (5):

$$\frac{dm}{dt} = kAS_{rel.} \quad \ldots\ldots\ldots\ldots\ldots\ldots \quad (A6.10)$$

where A is the surface area and m is the mass, of crystals at time t; and, k is a constant.

6. Volume and surface shape factors for all the substrate particles in the bed are equal.

7. Either plug flow of liquid through the bed or ideal mixing of liquid in the bed occurs.

A6.3 PLUG FLOW MODEL

The initial number surface mean radius of the substrate particles in the bed is:

$$\bar{r}_{s,o} = \sqrt{\frac{\Sigma\, n_i r_{i,o}}{\Sigma\, n_i}} \quad \ldots\ldots\ldots\ldots\ldots\ldots \quad (A6.11)$$

The number surface mean radius at time, t is:

$$\bar{r}_{s,t} = \sqrt{\frac{\Sigma\ n_i r_{i,t}}{\Sigma\ n_i}} \quad \ldots\ldots\ldots\ldots\ldots\ldots \quad (A6.12)$$

Assumptions 1 and 6 (above) result in the number of particles, n_x, in an element δx of the bed (Figure A6.1) being constant.

$$\text{i.e.} \quad n_x = \frac{m_o \delta x}{\rho_b H f_v \bar{r}_o^3} \quad \ldots\ldots\ldots\ldots\ldots\ldots \quad (A6.13)$$

where, m_o is the initial mass of bed material; ρ_b is the density of the bed material; f_v is the volume shape factor; H is the bed height; and, $\bar{r}_o$ is the number mass mean radius.

Thus, the surface area $A_{x,t}$ at any time, t in an element δx of the bed is:

$$A_{x,t} = n_x f_s (\bar{r}_{s,t})^2 = \frac{f_s m_o \delta x (\bar{r}_{s,t})^2}{\rho_b H f_v (\bar{r}_o)^3} \quad \ldots\ldots\ldots \quad (A6.14)$$

where, f_s is the surface shape factor.

A molar balance for barium chromate on the bed element δx at time, t (figure A6.1) gives:

$$a_b v_L C_{x,t} = a_b v_L (C_{x,t} + \delta C_{x,t}) + A_{x,t}\ k\ S_{x,t} \quad \ldots\ldots \quad (A6.15)$$

where, v_L is the superficial liquid velocity; and, a_b is the bed cross sectional area.

$$\text{i.e.} \quad \frac{\partial C_{x,t}}{\partial x} = -\left(\frac{f_s}{f_v}\right)\left(\frac{m_o}{\rho_b H a_b v_L}\right)\left(\frac{\bar{r}_{s,t}^2}{\bar{r}_o^3}\right)\left(\frac{k}{C_{e,t}}\right)(C_{x,t} - C_{e,t})$$

$$\ldots\ldots\ldots\ldots\ldots\ldots \quad (A6.16)$$

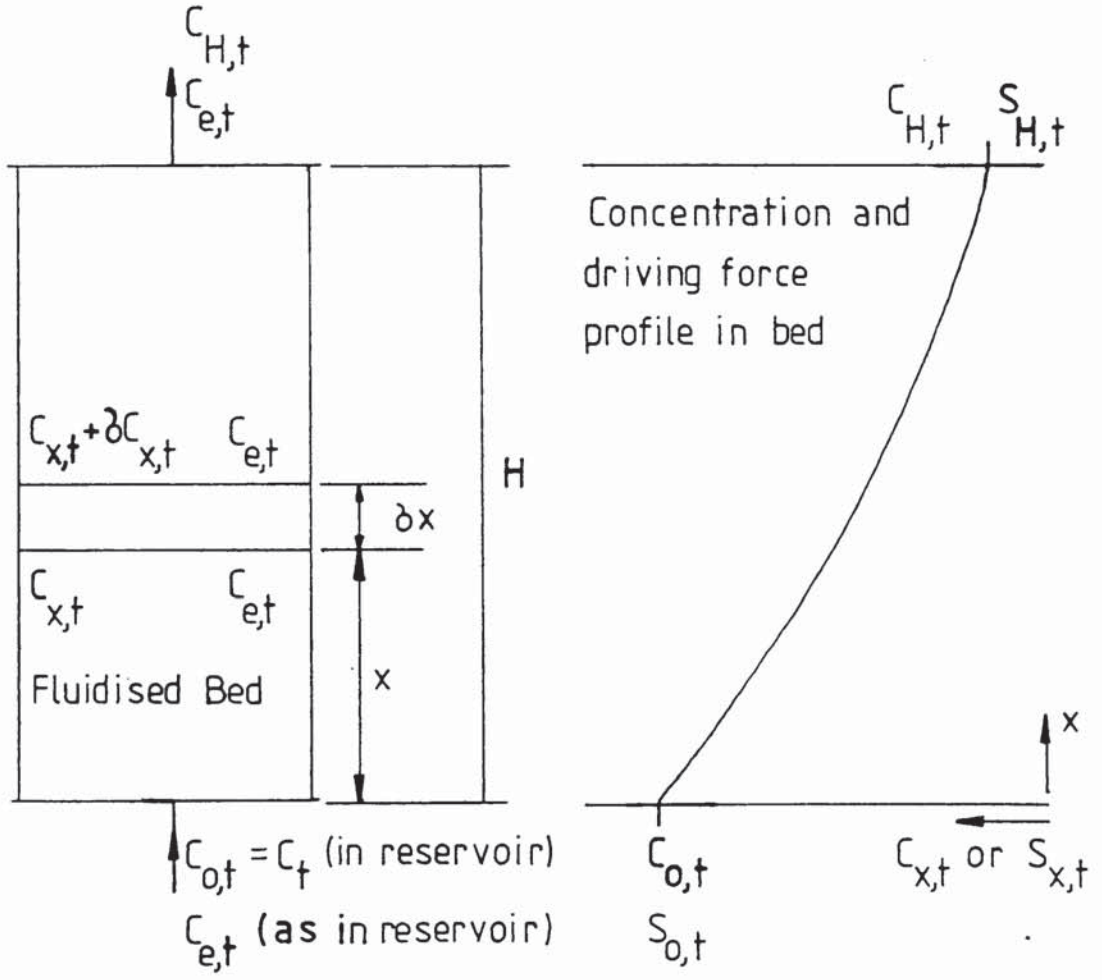

Figure A6.1 Plug Flow Model for Fluidised Bed Crystalliser

Integration with respect to x and use of the boundary condition $C_{x,t} = C_{o,t} = C_t$ (as in reservoir), eventually gives:

$$C_{x,t} = (C_{o,t} - C_{e,t})e^{-T_o x} + C_{e,t} \quad \ldots\ldots\ldots \quad (A6.17)$$

$$\text{where, } T_o = \left(\frac{f_s}{f_v}\right)\left(\frac{m_o}{\rho_b H a_b v_L}\right)\left(\frac{\bar{r}^2_{s,t}}{\bar{r}^3_o}\right)\left(\frac{k}{C_{e,t}}\right) \quad \ldots\ldots\ldots \quad (A6.18)$$

A6.4 IDEAL MIXING MODEL

A molar balance for barium chromate at time t over the whole of the bed (figure A6.2) gives:

$$a_b v_L C_t = a_b v_L C_{B,t} + k A_B S_{B,t} \quad \ldots\ldots\ldots\ldots\ldots \quad (A6.19)$$

Equation (A6.14) yields A_B, the overall bed surface area. Hence,

$$C_{B,t} = C_{e,t}((S_t/T') + 1) \quad \ldots\ldots\ldots\ldots\ldots \quad (A6.20)$$

$$\text{where, } T' = \left(\frac{f_s}{f_v}\right)\left(\frac{m_o}{\rho_b a_b v_L}\right)\left(\frac{\bar{r}^2_{s,t}}{\bar{r}^3_o}\right)\left(\frac{k}{C_{e,t}}\right) + 1 \quad \ldots\ldots\ldots \quad (A6.21)$$

A6.5 OVERALL MASS BALANCE

A molar balance for barium chromate at time, t (figure A6.3) gives:

$$a_b v_L(t) C_{o,t} - a_b v_L(t) C_{H,t} = -V_R \frac{dC_t}{dt} \quad \ldots\ldots\ldots \quad (A6.22)$$

$$v_L(t) = -\left(\frac{V_R}{a_b}\right)\left(\frac{dC_t}{dt}\right)\left(\frac{1}{C_{o,t} - C_{H,t}}\right) \quad \ldots\ldots\ldots \quad (A6.23)$$

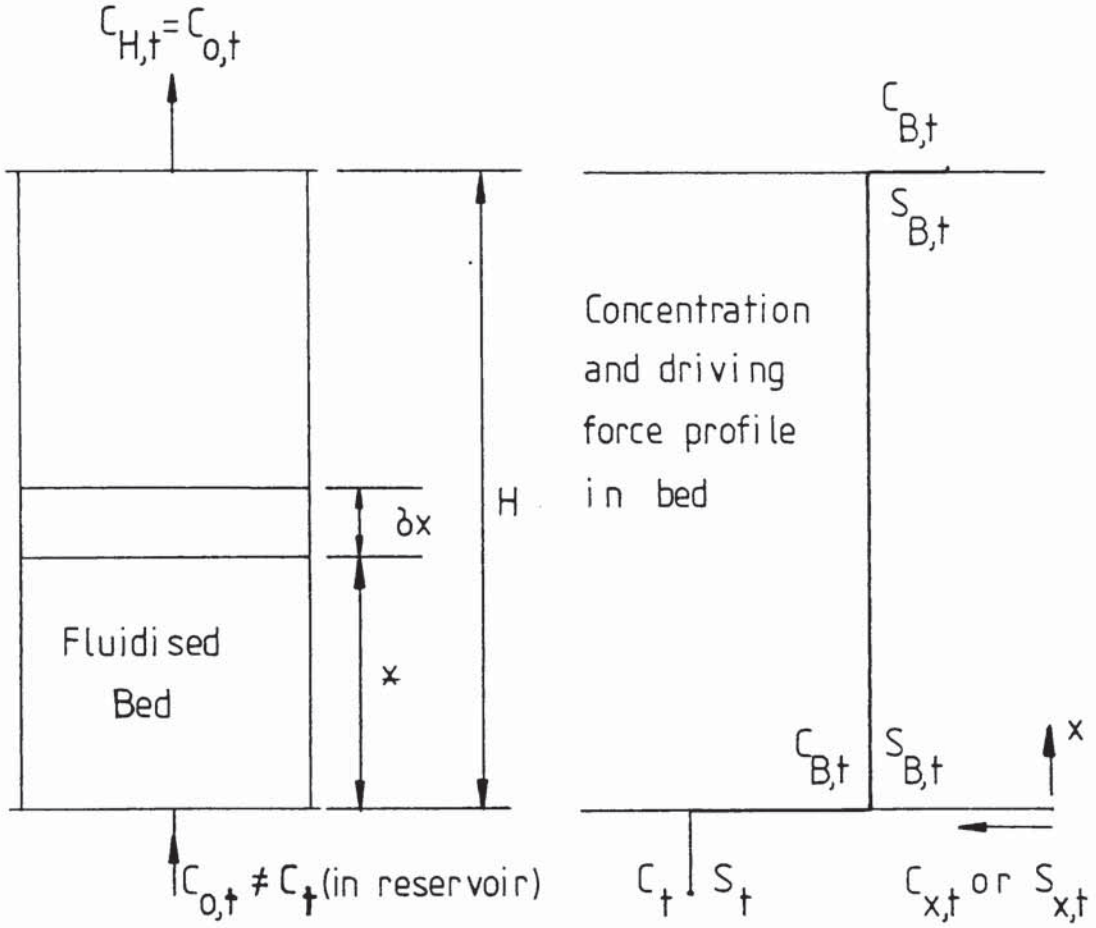

Figure A6.2 Ideal Mixing Model for Fluidised Bed Crystalliser

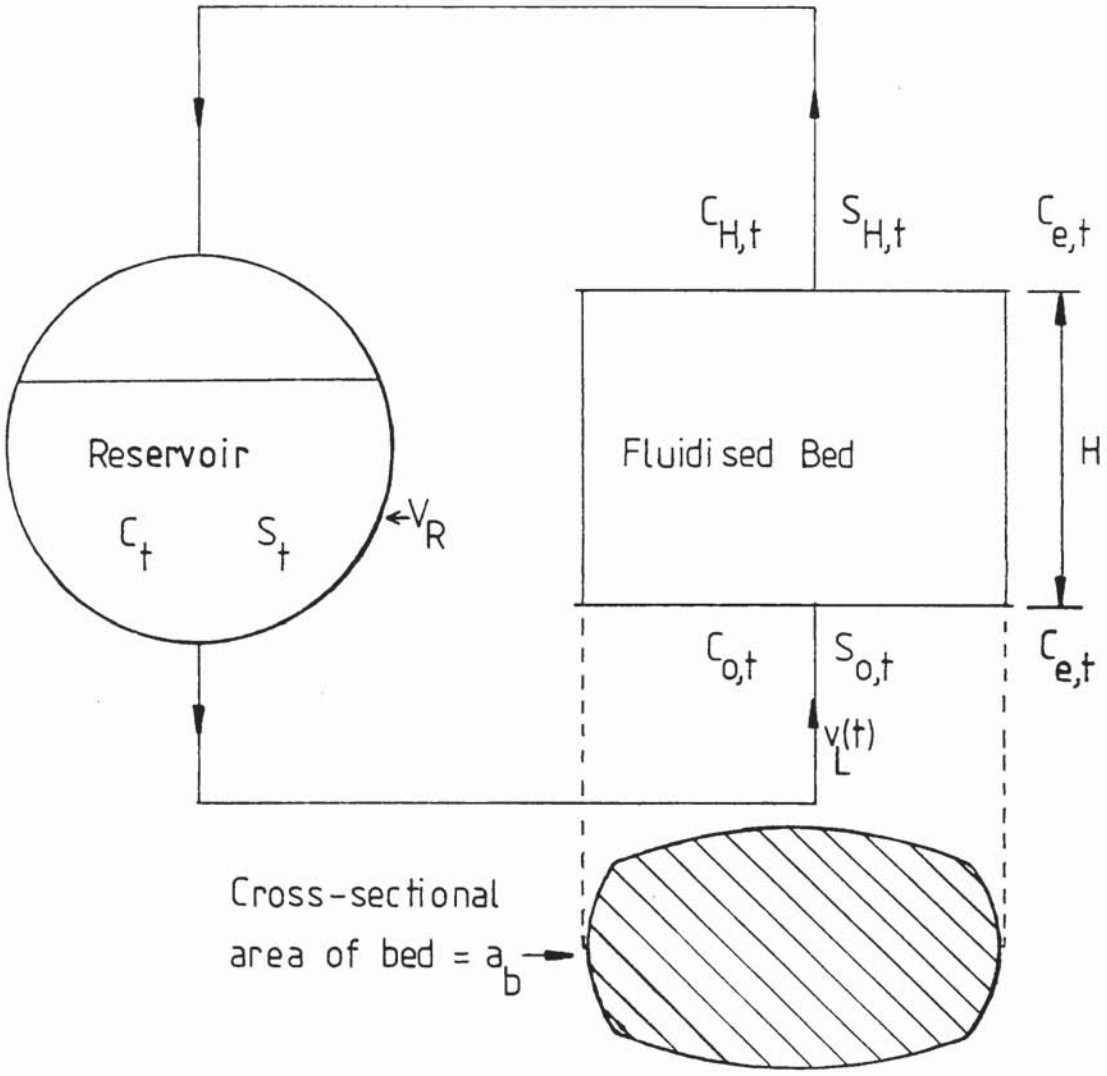

Figure A6.3 Overall Mass Balance for Fluidised Bed Crystalliser

The plug flow model (equations A6.9 and A6.17) gives:

$$v_L(t) = \frac{2V_R(1+S_t)k_uA_1Cu_oe^{-k_ut}}{a_bS_t(1-e^{-ToH})\,[\,C_{H_o^+} - 2C_{u_o}(1-e^{-k_ut})]} \qquad \text{..... (A6.24)}$$

Since T_o is a function of $\bar{r}^2_{s,t}$ and v_L, this equation has to be solved iteratively and the manner of variation of $\bar{r}^2_{s,t}$ with time must be known.

The ideal mixing model (equations A6.9 and A6.20), for which $C_{o,t} = C_t$ in equation A6.23, gives:

$$v_L(t) = \frac{[2V_R(1+S_t)k_uA_1Cu_oe^{-k_ut}]/a_b}{\Big[S_t(C_{H_o^+} - 2C_{u_o}(1-e^{-k_ut})) - 2V_R(1+S_t)k_uA_1C_{u_o}e^{-k_ut}A_2\Lambda(C_{H_o^+} - 2C_{u_o}(1-e^{-k_ut}))^{A_1}\Big]} \qquad \text{..... (A6.25)}$$

where, $\Lambda = (\frac{f_v}{f_s})(\frac{\rho_b}{m_ok})(\frac{\bar{r}^3_o}{\bar{r}^2_{s,t}})$ ..... (A6.26)

In this case too an explicit solution for v_L requires a knowledge of $\bar{r}^2_{s,t}$ which is a function of time.

A6.6 NUMERICAL RESULTS

Although equations A6.24 and A6.25 appear to be unwieldly, they can be simplified considerably by limiting the investigation to the initial flow rate required.

For example, for the ideal mixing model, equation A6.25 gives:

$$v_L(0) = p_o\alpha^*_o/a_b(1 - p_oA_2\Lambda\alpha^*_oC^{A_1}_{H^+}) \qquad \text{..... (A6.27)}$$

where, $p_o = 2V_R(1 + S_o)k_u A_1/S_o$ ..... (A6.28)

and, $\alpha_o^* = C_{u_o}/C_{H_o^+}$ ..... (A6.29)

Subject to some reasonable numerical assumptions concerning the parameters involved, it is possible to obtain an order of magnitude picture of the values of volumetric flow rate involved. Table A6.1 gives such values for the ideal mixing model and is based on the following numerical assumptions:

$f_v/f_s = 0.333$ (i.e. spherical particles)

$A_1 = 0.667$, and $A_2 = 0.062$ (322)

$\bar{r}_o^3/\bar{r}_{s,t}^2 = 10\ \mu m$

$k = 0.07$

$\rho_b = 19300\ kg/m^3$ (the density of tungsten)

$m_o = 25$ grammes

$S_o = 0.1$ (a low relative supersaturation)

$C_{H_o^+} = 1.0\ kmol/m^3$

These assumptions lead to a value of 36.8 for Λ, and makes the term containing Λ in the denominator of equation A6.27 very small. It is thus possible to further simplify this equation to:

$$v_L(0) = p_o \alpha_o^*/a_b \quad \text{..... (A6.30)}$$

The values for p_o, $C_{H_o^+}$ and A_2 are quite small, and even if Λ was assigned a value 10 times greater, the term containing Λ would still be negligible. It

TABLE A6.1

Variation of Initial Volumetric Flow Rate to Bed with Process Parameters, for Ideal Mixing Model

Temperature (^{o}C)	k_u (103) (1/h)	V_R (dm^3)	$v_L(0).a_b$ (dm^3/h)	$v_L(0).a_b$ (cm^3/min)	α^*_o (-)	Approximate Time for Complete Neutralisation (h)
66	0.002	10	0.293	5	1	∿350
90	0.045	10	6.60	110	1	∿ 16
100	0.145	10	21.3	354	1	∿ 5
66	0.002	10	0.587	10	2	∿144
90	0.045	10	13.2	220	2	∿6.5
100	0.145	10	42.5	709	2	∿ 2
66	0.002	10	2.93	49	10	∿ 26
90	0.045	10	66.0	1100	10	∿ 1
100	0.145	10	213	3540	10	∿0.4
66	0.002	2	0.059	1	1	∿350
90	0.045	2	1.32	22	1	∿ 16
100	0.145	2	4.25	71	1	∿ 5
66	0.002	2	0.117	2	2	∿144
90	0.045	2	2.64	44	2	∿6.5
100	0.145	2	8.51	142	2	∿ 2
66	0.002	2	0.587	10	10	∿26
90	0.045	2	13.2	220	10	∿ 1
100	0.145	2	42.5	709	10	∿0.4

therefore appears that, neither the amount of substrate material in the bed, nor the surface area of the bed material, are of critical effect. The controlling factors seem to be the parameters affecting the rate of hydrolysis of urea alone.

Assuming that the solution has physical properties similar to that of water, Stokes law (323) can be used to compute the flow rates for elutriation of tungsten from beds of different diameter. These computations are given in Table A6.2. A comparison of the flow rates in tables A6.1 and A6.2 show that the flow rate required to prevent a build-up of supersaturation in the reservoir is far too high to permit operation with a stable bed. For example, for a 10 dm^3 capacity rig, at $100^{o}C$ and with $\alpha_o^* = 2$, the time for complete hydrolysis is, from table A6.1, 2 hours and a circulation rate of 709 cm^3/min is required; now, table A6.2 shows that even 10 μm diameter tungsten particles would require a bed of diameter greater than 100 mm in order to maintain a stable bed at this flow rate. Conversely, the more reasonable particle size of 1 μm would require a bed of diameter greater than 1000 mm to prevent elutriation.

TABLE A6.2

Flow Rates (cm^3/min) for Elutriation of Tungsten

Stokes Diameter (μm)	Bed Diameter (mm)						
	25	50	100	200	500	1000	2000
1	0.294	1.18	4.70	18.8	117	470	1880
2	1.18	4.70	18.8	75.2	470	1880	7520
5	7.34	29.4	117	470	2937	11750	46999
10	29.4	118	470	1880	11750	46999	187996
15	66.1	264	1057	4230	26437	105748	422991
20	118	470	1880	7520	46999	187996	751984
25	184	734	2937	11750	73436	293744	1174975

APPENDIX 7

SHAPE FACTORS FOR BARIUM CHROMATE CRYSTALS

A7.1 VOLUME SHAPE FACTORS

Consider the (111) form of a barium chromate crystal as shown in figure A7.1.1. The crystal is comprised of eight pyramidal segments of the type shown in figure A7.1.2.

$$\text{Volume of a single pyramid} = \frac{1}{3} \cdot \frac{1}{2} (OP)(OQ)(OR)$$

$$\therefore \text{Volume of crystal} = 8 \cdot \frac{1}{6} (OP)(OQ)(OR)$$

$$= 492.10 \ (\mathring{A})^3$$

If d_v is the equivalent spherical volume diameter,

$$\frac{\pi}{6} d_{v.}^3 = 492.10$$

$$\therefore \quad d_v = 9.795 \ \mathring{A}$$

Figure 7.1.1 shows the equivalent sphere of this diameter superimposed on the crystal. Now, the maximum, second largest and smallest dimensions of the crystal are: $2a_o$ (=18.206 $\mathring{A}$), $2c_o$ (=14.674 $\mathring{A}$), and $2b_o$ (=11.052 $\mathring{A}$) respectively.

Consider the following ratios,

$$\frac{d_v}{2a_o} = \frac{9.795}{18.206} = 0.538$$

$$\frac{d_v}{2c_o} = \frac{9.795}{14.674} = 0.668$$

$$\frac{d_v}{2b_o} = \frac{9.795}{11.052} = 0.886$$

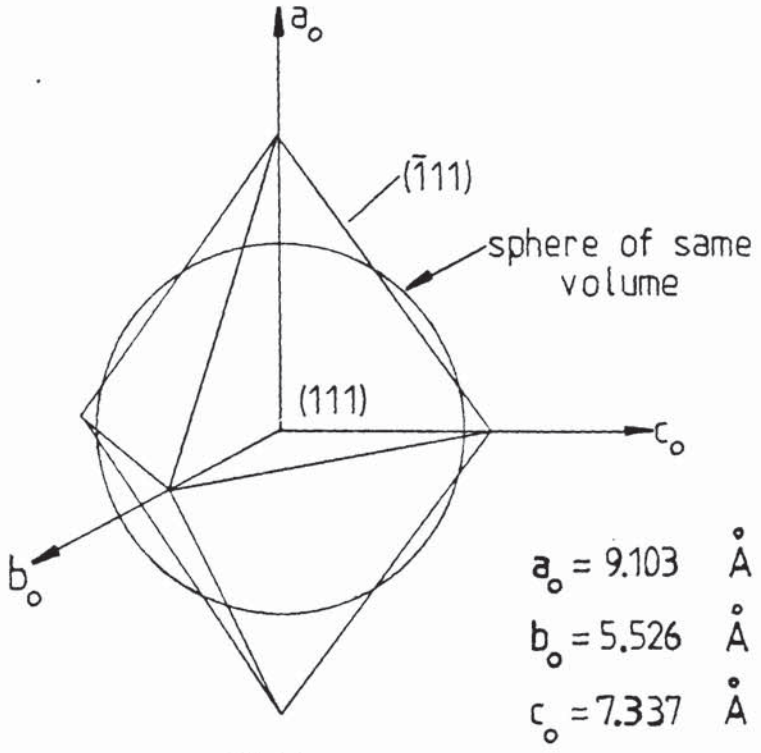

A7.1.1

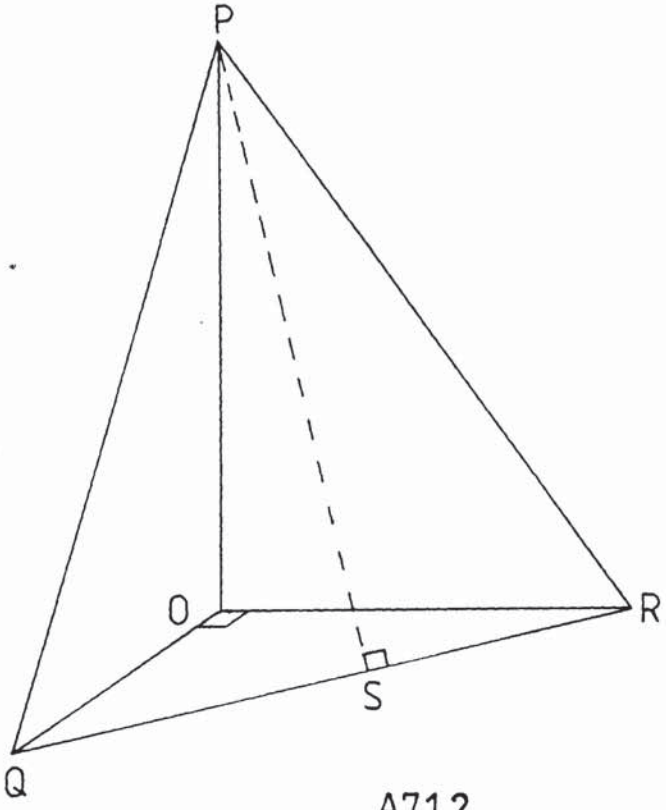

A7.1.2

Figure A7.1

A7.1.1 The (111) form of a barium chromate crystal

A7.1.2 A pyramidal segment of the (111) crystal form

Since sieve analysis usually tends to give the second largest dimension of the material being analysed (205,239), the ratio of equivalent volume diameter (as measured by the Coulter counter, say) to sieve diameter should in theory be 0.668. In any case the ratio would be expected to be between the limits 0.538 and 0.886. Experiments reported in Chapter 8 gave a value of 0.875 which is in this range.

A7.2 SPHERICITY

The definition of sphericity (ϕ) is (205):

$$\phi = \frac{\text{surface area of sphere of same volume as crystal}}{\text{surface area of crystal}}$$

For the (111) crystal form,

$$\text{surface area of crystal} = 8[\tfrac{1}{2}(PS)(QR)]$$
$$= 371.84 \ (\mathring{A})^2$$

$$\text{surface area of equivalent sphere} = \pi d_v^2$$
$$= 301.43 \ (\mathring{A})^2$$

$$\therefore \quad \text{sphericity } (\phi) = \frac{301.43}{371.84} = 0.811$$

This value of sphericity was used in calculating crystal surface areas from the differential number - equivalent volume diameter distributions of the barium chromate batch crystallisation products. Since sphericity is around 0.8 for even fairly irregular particles (209), use of the above value was considered reasonable.

APPENDIX 8

SOLUBILITY DATA OF SKANDER AND FALANGAS

The solubility data of Skander (4) and Falangas (5), which were correlated by means of the empirical expressions presented in Chapter 7, are collectively presented in this appendix. This data listing has been computer generated, and hence the symbol E denotes exponents to the base ten. The columns of data denote, from left to right, the solubility (C_e) in kmol/m^3, the pH of the solution at equilibrium and the temperature in ^oC.

A8.1. SKANDER'S DATA

A8.1.1. SOLUBILITY IN HYDROCHLORIC ACID

0.118E-03	4.18	31.1
0.165E-03	3.80	31.1
0.329E-03	3.50	31.1
0.580E-03	3.05	31.1
0.849E-03	2.80	31.1
1.680E-03	2.40	31.1
2.805E-03	2.10	31.1
4.572E-03	1.75	31.1
5.801E-03	1.55	31.1
8.052E-03	1.40	31.1
8.659E-03	1.30	31.1
13.870E-03	1.00	31.1
18.180E-03	0.75	31.1
39.820E-03	0.60	31.1
0.069E-03	5.5	40.5
0.086E-03	4.75	40.5
0.121E-03	4.40	40.5
0.259E-03	3.90	40.5
0.483E-03	3.50	40.5
0.725E-03	3.25	40.5
0.949E-03	3.05	40.5
2.037E-03	2.55	40.5
2.342E-03	2.40	40.5
3.021E-03	2.20	40.5
5.351E-03	1.90	40.5
11.570E-03	1.45	40.5
21.400E-03	1.05	40.5
30.940E-03	0.8	40.5
39.440E-03	0.65	40.5
0.247E-03	4.25	49.80
1.314E-03	3.15	49.80
1.513E-03	2.90	49.85
2.097E-03	2.70	49.80
2.527E-03	2.55	49.80
3.782E-03	2.35	49.75
7.427E-03	1.95	49.80
11.948E-03	1.65	49.85
18.560E-03	1.40	49.70
21.320E-03	1.20	49.70
32.630E-03	0.95	49.70
49.620E-03	0.85	49.70
72.080E-03	0.60	49.75
90.640E-03	0.35	49.70
0.411E-03	4.25	69.5
0.685E-03	3.80	69.5
1.182E-03	3.45	69.5
1.799E-03	3.15	69.5
2.467E-03	2.95	69.5
3.735E-03	2.75	69.5

4.455E-03	2.55	69.5
11.528E-03	2.25	69.5
24.089E-03	1.59	69.5
37.424E-03	1.15	69.5
37.682E-03	1.05	69.5
55.491E-03	0.90	69.5
66.244E-03	0.80	69.5
77.428E-03	0.70	69.5
92.064E-03	0.60	69.5
0.461E-03	4.50	89.6
0.727E-03	4.15	89.5
1.118E-03	3.85	89.6
1.685E-03	3.60	89.5
2.475E-03	3.25	89.6
3.550E-03	2.95	89.5
4.594E-03	2.85	89.4
13.750E-03	2.10	89.5
16.344E-03	2.00	89.5
19.595E-03	1.85	89.5
25.384E-03	1.60	89.5
44.088E-03	1.20	89.5
61.011E-03	1.10	89.5
70.808E-03	1.00	89.5
102.420E-03	0.80	89.5
106.880E-03	0.75	89.5

A8.2. FALANGAS'S DATA

A8.2.1. SOLUBILITY IN NITRIC ACID

1.579E-5	5.81	35.0
3.237E-5	5.52	35.0
1.938E-4	5.25	35.0
7.105E-5	5.10	34.1
4.618E-5	5.08	35.0
1.662E-4	4.40	35.0
2.305E-4	4.20	35.0
3.414E-4	3.75	35.0
8.289E-4	3.46	35.0
1.259E-3	3.15	34.5
6.580E-4	3.14	35.0
9.276E-4	3.00	35.0
1.468E-3	2.92	35.0
1.263E-3	2.90	33.9
1.161E-3	2.89	35.0
1.307E-3	2.80	34.7
1.626E-3	2.69	35.0
2.171E-3	2.61	35.0
2.368E-3	2.55	35.0

1.934E-3	2.45	35.0
2.447E-3	2.42	35.0
3.158E-3	2.26	35.0
2.708E-3	2.25	35.0
3.158E-3	2.22	35.0
3.158E-3	2.19	35.0
3.158E-3	2.00	35.0
5.842E-3	1.77	35.0
6.789E-3	1.72	35.0
9.197E-3	1.44	35.0
1.729E-2	1.0	35.0
2.913E-2	0.77	35.0
5.053E-5	6.02	52.2
5.921E-5	5.75	52.0
6.434E-5	4.95	52.0
1.938E-4	4.30	52.0
2.372E-4	4.05	52.0
8.289E-4	3.58	52.0
8.684E-4	3.06	52.0
1.125E-3	2.99	52.0
1.579E-3	2.91	52.0
1.216E-3	2.89	52.0
1.504E-3	2.75	52.0
2.960E-3	2.60	52.0
5.960E-3	2.25	52.0
3.039E-3	2.20	52.0
9.079E-3	2.16	52.0
3.158E-3	2.01	52.0
3.710E-3	2.00	52.0
6.474E-3	1.90	52.0
3.947E-3	1.86	52.0
1.413E-2	1.65	52.0
1.060E-2	1.62	52.0
9.276E-3	1.45	52.0
1.776E-2	1.25	52.0
1.105E-2	1.12	52.0
1.828E-2	1.00	52.0
2.250E-2	0.74	52.0
2.657E-2	0.73	52.0
3.328E-2	0.61	52.0
3.789E-2	0.48	52.0
5.092E-2	0.15	52.0
6.158E-5	6.61	65.0
2.763E-5	6.17	65.0
5.487E-5	5.65	65.0
3.039E-5	4.80	65.0
1.014E-5	4.70	65.0
2.305E-4	4.14	65.0
7.105E-4	3.70	65.0
1.382E-3	3.05	65.0
2.013E-3	3.00	65.0
1.384E-2	2.90	65.0
2.882E-3	2.78	65.0
1.382E-3	2.53	65.0
2.882E-3	2.51	65.0
1.255E-2	2.42	65.0
4.500E-3	2.41	65.0
1.697E-3	2.26	65.0

2.084E-2	2.15	65.0
3.079E-3	2.05	65.0
2.566E-3	1.96	65.0
2.882E-3	1.93	65.0
2.882E-3	1.90	65.0
3.158E-3	1.86	65.0
4.579E-3	1.71	65.0
6.276E-3	1.50	65.0
9.276E-3	1.45	65.0
7.421E-3	1.39	65.0
4.974E-2	1.20	65.0
3.710E-2	1.05	65.0
6.552E-2	0.80	65.0
8.289E-2	0.50	65.0

A8.2.2. SOLUBILITY IN NITRIC ACID (RESIDUE WEIGHT METHOD)

3.158E-4	5.08	35.0
1.105E-3	4.40	34.8
3.118E-3	4.20	34.6
1.658E-3	3.16	35.4
3.829E-3	2.92	35.1
2.210E-3	2.89	35.1
3.513E-3	2.69	34.7
3.710E-3	2.42	34.0
7.263E-3	2.25	34.7
1.216E-2	1.77	33.8
1.176E-2	1.72	34.2
3.197E-3	1.45	34.8
1.358E-2	1.44	33.8
1.764E-2	1.20	34.6
2.858E-2	1.0	34.0
3.497E-2	0.93	34.7
4.330E-2	0.77	34.2
5.483E-2	0.64	35.1
1.342E-3	4.3	52.0
3.276E-3	4.05	52.0
2.053E-3	3.06	52.3
3.158E-3	2.89	52.0
5.526E-3	2.75	52.0
4.737E-4	2.25	52.0
3.039E-3	2.20	52.6
1.184E-3	1.90	53.0
4.342E-3	1.65	52.0
1.101E-2	1.62	52.2
1.062E-2	1.45	53.1
2.712E-2	1.25	52.4
2.684E-2	1.25	52.4
1.488E-2	1.12	52.1
3.474E-2	0.74	52.4
5.297E-2	0.38	52.4
7.105E-4	3.70	65.0
2.803E-3	3.08	67.8

5.802E-3	2.53	64.6
4.776E-3	2.42	66.4
1.697E-3	2.26	64.5
1.816E-3	2.15	65.0
5.131E-3	1.96	64.5
3.710E-3	1.93	63.0
1.038E-2	1.50	65.6
1.255E-2	1.39	63.0
3.371E-2	1.31	65.6
2.949E-2	1.31	65.6
3.201E-2	0.72	63.1
4.113E-2	0.64	63.4
8.917E-2	0.05	63.5

A8.2.3. SOLUBILITY IN HYDROCHLORIC ACID

5.526E-4	3.78	34.5
8.684E-4	3.20	34.8
1.066E-3	3.00	34.9
5.526E-3	1.92	34.6
5.921E-3	1.88	34.0
5.724E-3	1.83	34.8
4.500E-3	1.78	34.5
1.449E-2	1.095	34.5
1.472E-2	1.05	34.5
1.500E-2	1.02	33.8
6.118E-2	0.50	34.6
5.921E-6	6.42	51.4
2.368E-4	4.80	52.3
6.710E-4	4.20	51.5
7.895E-4	3.50	52.4
2.566E-3	2.50	52.7
4.855E-3	1.98	51.7
8.289E-3	1.80	51.0
1.303E-2	1.20	52.2
5.881E-2	0.65	52.0
8.763E-2	0.38	52.1
5.131E-5	5.80	61.8
3.553E-3	3.50	62.0
2.053E-3	3.05	66.5
2.400E-3	2.40	62.0
4.816E-3	1.90	62.3
9.868E-3	1.50	63.0
7.421E-2	0.70	62.0
5.329E-5	5.90	100.0
3.446E-3	2.82	100.0
6.079E-3	2.80	100.0
7.421E-3	2.20	100.0
1.279E-2	1.60	100.0
1.820E-2	1.41	100.0
2.329E-2	1.22	100.0
3.355E-2	1.1	100.0
4.381E-2	0.65	100.0

A8.2.4. SOLUBILITY IN HYDROCHLORIC ACID (WITH 20 GM./LT. UREA)

1.066E-3	3.25	21.0
1.224E-3	2.90	21.0
2.072E-3	2.35	21.0
4.046E-3	1.70	21.0
1.007E-2	1.45	21.0
1.342E-2	1.10	21.0
7.145E-4	3.80	52.0
1.133E-3	2.95	52.0
3.564E-3	2.55	52.0
8.459E-3	1.95	52.0
1.061E-2	1.75	52.0
2.485E-2	1.10	52.0
4.518E-2	0.85	52.0
2.416E-3	3.60	65.0
2.716E-3	2.80	65.0
7.800E-3	2.40	65.0
5.013E-3	1.95	65.0
2.420E-2	1.30	65.0
6.668E-2	0.80	65.0
6.868E-3	3.20	91.5
1.149E-2	2.40	90.0
1.303E-2	2.10	94.0
1.709E-2	1.90	92.5
3.020E-2	1.65	90.0
3.829E-2	1.20	90.0
4.224E-2	0.95	90.0
1.401E-1	0.50	90.0

APPENDIX 9

SPECIFICATIONS OF PHILIPS IS 561 BARIUM ION SELECTIVE ELECTRODE

The barium ion selective electrode used for solubility measurements has the following specifications.

Sensitivity : 23 ± 3 mV/decade

Measuring range : 1 to 10^{-6} kmol/m^3

Reproducibility : ± 0.5 mV

Response time : < 30 s

Stability : < 1 mV/day

Light sensitivity : < 1 mV

pH range :

10^{-1} M : 1.7 to 7

10^{-2} M : 2 to 7

10^{-3} M : 2.5 to 7

Temperature range : 0 to 50°C

Operational life : 4 to 6 months

Selectivity coefficients:

H^+ : 6×10^{-2}

NH_4^+ : 4×10^{-3}

Li^+ : 5×10^{-4}

Na^+ : 3×10^{-3}

K^+ : 2×10^{-2}

Rb^+ : 1×10^{-2}

Cs^+ : 3×10^{-3}

Mg^{2+} : 8×10^{-6}

Ca^{2+} : 2×10^{-4}

Sr^{2+} : 3×10^{-2}

Reference electrode:

Type : RH 44/2-SD/1. Double junction with ground glass sleeve. Inner compartment filling solution : saturated KCl. Outer compartment filling solution : 0.1 M NH_4NO_3.

APPENDIX 10

RESULTS OF SOLUBILITY MEASUREMENTS USING BARIUM ION SELECTIVE ELECTRODE

These results are tabulated in tables A10.1 to A10.6. Each test gave two sets of values for the barium and hydrogen ion concentrations depending on whether the Cr(VI) ionic species in solution were assumed to be all univalent or all divalent. The activity coefficients were calculated using a modified form of the Debye-Huckel equation.

$$\text{i.e.} \quad \log_{10} \gamma = \frac{- A_o \sqrt{I_c}}{1 + B_o d_o \sqrt{I_c}} + C_o' I_c \quad \ldots\ldots\ldots\ldots \quad (A10.1)$$

where, C_o' is a constant and the other symbols are the same as in equations 7.14, 7.15, 7.16 and 7.17. The constant C_o' was calculated for any given temperature by fitting a least squares straight line to the calibration test data for the electrode. The optimum value of C_o' was taken to be that which minimised the standard error of the fit. The spread of the two sets of concentration values provided a measure of the uncertainty involved in the calculations.

TABLE A10.1

Solubility Measurements in Hydrochloric Acid at 20°C Using Barium Electrode

Test No.	pH	Ratio of Univalent Cr(VI) to Total Cr(VI)	Activities ($x10^5$) ($kmol/m^3$)		Concentrations ($x10^5$) ($kmol/m^3$)	
			Ba^{2+}	H^+	Ba^{2+}	H^+
01/25. 11. 80.	5. 54	0. 0	3. 23	0. 29	3. 41	0. 29
		1. 0			3. 38	0. 29
10/05. 12. 80.	3. 38	0. 0	101. 00	41. 69	138. 40	44. 62
		1. 0			133. 20	44. 30
25/05. 01. 81.	3. 18	0. 0	87. 61	66. 07	118. 40	70. 47
		1. 0			114. 40	70. 04
19/18. 12. 80.	2. 85	0. 0	135. 10	141. 30	198. 10	152. 90
		1. 0			190. 10	151. 90
07/03. 12. 80.	2. 83	0. 0	78. 85	147. 90	107. 50	157. 80
		1. 0			104. 50	157. 10

TABLE A10.1 (Continued)

Solubility Measurements in Hydrochloric Acid at 20°C Using Barium Electrode

Test No.	pH	Ratio of Univalent Cr(VI) to Total Cr(VI)	Activities ($x10^5$) (kmol/m^3)		Concentrations ($x10^5$) (kmol/m^3)	
			Ba^{2+}	H^+	Ba^{2+}	H^+
04/28.11.80./B	2.57	0.0	93.81	269.20	134.20	289.30
		1.0			130.40	288.10
13/10.12.80.	2.54	0.0	140.70	288.40	213.60	313.90
		1.0			205.70	312.10
04/28.11.80./A	2.48	0.0	101.90	331.10	149.00	357.00
		1.0			144.80	355.50
31/12.01.81.	2.28	0.0	106.30	524.80	148.50	528.70
		1.0			146.50	532.20
37/14.01.81.	1.97	0.0	57.14	1072.00	90.80	1171.00
		1.0			89.75	1169.00

TABLE A10.2

Solubility Measurements in Hydrochloric Acid at 30°C Using Barium Electrode

Test No.	pH	Ratio of Univalent Cr(VI) to Total Cr(VI)	Activities ($x10^5$) (kmol/m^3)		Concentrations ($x10^5$) (kmol/m^3)	
			Ba^{2+}	H^+	Ba^{2+}	H^+
02/26. 11. 80.	5. 62	0. 0	2. 92	0. 24	3. 08	2. 43
		1. 0			3. 06	2. 42
11/08. 12. 80.	3. 37	0. 0	99. 29	42. 66	136. 60	45. 69
		1. 0			131. 30	45. 37
26/07. 01. 81.	3. 30	0. 0	83. 17	50. 12	111. 90	53. 46
		1. 0			108. 00	53. 11
20/19. 12. 81.	2. 92	0. 0	164. 90	120. 20	250. 80	130. 90
		1. 0			239. 10	129. 90
08/04. 12. 80.	2. 86	0. 0	162. 00	138. 00	244. 40	149. 20
		1. 0			233. 70	148. 40

TABLE A10.2 (Continued)

Solubility Measurements in Hydrochloric Acid at 30°C Using Barium Electrode

Test No.	pH	Ratio of Univalent Cr(VI) to Total Cr(VI)	Activities ($x10^5$) (kmol/m^3)		Concentrations ($x10^5$) (kmol/m^3)	
			Ba^{2+}	H^+	Ba^{2+}	H^+
14/11. 12. 80.	2. 60	0. 0	64. 58	251. 20	89. 56	269. 50
		1. 0			87. 53	268. 30
05/01. 12. 80.	2. 55	0. 0	125. 10	281. 80	186. 60	304. 20
		1. 0			180. 40	302. 90
32/13. 01. 81.	2. 35	0. 0	201. 00	446. 70	333. 80	492. 00
		1. 0			319. 30	489. 30

TABLE A10.3

Solubility Measurements in Hydrochloric Acid at 40°C Using Barium Electrode

Test No.	pH	Ratio of Univalent Cr(VI) to Total Cr(VI)	Activities ($x10^5$) (kmol/m^3)		Concentrations ($x10^5$)(kmol/m^3)	
			Ba^{2+}	H^+	Ba^{2+}	H^+
03/27. 11. 80.	5. 71	0. 0	3. 36	0. 19	3. 56	0. 20
		1. 0			3. 53	0. 20
12/09. 12. 80.	3. 48	0. 0	95. 68	33. 11	129. 40	34. 99
		1. 0			124. 90	34. 86
27/08. 01. 81.	3. 41	0. 0	121. 90	38. 90	174. 20	41. 96
		1. 0			166. 50	41. 63
21/22. 12. 80.	2. 96	0. 0	132. 60	109. 60	190. 80	116. 30
		1. 0			183. 80	116. 10
09/04. 12. 80.	2. 93	0. 0	293. 60	117. 50	494. 30	126. 90
		1. 0			466. 90	126. 80

TABLE A10.3 (Continued)

Solubility Measurements in Hydrochloric Acid at 40°C Using Barium Electrode

Test No.	pH	Ratio of Univalent Cr(VI) to Total Cr(VI)	Activities ($x10^5$) ($kmol/m^3$)		Concentrations ($x10^5$) ($kmol/m^3$)	
			Ba^{2+}	H^+	Ba^{2+}	H^+
15/12.12.80.	2.64	0.0	82.83	229.10	115.60	242.70
		1.0			112.70	242.20
06/02.12.80.	2.62	0.0	223.50	239.90	362.50	259.10
		1.0			345.60	258.50
33/14.01.81.	2.43	0.0	341.10	371.50	632.80	414.00
		1.0			593.80	411.70

TABLE A10.4

Solubility Measurements in Hydrochloric Acid (with 20 kg/m^3 Urea) at 20°C Using Barium Electrode

Test No.	pH	Ratio of Univalent Cr(VI) to Total Cr(VI)	Activities ($x10^5$) (kmol/m^3)		Concentrations ($x10^5$) (kmol/m^3)	
			Ba^{2+}	H^+	Ba^{2+}	H^+
28/05.01.81.	3.35	0.0	114.60	44.67	155.90	47.08
		1.0			150.50	46.95
22/19.12.80.	3.03	0.0	199.00	93.33	329.90	108.30
		1.0			306.60	105.60
16/17.12.80.	2.66	0.0	90.96	218.80	132.80	243.20
		1.0			128.00	240.40
34/12.01.81.	2.43	0.0	234.40	371.50	366.50	389.60
		1.0			353.80	391.30
41/14.01.81.	2.13	0.0	158.50	741.30	246.00	778.30
		1.0			240.30	780.50

TABLE A10.5

Solubility Measurements in Hydrochloric Acid (with 20 kg/m^3 Urea) at 30°C Using Barium Electrode

Test No.	pH	Ratio of Univalent Cr(VI) to Total Cr(VI)	Activities ($x10^5$) (kmol/m^3)		Concentrations ($x10^5$) (kmol/m^3)	
			Ba^{2+}	H^+	Ba^{2+}	H^+
29/07. 01. 81.	3. 53	0. 0	93. 69	29. 51	125. 30	31. 24
		1. 0			121. 00	31. 09
23/23. 12. 80.	3. 08	0. 0	302. 40	83. 18	553. 30	97. 58
		1. 0			506. 60	95. 09
17/18. 12. 80.	2. 73	0. 0	113. 10	186. 20	167. 50	205. 70
		1. 0			160. 70	203. 50
35/13. 01. 81.	2. 50	0. 0	310. 60	316. 20	521. 70	337. 30
		1. 0			497. 60	338. 30

TABLE A10.6

Solubility Measurements in Hydrochloric Acid (with 20 kg/m^3 Urea) at 40°C Using Barium Electrode

Test No.	pH	Ratio of Univalent Cr(VI) to Total Cr(VI)	Activities ($x10^5$) (kmol/m^3)		Concentrations ($x10^5$) (kmol/m^3)	
			Ba^{2+}	H^+	Ba^{2+}	H^+
30/08.01.81.	4.10	0.0	72.39	7.94	94.12	8.41
		1.0			90.94	8.36
24/23.12.80.	3.35	0.0	89.36	44.67	120.30	47.44
		1.0			116.20	47.19
18/19.12.80.	2.80	0.0	132.60	158.50	193.60	170.00
		1.0			186.40	169.30
36/14.01.81.	2.55	0.0	431.80	281.80	817.70	310.60
		1.0			764.80	310.10

APPENDIX 11

DETAILS OF OPENINGS IN LID OF BATCH CRYSTALLISATION VESSEL

Opening	Socket Specification	Inclination to Vertical
Central (C)	24/29	0°
Peripheral (P1)	19/26	0°
Peripheral (P2)	19/26	5°
Peripheral (P3)	34/35	15°
Peripheral (P4)	19/26	10°

APPENDIX 12

BATCH CRYSTALLISATION MODEL FOR CONCURRENT NUCLEATION AND GROWTH

A12.0 INTRODUCTION

Modelling batch crystallisation with simultaneous nucleation and growth was originally carried out by Bransom and Dunning (252), and a similar approach is adopted here.

A12.1 ASSUMPTIONS

1. Nucleation effectively occurs at zero size and nucleation rate B_N is independent of crystal size, being expressed only as a function of driving force and other relevant process conditions, such as pH and temperature, T.

   i.e. $B_N = f_N(S) \cdot h_N(pH,T) = F_N$ ..... (A12.1)

2. Linear growth rate, G is also independent of crystal size and can be expressed similarly to nucleation rate.

   i.e. $G = f_G(S) \cdot h_G(pH,T) = F_G$ ..... (A12.2)

3. Effects of other possible causes of crystal birth or loss such as attrition and agglomeration are neglected.

4. The volume shape factor, f_v, surface shape factor, f_s, sphericity, ϕ, and crystal density, ρ, are constants for the whole population and so is the system volume, V.

5. The measurement of time commences from the moment nucleation first occurs.

A12.2 MODEL

If $N(L,t)$ denotes the total number of crystals present at time, t having a size greater than, L, by definition:

$$N(L,t) = \int_L^\infty n(L,t)\,dL \quad \ldots\ldots\ldots\ldots\ldots\ldots \quad (A12.3)$$

where $n(L,t)$ is the population density function.
Also, from assumption 1:

$$B_N = \frac{\partial N(O,t)}{\partial t} = f_N(S) \cdot h_N(pH,t) = F_N \quad \ldots\ldots\ldots \quad (A12.4)$$

For the case considered here, the general population balance represented by equation 9.1, in Chapter 9, reduces to:

$$\frac{\partial n}{\partial t} + G\frac{\partial n}{\partial L} = O, \quad \ldots\ldots\ldots\ldots\ldots\ldots\ldots \quad (A12.5)$$

since growth rate is independent of size.
Integrating equation A12.5 with respect to size then gives,

$$\frac{\partial}{\partial t}\left[\int_L^\infty n(L,t)\,dL\right] + G\frac{\partial}{\partial L}\left[\int_L^\infty n(L,t)\,dL\right] = O \quad \ldots\ldots\ldots\ldots\ldots \quad (A12.6)$$

i.e. $$\frac{\partial N(L,t)}{\partial t} + G\frac{\partial N(L,t)}{\partial L} = O \quad \ldots\ldots\ldots\ldots\ldots\ldots \quad (A12.7)$$

Now, the mass of crystals, m_t produced upto time t can be expressed as,

$$m_t = f_v \rho \int_0^{L_{t(max)}} \left[-\frac{\partial N(L,t)}{\partial L} \right] L^3 dL = f_v \rho \int_0^{L_{t(max)}} n(L,t) L^3 dL$$

..... (A12.8)

where, $L_{t(max)}$ is the diameter of the largest crystals present in the suspension at time t.

As Bransom and Dunning (252) have shown, m_t can also be expressed in terms of the nucleation and growth rates.

i.e. $$m_t = f_v \rho \int_0^t F_{N\theta} \cdot \{ \int_\theta^t F_{G\zeta} \, d\zeta \}^3 \, d\theta$$ ..... (A12.9)

where, $0<\theta<t$ and $\theta<\zeta<t$.

The final product mass m_∞ is also given by equation A12.8.

i.e. $$m_\infty = f_v \rho \int_0^{L_{\infty}(max)} n(L,\infty) L^3 \, dL$$ ..... (A12.10)

where, $n(L,\infty)$ is the final product population density function; and, $L_{\infty(max)}$ is the size of the largest crystals present in the final product. These largest crystals are obviously those nucleated first, in the initial time interval from t = 0 to t = dt. Similarly, all particles in the size range (say) L_θ to $L_\theta + dL_\theta$, of the final size distribution, would have been nucleated in an identifiable time interval from $t = \theta$ to $t = \theta + d\theta$. Thus, the following identity can be established:

$$n(L,\infty)_{(L=L_\theta)} \cdot dL_\theta = F_{N\theta} \cdot d\theta$$ ..... (A12.11)

$$\therefore \quad F_{N\theta} = n(L,\infty)_{(L=L_\theta)} \cdot \left(\frac{dL}{dt}\right)_{(t=\theta, L=L_\theta)}$$ ..... (A12.12)

$$\text{i.e.} \quad n(L,\infty)_{(L=L_\theta)} = \frac{F_{N\theta}}{F_{G\theta}} \quad \ldots\ldots\ldots\ldots\ldots\ldots \quad (A12.13)$$

Since growth rate is independent of size, for crystals nucleated in the time interval from t to t+dt, and having a final size of L_t,

$$dL_t = - F_{Gt}\, dt \quad \ldots\ldots\ldots\ldots\ldots\ldots\ldots \quad (A12.14)$$

It is therefore possible to combine equations, A12.9, A12.13 and A12.14 to obtain, with suitable changes to the limits of integration, the following relation,

$$m_t = f_v \rho \int_{L_t}^{L_\infty(max)} [n(L,\infty)]_{(L=L_\theta)} \left(\int_{L_t}^{L_\theta} dL_\zeta\right)^3 dL_\theta \quad \ldots\ldots\ldots\ldots\ldots \quad (A12.15)$$

where $L_t < L_\theta < L_\infty$.

This reduces to,

$$m_t = f_v \rho \int_{L_t}^{L_\infty(max)} [n(L,\infty)]_{(L=L_\theta)} (L_\theta - L_t)^3 dL_\theta = f_v \rho I \quad \ldots\ldots\ldots\ldots\ldots\ldots \quad (A12.16)$$

$$\text{where,} \quad I = \int_{L_t}^{L_\infty(max)} [n(L,\infty)]_{(L=L_\theta)} (L_\theta - L_t)^3 dL_\theta \quad \ldots \quad (A12.17)$$

The integral I can be evaluated numerically from the final product population density function, and so also the ratio of nucleation rate to growth rate, as expressed by equation A12.13.

A mass balance for the solute, in turn relates solute concentration, C_t at time, t to the crystal mass, m_t.

$$\text{i.e.} \quad C_t = (m_o - m_t)/(MV) \quad \ldots\ldots\ldots\ldots\ldots\ldots \quad (A12.18)$$

where m_o is the initial mass of solute taken; M is the molecular weight of the solute; and, V is the system volume.

It is also possible to use the crystal population density function at any given time, t to calculate the mass of crystals produced upto that time.

i.e. $$m_t = f_v \rho \int_0^{L_{t(max)}} [n(L,t)] (L)^3 \, dL \quad \ldots\ldots\ldots \text{(A12.19)}$$

The relations derived so far can be applied to a series of experiments, starting with the same initial conditions and employing the same operating conditions, with each experiment terminated at progressively longer times from commencement. Analysis of the products from such a series of experiments would give a series of crystal size distributions, and hence population density functions, culminating in the final product size distribution. For an experiment terminated after a time, t the population density function can be used to numerically evaluate m_t by equation A12.19. This can then be related to the final product population density by equation A12.16. An iterative procedure can thus be used to determine L_t, the lower limit of integration of the integral I (equations A12.16 and A12.17). This technique therefore enables the final size, L_t of crystals nucleated at any time, t to be determined. Consequently, the ratio of nucleation rate to growth rate at any time can be evaluated using equation A12.13.

However, separate determination of nucleation rate, F_N and growth rate, F_G requires another relation. For this purpose, equation A12.9 may be differentiated with respect to time.

$$\text{i.e.} \quad \frac{dm_t}{dt} = 3f_v\rho \, F_{Gt} \int_0^t F_{N\theta} \cdot \{\int_\theta^t F_{G\zeta} \, d\zeta\}^2 \, d\theta \quad .. \quad (A12.20)$$

The total crystal surface area, A at any time is given by,

$$A = f_s \int_0^t F_{N\theta} \cdot \{\int_\theta^t F_{G\zeta} \, d\zeta\}^2 \, d\theta \quad ..... \quad (A12.21)$$

Equations A12.20 and A12.21 can be combined to give,

$$\frac{dm_t}{dt} = \frac{3f_v\rho}{f_s} F_{Gt} \, A \quad ..... \quad (A12.22)$$

If crystal size distributions are based on equivalent volume diameters, the crystal surface area, A can be estimated from the population density function, n(L,t), provided crystal sphericity, ϕ is known.

$$\text{i.e.} \quad A = \frac{f_s}{\phi} \int_0^{L_{t(max)}} [n(L,t)]_{(L=L_\theta)} \, L_\theta^2 \, dL_\theta \quad .... \quad (A12.23)$$

Equations A12.22 and A12.23 enables the growth rate, F_G to be evaluated for any time, t. Subsequently, equation A12.13 can be used to determine the corresponding nucleation rate.

A12.3 APPLICATION OF MODEL

This model is applicable to a batch process in which concurrent nucleation and growth occurs continuously during crystallisation. Furthermore, in accordance

with the model, both nucleation and growth are considered to be independent of crystal size. In the barium chromate batch crystallisation experiments nucleation was considered to have occurred in an initial 'burst', and therefore, this model was not employed in analysing the experimental data. However, under conditions in which nucleation occurs during the whole process, this model would be of relevance. Moreover, it could be extended to cover conditions under which agglomeration as well as nucleation and growth occurs all the time.

APPENDIX 13

LISTING OF COMPUTER PROGRAM 'GRAPHICS'

The computer program written to fit a cumulative normal distribution on a mass basis to experimental crystal size distribution data, using the Gauss-Newton non-linear optimisation technique (201), and consequently to derive values of relevant variables, is listed in this appendix. The program is named GRAPHICS and was written in a version of Fortran IV suitable for a Harris 500 computer. The function of each program segment is explained in comment statements included in the listing.

```
C**********************************************************************
C     PROGRAM TO FIT CUMULATIVE NORMAL DISTRIBUTIONS TO SETS  **
C     OF EXPERIMENTAL CUMULATIVE SIZE DISTRIBUTION DATA, TO   **
C     THEREBY DERIVE VALUES OF MEAN CRYSTAL SIZE, CRYSTAL     **
C     SURFACE AREA AND CRYSTAL POPULATION, AND TO PLOT        **
C     GRAPHS OF CUMULATIVE SIZE DISTRIBUTION ON A MASS        **
C     BASIS AND DIFFERENTIAL SIZE DISTRIBUTION ON A NUMBER    **
C     BASIS                                                   **
C**********************************************************************
C
C
C     MAIN SEGMENT
C     ************
C
C
C     TYPE SPECIFICATION STATEMENTS
C
      REAL C(30),D(30),X(5),T(5)
      REAL E(5), F(5), G(5), A(2,2), B(2,2), W(2,2)
      REAL TOL, P, SUM, SNEW
      REAL R, WW, Z, D1, D2, D3, YMAX, XMAX
      REAL XX(1000), YY(1000)
      REAL FIT(30), RES(30)
      REAL Z1, Z2, Z3, TIME(30), CRYS(30)
      REAL PHI, SURF(30), WE(30), PN(30), SCA
C
      INTEGER  I, J, K, K1, L, IFLAG, INDEX, INX
      INTEGER NTOT, IA(30), ITOT, IFAIL, ISTOP, IY
      INTEGER ILIT, ISX, IMAT
C
C     INPUT NUMBER OF DISTINCT DATA SETS, CRYSTAL DENSITY,
C     CRYSTAL SHAPE FACTOR AND SCALE FACTOR FOR GRAPH PLOT
C
      READ(11,-) NTOT, R, PHI, SCA
C
C     CALL SUBROUTINE TO INITIALISE GRAPH PLOTTING PACKAGE
C
      CALL FIRST(NTOT,SCA)
C
C     DO LOOP WHICH SETS UP COMPUTATIONS FOR THE SERIES OF DATA SETS
C
      DO 800 ITOT = 1, NTOT
C
C     INPUT LABEL FOR TITLE OF GRAPH AND HEADING FOR NUMERICAL
C     OUTPUT FOR EACH DATA SET
C
      READ(11,12) (IA(I), I = 1, 20)
   12 FORMAT(20A3)
C
C     INPUT CRYSTAL MASS AND CRYSTALLISATION TIME
C
      READ(11,-) WW, TIME(ITOT)
C
C     INPUT NUMBER OF PARAMETERS, NUMBER OF DATA POINTS
C     AND MAXIMUM NUMBER OF ITERARTIONS
C
      READ(11,-)  N, K, INX
C
```

```
C     INPUT INITIAL VALUES FOR THE PARAMETERS
C
      READ(11,-)  (X(I), I = 1, N)
C
C     INPUT STOPPING TOLERANCE CRITERIA FOR THE INDIVIDUAL PARAMETERS
C
      READ(11,-)  (T(I), I = 1, N)
C
C     INPUT STOPPING TOLERANCE CRITERION FOR THE OBJECTIVE FUNCTION
C
      READ(11,-)    TOL
C
C     INITIALISE CONTROL VARIABLES AND FLAGS
C
      K1=31-K
      INDEX=0
      SNEW=0.0
      IFAIL=0
C
C     CALL SUBROUTINE TO INPUT EXPERIMENTAL SIZE DISTRIBUTION DATA
C
      CALL DATA(K,C(K1),D(K1))
C
C     CALL SUBROUTINE TO PRINT OUT HEADING FOR NUMERICAL RESULTS
C
      CALL PRINTI(IA)
C
C     CALL SUBROUTINE TO PRINT OUT INITIAL VALUES OF THE
C     PARAMETERS FOR OPTIMISATION AND THEIR STOPPING
C     TOLERANCES
C
      CALL OUTPUT(N,X(1),T(1),TOL)
C
C     CONVERT SIEVE DIAMETERS TO EQUIVALENT VOLUME DIAMETERS
C
      DO 65 I = K1, 30
      D(I) = PHI*D(I)
   65 CONTINUE
C
C     INITIALISE VARIABLES AND ARRAYS FOR OPTIMISATION BY THE
C     GAUSS - NEWTON NONLINEAR OPTIMISATION METHOD WHICH
C     INVOLVES LINEARISATION OF THE MODEL BY MEANS OF A
C     TRUNCATED TAYLOR SERIES
C
   70 SUM=0.0
      DO 100 I = 1, N
      E(I)=0.0
      F(I)=0.0
      G(I)=0.0
      DO  80 J = 1, N
      A(I,J)=0.0
      B(I,J)=0.0
   80 CONTINUE
  100 CONTINUE
C
C     COMPUTATION SECTION FOR OPTIMISATION METHOD
C
      DO 300 L = K1, 30
```

```
C
C     CALL SUBROUTINES TO CALCULATE DERIVATIVES OF OBJECTIVE
C     FUNCTION WITH RESPECT TO THE MODEL PARAMETERS AND THE
C     OBJECTIVE FUNCTION ITSELF
C
      CALL SIGMA(D(L),X(1),N,E(2))
      CALL MUE(D(L),X(1),N,E(1))
      CALL FRAC(C(L),D(L),X(1),N,P)
C
      RES(L)=P
      FIT(L)=C(L)-P
      SUM=SUM+(P**2.0)
C
      DO 280 I = 1, N
C
      G(I)=G(I)+E(I)*P
C
      DO 260 J = 1, N
C
      B(I,J)=B(I,J)+E(I)*E(J)
C
  260 CONTINUE
C
  280 CONTINUE
C
  300 CONTINUE
C
      DO 320 I = 1, N
C
      E(I)=ABS(B(I,I))
C
  320 CONTINUE
C
      DO 360 I = 1, N
C
      DO 340 J = 1, N
C
      A(I,J)=B(I,J)/(SQRT(E(I)*E(J)))
C
  340 CONTINUE
C
  360 CONTINUE
C
C     CALL SUBROUTINE TO CARRY OUT MATRIX INVERSION
C
      CALL  MATIN(N,A     ,B     ,IMAT)
      IF(IMAT.LT.0)  GO  TO  500
C
      DO 375 I = 1, N
C
      DO 370 J = 1, N
C
      B(I,J) = B(I,J)/SQRT(E(I)*E(J))
C
  370 CONTINUE
C
  375 CONTINUE
C
```

```
C     CALL SUBROUTINE TO CARRY OUT MATRIX MULTIPLICATION
C
      CALL MATPR(N,N,N,B     ,G(1),F(1),IMAT)
      IF(IMAT.LT.0)  GO  TO  500
C
      DO 400 I = 1, N
C
      G(I)=F(I)
C
      DO 380 J = 1, N
C
      W(I,J)=B(I,J)
C
  380 CONTINUE
C
  400 CONTINUE
C
C     CALL SUBROUTINE TO TEST STOPPING TOLERANCE CRITERIA
C     FOR PARAMETERS AND OBJECTIVE FUNCTION
C
      CALL TEST(N,G(1),X(1),T(1),TOL,SUM,IFLAG,INDEX,SNEW)
C
      IF(IFLAG.GT.0)  GO  TO  500
C
      IF(INDEX.GT.INX)  GO TO  500
C
      GO   TO  70
C
C     COMPUTE STANDARD ERRORS OF OPTIMISED MODEL PARAMETERS
C
  500 DO 520 I = 1, N
C
      G(I)=SQRT(ABS(W(I,I)*SNEW/FLOAT(K-N)))
C
  520 CONTINUE
C
C     CALL SUBROUTINE TO PRINT OUT RESULTS OF OPTIMISATION
C
      CALL RESULT(N,X(1),G(1),INDEX,SNEW,K)
C
C     CALL SUBROUTINE TO PRINT OUT EXPERIMENTAL AND FITTED
C     VALUES OF CUMULATIVE CRYSTAL MASS
C
      CALL PRINT2(K,C(K1),D(K1),FIT(K1),RES(K1))
C
C     INITIALISE CONTROL VARIABLES
C
      ILIT=1000
      XX(1)=0.0
      YY(1)=1.0
C
C     COMPUTE VALUES OF CUMULATIVE CRYSTAL MASS FRACTION FOR
C     FIXED INCREMENTS OF VOLUME DIAMETER, FOR USE IN
C     PLOTTING FITTED CUMULATIVE NORMAL DISTRIBUTION CURVE
C
      DO 530 I = 2, 1000
C
      XX(I)=FLOAT(I-1)
```

```
      Z=(XX(I)-X(1))/X(2)
      YY(I)=S15ACF(Z,IFAIL)
      IF(YY(I).LT.1.0E-09)  ILIT=I
      IF(YY(I).LT.1.0E-09) GO TO 535
C
  530 CONTINUE
C
C     CALL SUBROUTINE TO PRINT TITLE ON THE GRAPH OF THE
C     CUMULATIVE SIZE DISTRIBUTION
C
  535 CALL TITLE(IA)
C
C     CALL SUBROUTINE TO PLOT GRAPH OF CUMULATIVE SIZE
C     DISTRIBUTION ON A MASS BASIS
C
      CALL PLOT1(K,D(K1),C(K1),XX(1),YY(1),ILIT)
C
C     INITIALISE ARRAYS AND VARIABLES FOR COMPUTING CRYSTAL
C     POPULATION, CRYSTAL SURFACE AREA AND DATA FOR
C     DIFFERENTIAL SIZE DISTRIBUTION ON A NUMBER BASIS
C
      DO 540 I = 1, 1000
C
      XX(I) = 0.0
      YY(I) = 0.0
C
  540 CONTINUE
C
      IFAIL = 0
      SUM = 0.0
      YMAX = 0.0
      ISTOP = 1000
      Z1=0.0
      Z3=0.0
C
C     COMPUTATION SECTION FOR DIFFERENTIAL SIZE DISTRIBUTION
C     ON A NUMBER BASIS, CRYSTAL SURFACE AREA AND CRYSTAL
C     POPULATION
C
      DO 550 I = 1, 1000
C
      XX(I) = FLOAT(I)
      Z=(XX(I)-X(1))/X(2)
      D1=(1.0E15)*WW*6.0/R
      D2=2.0*(ASIN(1.0))*(XX(I)**3.0)
      D3=1.0/(SQRT(4.0*ASIN(1.0)))
      D3=(D3/X(2))*EXP(-0.5*(Z**2.0))
      Z2=(D3*D1)/(0.811*XX(I)*(1.0E12))
      YY(I) = D1*D3/D2
      Z3=Z3+0.5*(Z1+Z2)
      Z1=Z2
      SUM=SUM+YY(I)
C
      IF(YY(I).LT.1.0.AND.I.GT.25)  ISTOP = I-1
C
      IF(YY(I).LT.1.0.AND.I.GT.25)  GO  TO  570
C
  550 CONTINUE
```

```
C
  570 DO 600 I = 1, ISTOP
C
      YMAX=AMAX1(YMAX,YY(I))
C
  600 CONTINUE
C
      ISX=ISTOP
C
      PN(ITOT)=SUM
C
      SURF(ITOT)=Z3
C
      XMAX=10.0*(AINT(((FLOAT(ISTOP))/10.0)+1.0))
      ISTOP=INT(XMAX/10.0)
      IY=INT(ALOG10(YMAX)+2.0)
      YMAX=10.0**(FLOAT(IY))
C
C     CALL SUBROUTINE TO PRINT TITLE ON THE GRAPH OF THE
C     DIFFERENTIAL SIZE DISTRIBUTION
C
      CALL TITLE(IA)
C
C     CALL SUBROUTINE TO PLOT GRAPH OF THE DIFFERENTIAL
C     SIZE DISTRIBUTION ON A NUMBER BASIS
C
      CALL PLOT(XX(1),YY(1),ITOT,ISX,XMAX,YMAX,IY)
C
C     CALL SUBROUTINE TO PRINT OUT RESULTS FROM DIFFERENTIAL
C     NUMBER SIZE DISTRIBUTION
C
      CALL PRINT(XX(1),YY(1),ISX,SUM,WW)
C
C     COMPUTE CORRECTED CRYSTAL MASS
C
      Z1=(0.0-X(1))/X(2)
      Z2=(XMAX-X(1))/X(2)
      CRYS(ITOT)=WW*(ABS((S15ACF(Z1,IFAIL))-(S15ACF(Z2,IFAIL))))
C
      WE(ITOT)=WW
C
      IF(ITOT.LT.NTOT) GO TO 800
C
C     PRINT OUT COLLECTED RESULTS FROM ALL THE DATA SETS
C
      WRITE(100,620)
  620 FORMAT(1H ,5X,8HTIME (S),5X,26HCRYSTAL    MASS  (GRAMMES),
     1       5X,15HCRYSTAL SURFACE,5X,7HCRYSTAL,/,19X,
     2       26H(EXPERIMENTAL) (CORRECTED),5X,15HAREA   (SQ. M.),
     3       5X,14HPOPULATION (-),/)
C
      DO 750 L = 1, NTOT
C
      WRITE(100,700) TIME(L), WE(L), CRYS(L), SURF(L), PN(L)
  700 FORMAT(1H ,4X,F9.2,6X,F8.5,7X,F8.5,8X,1PE12.5,8X,1PE12.5)
C
  750 CONTINUE
C
```

```
  800 CONTINUE
C
      WRITE(100,850)
  850 FORMAT(1H ,1X,130(1H*),/)
C
C     CALL SUBROUTINE TO TERMINATE GRAPH PLOTTING PACKAGE
C
      CALL LAST
C
      STOP
C
      END
C
C
C
C     THE SUBROUTINE 'TITLE' PRINTS THE TITLE OF THE GRAPH
C     PLOT AT THE TOP OF EACH GRAPH
C     ****************************************************
C
      SUBROUTINE TITLE(IA)
C
      INTEGER IA(20)
C
      CALL CHASIZ(2.0,2.75)
      CALL MOVTO2(0.0,0.0)
C
      CALL LINTO2(0.0,210.5)
      CALL LINTO2(297.5,210.5)
      CALL LINTO2(297.5,0.0)
      CALL LINTO2(0.0,0.0)
C
      CALL SHIFT2(48.0,35.0)
C
      CALL MOVTO2(10.0,115.0)
      CALL CHAARR(IA,20,3)
C
      RETURN
C
      END
C
C
C
C     THE SUBROUTINE 'PRINT' PRINTS OUT THE CRYSTAL SIZE AND
C     NUMBER FREQUENCY PER  MICRON DATA  USED FOR THE
C     DIFFERENTIAL NUMBER SIZE DISTRIBUTION AS WELL AS THE
C     CRYSTAL POPULATION AND THE EXPERIMENTAL CRYSTAL MASS
C     ********************************************************
C
      SUBROUTINE PRINT(XX,YY,ISTOP,SUM,WW)
C
      REAL WW, SUM
      REAL XX(ISTOP), YY(ISTOP)
C
      INTEGER ISTOP, I
C
     WRITE(100,40)
   40 FORMAT(1H ,20X,14HSIZE (MICRONS),12X,
     127HNUMBER FREQUENCY PER MICRON,/)
```

```
C
      WRITE(100,60) XX(1), YY(1)
   60 FORMAT(22X,G10.5,15X,F20.5)
C
      DO 80 I = 10, ISTOP, 10
      WRITE(100,60)  XX(I), YY(I)
   80 CONTINUE
C
      WRITE(100,60) XX(ISTOP), YY(ISTOP)
C
      WRITE(100,100) SUM
  100 FORMAT(1H ,15X,24HTOTAL PARTICLE NUMBER = ,G20.5,/)
C
      WRITE(100,120)    WW
  120 FORMAT(1H ,15X,28HEXPERIMENTAL CRYSTAL MASS = ,F8.5,8H GRAMMES,/)
C
      WRITE(100,300)
  300 FORMAT(1H ,1X,130(1H*),/)
C
      RETURN
C
      END
C
C
C
C     THE SUBROUTINE 'FIRST' CALLS ALL THE INITIALISATION AND
C     SCALING ROUTINES REQUIRED BY THE GINO GRAPH PLOTTING
C     PACKAGE. NOTE THAT WITH A UNIT SCALE FACTOR, THE SYSTEM
C     LIMIT TO THE MAXIMUM LENGTH OF GRAPH PLOTTER PAPER THAT
C     CAN BE USED, RESTRICTS THE TOTAL NUMBER OF GRAPHS THAT
C     CAN BE PLOTTED AT ANY ONE TIME TO SIX
C     ************************************************************
C
      SUBROUTINE FIRST(NTOT,SCA)
C
      REAL U, SCA
C
      INTEGER NTOT
C
      U=1000.0*FLOAT(2*NTOT)
C
      CALL OPEN
      CALL DEVPAP(U,350.0,0)
      CALL ERRMAX(100)
      CALL CHASWI(1)
      CALL SCALE(SCA)
      CALL SHIFT2(10.0,10.0)
      CALL CHASIZ(3.0,5.0)
C
      RETURN
C
      END
C
C
C
C     THE SUBROUTINE 'PRINTI' PRINTS OUT THE HEADING FOR THE
C     NUMERICAL RESULTS THAT ARE PRODUCED FOR EACH DATA SET
C     ************************************************************
```

```
C
      SUBROUTINE PRINTI(IA)
C
      INTEGER IA(20), I
C
      WRITE(100,20)   (IA(I), I = 1, 20)
   20 FORMAT(1H ,20X,20A3)
C
      RETURN
C
      END
C
C
C
C     THE SUBROUTINE 'LAST' TERMINATES THE USE OF THE GINO
C     GRAPH PLOTTING PACKAGE
C     ******************************************************
C
      SUBROUTINE LAST
C
      CALL DEVEND
C
      RETURN
C
      END
C
C
C
C     THE SUBROUTINE 'PLOT' USES THE ROUTINES OF THE GINO GRAPH
C     PLOTTING PACKAGE TO PRODUCE A GRAPH OF THE DIFFERENTIAL
C     CRYSTAL SIZE DISTRIBUTION ON A NUMBER BASIS
C     ************************************************************
C
      SUBROUTINE PLOT(XX,YY,N,ISTOP,XMAX,YMAX,IY)
C
      REAL XX(ISTOP), YY(ISTOP), XMAX, YMAX
C
      INTEGER N, IY, ISTOP
C
      CALL CHASIZ(1.5,2.5)
      CALL AXIPOS(0,0.0,0.0,220.0,1)
      CALL AXIPOS(0,0.0,0.0,110.0,2)
      CALL AXISCA(3,10,0.0,XMAX,1)
      CALL AXISCA(4,IY,1.0,YMAX,2)
      CALL AXIDRA(-2,1,1)
      CALL AXIDRA(2,-1,2)
C
      CALL CHASIZ(3.0,5.0)
C
      CALL MOVTO2(20.0,-20.0)
      CALL CHAHOL(29HPARTICLE DIAMETER (MICRONS)*.)
C
      CALL MOVTO2(-20.0,2.0)
      CALL CHAANG(90.0)
      CALL CHAHOL(40HPARTICLE NUMBER FREQUENCY (NO./MICRON)*.)
      CALL CHAANG(0.0)
C
      CALL GRACUR(XX,YY,ISTOP)
```

```
C
      CALL SHIFT2(300.0,-35.0)
C
      RETURN
C
      END
C
C
C
C     THE SUBROUTINE 'DATA' READS IN ONE SET OF EXPERIMENTAL
C     SIZE DISTRIBUTION DATA, AT A TIME. THIS CONSISTS OF
C     PAIRS OF SIEVE DIAMETER AND CUMULATIVE CRYSTAL MASS DATA
C     ********************************************************
C
      SUBROUTINE DATA(K,C,D)
C
      REAL C(K),D(K)
C
      INTEGER  K, I
C
      DO 40 I = 1, K
      READ(11,-) D(I), C(I)
   40 CONTINUE
C
      RETURN
C
      END
C
C
C
C     THE SUBROUTINE 'OUTPUT' PRINTS OUT THE INITIAL VALUES
C     OF THE MODEL PARAMETERS AND THE STOPPING TOLERANCES
C     FOR THE PARAMETERS AND FOR THE OBJECTIVE FUNCTION
C     ****************************************************
C
      SUBROUTINE OUTPUT(N,X,T,TOL)
C
      REAL X(N), T(N), TOL
C
      INTEGER N, I
C
      WRITE(100,100)
  100 FORMAT(1H /12X,8HVARIABLE,22X,13HINITIAL VALUE,19X,9HTOLERANCE/)
C
      DO 140 I = 1, N
      WRITE(100,120)   I, X(I), T(I)
  120 FORMAT(1H ,10X,I5, 9X,2(10X,G20.5))
  140 CONTINUE
C
      WRITE(100,160)   TOL
  160 FORMAT(1H /2X,31HOBJECTIVE FUNCTION TOLERANCE = ,G20.5)
C
      RETURN
C
      END
C
C
C
```

```
C     THE SUBROUTINE 'SIGMA' CALCULATES THE VALUE OF THE DERIVATIVE
C     OF THE OBJECTIVE FUNCTION WITH RESPECT TO THE SECOND MODEL
C     PARAMETER, WHICH IS THE STANDARD DEVIATION OF THE NORMAL
C     DISTRIBUTION
C     ****************************************************************
C
      SUBROUTINE SIGMA(D,Q,N,V)
C
      REAL V, D, Q(N), F, Z
C
      INTEGER N
C
      F=1.0/(SQRT(4.0*ASIN(1.0)))
      Z=(D-Q(1))/Q(2)
      V= 1.0*F*(Z/Q(2))*EXP(-1.0*(Z**2.0)/2.0)
C
      RETURN
C
      END
C
C
C
C     THE SUBROUTINE 'MUE' CALCULATES THE VALUE OF THE DERIVATIVE
C     OF THE OBJECTIVE FUNCTION WITH RESPECT TO THE FIRST MODEL
C     PARAMETER, WHICH IS THE MEAN OF THE NORMAL DISTRIBUTION
C     ****************************************************************
C
      SUBROUTINE MUE(D,Q,N,W)
C
      REAL W,D,Q(N),F,Z
C
      INTEGER N
C
      F=1.0/(SQRT(4.0*ASIN(1.0)))
      Z=(D-Q(1))/Q(2)
      W= 1.0*(F/Q(2))*EXP(-1.0*(Z**2.0)/2.0)
C
      RETURN
C
      END
C
C
C
C     THE SUBROUTINE 'FRAC' CALCULATES THE VALUE
C     OF THE OBJECTIVE FUNCTION
C     ****************************************
C
      SUBROUTINE FRAC(C,D,Q,N,A)
C
      REAL C, D, Z, Q(N), A
C
      INTEGER N, IFAIL
C
      Z=(D-Q(1))/Q(2)
      IFAIL=0
      Y=S15ACF(Z,IFAIL)
      A=C-Y
C
```

```
      RETURN
C
      END
C
C
C
C     THE SUBROUTINE 'TEST' EXAMINES THE STOPPING TOLERANCE
C     CRITERIA FOR THE OBJECTIVE FUNCTION AND THE MODEL
C     PARAMETERS, AND SETS UP NEW VALUES OF THE MODEL
C     PARAMETERS FOR THE NEXT ITERATION
C     ******************************************************
C
      SUBROUTINE TEST(N,R,X,T,TOL,SUM,IFLAG,INDEX,SNEW)
C
      REAL R(N),X(N),T(N),TOL,SUM,SNEW
C
      INTEGER N, IFLAG, INDEX, I
C
      IF(ABS(SUM-SNEW).GT.TOL) GO TO 80
C
      DO 40 I = 1, N
C
      IF(ABS(R(I)).GT.T(I)) GO TO 80
C
   40 CONTINUE
C
      IFLAG=10
C
      GO TO 100
C
   80 IFLAG=-10
C
  100 INDEX=INDEX+1
C
      SNEW=SUM
      DO 120 I = 1, N
      X(I)=X(I)+R(I)
  120 CONTINUE
C
      RETURN
C
      END
C
C
C
C     THE SUBROUTINE 'RESULT' PRINTS OUT THE VALUES OF THE
C     PARAMETERS AND THE OBJECTIVE FUNCTION AT THE MINIMUM,
C     THE NUMBER OF ITERATIONS, THE STANDARD ERRORS OF THE
C     OPTIMISED PARAMETERS AND THE MEAN SQUARED ERROR OF
C     THE FIT
C     ******************************************************
C
      SUBROUTINE RESULT(N,X,Y,INDEX,SNEW,K)
C
      REAL X(N), Y(N), SNEW, F
C
      INTEGER N, K, INDEX, I
C
```

```
      WRITE(100,20)  INDEX
   20 FORMAT(1H /60X,7HRESULTS/60X,7(1H-)/50X,16HITERATION NO. = ,I6)
C
      WRITE(100,30)
   30 FORMAT(1H /25X,8HVARIABLE,22X,5HVALUE,20X,14HSTANDARD ERROR/)
C
      DO 60 I = 1, N
      WRITE(100,40) I, X(I), Y(I)
   40 FORMAT(23X,I6, 6X,2(10X,G20.5))
   60 CONTINUE
C
      F=SNEW/FLOAT(K-N)
C
      WRITE(100,80)   F
   80 FORMAT(1H /2X,21HMEAN SQUARED ERROR = ,G20.5)
C
      RETURN
C
      END
C
C
C
C     THE SUBROUTINE 'PRINT2' PRINTS OUT VALUES OF VOLUME
C     DIAMETER, EXPERIMENTAL CUMULATIVE CRYSTAL MASS,
C     FITTED CUMULATIVE CRYSTAL MASS AND ERROR OF FIT
C     ***************************************************
C
      SUBROUTINE PRINT2(K,C,D,FIT,RES)
C
      REAL C(K), D(K), FIT(K), RES(K)
C
      INTEGER K, I
C
      WRITE(100,40)
   40 FORMAT(1H ,20X,6HVOLUME,31X,24HCUMULATIVE MASS FRACTION,
     130X,8HRESIDUAL,/20X,8HDIAMETER,21X,12HEXPERIMENTAL,18X,
C
     29HOPTIMISED,/)
      DO 120 I = 1, K
      WRITE(100,80) D(I), C(I), FIT(I), RES(I)
   80 FORMAT(1X,4(10X,G20.5))
  120 CONTINUE
C
      RETURN
C
      END
C
C
C
C     THE SUBROUTINE 'PLOT1' USES THE ROUTINES OF THE GINO
C     GRAPH PLOTTING PACKAGE, TO PRODUCE A GRAPH OF THE
C     CUMULATIVE CRYSTAL SIZE DISTRIBUTION ON A MASS BASIS,
C     SHOWING THE EXPERIMENTAL POINTS AND THE FITTED CURVE
C     ***************************************************
C
      SUBROUTINE PLOT1(K,D,C,XX,YY,N)
C
      REAL D(K), C(K), XX(N), YY(N), Q
```

```
C
      INTEGER K, N
      INTEGER ILIM
C
      CALL CHASIZ(1.5,2.5)
C
      ILIM=N-1
C
      IF(D(K).GT.FLOAT(ILIM)) ILIM=INT(D(K))+1
C
      Q=10.0*(AINT(((FLOAT(ILIM))/10.0)+1.0))
C
      CALL AXIPOS(0,0.0,0.0,220.0 ,1)
      CALL AXIPOS(0,0.0,0.0,110.0,2)
      CALL AXISCA(3,10,0.0, Q  ,1)
      CALL AXISCA(3,5,0.0,1.0,2)
      CALL AXIDRA(-2,1,1)
      CALL AXIDRA(2,-1,2)
C
      CALL CHASIZ(3.0,5.0)
C
      CALL MOVTO2(20.0,-20.0)
      CALL CHAHOL(29HPARTICLE DIAMETER (MICRONS)*.)
C
      CALL MOVTO2(-20.0,10.0)
      CALL CHAANG(90.0)
      CALL CHAHOL(30HCUMULATIVE MASS FRACTION (-)*.)
      CALL CHAANG(0.0)
C
      CALL CHASIZ(1.5,2.5)
C
      CALL GRACUR(XX,YY,N)
C
      CALL GRASYM(D,C,K,5,0)
C
      CALL SHIFT2(300.0,-35.0)
C
      RETURN
C
      END
C
C
C
C     THE SUBROUTINE 'MATIN' INVERTS ANY SUPPLIED
C     MATRIX OF SIZE N X N
C     ******************************************
C
      SUBROUTINE MATIN(N,BORI,BINV,IMAT)
C
      REAL BORI(N,N), BINV(N,N), P, Q, T
C
      INTEGER I, J, K, L, M, N, IMAT
C
      IMAT=1
C
      DO 40 K = 1, N
C
      DO 20 L = 1, N
```

```
      BINV(K,L)=0.0E0
   20 CONTINUE
C
   40 CONTINUE
C
      DO 60 K = 1, N
      BINV(K,K)=1.0E0
   60 CONTINUE
C
      DO 220 M = 1, N
C
      IF(M.EQ.N) GO TO 140
C
      J=M+1
C
      P=BORI(M,M)
      Q=BORI(M+1,M)
C
      IF( ABS(P).GE. ABS(Q)) I=M
C
      DO 100 K = J, N
C
      Q=BORI(K,M)
C
      IF( ABS(P).GE. ABS(Q)) GO TO 100
C
      P=Q
      I=K
C
  100 CONTINUE
C
      IF(I.EQ.M) GO TO 140
C
      DO 120 L = 1, N
C
      T=BORI(I,L)
      BORI(I,L)=BORI(M,L)
      BORI(M,L)=T
C
      T=BINV(I,L)
      BINV(I,L)=BINV(M,L)
      BINV(M,L)=T
C
  120 CONTINUE
C
  140 IF( ABS(BORI(M,M)).LT.1.0E-20) GO TO 240
C
      P=BORI(M,M)
C
      DO 160 L = 1, N
      BORI(M,L)=BORI(M,L)/P
      BINV(M,L) =BINV(M,L)/P
  160 CONTINUE
C
      DO 200 K = 1, N
C
      IF(K.EQ.M) GO TO 200
C
```

```
      P=BORI(K,M)
C
      DO 180 L = 1, N
      BORI(K,L)=BORI(K,L)-BORI(M,L)*P
      BINV(K,L)=BINV(K,L)-BINV(M,L)*P
  180 CONTINUE
C
  200 CONTINUE
C
  220 CONTINUE
C
      GO TO 280
C
  240 WRITE(100,260)
  260 FORMAT(1H ,43HSUBROUTINE MATIN FAILS : MATRIX IS SINGULAR)
C
      IMAT=-1
C
  280 RETURN
C
      END
C
C
C
C     THE SUBROUTINE 'MATPR' MULTIPLIES TWO SUPPLIED MATRICES
C     ********************************************************
C
      SUBROUTINE MATPR(NR1,NR2,NC1,P,Q,R,IMAT)
C
      REAL             P(NR1,NC1), Q(NR2), R(NC1), SUM
C
      INTEGER K, M, IMAT
      INTEGER NR1, NR2, NC1
C
      IMAT=1
C
      IF(.NOT.NC1.EQ.NR2) GO TO 80
C
      DO 60 K = 1, NR1
C
      SUM=0.0E0
C
      DO 20 M = 1, NR2
      SUM=SUM+P(K,M)*Q(M)
   20 CONTINUE
C
      R(K)=SUM
C
   60 CONTINUE
C
      GO TO 120
C
   80 WRITE(100,100)
  100 FORMAT(1H ,22HSUBROUTINE MATPR FAILS)
C
      IMAT=-1
C
  120 RETURN
```

```
C
      END
C
C
C
C     END OF PROGRAM
C     **************
```

APPENDIX 14

LISTING OF COMPUTER PROGRAM 'MASFITL'

The computer program written to fit pairs of straight lines to sets of experimental crystal mass-time data, using the linear regression routine G02CAF from the NAG library (301), is listed in this appendix. The program is named MASFITL and was written in a version of Fortran IV suitable for a Harris 500 computer. Comment statements have been included in the listing to explain the function of each program segment.

```
C*************************************************************************
C     PROGRAM  TO  FIT  EMPIRICAL  RELATIONS  TO  THE  CHANGE  IN     **
C     CRYSTAL  MASS  WITH  TIME                                        **
C*************************************************************************
C
C
C     MAIN SEGMENT
C     ************
C
C
C     TYPE SPECIFICATION STATEMENTS
C
      REAL T(50), P(50), W(50), V(50), TL
      REAL SL1(2), SL2(2), STOL, SCA, PL, CR(2)
C
      INTEGER I, N, IFAIL, ITX(10), ITY(15), KO, LL
C
C     INPUT AXIS LABELS FOR GRAPH OF RESULTS
C
      READ(11,20) (ITX(I), I = 1, 10)
   20 FORMAT(10A3)
C
      READ(11,40) (ITY(I), I = 1, 15)
   40 FORMAT(15A3)
C
C     INPUT NUMBER OF DATA POINTS, TOLERANCE FACTOR FOR FITTING
C     AND SCALE FACTOR FOR GRAPHICAL OUTPUT
C
      READ(11,-) N, STOL, SCA
C
C     CALL MAIN DATA INPUT SUBROUTINE
C
      CALL INPUT(N,T(1),P(1),W(1),V(1),KO)
C
C     CALL SUBROUTINE TO SORT OUT INPUT DATA
C
      CALL SORT(N,T(1),P(1),W(1),V(1),KO)
C
C     CALL SUBROUTINE TO CARRY OUT OPTIMISATION
C
      CALL FIT(N,T(1),P(1),W(1),V(1),SL1,SL2,STOL,
     1         TL, PL, IFAIL, CR, LL)
C
C     CALL SUBROUTINE TO PRINT OUT NUMERICAL RESULTS
C
      CALL OUTPUT(N,T(1),P(1),W(1),V(1),SL1,SL2,CR,LL)
C
C     CALL GRAPHICAL OUTPUT SUBROUTINE
C
      CALL PLOT(N,T(1),P(1),SL1,SL2,TL,PL,ITX,ITY,SCA)
C
      STOP
C
      END
C
C
C
C     THE OPTIMISATION SUBROUTINE 'FIT' FITS THE EXPERIMENTAL DATA
```

```
C     TO TWO CONSECUTIVE STRAIGHT LINES,THE SECOND OF WHICH HAS A
C     VERY SMALL SLOPE. THE STRAIGHT LINES ARE FITTED USING THE
C     LINEAR REGRESSION ROUTINE 'G02CAF' FROM THE NAG LIBRARY.A
C     TRIAL-AND-ERROR METHOD OF CONSIDERING THE SLOPES OF LINES
C     FITTED TO A PROGRESSIVELY GREATER NUMBER OF THE DATA POINTS,
C     UNTIL A COMPARATIVELY SHARP, PRESET, DIFFERENCE IN THE SLOPE
C     IS DETECTED, IS USED TO SET THE REGION OF APPLICABILITY OF
C     EACH FITTED LINE
C     ****************************************************************
C
      SUBROUTINE FIT(KNO,T,P,W,V,SL1,SL2,ST,TL,PL,IFAIL,CR,NK)
C
      REAL T(KNO), P(KNO), W(KNO), V(KNO), SL1(2), SL2(2), R(20)
      REAL ST, TL, PL, XS, XI,   CR(2)
C
      INTEGER K, KNO, I, NK, NL, NR, IFAIL
C
      K=KNO
C
:SKFZ 23
C
      K=KNO-2
C
:ESKP
C
      XS=(P(K)-P(K-1))/(T(K)-T(K-1))
      XI=P(K)-(XS*T(K))
C
      NL=K-2
C
      DO 100 I = 1, NL
C
      NK=NL+1-I
      NR=I+2
C
      CALL G02CAF(NR,T(NK), P(NK),R,IFAIL)
C
      IF((ABS(R(6)-XS)).GT.(ABS(ST*XS)))  GO  TO  200
C
      SL1(2)=R(6)
      SL2(2)=R(7)
      CR(2)=R(5)
C
  100 CONTINUE
C
  200 IF(NR.LE.3) SL1(2)=XS
      IF(NR.LE.3) SL2(2)=XI
      IF(NR.LE.3) CR(2)=1.00
C
      CALL G02CAF(NK,T(1),P(1),R,IFAIL)
C
      SL1(1)=R(6)
      SL2(1)=R(7)
      CR(1)=R(5)
C
      TL=(SL2(2)-SL2(1))/(SL1(1)-SL1(2))
C
      PL=(SL1(1)*TL)+SL2(1)
```

```
C
      RETURN
C
      END
C
C
C
C     THE SUBROUTINE 'OUTPUT' PRINTS OUT ALL THE NUMERICAL RESULTS
C     FROM THE EMPIRICAL FITTING PROCESS
C     ************************************************************
C
      SUBROUTINE OUTPUT(K,T,P,W,V,SL1,SL2,CR,NK)
C
      REAL T(K), P(K), W(K), V(K), SL1(2), SL2(2)
      REAL  CR(2), Y, RS
C
      INTEGER I, K, NK
C
      WRITE(16,40)
   40 FORMAT(1H ,//30X,8HLINE NO.,10X,5HSLOPE,10X,9HINTERCEPT,10X,
     1       12HCORR. COEFF.,/)
C
      DO 120 I = 1, 2
C
      WRITE(16,80) I, SL1(I), SL2(I), CR(I)
   80 FORMAT(30X,I4,11X,1PE11.4,6X,1PE11.4,11X,0PF8.5)
C
  120 CONTINUE
C
      WRITE(16,160)
  160 FORMAT(1H ,//,10X,31HVALUES OF INDEPENDENT VARIABLES,10X,
     1       28HVALUES OF DEPENDENT VARIABLE,12X,14HRESIDUAL ERROR,
     2       6X,9HWEIGHTING,/,10X,8HTIME (S),10X,13HVOLUME (LIT.),
     3       10X,12HEXPERIMENTAL,10X,6HFITTED,/)
C
      DO 240 I = 1, K
C
      Y=(SL1(1)*T(I))+SL2(1)
C
      IF(I.GT.NK) Y=(SL1(2)*T(I))+SL2(2)
C
      RS=P(I)-Y
C
      WRITE(16,200) T(I), V(I), P(I), Y, RS, W(I)
C
  200 FORMAT(9X,F8.1,13X,F6.4,15X,F9.6,10X,F9.6,12X,1PE13.6,7X,0PF6.2)
  240 CONTINUE
C
      WRITE(16,280)
  280 FORMAT(1H ,//,132(1H*))
C
      RETURN
C
      END
C
C
C
C     THE GRAPHICAL OUTPUT SUBROUTINE 'PLOT' USES THE ROUTINES OF
```

```
C     THE GINO GRAPH PLOTTING PACKAGE, TO PRODUCE A GRAPH SHOWING
C     THE EXPERIMENTAL DATA AND THE FITTED EMPIRICAL RELATIONS.
C     THE PLOT CAN BE SCALED TO ANY SIZE BY CHANGING THE SCALE
C     FACTOR, INPUT AS DATA IN THE MAIN SEGMENT. COMPILATION
C     OPTIONS 1, 2 AND 3 PERMIT DISPLAY OF THE GRAPH ON A T4010
C     GRAPHICS TERMINAL, PLOTTING A HARDCOPY OF THE GRAPH, AND
C     DISPLAY OF THE GRAPH ON AN IMLAC DYNAGRAPHICS TERMINAL,
C     RESPECTIVELY
C     ************************************************************
C
      SUBROUTINE PLOT(K,T,P,SL1,SL2,TL,PL,ITX,ITY,SCA)
C
      REAL T(K), P(K), SL1(2), SL2(2), TL, PL, SCA, XO, YO, XLT
C
      INTEGER K, ITX(10), ITY(15), NL
C
C
:SKFZ 1
      CALL T4010
:ESKP
C
:SKFZ 2
      CALL OPEN
:ESKP
C
:SKFZ 3
      CALL APDS4
:ESKP
C
C
      CALL ERRMAX(100)
C
      CALL SHIFT2(10.0,10.0)
C
      CALL CHASWI(1)
C
      CALL SCALE(SCA)
C
      CALL CHASIZ(1.5,2.5)
C
      CALL MOVTO2(0.0,0.0)
C
      CALL LINTO2(0.0,210.5)
      CALL LINTO2(297.5,210.5)
      CALL LINTO2(297.5,0.0)
      CALL LINTO2(0.0,0.0)
C
      CALL SHIFT2(46.0,35.0)
C
      CALL AXIPOS(0,0.0,0.0,110.0,2)
      CALL AXISCA(3,5,0.0,5.0,2)
      CALL AXIDRA(2,-1,2)
C
      XLT=100.0*(AINT((T(K)/100.0)+1.0))
C
      CALL AXIPOS(0,0.0,0.0,220.0,1)
      CALL AXISCA(3,10,0.0,XLT,1)
      CALL AXIDRA(-2,1,1)
```

```
C
      CALL GRASYM(T,P,K,5,0)
C
      XO=-1.0*SL2(1)/SL1(1)
      YO=0.0
      IF(XO.LT.0.0) YO=SL2(1)
      IF(XO.LT.0.0) XO=0.0
C
      XO=XO*220.0/XLT
      YO=YO*110.0/5.0
C
      CALL MOVTO2(XO,YO)
C
      NL=INT(T(K))
C
      XO=TL*220.0/XLT
      YO=PL*110.0/5.0
C
      CALL LINTO2(XO,YO)
C
      XO=T(K)*220.0/XLT
      YO=P(K)*110.0/5.0
C
      CALL LINTO2(XO,YO)
C
      CALL CHASIZ(3.0,5.0)
C
      CALL MOVTO2(50.0,-20.0)
C
      CALL CHAARR(ITX,10,3)
C
      CALL MOVTO2(-14.0,5.0)
      CALL CHAANG(90.0)
C
      CALL CHAARR(ITY,15,3)
C
      CALL CHAANG(0.0)
C
      CALL DEVEND
C
      RETURN
C
      END
C
C
C
C     THE DATA INPUT SUBROUTINE 'INPUT' READS IN THE CRYSTAL
C     MASS - TIME DATA FROM A SERIES OF CRYSTALLISATION
C     EXPERIMENTS. INITIAL SOLUTE MASS [CO], MOLECULAR WEIGHT
C     OF THE SOLUTE [WM] AND SYSTEM VOLUME [V(I)], ARE ALSO
C     INPUT TO FACILITATE SUBSEQUENT EXTENSION OF THE
C     PROGRAM IF NECESSARY, BUT ARE NOT USED IN THE CURRENT
C     VERSION. PROVISION FOR WEIGHTING THE DATA IS AVAILABLE
C     AS WELL
C     ********************************************************
C
      SUBROUTINE INPUT(K,T,P,W,V,KO)
C
```

```
      REAL T(K), P(K), W(K), V(K), A, WM, CO
C
      INTEGER K, KO, I
C
      READ(11,-) KO
C
      READ(11,-)  CO, WM
C
      DO 80 I = 1, K
      IF(KO.GT.0) READ(11,-) T(I), A, V(I), W(I)
C
      IF(KO.LT.1) READ(11,-) T(I), A, V(I)
      IF(KO.LT.1) W(I)=1.0
C
      P(I)=A
C
   80 CONTINUE
C
      RETURN
C
      END
C
C
C
C     THE DATA SORTING SUBROUTINE 'SORT' CARRIES OUT A BUBBLE
C     SORT ON THE CRYSTAL MASS - TIME DATA TO ARRANGE IT IN
C     INCREASING ORDER OF TIME
C     ********************************************************
C
      SUBROUTINE SORT(N,T,P,W,V,KO)
C
      REAL T(N), P(N), W(N), V(N), A
C
      INTEGER N,    KO, ITOP, ILOW
C
      ITOP=N
   20 ILOW=1
C
   40 IF(.NOT.T(ILOW).GT.T(ILOW+1))  GO  TO  60
C
      A=T(ILOW+1)
      T(ILOW+1)=T(ILOW)
      T(ILOW)=A
C
      A=P(ILOW+1)
      P(ILOW+1)=P(ILOW)
      P(ILOW)=A
C
      A=V(ILOW+1)
      V(ILOW+1)=V(ILOW)
      V(ILOW)=A
C
      IF(.NOT.KO.GT.0)  GO  TO  60
C
      A=W(ILOW+1)
      W(ILOW+1)=W(ILOW)
      W(ILOW)=A
C
```

```
   60 ILOW=ILOW+1
C
      IF(.NOT.ILOW.EQ.ITOP)  GO  TO  40
C
      ITOP=ITOP-1
C
      IF(.NOT.ITOP.EQ.1)  GO  TO  20
C
      RETURN
C
      END
C
C
C
C     END OF PROGRAM
C     **************
```

APPENDIX 15

LISTING OF COMPUTER PROGRAM 'PHFIT'

The computer program written to fit an empirical curve to sets of experimental pH-time data, using a comprehensive quasi-Newton non-linear optimisation algorithm (267) provided by the routine E04KBF from the NAG library (301), is listed in this appendix. The program is called PHFIT and was written in a version of Fortran IV suitable for a Harris 500 computer. The listing includes comment statements which describe the function of each program segment.

```
C*****************************************************************
C     PROGRAM  TO  FIT  AN  EMPIRICAL  CURVE  TO  THE  CHANGE   **
C     IN  PH  WITH  TIME                                          **
C*****************************************************************
C
C
C     MAIN  SEGMENT
C     *************
C
C
C     TYPE SPECIFICATION AND COMMON STATEMENTS
C
      REAL T(600), P(600),   W(600)
      REAL X(6), DX(6), BL(6), BU(6), S(6)
      REAL XTOL, FEST, ET
C
C
      INTEGER I, N, KO, IB
      INTEGER NFIT, IFAIL, IPR
      INTEGER ITX(10), ITY(10)
C
C
      COMMON // T, P, W, N, S
C
C
C     INPUT AXIS LABELS FOR GRAPH OF RESULTS
C
      READ(11,10) (ITX(I), I = 1, 10)
   10 FORMAT(10A3)
C
      READ(11,10) (ITY(I), I = 1, 10)
C
C     INPUT VALUES OF CONTROL VARIABLES FOR DATA INPUT,
C     FOR GRAPHICAL OUTPUT AND FOR THE OPTIMISATION
C     ROUTINE, AS WELL AS INITIAL VALUES OF THE FITTING
C     PARAMETERS
C     ************************************************
C
      READ(11,-) N, NFIT, IPR, SCA
C
      READ(11,-) (X(I), I = 1, NFIT)
C
      READ(11,-) XTOL, FEST, ET, IB
C
C     CALL MAIN DATA INPUT SUBROUTINE
C
      CALL INPUT(N,T(1),P(1),W(1),KO)
C
C     CALL SUBROUTINE TO SORT OUT INPUT DATA
C
      CALL SORT(N,T(1),P(1),W(1),KO)
C
C     CALL SUBROUTINE TO CARRY OUT OPTIMISATION
C
      CALL FIT(NFIT,X(1),DX(1),BL(1),BU(1),IFAIL,XTOL,
     1         FEST,IPR,ET,IB)
C
C     CALL SUBROUTINE TO PRINT OUT NUMERICAL RESULTS
```

```
C
      CALL OUTPUT(N,T(1),P(1),W(1),NFIT,X(1))
C
C     CALL GRAPHICAL OUTPUT SUBROUTINE
C
      CALL PLOT(N,T(1),P(1),X(1),NFIT,SCA,ITX,ITY)
C
      STOP
C
      END
C
C
C
C     THE DATA INPUT SUBROUTINE 'INPUT' READS IN SETS OF
C     PH - TIME DATA FROM A SERIES OF CRYSTALLISATION
C     EXPERIMENTS. THE TIME VALUES FED IN ARE RAW DATA,
C     WHICH ARE THEN TRANSFORMED WITH RESPECT TO THE
C     NUCLEATION TIMES, WHICH ARE ALSO READ IN, AND
C     CONVERTED TO CONSISTENT UNITS. PROVISION FOR
C     WEIGHTING THE DATA IS ALSO AVAILABLE AS AN OPTION
C     ************************************************
C
      SUBROUTINE INPUT(K,T,P,W,KO)
C
      REAL T(K), P(K), W(K), A, B, Q(2,40), FAC
C
      INTEGER K, KO, I, KNUC, NSET, IFAC, IS, J
C
      READ(11,-) KO, KNUC, NSET
C
      READ(11,-) (Q(1,J), J = 1, NSET)
C
      READ(11,-) (Q(2,J), J = 1, NSET)
C
      DO 80 I = 1, K
      IF(KO.GT.0) READ(11,-) A, B, P(I), W(I)
C
      IF(KO.LT.1) READ(11,-) A, B, P(I)
      IF(KO.LT.1) W(I)=1.0
C
      T(I)=(A*60.0)+B
C
      IF(.NOT.KNUC.GT.0)  GO  TO  80
C
      IS = 0
      IFAC = 0
C
      DO 70 J = 1, NSET
C
      IS=IS+INT(Q(1,J)+0.5)
C
      IFAC = IS - I
C
      IF(IFAC.GE.0)  FAC=60.0*Q(2,J)
      IF(IFAC.GE.0)  GO  TO  75
C
   70 CONTINUE
C
```

```
   75 T(I)=T(I)-FAC
C
   80 CONTINUE
C
      RETURN
C
      END
C
C
C
C     THE DATA SORTING SUBROUTINE 'SORT' CARRIES OUT A
C     BUBBLE SORT ON THE PH - TIME DATA SETS, TO
C     ARRANGE ALL THE DATA IN INCREASING ORDER OF TIME
C     ************************************************
C
      SUBROUTINE SORT(N,T,P,W,KO)
C
      REAL T(N), P(N), W(N), A
C
      INTEGER N,    KO, ITOP, ILOW
C
      ITOP=N
   20 ILOW=1
C
   40 IF(.NOT.T(ILOW).GT.T(ILOW+1))  GO  TO  60
C
      A=T(ILOW+1)
      T(ILOW+1)=T(ILOW)
      T(ILOW)=A
C
      A=P(ILOW+1)
      P(ILOW+1)=P(ILOW)
      P(ILOW)=A
C
      IF(.NOT.KO.GT.0)  GO  TO  60
C
      A=W(ILOW+1)
      W(ILOW+1)=W(ILOW)
      W(ILOW)=A
C
   60 ILOW=ILOW+1
C
      IF(.NOT.ILOW.EQ.ITOP)  GO  TO  40
C
      ITOP=ITOP-1
C
      IF(.NOT.ITOP.EQ.1)  GO  TO  20
C
      RETURN
C
      END
C
C
C
C     THE OPTIMISATION SUBROUTINE 'FIT' CALLS THE NAG LIBRARY
C     ROUTINE 'E04KBF' TO CARRY OUT THE NONLINEAR OPTIMISATION
C     ********************************************************
C
```

```
      SUBROUTINE FIT(K,X,DX,BL,BU,IFAIL,XT,FE,IP,ET,IB)
C
      REAL X(K), DX(K), BL(K), BU(K), HL(15), HD(6)
      REAL F, W(54), XT, FE, ET
C
      INTEGER IFAIL, K, IS(6), IW(2), IP, IB
C
      LOGICAL LOCSCH
C
      EXTERNAL FUNCT, MONIT, E04LBS
C
      IFAIL=1
C
      LOCSCH=.TRUE.
C
      CALL E04KBF(K,FUNCT,MONIT,IP,LOCSCH,0,E04LBS,3000,ET,XT,
     1            1.0E05,FE, IB,BL,BU,X,HL,15,HD,IS,F,DX,IW,2,
     2            W,54,IFAIL)
C
      WRITE(16,40) IFAIL
   40 FORMAT(1H ,/,132(1H*),/,30X,8HIFAIL = ,I3,/,132(1H*))
C
      RETURN
C
      END
C
C
C
C     THE SUBROUTINE 'OUTPUT' PRINTS OUT THE MAIN NUMERICAL
C     RESULTS FROM THE EMPIRICAL FITTING PROCESS
C     ******************************************************
C
      SUBROUTINE OUTPUT(N,T,P,W,NFIT,X)
C
      REAL T(N), P(N), W(N), X(N), CN, Y, RS
C
      INTEGER N,   I
C
      WRITE(16,20)
   20 FORMAT(1H ,//,10X,30HVALUES OF INDEPENDENT VARIABLE,10X,
     128HVALUES OF DEPENDENT VARIABLE,12X,14HRESIDUAL ERROR,6X,
     29HWEIGHTING,/,21X,8HTIME (S),21X,12HEXPERIMENTAL,10X,6HFITTED,/)
C
      DO 60 I = 1, N
C
      IFAIL=0
C
      CN=((T(I)/T(N))-X(2))/X(3)
C
      Y=((P(N)-X(1)-X(4))*S15ABF(CN,IFAIL))+X(1)+(X(4)*T(I)/T(N))
C
      RS=P(I)-Y
C
      WRITE(16,40)  T(I), P(I), Y, RS, W(I)
   40 FORMAT(18X,F8.1,25X,F7.3,11X,F9.6,11X,E13.6,6X,F6.2)
C
   60 CONTINUE
C
```

```
      WRITE(16,80)
   80 FORMAT(1H ,//,132(1H*))
C
      RETURN
C
      END
C
C
C
C     THE GRAPHICAL OUTPUT SUBROUTINE 'PLOT' USES THE ROUTINES
C     OF THE GINO GRAPH PLOTTING PACKAGE TO PRODUCE A GRAPH
C     SHOWING THE EXPERIMENTAL DATA AND THE FITTED EMPIRICAL
C     CURVE. THE PLOT CAN BE SCALED TO ANY SIZE BY CHANGING
C     THE SCALE FACTOR, INPUT AS DATA IN THE MAIN SEGMENT.
C     COMPILATION OPTION 1 PERMITS DISPLAY OF THE GRAPH ON A
C     T4010 GRAPHICS TERMINAL; OPTION 2 GIVES A HARDCOPY OF
C     THE PLOT; AND, OPTION 3 ALLOWS DISPLAY OF THE GRAPH ON
C     AN IMLAC DYNAGRAPHICS TERMINAL
C     ********************************************************
C
      SUBROUTINE PLOT(N,T,P,F,NFIT,SCA,ITX,ITY)
C
      REAL T(N), P(N), F(NFIT), SCA, XLT, XST, YST, X, Y, CN
C
      INTEGER N, IFAIL, NL1, NL2, I, ITX(10), ITY(10)
      INTEGER NFIT
C
C
:SKFZ 1
      CALL T4010
:ESKP
C
:SKFZ 2
      CALL OPEN
:ESKP
C
:SKFZ 3
      CALL APDS4
:ESKP
C
C
      CALL ERRMAX(50)
C
      CALL SHIFT2(10.0,10.0)
C
      CALL CHASWI(1)
C
      CALL SCALE(SCA)
C
      CALL CHASIZ(1.5,2.5)
C
      CALL MOVTO2(0.0,0.0)
C
      CALL LINTO2(0.0,210.5)
      CALL LINTO2(297.5,210.5)
      CALL LINTO2(297.5,0.0)
      CALL LINTO2(0.0,0.0)
C
```

```
      CALL SHIFT2(42.0,35.0)
C
      CALL AXIPOS(0,0.0,0.0,110.0,2)
      CALL AXISCA(3,7,0.0,7.0,2)
      CALL AXIDRA(2,-1,2)
C
      XLT=1000.0*(AINT((T(N)/1000.0)+1.0))
C
      CALL AXIPOS(0,0.0,0.0,220.0,1)
      CALL AXISCA(3,10,0.0,XLT,1)
      CALL AXIDRA(-2,1,1)
C
      IFAIL=0
C
      CN=((T(1)/T(N))-F(2))/F(3)
C
      YST=((P(N)-F(1)-F(4))*S15ABF(CN,IFAIL))+F(1)+(F(4)*T(1)/T(N))
C
      YST=110.0*YST/7.0
C
      XST=220.0*T(1)/XLT
C
      CALL MOVTO2(XST,YST)
C
      NL1=INT(T(1))+1
      NL2=INT(T(N))
C
      DO 40 I = NL1, NL2
C
      X=FLOAT(I)
      IFAIL=0
C
      CN=((X/T(N))-F(2))/F(3)
C
      Y=((P(N)-F(1)-F(4))*S15ABF(CN,IFAIL))+F(1)+(F(4)*X/T(N))
C
      X=220.0*X/XLT
      Y=110.0*Y/7.0
C
      CALL LINTO2(X,Y)
C
   40 CONTINUE
C
      CALL GRASYM(T,P,N,5,0)
C
      CALL CHASIZ(3.0,5.0)
C
      CALL MOVTO2(50.0,-20.0)
C
      CALL CHAARR(ITX,10,3)
C
      CALL MOVTO2(-15.0,25.0)
C
      CALL CHAANG(90.0)
C
      CALL CHAARR(ITY,10,3)
C
      CALL CHAANG(0.0)
```

```
C
      CALL DEVEND
C
      RETURN
C
      END
C
C
C
C     THE SUBROUTINE 'FUNCT' IS CALLED BY THE OPTIMISATION
C     ROUTINE 'E04KBF', TO PROVIDE THE FUNCTION TO BE
C     MINIMISED AND THE DERIVATIVES OF THAT FUNCTION WITH
C     RESPECT TO THE PARAMETERS FOR OPTIMISATION. THE
C     FUNCTION USED HERE IS A LEAST SQUARES OBJECTIVE
C     FUNCTION, WITH THE MODEL FOR PH BEING AN EMPIRICAL
C     COMBINATION OF A STRAIGHT LINE AND A CUMULATIVE
C     NORMAL DISTRIBUTION, BOTH EXPRESSED AS FUNCTIONS OF
C     TIME
C     ******************************************************
C
      SUBROUTINE FUNCT(IFLAG,N,XC,FC,GC,IW,LIW,WX,LW)
C
      REAL T(600), P(600), W(600)
      REAL XC(N),   GC(N), WX(LW), SUM, CN, Y, FC
      REAL S(6), SX, A, B, C, D
C
      INTEGER IFLAG, N, IW(LIW), LIW, LW
      INTEGER I, K, IFAIL
C
      COMMON // T, P, W, K, S
C
      SUM=0.0
C
      DO 20 I = 1, N
      S(I)=0.0
   20 CONTINUE
C
      DO 40 I = 1, K
C
      IFAIL = 0
C
      CN=((T(I)/T(K))-XC(2))/XC(3)
C
      Y=((P(K)-XC(1)-XC(4))*S15ABF(CN,IFAIL))+XC(1)+(XC(4)*T(I)/T(K))
C
      SUM=SUM+((W(I)*(P(I)-Y))**2.0)
C
      SX=2.0*(W(I)**2.0)*(Y-P(I))
C
      A=1.0-S15ABF(CN,IFAIL)
C
      S(1)=S(1)+(SX*A)
C
      B=(P(K)-XC(1)-XC(4))*(EXP(-0.5*(CN**2.0)))/
     1  (2.0*((ASIN(1.0))**0.5))
C
      C=-1.0/XC(3)
C
```

```
      D=(XC(2)-(T(I)/T(K)))/(XC(3)**2.0)
C
      S(2)=S(2)+(SX*B*C)
C
      S(3)=S(3)+(SX*B*D)
C
      S(4)=S(4)+(SX*((T(I)/T(K))-S15ABF(CN,IFAIL)))
C
   40 CONTINUE
C
      FC=SUM
C
      DO 60 I = 1, N
C
      GC(I)=S(I)
C
   60 CONTINUE
C
      RETURN
C
      END
C
C
C
C     THE SUBROUTINE 'MONIT' IS CALLED BY THE OPTIMISATION ROUTINE
C     'E04KBF', TO PROVIDE MONITORING OF THE COURSE OF OPTIMISATION.
C     VALUES OF MODEL PARAMETERS, THEIR GRADIENTS AND THE OBJECTIVE
C     FUNCTION, AS WELL AS THE NUMBER OF ITERATIONS AND FUNCTION
C     EVALUATIONS, AND THE STATUS OF THE PARAMETERS, ARE PRINTED OUT
C     AT INTERVALS DETERMINED BY THE PRINT FACTOR, WHICH IS INPUT
C     AS DATA IN THE MAIN SEGMENT, AND ALSO AT THE END OF THE
C     OPTIMISATION
C     ****************************************************************
C
      SUBROUTINE MONIT(N,XC,FC,GC,IS,GPJ,CON,POS,NIT,NF,IW,LIW,W,LW)
C
      REAL XC(N), FC, GC(N), GPJ, CON, W(LW)
C
      INTEGER N, IS(N), NIT, NF, IW(LIW), LIW, LW, J, ISJ
C
      LOGICAL POS
C
      WRITE(16,20)  NIT, NF, FC, GPJ
   20 FORMAT(1H ,/,12X,4HITNS,5X,8HFN EVALS,13X,8HFN VALUE,13X,
     121HNORM OF PROJ GRADIENT,/,10X,I4,6X,I5,2(6X,1PE20.4))
C
      WRITE(16,40)
   40 FORMAT(1H ,/,12X,1HJ,14X,4HX(J),17X,4HG(J),7X,6HSTATUS)
C
      DO 400 J = 1, N
C
      ISJ=IS(J)
C
      IF(ISJ.GT.0)  GO  TO  60
C
      ISJ=-ISJ
C
      GO  TO  (100,140,180),  ISJ
```

```
C
   60 WRITE(16,80) J, XC(J), GC(J)
   80 FORMAT(11X,I2,1X,1P2E20.4,5X,4HFREE)
C
      GO  TO  400
C
  100 WRITE(16,120) J, XC(J), GC(J)
  120 FORMAT(11X,I2,1X,1P2E20.4,5X,11HUPPER BOUND)
C
      GO  TO  400
C
  140 WRITE(16,160) J, XC(J), GC(J)
  160 FORMAT(11X,I2,1X,1P2E20.4,5X,11HLOWER BOUND)
C
      GO  TO  400
C
  180 WRITE(16,200) J, XC(J), GC(J)
  200 FORMAT(11X,I2,1X,1P2E20.4,5X,8HCONSTANT)
C
  400 CONTINUE
C
      WRITE(16,420) CON
  420 FORMAT(11X,50HESTIMATED CONDITION NUMBER OF PROJECTED HESSIAN = ,
     11PE10.2)
C
      RETURN
C
      END
C
C
C
C     END OF PROGRAM
C     **************
```

APPENDIX 16

LISTING OF COMPUTER PROGRAM 'TOTE'

The computer program written to fit sets of experimental batch crystallisation data to the empirical power law type models presented in Chapter 9 is listed in this appendix. This program uses a comprehensive quasi-Newton non-linear optimisation algorithm (267), provided by the routine E04KBF from the NAG library (301). The program is named TOTE and was written in a version of Fortran IV suitable for a Harris 500 computer. The function of each program segment is detailed by comment statements included in the listing.

```
C*************************************************************************
C     PROGRAM TO FIT AN EMPIRICAL POWER LAW TYPE CURVE TO      **
C     CRYSTAL GROWTH RATE PER UNIT SURFACE AREA                **
C*************************************************************************
C
C
C     MAIN SEGMENT
C     ************
C
C     TYPE SPECIFICATION STATEMENTS
C
      REAL SCA, XTOL, ET, FEST, FSCA, Q1X, FNT
      REAL Z(150), E(150), D(150), Y(150), T(150), TL
      REAL X(10), BL(10), BU(10), H(10), DX(10), U(10)
      REAL P(150), Q(150), RPM(150), TMP(150)
C
      INTEGER I, N, IPLT, NFIT, IPR, IB, ITP
      INTEGER IS(6), ITX(10), ITY(15)
C
C     COMMON BLOCKS
C
      COMMON // Z, D, U, FSCA, Q1X, N, RPM, TMP
      COMMON /BLK1/ H
      COMMON /BLK2/ Q, Y, E, P
C
C     INPUT UPPER LIMIT OF TIME VARIABLE, NUMBER OF DATA POINTS AND
C     FLAG TO CALL GRAPHICAL OUTPUT SUBROUTINE
C
      READ(11,-) TL, N, IPLT
C
C     INPUT CONTROL VARIABLES FOR NONLINEAR OPTIMISATION ROUTINE,
C     SCALE FACTOR FOR OBJECTIVE FUNCTION AND SCALE FACTOR FOR
C     GRAPHICAL OUTPUT
C
      READ(11,-) NFIT, IPR, IB, ITP, SCA, XTOL,
     1           ET, FEST, FSCA, Q1X
C
C     CALL MAIN DATA INPUT SUBROUTINE
C
      CALL DATAIN(N,T(1),Z(1),D(1),E(1),Y(1),BL(1),
     1            BU(1),X(1),H(1),IS(1),NFIT,RPM(1),TMP(1))
C
C     INPUT AXIS LABELS FOR ONE OF THE PLOTS AVAILABLE AS
C     GRAPHICAL OUTPUT
C
      READ(11,20) (ITX(I), I = 1, 10)
   20 FORMAT(10A3)
C
      READ(11,40) (ITY(I), I = 1, 15)
   40 FORMAT(15A3)
C
C     CALL SUBROUTINE TO SORT OUT INPUT DATA
C
      CALL SORT(N,T(1),Z(1),D(1),E(1),Y(1),RPM(1),TMP(1))
C
C     CALL SUBROUTINE TO CARRY OUT OPTIMISATION
C
      CALL FIT(NFIT, IPR, ET, XTOL, IB, BL(1), BU(1), X(1),
```

```
     1         DX(1), FEST, FNT, ITP, IS(1))
C
C     COMPUTE UNSCALED VALUES OF OPTIMISED PARAMETERS
C
      DO 60 I = 1, NFIT
      U(I)=H(I)*X(I)
   60 CONTINUE
C
C     CALL SUBROUTINE TO PRINT OUT NUMERICAL RESULTS
C
      CALL OUTPUT(N,T(1),Z(1),D(1),E(1),Y(1),Q(1))
C
C     DEPENDING ON WHETHER OR NOT THE PLOT FLAG IS SET,
C     CALL SUBROUTINE TO PRODUCE GRAPHICAL OUTPUT
C
      IF(IPLT.GT.0)  CALL PLOT(N,T(1),Y(1),Q(1),SCA,
     1                         ITX,ITY,P(1),E(1),IS(1),NFIT)
C
C     CALL SUBROUTINE TO CALCULATE AND PRINT OUT
C     STATISTICAL PARAMETERS FOR FIT
C
      CALL STAT(N,Y,Q,FNT,FSCA,IS,NFIT)
C
      STOP
C
      END
C
C
C
C     THE DATA INPUT SUBROUTINE 'DATAIN' READS IN EXPERIMENTAL
C     DATA CONSISTING OF TIME, HYDROGEN ION ACTIVITY,CRYSTAL
C     SIZE, DRIVING FORCE,EXPERIMENTAL GROWTH RATE PER UNIT
C     SURFACE AREA, STIRRER SPEED AND TEMPERATURE, IN EACH SET
C     THAT IS READ IN. INITIAL VALUES OF MODEL PARAMETERS, THEIR
C     LOWER AND UPPER LIMITS AND SCALE FACTORS, AS WELL AS
C     VALUES OF FLAGS TO INDICATE THE STATUS OF THE MODEL
C     PARAMETERS ARE ALSO INPUT
C     ************************************************************
C
      SUBROUTINE DATAIN(K,T,Z,D,E,Y,BL,BU,X,H,IS,N,RPM,TMP)
C
      REAL Z(K), T(K), D(K), E(K), Y(K)
      REAL BL(N), BU(N), X(N), H(N), RPM(K), TMP(K)
C
      INTEGER K, N, I, IS(N)
C
      DO 80 I = 1, K
C
      READ(11,-) T(I), Z(I), D(I), E(I), Y(I), RPM(I), TMP(I)
C
      RPM(I)=RPM(I)/500.0
      TMP(I)=TMP(I)+273.0
C
   80 CONTINUE
C
      READ(11,-)  (X(I), I = 1, N)
C
      READ(11,-)  (BL(I), I = 1, N)
```

```
C
      READ(11,-)  (BU(I), I = 1, N)
C
      READ(11,-) (H(I), I = 1, N)
C
      READ(11,-) (IS(I), I = 1, N)
C
      RETURN
C
      END
C
C
C
C     THE DATA SORTING SUBROUTINE 'SORT' CARRIES OUT A BUBBLE
C     SORT ON THE EXPERIMENTAL DATA TO ARRANGE IT IN SETS
C     WHICH ARE ACCORDING TO INCREASING ORDER OF TIME
C     ***********************************************************
C
      SUBROUTINE SORT(N,T,Z,D,E,Y,RPM,TMP)
C
      REAL Z(N), T(N), E(N), D(N), Y(N), B, RPM(N), TMP(N)
C
      INTEGER N, ITOP, ILOW
C
      ITOP=N
C
   20 ILOW=1
C
   40 IF(.NOT.T(ILOW).GT.T(ILOW+1))  GO  TO  60
C
      B=T(ILOW+1)
      T(ILOW+1)=T(ILOW)
      T(ILOW)=B
C
      B=Y(ILOW+1)
      Y(ILOW+1)=Y(ILOW)
      Y(ILOW)=B
C
      B=D(ILOW+1)
      D(ILOW+1)=D(ILOW)
      D(ILOW)=B
C
      B=Z(ILOW+1)
      Z(ILOW+1)=Z(ILOW)
      Z(ILOW)=B
C
      B=E(ILOW+1)
      E(ILOW+1)=E(ILOW)
      E(ILOW)=B
C
      B=RPM(ILOW+1)
      RPM(ILOW+1)=RPM(ILOW)
      RPM(ILOW)=B
C
      B=TMP(ILOW+1)
      TMP(ILOW+1)=TMP(ILOW)
      TMP(ILOW)=B
C
```

```
   60 ILOW=ILOW+1
C
      IF(.NOT.ILOW.EQ.ITOP)  GO  TO  40
C
      ITOP=ITOP-1
C
      IF(.NOT.ITOP.EQ.1)  GO  TO  20
C
      RETURN
C
      END
C
C
C
C     THE OPTIMISATION SUBROUTINE 'FIT' CALLS THE NAG LIBRARY
C     ROUTINE 'E04KBF' TO CARRY OUT TNE NONLINEAR OPTIMISATION
C     ********************************************************
C
      SUBROUTINE FIT(K,IP,ET,XT,IB,BL,BU,X,DX,FEST,F,ITP,IS)
C
      REAL ET, XT, W(90), BL(K), BU(K), X(K), DX(K)
      REAL  FEST, F, HL(45), HD(10)
C
      INTEGER K, IP, IB, IW(2), IS(K), ITP, IFAIL, LH, LW
C
      LOGICAL LAM
C
      EXTERNAL E04LBS, FUNCT2, MONIT
C
      IF(ITP.EQ.0)  GO  TO  30
C
      IFAIL=0
C
      CALL FUNCT2(IFAIL,K,X,F,DX,IW,2,W,90)
C
      LH=K*(K-1)/2
      LW=9*K
C
      DO 10 I = 1, LH
C
      HL(I)=0.0
C
   10 CONTINUE
C
      DO 20 I = 1, K
C
      HD(I)=1.0
C
   20 CONTINUE
C
   30 IFAIL=1
C
      LAM=.TRUE.
C
      CALL E04KBF(K,FUNCT2,MONIT,IP,LAM,ITP,E04LBS,3000,ET,
     1            XT,1.0E05,FEST,IB,BL,BU,X,HL(1),LH,HD(1),IS,F,
     2            DX,IW,2,W(1),LW,IFAIL)
C
```

```
      WRITE(100,40) IFAIL
   40 FORMAT(1H ,/,132(1H*),/,35X,8HIFAIL = ,I3,/,132(1H*))
C
      IFAIL=0
C
      CALL FUNCT2(IFAIL,K,X,F,DX,IW,2,W,54)
C
      RETURN
C
      END
C
C
C
C     THE SUBROUTINE 'MONIT' IS CALLED BY THE OPTIMISATION ROUTINE
C     'E04KBF' TO PROVIDE MONITORING OF THE COURSE OF OPTIMISATION.
C     VALUES OF MODEL PARAMETERS, THEIR GRADIENTS AND THE OBJECTIVE
C     FUNCTION, AS WELL AS THE NUMBER OF ITERATIONS AND FUNCTION
C     EVALUATIONS AND THE STATUS OF EACH PARAMETER ARE PRINTED OUT
C     AT INTERVALS DETERMINED BY THE PRINT FACTOR, INPUT AS DATA IN
C     THE MAIN SEGMENT, AND ALSO AT THE END OF THE OPTIMISATION
C     ************************************************************
C
      SUBROUTINE MONIT(N,XC,FC,GC,IS,GPJ,CON,POS,NIT,NF,IW,LIW,W,LW)
C
      REAL XC(N), FC, GC(N), GPJ, CON, W(LW), H(10)
C
      INTEGER N, IS(N), NIT, NF, IW(LIW), LIW, LW, J, ISJ
C
      COMMON /BLK1/ H
C
      LOGICAL POS
C
      WRITE(100,20) NIT, NF, FC, GPJ
   20 FORMAT(1H ,/,12X,4HITNS,5X,8HFN EVALS,13X,8HFN VALUE,13X,
     121HNORM OF PROJ GRADIENT,/,10X,I4,6X,I5,2(6X,1PE20.4))
C
      WRITE(100,40)
   40 FORMAT(1H ,/,12X,1HJ,14X,4HX(J),17X,4HG(J),7X,6HSTATUS,
     1       7X,12HSCALE FACTOR)
C
      DO 400 J = 1, N
C
      ISJ=IS(J)
C
      IF(ISJ.GT.0)  GO  TO  60
C
      ISJ=-ISJ
C
      GO  TO  (100,140,180), ISJ
C
   60 WRITE(100,80) J, XC(J), GC(J), H(J)
   80 FORMAT(11X,I2,1X,1P2E20.5,5X,4HFREE,7X,1PE12.2)
C
      GO  TO  400
C
  100 WRITE(100,120) J, XC(J), GC(J), H(J)
  120 FORMAT(11X,I2,1X,1P2E20.5,5X,11HUPPER BOUND,1PE12.2)
C
```

```
      GO  TO  400
C
  140 WRITE(100,160) J, XC(J), GC(J), H(J)
  160 FORMAT(11X,I2,1X,1P2E20.5,5X,11HLOWER BOUND,1PE12.2)
C
      GO  TO  400
C
  180 WRITE(100,200) J, XC(J), GC(J), H(J)
  200 FORMAT(11X,I2,1X,1P2E20.5,5X,8HCONSTANT,3X,1PE12.2)
C
  400 CONTINUE
C
      WRITE(100,420)  CON
  420 FORMAT(11X,50HESTIMATED CONDITION NUMBER OF PROJECTED HESSIAN = ,
     11PE10.2)
C
      RETURN
C
      END
C
C
C
C     THE SUBROUTINE 'FUNCT2' IS CALLED BY THE OPTIMISATION ROUTINE
C     'E04KBF' TO PROVIDE THE FUNCTION TO BE MINIMISED AND THE
C     DERIVATIVES OF THAT FUNCTION WITH RESPECT TO EACH MODEL
C     PARAMETER. A LEAST SQUARES OBJECTIVE FUNCTION WITH PROVISION
C     FOR SCALING THE FUNCTION AND THE PARAMETERS WAS USED WITH A
C     POWER LAW TYPE MODEL FOR CRYSTAL GROWTH RATE PER UNIT
C     SURFACE AREA. THE VARIABLES INCLUDED IN THE POWER LAW MODEL
C     DEPENDED ON THE COMPILATION OPTION CHOSEN. WITH OPTION 6,
C     CRYSTAL SIZE, HYDROGEN ION ACTIVITY AND DRIVING FORCE ARE
C     INCLUDED. STIRRER SPEED IS ADDED TO THESE WHEN OPTION 7 IS
C     USED, AND WITH OPTION 8, TEMPERATURE IS TAKEN INTO ACCOUNT
C     AS WELL
C     ****************************************************************
C
      SUBROUTINE FUNCT2(IFLAG,N,XC,FC,GC,IW,LIW,WX,LW)
C
      REAL XC(N), GC(N), FC, Z(150), S(10), Q(150), Y(150)
      REAL SUM, H(10), U(10), WX(LW), FSCA, Q1X, SDF, SX, RPM(150)
      REAL DR1, DR2, DR3, DR4, XG, E(150), P(150), D(150), TMP(150)
:SKFZ 7, 8
      REAL DR5
:ESKP
C
:SKFZ 8
      REAL DR6
:ESKP
C
      INTEGER I, K, IFLAG, IW(LIW), LW, LIW
C
      COMMON // Z, D, U, FSCA, Q1X, K, RPM, TMP
      COMMON /BLK1/ H
      COMMON /BLK2/ Q, Y, E, P
C
      SUM=0.0
      DO 50 I = 1, N
      S(I)=0.0
```

```
      U(I)=XC(I)*H(I)
   50 CONTINUE
C
      DO 200 I = 1, K
C
      SDF=E(I)
C
:SKFZ 6
      XG=U(1)*(Z(I)**U(2))*(D(I)**U(3))*(SDF**U(4))
:ESKP
C
:SKFZ 7
      XG=U(1)*(Z(I)**U(2))*(D(I)**U(3))*(SDF**U(4))*
     1   (RPM(I)**U(5))
:ESKP
C
:SKFZ 8
      XG=U(1)*(Z(I)**U(2))*(D(I)**U(3))*(SDF**U(4))*
     1   (RPM(I)**U(5))*(EXP(-U(6)/TMP(I)))
:ESKP
C
      Q(I)=XG
C
      P(I)=(Y(I)*(SDF**U(4))/Q(I))**(1.0/U(4))
C
      SUM=SUM+((FSCA*(Q(I)-Y(I)))**2.0)
      SX=2.0*(FSCA**2.0)*(Q(I)-Y(I))
C
      DR1=XG/U(1)
      DR2=XG*(ALOG(Z(I)))
      DR3=XG*(ALOG(D(I)))
C
      DR4=XG*(ALOG(SDF))
C
:SKFZ 7, 8
      DR5=XG*(ALOG(RPM(I)))
:ESKP
C
:SKFZ 8
      DR6=-1.0*XG*U(6)/TMP(I)
:ESKP
C
      S(1)=S(1)+(SX*DR1*H(1))
      S(2)=S(2)+(SX*DR2*H(2))
      S(3)=S(3)+(SX*DR3*H(3))
      S(4)=S(4)+(SX*DR4*H(4))
C
:SKFZ 7, 8
      S(5)=S(5)+(SX*DR5*H(5))
:ESKP
C
:SKFZ 8
      S(6)=S(6)+(SX*DR6*H(6))
:ESKP
C
  200 CONTINUE
C
      FC=SUM
```

```
C
      DO 250 I = 1, N
      GC(I)=S(I)
  250 CONTINUE
C
      RETURN
C
      END
C
C
C
C     THE SUBROUTINE 'OUTPUT' PRINTS OUT THE MAIN NUMERICAL
C     RESULTS FROM THE EMPIRICAL FITTING PROCESS
C     ******************************************************
C
      SUBROUTINE OUTPUT(K,T,Z,D,E,Y,Q)
C
      REAL T(K), Z(K), E(K), D(K), Y(K), Q(K), R
C
      INTEGER I, K
C
      WRITE(100,10)
   10 FORMAT(1H ,///)
C
      WRITE(100,20)
   20 FORMAT(5X,8HTIME (S),8X,2HAH,8X,14HMASS MEAN SIZE,5X,
     1       13HDRIVING FORCE,22X,11HGROWTH RATE,/,71X,
     2       12HEXPERIMENTAL,5X,10HCALCULATED,7X,8HRESIDUAL,//)
C
      DO 200 I = 1, K
C
      R=Q(I)-Y(I)
C
      WRITE(100,100) T(I), Z(I), D(I), E(I), Y(I), Q(I), R
  100 FORMAT(4X,F8.1,3X,1PE12.5,4X,1PE12.5,7X,1PE12.5,8X,1PE12.5,
     1       4X,1PE12.5,4X,1PE12.5)
C
  200 CONTINUE
C
      WRITE(100,300)
  300 FORMAT(1H ,//,132(1H*))
C
      RETURN
C
      END
C
C
C
C     THE GRAPHICAL OUTPUT SUBROUTINE 'PLOT' USES THE ROUTINES OF
C     THE GINO GRAPH PLOTTING PACKAGE TO PRODUCE GRAPHS SHOWING
C     THE RESULTS OF THE OPTIMISATION. THE PLOT CAN BE SCALED TO
C     ANY SIZE BY CHANGING THE SCALE FACTOR, INPUT AS DATA IN
C     THE MAIN SEGMENT. COMPILATION OPTIONS 1, 2 AND 3 PERMIT
C     DISPLAY OF THE GRAPH ON A T4010 GRAPHICS TERMINAL, PLOTTING
C     A HARDCOPY OF THE GRAPH AND DISPLAY OF THE GRAPH ON AN
C     IMLAC DYNAGRAPHICS TERMINAL, RESPECTIVELY.COMPILATION
C     OPTION 21 GIVES A POINT PLOT OF EXPERIMENTAL AND CALCULATED
C     CRYSTAL GROWTH RATES PER UNIT SURFACE AREA WITH TIME.
```

```
C     OPTION 22 GIVES A LOG-LOG PLOT OF THE FITTED MODEL AGAINST
C     DRIVING FORCE, AND A LINEAR VERSION OF THIS GRAPH IS
C     OBTAINED IN ADDITION, WHEN THE HARDCOPY OPTION IS SET
C     CONCURRENTLY
C     ************************************************************
C
      SUBROUTINE PLOT(K,T,Y,Q,SCA,ITX,ITY,P,E,IS,N)
C
      REAL T(K), Y(K), Q(50), SCA, YD, YT, P(50), E(50)
:SKFZ 21
      REAL XLT, XST, YST
:ESKP
C
:SKFZ 22
      REAL AU, AL
:ESKP
C
      INTEGER ITX(10), ITY(15), K, IYL, IYU, IYD, ISC
      INTEGER N, IS(N)
C
:SKFZ 1
      CALL T4010
:ESKP
C
:SKFZ 2
      CALL OPEN
:ESKP
C
:SKFZ 3
      CALL APDS4
:ESKP
C
      CALL ERRMAX(100)
      CALL DEVPAP(3000.0,350.0,0)
      CALL SHIFT2(10.0,10.0)
      CALL CHASWI(1)
      CALL SCALE(SCA)
C
:SKFZ 21
C
      CALL CHASIZ(1.5,2.5)
      CALL MOVTO2(0.0,0.0)
C
      CALL LINTO2(0.0,210.5)
      CALL LINTO2(297.5,210.5)
      CALL LINTO2(297.5,0.0)
      CALL LINTO2(0.0,0.0)
C
      CALL SHIFT2(48.0,35.0)
C
      XST=0.0
      YST=1.0E25
C
      DO 20 I = 1, K
      XST=AMAX1(XST,Q(I))
      YST=AMIN1(YST,Q(I))
   20 CONTINUE
C
```

```
      DO 40 I = 1, K
      XST=AMAX1(XST,Y(I))
      YST=AMIN1(YST,Y(I))
   40 CONTINUE
C
      CALL AXIPOS(1,0.0,0.0,110.0,2)
      CALL AXISCA(4,0,YST,XST,2)
      CALL AXIDRA(2,0,2)
C
      XLT=100.0*(AINT((T(K)/100.0)+1.0))
C
      CALL AXIPOS(1,0.0,0.0,220.0,1)
      CALL AXISCA(3,10,0.0,XLT,1)
      CALL AXIDRA(-2,1,1)
C
      IYL=INT((ALOG10(YST))-1.0)
      IYU=INT((ALOG10(XST)))
      IYD=IYU-IYL
      YD=110.0/FLOAT(IYD)
      IYD=IYD+1
C
      DO 70 I = 1, IYD
      YT=(YD*FLOAT(I-1))-1.0
      CALL MOVTO2(-9.0,YT)
      CALL CHAHOL(4H10*.)
      CALL MOVBY2(0.0,2.5)
      ISC=IYL+I-1
      CALL CHAINT(ISC,3)
      CALL MOVBY2(-7.5,-2.5)
   70 CONTINUE
C
      CALL GRASYM(T,Y,K,5,0)
C
      CALL GRASYM(T,Q,K,8,0)
C
      CALL CHASIZ(3.0,5.0)
C
      CALL MOVTO2(50.0,-20.0)
      CALL CHAARR(ITX,10,3)
C
      CALL MOVTO2(-10.5,8.0)
      CALL CHAANG(90.0)
      CALL CHAARR(ITY,15,3)
C
      CALL CHAANG(0.0)
C
      CALL SHIFT2(300.0,-35.0)
C
:ESKP
C
:SKFZ 22
C
      AU=0.0
      AL=1.0E25
C
      DO 120 I = 1, K
      AU=AMAX1(AU,P(I))
      AL=AMIN1(AL,P(I))
```

```
  120 CONTINUE
C
      DO 140 I = 1, K
      AU=AMAX1(AU,E(I))
      AL=AMIN1(AL,E(I))
  140 CONTINUE
C
      CALL CHASIZ(1.5,2.5)
C
      CALL MOVTO2(0.0,0.0)
C
      CALL LINTO2(0.0,210.5)
      CALL LINTO2(297.5,210.5)
      CALL LINTO2(297.5,0.0)
      CALL LINTO2(0.0,0.0)
C
      CALL SHIFT2(103.0,35.0)
C
      CALL AXIPOS(1,0.0,0.0,110.0,2)
      CALL AXISCA(4,0,AL,AU,2)
      CALL AXIDRA(2,0,2)
C
      CALL AXIPOS(1,0.0,0.0,110.0,1)
      CALL AXISCA(4,0,AL,AU,1)
      CALL AXIDRA(-2,0,1)
C
      CALL GRID(0,0,0)
C
      CALL MOVTO2(0.0,0.0)
      CALL LINTO2(110.0,110.0)
C
      CALL GRASYM(E,P,K,5,0)
C
      CALL CHASIZ(3.0,5.0)
C
      CALL MOVTO2(52.0,-17.5)
      CALL SYMBOL(1)
      CALL MOVBY2(3.0,-2.5)
      CALL CHAHOL(5H*UC*.)
      CALL CHASIZ(1.5,2.5)
      CALL MOVBY2(1.0,-2.5)
      CALL CHAHOL(5H*LT*.)
      CALL CHASIZ(3.0,5.0)
C
      CALL MOVTO2(-22.0,20.0)
      CALL CHAANG(90.0)
C
      CALL CHAHOL(13H*U[(R  /*LK*.)
      CALL MOVTO2(-20.0,30.0)
      CALL CHASIZ(1.5,2.5)
      CALL CHAHOL(5H*UG*.)
      CALL MOVTO2(-20.0,41.5)
      CALL CHAHOL(5H*U1*.)
      CALL MOVTO2(-22.0,43.0)
      CALL CHASIZ(3.0,5.0)
      CALL CHAHOL(5H*U)*.)
C
      IF(IS(2).EQ.-3)  GO  TO  160
```

```
C
      CALL CHAHOL(13H*U(*LA  *U)*.)
      CALL MOVTO2(-20.0,53.0)
      CALL CHASIZ(1.5,2.5)
      CALL CHAHOL(5H*UH*.)
      CALL MOVBY2(-2.0,0.5)
      CALL CHAHOL(5H*U+*.)
      CALL MOVTO2(-27.0,62.5)
      CALL CHAHOL(8H*U-*LK*.)
      CALL MOVBY2(2.0,0.5)
      CALL CHAHOL(5H*U2*.)
      CALL MOVTO2(-22.0,67.5)
C
  160 IF(IS(3).EQ.-3)  GO  TO  180
C
      CALL CHASIZ(3.0,5.0)
      CALL CHAHOL(7H*U(L)*.)
      CALL MOVBY2(-5.0,0.5)
      CALL CHASIZ(1.5,2.5)
      CALL CHAHOL(8H*U-*LK*.)
      CALL MOVBY2(2.0,0.5)
      CALL CHAHOL(5H*U3*.)
      CALL MOVBY2(3.0,0.5)
C
  180 IF(N.LT.5)  GO  TO  220
C
      IF(IS(5).EQ.-3)  GO  TO  200
C
      CALL CHASIZ(3.0,5.0)
      CALL CHAHOL(11H*U(*LW*U)*.)
      CALL MOVBY2(-5.0,0.5)
      CALL CHASIZ(1.5,2.5)
      CALL CHAHOL(8H*U-*LK*.)
      CALL MOVBY2(2.0,0.5)
      CALL CHAHOL(5H*U5*.)
      CALL MOVBY2(3.0,0.5)
C
  200 IF(N.LT.6)  GO  TO  220
C
      IF(IS(6).EQ.-3)  GO  TO  220
C
      CALL CHASIZ(3.0,5.0)
      CALL CHAHOL(26H*U(*LEXP*U(-*LK*U  /RT))*.)
      CALL MOVBY2(2.0,-20.5)
      CALL CHASIZ(1.5,2.5)
      CALL CHAHOL(5H*U6*.)
      CALL MOVBY2(-2.0,21.0)
C
  220 CALL CHASIZ(3.0,5.0)
      CALL CHAHOL(5H*U]*.)
      CALL MOVBY2(-5.0,0.5)
      CALL CHASIZ(1.5,2.5)
      CALL CHAHOL(10H*U(1/*LK*.)
      CALL MOVBY2(2.0,0.5)
      CALL CHAHOL(5H*U4*.)
      CALL MOVBY2(-2.0,0.5)
      CALL CHAHOL(5H*U)*.)
C
```

```
      CALL CHAANG(0.0)
C
      IYL=INT((ALOG10(AL))-1.0)
      IYU=INT(ALOG10(AU))
      IYD=IYU-IYL
      YD=110.0/FLOAT(IYD)
      IYD=IYD+1
C
      DO 240 I = 1, IYD
      YT=(YD*FLOAT(I-1))-1.0
      CALL MOVTO2(-9.0,YT)
      CALL CHAHOL(4H10*.)
      CALL MOVBY2(0.0,2.5)
      ISC=IYL+I-1
      CALL CHAINT(ISC,3)
      CALL MOVBY2(-7.5,-2.5)
  240 CONTINUE
C
      DO 300 I = 1, IYD
      YT=(YD*FLOAT(I-1))-1.0
      CALL MOVTO2(YT,-9.0)
      CALL CHAHOL(4H10*.)
      CALL MOVBY2(0.0,2.5)
      ISC=IYL+I-1
      CALL CHAINT(ISC,3)
      CALL MOVBY2(-7.5,-2.5)
  300 CONTINUE
C
:ESKP
C
:SKFZ 1,3
      GO  TO  900
:ESKP
C
:SKFZ 2
C
      AU=1.0E-02*(AINT((1.0E02*AU)+1.0))
C
      CALL SHIFT2(300.0,-35.0)
C
      CALL MOVTO2(0.0,0.0)
C
      CALL LINTO2(0.0,210.5)
      CALL LINTO2(297.5,210.5)
      CALL LINTO2(297.5,0.0)
      CALL LINTO2(0.0,0.0)
C
      CALL SHIFT2(103.0,35.0)
C
      CALL AXIPOS(1,0.0,0.0,110.0,2)
      CALL AXISCA(3,4,0.0,AU,2)
      CALL AXIDRA(2,0,2)
C
      CALL AXIPOS(1,0.0,0.0,110.0,1)
      CALL AXISCA(3,4,0.0,AU,1)
      CALL AXIDRA(-2,0,1)
C
      CALL GRID(0,0,0)
```

```
C
      CALL MOVTO2(0.0,0.0)
      CALL LINTO2(110.0,110.0)
C
      CALL GRASYM(E,P,K,5,0)
C
      CALL CHASIZ(3.0,5.0)
C
      CALL MOVTO2(52.0,-17.5)
      CALL SYMBOL(1)
      CALL MOVBY2(3.0,-2.5)
      CALL CHAHOL(5H*UC*.)
      CALL CHASIZ(1.5,2.5)
      CALL MOVBY2(1.0,-2.5)
      CALL CHAHOL(5H*LT*.)
      CALL CHASIZ(3.0,5.0)
C
      CALL MOVTO2(-22.0,20.0)
      CALL CHAANG(90.0)
C
      CALL CHAHOL(13H*U[(R  /*LK*.)
      CALL MOVTO2(-20.0,30.0)
      CALL CHASIZ(1.5,2.5)
      CALL CHAHOL(5H*UG*.)
      CALL MOVTO2(-20.0,41.5)
      CALL CHAHOL(5H*U1*.)
      CALL MOVTO2(-22.0,43.0)
      CALL CHASIZ(3.0,5.0)
      CALL CHAHOL(5H*U)*.)
C
      IF(IS(2).EQ.-3)  GO  TO  340
C
      CALL CHAHOL(13H*U(*LA  *U)*.)
      CALL MOVTO2(-20.0,53.0)
      CALL CHASIZ(1.5,2.5)
      CALL CHAHOL(5H*UH*.)
      CALL MOVBY2(-2.0,0.5)
      CALL CHAHOL(5H*U+*.)
      CALL MOVTO2(-27.0,62.5)
      CALL CHAHOL(8H*U-*LK*.)
      CALL MOVBY2(2.0,0.5)
      CALL CHAHOL(5H*U2*.)
      CALL MOVTO2(-22.0,67.5)
C
  340 IF(IS(3).EQ.-3)  GO  TO  360
C
      CALL CHASIZ(3.0,5.0)
      CALL CHAHOL(7H*U(L)*.)
      CALL MOVBY2(-5.0,0.5)
      CALL CHASIZ(1.5,2.5)
      CALL CHAHOL(8H*U-*LK*.)
      CALL MOVBY2(2.0,0.5)
      CALL CHAHOL(5H*U3*.)
      CALL MOVBY2(3.0,0.5)
C
  360 IF(N.LT.5)  GO  TO  400
C
      IF(IS(5).EQ.-3)  GO  TO  380
```

```
C
      CALL CHASIZ(3.0,5.0)
      CALL CHAHOL(11H*U(*LW*U)*.)
      CALL MOVBY2(-5.0,0.5)
      CALL CHASIZ(1.5,2.5)
      CALL CHAHOL(8H*U-*LK*.)
      CALL MOVBY2(2.0,0.5)
      CALL CHAHOL(5H*U5*.)
      CALL MOVBY2(3.0,0.5)
C
  380 IF(N.LT.6)  GO  TO  400
C
      IF(IS(6).EQ.-3)  GO  TO  400
C
      CALL CHASIZ(3.0,5.0)
      CALL CHAHOL(26H*U(*LEXP*U(-*LK*U  /RT))*.)
      CALL MOVBY2(2.0,-20.5)
      CALL CHASIZ(1.5,2.5)
      CALL CHAHOL(5H*U6*.)
      CALL MOVBY2(-2.0,21.0)
C
  400 CALL CHASIZ(3.0,5.0)
      CALL CHAHOL(5H*U]*.)
      CALL MOVBY2(-5.0,0.5)
      CALL CHASIZ(1.5,2.5)
      CALL CHAHOL(10H*U(1/*LK*.)
      CALL MOVBY2(2.0,0.5)
      CALL CHAHOL(5H*U4*.)
      CALL MOVBY2(-2.0,0.5)
      CALL CHAHOL(5H*U)*.)
C
      CALL CHAANG(0.0)
C
      DO 500 I = 1, 5
      YT=(27.5*(FLOAT(I-1)))-1.0
      YD=(AU/4.0)*(FLOAT(I-1))
      CALL MOVTO2(-11.0,YT)
      CALL CHAHOL(3H0*.)
      CALL CHAFIX(YD,5,4)
  500 CONTINUE
C
      DO 600 I = 1, 5
      YT=(27.5*(FLOAT(I-1)))-2.0
      YD=(AU/4.0)*(FLOAT(I-1))
      CALL MOVTO2(YT,-6.0)
      CALL CHAHOL(3H0*.)
      CALL CHAFIX(YD,5,4)
  600 CONTINUE
C
:ESKP
C
  900 CALL DEVEND
C
      RETURN
C
      END
C
C
```

```
C
C     THE SUBROUTINE 'STAT' USES THE EXPERIMENTAL AND FITTED
C     DATA TO CALCULATE AND PRINT OUT RELEVANT STATISTICAL
C     PARAMETERS, WHICH INDICATE THE DEGREE OF FIT OF THE
C     MODEL. VALUES OF EXPERIMENTAL AND CALCULATED CRYSTAL
C     GROWTH RATES PER UNIT SURFACE AREA ARE ALSO OUTPUT TO
C     A SEPARATE RESULTS FILE FOR POSSIBLE USE AS DATA IN
C     OTHER STATISTICAL ANALYSIS PROGRAMS
C     ******************************************************
C
      SUBROUTINE STAT(K,Y,Q,FNT,FS,IS,N)
C
      REAL Y(K), Q(K), SUM, SST, SSD, SSR, AV, FNT, FS
C
      INTEGER K, N, IS(N), NF
C
      NF=0
C
      DO 20 I = 1, N
      IF(IS(I).GT.0.OR.IS(I).NE.-3)  NF=NF+1
   20 CONTINUE
C
      SUM=0.0
C
      DO 40  I = 1, K
      SUM=SUM+Y(I)
   40 CONTINUE
C
      AV=SUM/FLOAT(K)
C
      SUM=0.0
C
      DO 60 I = 1, K
      SUM=SUM+((Y(I)-AV)**2.0)
   60 CONTINUE
C
      SST=SUM/FLOAT(K-1)
C
      SUM=0.0
C
      DO 80 I = 1, K
      SUM=SUM+((Q(I)-AV)**2.0)
   80 CONTINUE
C
      SSR=SUM/FLOAT(NF)
C
      SSD=FNT/((FS**2.0)*FLOAT(K-1-NF))
C
      WRITE(100,100) AV, SST, SSD, SSR
  100 FORMAT(1H ,///,30X,39HAVERAGE OF OBSERVED VALUES OF DEPENDENT,
     1       12H VARIABLE = ,1PE14.5,/,30X,17HTOTAL MEAN SQUARE,32X,
     2       2H= ,1PE14.5,/,30X,28HMEAN SQUARE ABOUT REGRESSION,21X,
     3       2H= ,1PE14.5,/,30X,29HMEAN SQUARE DUE TO REGRESSION,20X,
     4       2H= ,1PE14.5)
C
      WRITE(100,110) FS
  110 FORMAT(1H ,/,30X,21HFUNCTION SCALE FACTOR,28X,2H= ,1PE14.5,///)
C
```

```
      WRITE(100,120)
  120 FORMAT(1H ,/,132(1H*))
C
:SKFZ 23
      DO 180 I = 1, K
      WRITE(120,140) Y(I), Q(I)
  140 FORMAT(2(2X,1PE15.7))
  180 CONTINUE
:ESKP
C
      RETURN
C
      END
C
C
C
C     THE REAL FUNCTION 'EXP10' CALCULATES THE EXPONENTIAL TO THE
C     BASE TEN OF ANY REAL NUMBER, VARIABLE OR EXPRESSION
C     ***************************************************************
C
      REAL FUNCTION EXP10(X)
      EXP10=10.0**X
      RETURN
      END
C
C
C
C     END OF PROGRAM
C     **************
```

APPENDIX 17

LISTING OF COMPUTER PROGRAM 'AGLOM'

The computer program written to fit sets of experimental crystal population-time data, to the simple agglomeration model presented in Chapter 9, using a comprehensive quasi-Newton non-linear optimisation algorithm (267), provided by the routine E04KBF from the NAG library (301), is listed in this appendix. The program is called AGLOM and was written in a version of Fortran IV suitable for a Harris 500 computer. Comment statements in the body of this listing describe the function of each program segment.

```
C*********************************************************************
C     PROGRAM TO FIT EXPERIMENTAL CRYSTAL POPULATION - TIME **
C     DATA TO A SIMPLE AGGLOMERATION MODEL FOR BATCH         **
C     CRYSTALLISATION                                        **
C*********************************************************************
C
C
C     MAIN SEGMENT
C     ************
C
C
C     TYPE SPECIFICATION STATEMENTS
C
      REAL T(35), CN(35), Q(35), X(5), S(5), BL(5), BU(5)
      REAL DX(5), F, FS, FE, ET, XT, U(5), AV, SCA
C
      INTEGER  K, IN, IL(5), IP, IX, IB
C
C     COMMON BLOCKS
C
      COMMON // S
      COMMON /BLK2/T, CN, Q, K, U, FS
C
C     CALL SUBROUTINE TO INPUT ALL DATA
C
      CALL DATAIN(T,CN,K,IN,IP,IB,IX,XT,ET,FE,FS,X,BL,
     1            BU,S,IL,SCA)
C
C     CALL SUBROUTINE TO CARRY OUT OPTIMISATION
C       .
      CALL FIT(X(1),BL(1),BU(1),IL(1),DX(1),F,IP,IB,IX,
     1         XT,ET,FE,IN)
C
C     CALL SUBROUTINE TO PRINT OUT NUMERICAL RESULTS
C
      CALL OUTPUT(K,T(1),CN(1),Q(1),U(3))
C
C     CALL SUBROUTINE TO CALCULATE AND PRINT OUT RESULTS
C     DERIVED FROM OPTIMISED MODEL PARAMETERS
C
      CALL RESULT(K,T(1),CN(1),IN,U(1),AV)
C
C     CALL SUBROUTINE TO PRODUCE GRAPHICAL OUTPUT
C
      CALL PLOT(K,T(1),CN(1),IN,U(1),AV,SCA)
C
      STOP
C
      END
C
C
C
C     THE SUBROUTINE 'DATAIN' READS IN ALL THE DATA FOR THE
C     PROGRAM. THIS INCLUDES, CONTROL VARIABLES FOR THE
C     OPTIMISATION; SCALE FACTORS FOR GRAPHICAL OUTPUT,
C     MODEL PARAMETERS AND OBJECTIVE FUNCTION; INITIAL
C     VALUES, AND LOWER AND UPPER LIMITS OF MODEL
C     PARAMETERS; AND, EXPERIMENTAL CRYSTAL POPULATION - TIME
```

```
C     DATA
C     ********************************************************
C
      SUBROUTINE DATAIN(T,CN,K,IN,IP,IB,IX,XT,ET,FE,FS,X,
     1                  BL,BU,S,IL,SCA)
C
      REAL T(35), CN(35), XT, ET, FE, FS, X(5)
      REAL BL(5), BU(5), S(5), SCA
C
      INTEGER K, IN, IP, IB, IL(5), IX, I
C
      READ(11,-) K, IN, IP, IB, IX, XT, ET, FE, FS, SCA
C
      READ(11,-) (X(I), I = 1, IN)
      READ(11,-) (BL(I), I = 1, IN)
      READ(11,-) (BU(I), I = 1, IN)
      READ(11,-) (S(I), I = 1, IN)
      READ(11,-) (IL(I), I = 1, IN)
C
      DO 100 I = 1, K
      READ(11,-) T(I), CN(I)
  100 CONTINUE
C
      RETURN
C
      END
C
C
C
C     THE OPTIMISATION SUBROUTINE 'FIT' CALLS THE NAG LIBRARY
C     ROUTINE 'E04KBF' TO CARRY OUT THE NONLINEAR OPTIMISATION
C     ********************************************************
C
      SUBROUTINE FIT(X,BL,BU,IL,DX,F,IP,IB,IX,XT,ET,FE,N)
C
      REAL X(N), BL(N), BU(N), DX(N), HL(10), HD(5)
      REAL ET, FE, F, XT, W(45)
C
      INTEGER I, N, IL(N), IW(2), IP, IB, IX, IFAIL, LH, LW
C
      LOGICAL LAM
C
      EXTERNAL E04LBS, FUNCT, MONIT
C
      IF(IX.EQ.0)  GO  TO  30
C
      LH=N*(N-1)/2
      LW=9*N
      IFAIL=0
      CALL FUNCT(IFAIL,N,X(1),F,DX(1),IW,2,W(1),LW)
C
      DO 10 I = 1, LH
      HL(I)=0.0
   10 CONTINUE
C
      DO 20 I = 1, N
      HD(I)=1.0
   20 CONTINUE
```

```
C
   30 IFAIL=1
C
      LAM=.TRUE.
C
      CALL E04KBF(N,FUNCT,MONIT,IP,LAM,IX,E04LBS,3000,ET,XT,
     1            1.0E05,FE,IB,BL(1),BU(1),X(1),HL(1),LH,HD(1),
     2            IL(1),F,DX(1),IW,2,W(1),LW,IFAIL)
C
      WRITE(100,40) IFAIL
   40 FORMAT(1H ,//,132(1H*),/,38X,8HIFAIL = ,I3,/,132(1H*))
C
      IFAIL=0
C
      CALL FUNCT(IFAIL,N,X(1),F,DX(1),IW,2,W(1),LW)
C
      RETURN
C
      END
C
C
C
C     THE SUBROUTINE 'FUNCT' IS CALLED BY THE OPTIMISATION ROUTINE
C     'E04KBF', TO PROVIDE THE OBJECTIVE FUNCTION TO BE MINIMISED
C     AND THE DERIVATIVES OF THAT FUNCTION WITH RESPECT TO THE
C     MODEL PARAMETERS. THE AGGLOMERATION MODEL USED HERE, APPLIES
C     TO THE CASE OF TWO PARTICLE COLLISIONS, WITH NUCLEATION
C     RESTRICTED TO AN INITIAL BURST OF FINITE DURATION
C     ************************************************************
C
      SUBROUTINE FUNCT(IFLAG,N,XC,FC,GC,IW,LIW,WX,LW)
C
      REAL XC(N), GC(N), WX(LW), FS, SUM, Q(35), SQ
      REAL CN(35), T(35), DE(5), S(5), U(5), SX, DR(5)
C
      INTEGER I, N, LIW, LW, IW(LIW), J
C
      COMMON // S
      COMMON /BLK2/ T, CN, Q, K, U, FS
C
      SUM=0.0
C
      DO 20 I = 1, N
      DE(I)=0.0
      U(I)=XC(I)*S(I)
   20 CONTINUE
C
      DO 200 I = 1, K
C
      IF(T(I).LT.U(3))  GO  TO  200
C
      Q(I)=1.0/((U(1)*T(I))-(U(1)*U(3))+U(2))
      SQ=Q(I)**2.0
C
      SUM=SUM+((FS*(Q(I)-CN(I)))**2.0)
      SX=2.0*(FS**2.0)*(Q(I)-CN(I))
C
      DR(1)=-1.0*T(I)*SQ
```

```
      DR(2)=-1.0*SQ
      DR(3)=U(1)*SQ
C
      DO 100 J = 1, N
      DE(J)=DE(J)+(SX*DR(J)*S(J))
  100 CONTINUE
C
  200 CONTINUE
C
      FC=SUM
C
      DO 300 I = 1, N
      GC(I)=DE(I)
  300 CONTINUE
C
      RETURN
C
      END
C
C
C
C     THE SUBROUTINE 'MONIT' IS CALLED BY THE OPTIMISATION ROUTINE
C     'E04KBF', TO PROVIDE MONITORING OF THE COURSE OF OPTIMISATION.
C     VALUES OF THE MODEL PARAMETERS, THEIR GRADIENT VALUES AND THE
C     VALUE OF THE OBJECTIVE FUNCTION, AS WELL AS THE NUMBER OF
C     ITERATIONS, THE NUMBER OF FUNCTION EVALUATIONS AND THE STATUS
C     OF EACH PARAMETER, ARE PRINTED OUT AT INTERVALS DETERMINED BY
C     THE PRINT FACTOR, WHICH IS INPUT AS DATA IN THE MAIN SEGMENT,
C     AND ALSO AT THE END OF THE OPTIMISATION
C     ****************************************************************
C
      SUBROUTINE MONIT(N,XC,FC,GC,IS,GPJ,CON,POS,NIT,NF,IW,LIW,W,LW)
C
      REAL XC(N), FC, GC(N), GPJ, CON, W(LW), H(5)
C
      INTEGER N, IS(N), NIT, NF, IW(LIW), LIW, LW, J, ISJ
C
      COMMON // H
C
      LOGICAL POS
C
      WRITE(100,20) NIT, NF, FC, GPJ
   20 FORMAT(1H ,/,12X,4HITNS,5X,8HFN EVALS,13X,8HFN VALUE,13X,
     121HNORM OF PROJ GRADIENT,/,10X,I4,6X,I5,2(6X,1PE20.4))
C
      WRITE(100,40)
   40 FORMAT(1H ,/,12X,1HJ,14X,4HX(J),17X,4HG(J),7X,6HSTATUS,
     1       7X,12HSCALE FACTOR)
C
      DO 400 J = 1, N
C
      ISJ=IS(J)
C
      IF(ISJ.GT.0)  GO  TO  60
C
      ISJ=-ISJ
C
      GO  TO  (100,140,180), ISJ
```

```
C
   60 WRITE(100,80) J, XC(J), GC(J), H(J)
   80 FORMAT(11X,I2,1X,1P2E20.5,5X,4HFREE,7X,1PE12.2)
C
      GO  TO  400
C
  100 WRITE(100,120) J, XC(J), GC(J), H(J)
  120 FORMAT(11X,I2,1X,1P2E20.5,5X,11HUPPER BOUND,1PE12.2)
C
      GO  TO  400
C
  140 WRITE(100,160) J, XC(J), GC(J), H(J)
  160 FORMAT(11X,I2,1X,1P2E20.5,5X,11HLOWER BOUND,1PE12.2)
C
      GO  TO  400
C
  180 WRITE(100,200) J, XC(J), GC(J), H(J)
  200 FORMAT(11X,I2,1X,1P2E20.5,5X,8HCONSTANT,3X,1PE12.2)
C
  400 CONTINUE
C
      WRITE(100,420)  CON
  420 FORMAT(11X,50HESTIMATED CONDITION NUMBER OF PROJECTED HESSIAN = ,
     11PE10.2)
C
      RETURN
C
      END
C
C       .
C
C     THE SUBROUTINE 'OUTPUT' PRINTS OUT THE MAIN NUMERICAL RESULTS
C     FROM THE EMPIRICAL FITTING PROCESS
C     ****************************************************************
C
      SUBROUTINE OUTPUT(K,T,CN,Q,UT)
C
      REAL T(K), UT, Q(K), CN(K), R
C
      INTEGER I, K
C
      WRITE(100,20)
   20 FORMAT(1H ,//,30X,8HTIME (S),20X,18HCRYSTAL POPULATION,/,
     1       43X,12HEXPERIMENTAL,5X,10HCALCULATED,7X,8HRESIDUAL,//)
C
      DO 200 I = 1, K
C
      IF(T(I).LT.UT)  GO  TO  200
C
      R=Q(I)-CN(I)
C
      WRITE(100,100) T(I), CN(I), Q(I), R
  100 FORMAT(30X,F7.1,3(5X,1PE12.5))
C
  200 CONTINUE
C
      WRITE(100,300)
  300 FORMAT(1H ,//,132(1H*),//)
```

```
C
      RETURN
C
      END
C
C
C
C     THE SUBROUTINE 'RESULT' CALCULATES AND PRINTS OUT VALUES
C     OF VARIABLES RELEVANT TO THE AGGLOMERATION MODEL, USING
C     THE OPTIMISED VALUES OF THE MODEL PARAMETERS
C     ************************************************************
C
      SUBROUTINE RESULT(K,T,CN,N,U,AV)
C
      REAL  U(N), A1, A2, A3, SUM, AV, T(K), CN(K)
C
      INTEGER N, K, I
C
      A1=2.0*U(1)
C
      A2=1.0/U(2)
C
      A3=U(3)
C
      SUM=0.0
C
      DO 40 I = 1, K
      SUM=SUM+CN(I)
   40 CONTINUE
C
      AV=SUM/FLOAT(K)
C
      WRITE(100,80) A1, A2, A3, AV
   80 FORMAT(1H ,///,20X,26HCOLLISION FREQUENCY FACTOR,19X,2H= ,
     1        1PE15.5,2X,9H(1/NO.S.),//,20X,
     2        47HPOPULATION AFTER INITIAL BURST OF NUCLEATION = ,
     3        1PE15.5,2X,5H(NO.),//,20X,
     4        39HDURATION OF INITIAL BURST OF NUCLEATION,6X,2H= ,
     5        1PE15.5,2X,4H(S.),//,20X,
     6        18HAVERAGE POPULATION,27X,2H= ,1PE15.5,2X,5H(NO.),//)
C
      WRITE(100,120)
  120 FORMAT(1H ,///,132(1H*))
C
      RETURN
C
      END
C
C
C
C     THE GRAPHICAL OUTPUT SUBROUTINE 'PLOT' USES THE ROUTINES
C     OF THE GINO GRAPH PLOTTING PACKAGE, TO PRODUCE A GRAPH
C     SHOWING THE EXPERIMENTAL DATA AND THE FITTED EMPIRICAL
C     CURVE. THE PLOT CAN BE SCALED TO ANY SIZE BY CHANGING
C     THE SCALE FACTOR, INPUT AS DATA IN THE MAIN SEGMENT.
C     COMPILATION OPTION 1 PERMITS DISPLAY OF THE GRAPH ON A
C     T4010 GRAPHICS TERMINAL; OPTION 2 GIVES A HARDCOPY OF
C     THE PLOT; AND, OPTION 3 ALLOWS DISPLAY OF THE GRAPH ON
```

```
C     AN IMLAC DYNAGRAPHICS TERMINAL
C     ************************************************************
C
      SUBROUTINE PLOT(K,T,CN,N,U,AV,SCA)
C
      REAL T(K), CN(K), U(N), AV, SCA, XLT
      REAL YU, YL, YD, YT
:SKFZ 23
      REAL UT, XT, QT, YM
:ESKP
C
      INTEGER K, N, I, IYL, IYD, IXT, ISC, IZ
C
:SKFZ 1
      CALL T4010
:ESKP
C
:SKFZ 2
      CALL OPEN
:ESKP
C
:SKFZ 3
      CALL APDS4
:ESKP
C
      CALL ERRMAX(100)
      CALL SHIFT2(10.0,10.0)
      CALL CHASWI(1)
      CALL SCALE(SCA)
      CALL CHASIZ(1.5,2.5)
      CALL MOVTO2(0.0,0.0)
C
      CALL LINTO2(0.0,210.5)
      CALL LINTO2(297.5,210.5)
      CALL LINTO2(297.5,0.0)
      CALL LINTO2(0.0,0.0)
C
      CALL SHIFT2(48.0,35.0)
C
      XLT=100.0*(AINT((T(K)/100.0)+1.0))
      IXT=INT(((XLT-U(3))/5.0)+1.0)
C
      YU=0.0
      YL=1.0E25
C
      IZ=-1
C
      DO 40 I = 1, K
      YU=AMAX1(YU,CN(I))
      YL=AMIN1(YL,CN(I))
   40 CONTINUE
C
      IYL=INT((ALOG10(YL)))
      IYU=INT((ALOG10(YU))+1.0)
      IYD=IYU-IYL
      YD=110.0/FLOAT(IYD)
      IYD=IYD+1
C
```

```
      CALL AXIPOS(1,0.0,0.0,220.0,1)
      CALL AXISCA(3,10,0.0,XLT,1)
      CALL AXIDRA(-2,1,1)
C
      CALL AXIPOS(1,0.0,0.0,110.0,2)
      CALL AXISCA(4,0,YL,YU,2)
      CALL AXIDRA(2,0,2)
C
      DO 80 I = 1, IYD
      YT=(YD*FLOAT(I-1))-1.0
      CALL MOVTO2(-9.0,YT)
      CALL CHAHOL(4H10*.)
      CALL MOVBY2(0.0,2.5)
      ISC=IYL+I-1
      CALL CHAINT(ISC,3)
      CALL MOVBY2(-7.5,-2.5)
   80 CONTINUE
C
      CALL GRASYM(T,CN,K,5,0)
C
:SKFZ 23
C
      UT=220.0*U(3)/XLT
      CALL MOVTO2(UT,0.0)
C
      CALL DASHED(2,13.0,6.0,3.0)
      CALL LINTO2(UT,110.0)
C
      IF(U(3).LT.1.0)  GO  TO  120
C
      CALL DASHED(0,0.0,0.0,0.0)
      CALL MOVTO2(UT+5.0,4.0)
      CALL CHAANG(90.0)
      CALL CHAHOL(16HEND OF INITIAL*.)
      CALL MOVTO2(UT+10.0,4.0)
      CALL CHAHOL(12HNUCLEATION*.)
      CALL CHAANG(0.0)
C
  120 CALL DASHED(-2,6.0,1.5,1.5)
C
      YM=(10.0**(FLOAT(IYU)))
C
      DO 200 I = 1, IXT
C
      XT=(5.0*FLOAT(I-1))+U(3)
      QT=1.0/((U(1)*XT)-(U(1)*U(3))+U(2))
C
      IF(IZ.EQ.0)  GO  TO  150
C
      IF(QT.LE.YM)  IZ=1
C
      IF(IZ.LT.0)  GO  TO  200
C
      CALL GRAMOV(XT,QT)
      IZ=0
C
      GO  TO  200
C
```

```
  150 CALL GRALIN(XT,QT)
C
  200 CONTINUE
C
      CALL DASHED(0,0.0,0.0,0.0)
      CALL MOVBY2(-21.5,-6.0)
      CALL CHAHOL(15HAGGLOMERATION*.)
      CALL MOVBY2(-19.5,-5.0)
      CALL CHAHOL(7HMODEL*.)
C
:ESKP
C
      CALL DASHED(-2,8.0,2.0,2.0)
C
      CALL GRAMOV(0.0,AV)
      CALL GRALIN(XLT,AV)
C
      CALL DASHED(0,0.0,0.0,0.0)
C
      CALL MOVBY2(-17.0,7.5)
      CALL CHAHOL(9HAVERAGE*.)
      CALL MOVBY2(-10.5,-5.0)
      CALL CHAHOL(12HPOPULATION*.)
C
      CALL CHASIZ(3.0,5.0)
C
      CALL MOVTO2(50.0,-20.0)
      CALL CHAHOL(18HTIME   (SECONDS)*.)
C
      CALL MOVTO2(-14.0,15.0)
      CALL CHAANG(90.0)
      CALL CHAHOL(26HCRYSTAL POPULATION   (-)*.)
      CALL CHAANG(0.0)
C
      CALL DEVEND
C
      RETURN
C
      END
C
C
C
C     END  OF  PROGRAM
C     ****************
```

APPENDIX 18

ACTIVITIES AND CONCENTRATIONS OF CR(VI) IONIC SPECIES IN ACIDIC SOLUTION

The equilibria that prevail in a solution of barium chromate in hydrochloric acid have been detailed in Chapter 7. They are:

$$K_{sp} = a_{Ba^{2+}} a_{CrO_4^{2-}} \quad \ldots\ldots\ldots\ldots \text{(A18.1)}$$

$$K_1 = a_{HCrO_4^-} a_{H^+} / a_{H_2CrO_4} \quad \ldots\ldots\ldots\ldots \text{(A18.2)}$$

$$K_2 = a_{CrO_4^{2-}} a_{H^+} / a_{HCrO_4^-} \quad \ldots\ldots\ldots\ldots \text{(A18.3)}$$

$$K_3 = a_{Cr_2O_7^{2-}} / a^2_{HCrO_4^-} \quad \ldots\ldots\ldots\ldots \text{(A18.4)}$$

$$K_4 = a_{HCr_2O_7^-} a_{H^+} / a_{H_2Cr_2O_7} \quad \ldots\ldots\ldots\ldots \text{(A18.5)}$$

$$K_5 = a_{Cr_2O_7^{2-}} a_{H^+} / a_{HCr_2O_7^-} \quad \ldots\ldots\ldots\ldots \text{(A18.6)}$$

$$K_6 = a_{CrO_3Cl^-} / a_{HCrO_4^-} a_{H^+} a_{Cl^-} \quad \ldots\ldots\ldots\ldots \text{(A18.7)}$$

In the above relations 'a' denotes activities and in the relations developed below γ denotes activity coefficients and 'C' denotes concentrations.

If it is considered that the barium chromate in solution is completely dissociated into ions, equation A18.1 need not be considered. Moreover, a mass balance for total chromium in solution then gives:

$$C_{Cr(VI)} = C_{HCrO_4^-} + C_{H_2CrO_4} + C_{CrO_4^{2-}} + 2C_{Cr_2O_7^{2-}} + 2C_{H_2Cr_2O_7} + 2C_{HCr_2O_7^-} + C_{CrO_3Cl^-} \quad \ldots \text{(A18.8)}$$

Also, for each ionic species in solution,

$$C = a/\gamma \quad \ldots\ldots\ldots\ldots\ldots\ldots\ldots \quad (A18.9)$$

Equation A18.9 and equations A18.2 to A18.7 can be used to substitute expressions, involving only hydrogen ion activity and chromate ion activity, for the concentration of each of the other ionic species in equation A18.8. Furthermore, Skander (4) has assumed that hydrogen ion concentration and chlorine ion concentration are equal.

$$\text{i.e.} \quad C_{Cl^-} = C_{H^+} \quad \ldots\ldots\ldots\ldots\ldots\ldots \quad (A18.10)$$

If this assumption is adopted here as well, equation A18.8 finally rearranges to give:

$$U_1 a^2_{CrO_4^{2-}} + U_2 a_{CrO_4^{2-}} - C_{Cr(VI)} = 0 \quad \ldots\ldots\ldots \quad (A18.11)$$

where,

$$U_1 = (2K_3 a^2_{H^+}/K_2^2)\left[\frac{1}{\gamma_{Cr_2O_7^{2-}}} + \frac{a_{H^+}}{\gamma_{HCr_2O_7^-}K_5} + \frac{a^2_{H^+}}{\gamma_{H_2Cr_2O_7}K_4K_5}\right]$$

$$\ldots\ldots\ldots\ldots\ldots\ldots \quad (A18.12)$$

and,

$$U_2 = \frac{1}{\gamma_{CrO_4^{2-}}} + \frac{a_{H^+}}{\gamma_{HCrO_4^-}K_2} + \frac{a^2_{H^+}}{\gamma_{H_2CrO_4}K_1K_2} + \frac{\gamma_{Cl^-}a^3_{H^+}K_6}{\gamma_{H^+}\gamma_{CrO_3Cl^-}K_2}$$

$$\ldots\ldots\ldots\ldots\ldots\ldots \quad (A18.13)$$

The quadratic equation A18.11 can be solved for the chromate ion activity .

$$\text{i.e.} \quad a_{CrO_4^{2-}} = \frac{-U_2 + \sqrt{U_2^2 + 4U_1C_{Cr(VI)}}}{2U_1} \quad \ldots\ldots \quad (A18.14)$$

Once chromate ion activity is known, the equilibrium relations can be used to calculate the activities of the other ionic species.

i.e. $a_{HCrO_4^-} = a_{CrO_4^{2-}}\ a_{H^+}/K_2$ .. (A18.15)

$a_{H_2CrO_4} = a_{CrO_4^{2-}}\ a_{H^+}^2/K_1K_2$ .. (A18.16)

$a_{Cr_2O_7^{2-}} = a_{CrO_4^{2-}}^2\ a_{H^+}^2\ K_3/K_2^2$ .. (A18.17)

$a_{HCr_2O_7^-} = a_{CrO_4^{2-}}^2\ a_{H^+}^3\ K_3/K_2^2K_5$ .. (A18.18)

$a_{H_2Cr_2O_7} = a_{CrO_4^{2-}}^2\ a_{H^+}^4\ K_3/K_2^2K_4K_5$ .. (A18.19)

$a_{CrO_3Cl^-} = a_{CrO_4^{2-}}\ a_{H^+}^3\ \gamma_{Cl^-}\ K_6/\gamma_{H^+}K_2$ .. (A18.20)

As indicated in Chapter 7, activity coefficients can be calculated using the Debye-Huckel equation.

i.e. $\log_{10}(\gamma) = \dfrac{A_o\sqrt{I_c}}{1 + B_o d_o \sqrt{I_c}}$ ..... (A18.21)

where, $I_c = \frac{1}{2} \sum_i C_i Z_i^2$ ..... (A18.22)

and, A_o and B_o are empirical constants defined by equations 7.16 and 7.17 respectively, in Chapter 7.

Since ionic strength depends on the ionic concentrations, which in turn depend upon the activities and activity coefficients, an iterative calculation procedure is required. For a given total Cr(VI) concentration and hydrogen ion activity (i.e. pH), unit activity coefficients may be assumed for all species, and thus their activities and concentrations may be calculated using the relations given above.

Ionic strength can then be calculated and new estimates for the activity coefficients obtained in order to repeat the cycle of calculations. The iterative process may be terminated when no further significant change in the calculated value of ionic strength occurs.

REFERENCES

1. Miller, C.H.; in: Proc. 3rd Symp. Chem. Probl. connected Stab. Explos. 1973; ed.: Hanson, J.; Sekt. Detonik Foerbraenning, Joenkoeping, Sweden; pp: 285-301; 1974.

2. Gordon, L., Salutsky, M.L. and Willard, H.H.; Precipitation from Homogeneous Solution; Wiley, New York; 1959.

3. Walton, A.G.; The Formation and Properties of Precipitates; Interscience, New York; 1967.

4. Skander, J.L,; Ph.D. Thesis; University of Aston in Birmingham; 1979.

5. Falangas, E.; Ph.D. Thesis; University of Aston in Birmingham; 1980.

6. Salutsky, M.L., Stites, J.G. and Martin, A.W.; Anal. Chem.; Vol. 25 (11); pp: 1677-1681; 1953.

7. Gordon, L. and Firsching, F.H.; Anal. Chem.; Vol. 26; pp: 759-760; 1954.

8. Nancollas, G.H.; Adv. Coll. Interf. Sci.; Vol. 10; pp: 215-252; 1979.

9. Mullin, J.W.; Crystallisation; 2nd edition; Butterworths, London; 1972.

10. De Jong, E.J.; in: Proc. 7th Symp. Ind. Cryst.; ed.: De Jong, E.J. and Jancic, S.J.; North Holland, Amsterdam; pp: 25-27; 1979.

11. Strickland-Constable, R.F.; Chem. Engr.; No. 280 (December); pp: 603-604; 1973.

12. Mullin, J.W.; Chem. Ind.; No. 8 (3, May); pp: 372-377; 1980.

13. Nielsen, A.E.; Kinetics of Precipitation; Pergamon, Oxford; 1964.

14. Ohara, M. and Reid, R.C.; Modeling Crystal Growth Rates from Solution; Prentice-Hall, New Jersey; 1973.

15. Walton, A.G.; in: Dispersion of Powders in Liquids; 2nd edition; ed.: G.D. Parfitt; Applied Science Publishers, Barking; pp: 175-220; 1973.

16. Botsaris, G.D.; in: Proc. 6th Symp. Ind. Cryst.; ed.: Mullin, J.W.; Plenum Press, New York; pp: 3-22; 1976.

17. Garside, J. and Davey, R.J.; Chem. Eng. Commun.; Vol. 4; pp: 393-424; 1980.

18. Strickland-Constable, R.F.; AIChE Symp. Ser.; Vol. 68 (121); pp: 1-7; 1972.

19. Becker, R. and Doring, W.; Ann. Physik (Leipzig); Vol. 24; pp: 719-752; 1935.

20. Becker, R.; Disc. Farad. Soc.; Vol. 5; pp: 55-61; 1949.

21. Larson, M.A.; Chem. Eng. Commun.; Vol. 12 (1-3); pp: 161-169; 1981.

22. Ottens, E.P.K., Janse, A.H. and De Jong, E.J.; Jou. Cryst. Growth; Vol. 13/14; pp: 500-505; 1972.

23. Ottens, E.P.K. and De Jong, E.J.; Ind. Eng. Chem. (Fundam.); Vol. 12 (2); pp: 179-184; 1973.

24. Evans, T.W., Margolis, G. and Sarofim, A.F.; AIChE Jou.; Vol. 20 (5); pp: 950-958; 1974.

25. Garside, J., Rusli, I.T. and Larson, M.A.; AIChE Jou.; Vol. 25 (1); pp: 57-64; 1979.

26. Yamamoto, H. and Harano, Y.; Jou. Chem. Eng. Japan; Vol. 13 (4); pp: 313-318; 1980.

27. Denk, E.G. and Botsaris, G.D.; Jou. Cryst. Growth; Vol. 13/14; pp: 493-499; 1972.

28. Botsaris, G.D., Denk, E.G. and Chua, J.O.; AIChE Symp. Ser.; Vol. 68 (121); pp: 21-30; 1972.

29. Sung, C.Y., Estrin, J. and Youngquist, G.R.; AIChE Jou.; Vol. 19; pp: 957-962; 1973.

30. Wang, M.L. and Yang, H.M.; Chem. Eng. Commun.; Vol. 12 (4-6); pp: 241-251; 1981.

31. Mullin, J.W. and Leci, C.L.; AIChE Symp. Ser.; Vol. 68 (121); pp: 8-20; 1972.

32. Nyvlt, J., Rychly, R., Gottfried, J. and Wurzelova, J.; Jou. Cryst. Growth; Vol. 6; pp: 151-162; 1970.

33. Storm, T.D., Hazleton, R.A. and Lahti, L.E.; Jou. Cryst. Growth; Vol. 7; pp: 55-60; 1970.

34. Mullin, J.W. and Raven, K.D.; Nature; Vol. 190; p.251; 1961.

35. Mullin, J.W. and Raven, K.D.; Nature; Vol. 195; pp: 35-38; 1962.

36. Blackadder, D.A.; Chem. Engr.; Dec. 1964; pp: 303-320; 1964.

37. Mullin, J.W. and Jancic, S.J.; Trans. Instn. Chem. Engrs.; Vol. 57; pp: 188-193; 1979.

38. Nyvlt, J.; Industrial Crystallisation from Solutions; Butterworths, London; pp: 150-155; 1971.

39. Aquilano, D.; Mater. Chem.; Vol. 4 (3); pp: 237-261; 1979.

40. Bennema, P.; in: Proc. 6th Symp. Ind. Cryst.; ed: Mullin, J.W.; Plenum Press, New York; pp: 91-112; 1976.

41. Bennema, P.; in: Proc. 7th Symp. Ind. Cryst.; ed: De Jong, E.J. and Jancic, S.J.; North Holland, Amsterdam; pp: 115-133; 1979.

42. Mullin, J.W.; in: Proc. 7th Symp. Ind. Cryst.; ed: De Jong, E.J. and Jancic, S.J.; North Holland, Amsterdam; pp: 93-103; 1979.

43. Rousseau, R.W.; Chemtech; Vol. 10 (9); pp: 566-571; 1980.

44. Burton, W.K.; Cabrera, N. and Frank, F.C.; Phil. Trans. Roy. Soc.; Vol. A243; pp: 299-358; 1951.

45. Gilmer, G.H.; Science; Vol. 208; pp: 355-363; 1980.

46. Ranz, W.E. and Marshall, W.R.; Chem. Eng. Progr.; Vol. 48 (3); pp: 141-146; 1952.

47. Ranz, W.E. and Marshall, W.R.; Chem. Eng. Progr.; Vol. 48 (4); pp: 173-180; 1952.

48. Karpinski, P.H.; Chem. Eng. Sci.; Vol. 35; pp: 2321-2324; 1980.

49. Rowe, P.N., Claxton, K.T. and Lewis, J.B.; Trans. Instn. Chem. Engrs.; Vol. 43; pp: 14-31; 1965.

50. Levins, D.M. and Glastonbury, J.R.; Trans. Instn. Chem. Engrs.; Vol. 50; pp: 132-146; 1972.

51. Frossling, N.; Gerlands Beitr. Geophys.; Vol. 52; pp: 170-216; 1938.

52. Bourne, J.R.; AIChE Symp. Ser.; Vol. 76 (103); pp: 59-64; 1980.

53. Tavare, N.S., Garside, J. and Chivate, M.R.; Ind. Eng. Chem. (Proc. Des. Dev.); Vol. 19 (4); pp: 653-665; 1980.

54. Tavare, N.S. and Chivate, M.R.; Jou. Chem. Eng. Japan; Vol. 13 (5); pp: 371-379; 1980.

55. Blickle, T. and Halasz, S.; Krist. Tech.; Vol. 8 (6); pp: 679-687; 1973.

56. Nyvlt, J.; Collect. Czech. Chem. Commun.; Vol. 44; pp: 2173-2183; 1979.

57. Garside, J. and Jancic, S.J.; Chem. Eng. Sci.; Vol. 33; pp: 1623-1630; 1978.

58. Abegg, C.F., Stevens, J.D. and Larson, M.A.; AIChE Jou.; Vol. 14 (1); pp: 118-122; 1968.

59. Garside, J.; in: Proc. 7th Symp. Ind. Cryst.; ed: De Jong, E.J. and Jancic, S.J.; North Holland, Amsterdam; pp: 143-151; 1979.

60. Nienow, A.W., Bujac, P.D.B. and Mullin, J.W.; Jou. Cryst. Growth.; Vol. 13/14; pp: 488-492; 1972.

61. Levins, D.M. and Glastonbury, J.R.; Trans. Instn. Chem. Engrs.; Vol. 50; pp: 32-41; 1972.

62. Nienow, A.W.; Trans. Instn. Chem. Engrs.; Vol. 54; pp: 205-207; 1976.

63. Conti, R., Sicardi, S. and Specchia, V.; Chem. Eng. Jou.; Vol. 22; pp: 247-249; 1981.

64. Broul, M. and Nyvlt, J.; Chem. Listy; Vol. 74 (4); pp: 362-383; 1980.

65. Randolph, A.D. and Puri, A.D.; AIChE Jou.; Vol. 27 (1); pp: 92-99; 1981.

66. Glassner, A.; Mater. Res. Bull.; Vol. 6 (12); pp: 1361-1364; 1971.

67. Shor, S.M. and Larson, M.A.; Chem. Eng. Progr. Symp. Ser.; Vol. 67; pp: 32-42; 1971.

68. Nancollas, G.H.; Interactions in Electrolyte Solutions; Elsevier, Amsterdam; 1966.

69. Pazourek, K.; Czech. Jou. Phys.; B29 (2); pp: 222-226; 1979.

70. Davey, R.J. and Mullin, J.W.; Krist. Tech.; Vol. 11 (6); pp: 625-628; 1976.

71. Lewin, S.Z. and Vance, J.E.; Jou. Am. Chem. Soc.; Vol. 74; pp: 1433-1436; 1952.

72. Phillips, V.A., Kolbe, J.L. and Opperhauser, H.; Jou. Cryst. Growth; Vol. 41 (2); pp: 228-234; 1977.

73. Kuznetsov, D.A. and Hodorowicz, S.; Krist. Tech.; Vol. 13 (12); pp: 1413-1416; 1978.

74. Mullin, J.W. and Sohnel, O.; Chem. Eng. Sci.; Vol. 32; pp: 683-686; 1977.

75. Sohnel, O., Garside, J. and Jancic, S.J.; Jou. Cryst. Growth; Vol. 39; pp: 307-314; 1977.

76. Sohnel, O. and Mullin, J.W.; Chem. Eng. Sci.; Vol. 33; pp: 1535-1538; 1978.

77. Sohnel, O. and Garside, J.; Jou. Cryst. Growth; Vol. 46; pp: 238-240; 1979.

78. Christoffersen, J., Christoffersen, M.R., van Rosmalen, G.M. and Marchee, W.G.J.; Jou. Cryst. Growth; Vol. 47; pp: 607-612; 1979.

79. van Leeuwen, C.; Jou. Cryst. Growth; Vol. 46; pp: 91-95; 1979.

80. van Leeuwen, C. and Blomen, L.J.M.J.; Jou. Cryst. Growth; Vol. 46; pp: 96-104; 1979.

81. Sohnel, O. and Garside, J.; Jou. Cryst. Growth; Vol. 54; pp: 358-360; 1981.

82. Nielsen, A.E.; Krist. Tech.; Vol. 4 (1); pp: 17-38; 1969.

83. Barton, D. and Ollis, W.D. (ed.); Comprehensive Organic Chemistry, Vol. 1; Pergamon, Oxford; pp: 1108-1109; 1979.

84. Hartford, W.H. and Darrin, M.; Chem. Rev.; Vol. 58; pp: 1-61; 1958.

85. Knoblowitz, M. and Morrow, J.I.; Inorg. Chem.; Vol. 15 (7); pp: 1674-1677; 1976.

86. Nyholm, R.S.; Jou. Soc. Chem. Ind. (Lond.); Vol. 66; pp: 449-451; 1947.

87. Tong, J.Y. and King, E.L.; Jou. Am. Chem. Soc.; Vol. 82; pp: 3805-3809; 1960.

88. Ramette, R.W.; Jou. Chem. Educ.; Vol. 49 (4); pp: 270-271; 1972.

89. Epik, P.A. and Tolstikov, V.P.; Zhur. Obshchei. Khim.; Vol. 20; pp: 762-769; 1950.

90. Epik, P.A. and Orochko, A.I.; Zhur. Neorg. Khim.; pp: 1855-1864; 1958.

91. Jove, J. and Haissinsky, M.; Jou. Chim. Phys.; Vol. 63 (5); pp: 709-715; 1966.

92. Kalecinski, J.; Bull. Acad. Polon. Sci., Ser. Sci. Chim.; Vol. 14 (2); pp: 137-142; 1966.

93. Roder, M., Bakh, N.A. and Bugaenko, L.T.; Tr. 2-go (Vtorgo) Vses. Soveshch. po. Radiats. Khim. Akad. Nauk. SSSR, Otd. Khim. Nauk. Moscow; pp: 378-381; 1960.

94. Clarke, R., Kuhn, A. and Okoh, E.; Chem. Brit.; Vol. 11 (2); pp: 59-64; 1975.

95. Mellor, J.W.; Comprehensive Treatise on Inorganic and Theoretical Chemistry, Vol. 11; Longman, London; 1931.

96. Bindra, P.S.; Ph.D. Thesis; University of Southampton; 1974.

97. Takiyama, K.; Bull. Chem. Soc. Japan; Vol. 31 (8); pp: 950-953; 1958.

98. Benes, J.; Coll. Czech. Chem. Commun.; Vol. 34; pp: 1514-1522; 1969.

99. Heyn, A.H.A. and Schupak, E.; Anal. Chem.; Vol. 26 (7); pp: 1243-1245; 1954.

100. Elving, P.J. and van Atta, R.E.; Anal. Chem.; Vol. 22 (11); pp: 1375-1376; 1950.

101. Willard, H.H.; Anal. Chem.; Vol. 22 (11); pp: 1372-1374; 1950.

102. Burrus, H.L.; Jou. Appl. Chem.; Vol. 11; pp: 376-382; 1961.

103. Warner, R.C.; Jou. Bio. Chem.; Vol. 142; pp: 705-723; 1942.

104. Werner, E.A.; Jou. Chem. Soc. (Trans.); Vol. 113; pp: 84-99; 1918.

105. Werner, E.A.; Jou. Chem. Soc. (Trans.); Vol. 117; pp: 1078-1081; 1920.

106. Sengupta, S.K. and Varma, S.; Technology; Vol. 9 (2-3); pp: 201-203; 1972.

107. Nurakhmetov, N.N. and Beremzhanov, B.A.; Izv. Akad. Nauk. Kaz. SSR, Ser. Khim.; Vol. 18 (2); pp: 82-84; 1968.

108. Welles, H.L., Giaquinto, A.R. and Lindstrom, R.E.; Jou. Pharm. Sci.; Vol. 60 (8); pp: 1212-1216; 1971.

109. Shaw, W.H.R. and Bordeaux, J.J.; Jou. Am. Chem. Soc.; Vol. 77; pp: 4729-4733; 1955.

110. Freiser, H. and Fernando, Q.; Ionic Equilibria in Analytical Chemistry; Wiley, New York; 1963.

111. Castorina, T.C., McCahill, J.W., Graybush, R.J. and Helf, S.; The Chemistry of Hexamethylene-tetramine in an Acidic Aqueous Medium; Feltman Research and Engineering Laboratories; New Jersey; 1960.

112. Keene, B.R.T.; Chem. Brit.; Vol. 9; p. 424; 1973.

113. Davies, D.L.; Chem. Brit.; Vol. 10; p.359; 1974.

114. Bindra, P.S.; M.Sc. Thesis; University of Manchester Institute of Science and Technology; 1970.

115. Rychly, R.; Chem. Listy.; Vol. 65 (1); pp: 91-93; 1971.

116. Adamski, T.; Nature; Vol. 190; p. 524; 1961.

117. Adamski, T.; Bull. Soc. Fr. Mineral. Crystallogr.; Vol. 90 (1); pp: 113-114; 1967.

118. Adamski, T.; Mikrochim. Acta.; No. 1; pp: 67-80; 1967.

119. Adamski, T.; Mikrochim. Acta.; Supp. 2; pp: 1-15; 1967.

120. Packter, A.; Krist. Tech.; Vol. 9 (5); pp: 497-502; 1974.

121. Packter, A., Chauhan, P. and Saunders, D.; Z. Phys. Chem. (Leipzig); Vol. 242 (5/6); pp: 289-297; 1969.

122. Packter, A.; Krist. Tech.; Vol. 12 (2); pp: 117-121; 1976.

123. Packter, A. and Alleem, A.; Cryst. Res. Tech.; Vol. 16 (1); pp: 33-37; 1981.

124. Packter, A. and Sahay, S.; Krist. Tech.; Vol. 9 (5); pp: 485-496; 1974.

125. Packter, A.; Jou. Chem. Soc. (A); pp: 859-862; 1968.

126. Packter, A. and Sahay, S.; Krist. Tech.; Vol. 11 (10); pp: 1033-1039; 1976.

127. Reiss, H.; Jou. Chem. Phys.; Vol. 19 (4); pp: 482-487; 1951.

128. van der Merwe, J.H.; C.R.C. Crit. Rev. Solid State Mater. Sci.; Vol. 7; pp: 209-231; 1978.

129. Walton, A.G.; The Formation and Properties of Precipitates; Interscience, New York; pp: 12-41; 1967.

130. Koutsoukos, P.G. and Nancollas, G.H.; Jou. Cryst. Growth; Vol. 53; pp: 10-19; 1981.

131. Gill, J.S. and Nancollas, G.H.; Desalination; Vol. 29 (3); pp: 247-253; 1979.

132. Liu, S.T. and Nancollas, G.H.; Jou. Cryst. Growth; Vol. 6; pp: 281-289; 1970.

133. Nancollas, G.H. and Liu, S.T.; Soc. Pet. Eng. Jou.; Vol. 15 (6); pp: 509-516; 1975.

134. Reddy, M.M. and Nancollas, G.H.; Jou. Coll. Interf. Sci.; Vol. 36 (2); pp: 166-177; 1971.

135. Nancollas, G.H. and Reddy, M.M.; Jou. Coll. Interf. Sci.; Vol. 37 (4); pp: 824-830; 1971.

136. Barone, J.P. and Nancollas, G.H.; Jou. Coll. Interf. Sci.; Vol. 62 (3); pp: 421-431; 1977.

137. Pashley, D.W.; in: Epitaxial Growth, Part A; ed.: J.W. Matthews; Academic Press, New York; pp: 1-27; 1975.

138. van der Merwe, J.H.; Disc. Farad. Soc.; No. 5; pp: 201-214; 1949.

139. Grunbaum, E.; in: Epitaxial Growth, Part B; ed.: J.W. Matthews; Academic Press, New York; pp: 611-673; 1975.

140. Pashley, D.W.; Recent Progr. Surface Sci.; Vol. 3; pp: 23-69; 1970.

141. Abbott, H.M. and Kerrigan, J.V.; U.S. Atomic Energy Commission; Report No. NP.-13168; 77 pp.; 1963.

142. Ickert, L.; Z. Phys. Chem. (Leipzig); Vol. 221; pp: 301-327; 1962.

143. Ickert, L.; Z. Phys. Chem. (Leipzig); Vol. 221; pp: 328-345; 1962.

144. Dankov, P.D.; Zh. Fiz. Khim.; Vol. 20; pp: 853-867; 1946.

145. Frank, F.C. and van der Merwe, J.H.; Proc. Royal Soc. (Lond.); Vol. 198A; pp: 205-216; 1949.

146. Frank, F.C. and van der Merwe, J.H.; Proc. Royal Soc. (Lond.); Vol. 198A; pp: 216-225; 1949.

147. Frank, F.C. and van der Merwe, J.H.; Proc. Royal Soc. (Lond.); Vol. 200A; pp: 125-134; 1949.

148. Zalkin, V.M.; Russ. Jou. Phys. Chem.; Vol. 36; pp: 716-717; 1962.

149. Blisnakov, G.; Compt. Rend.; Vol. 242; pp: 656-657; 1956.

150. Newkirk, J.B. and Turnbull, D.; Jou. Appl. Phys.; Vol. 26 (5); pp: 579-583; 1955.

151. Turnbull, D. and Vonnegut, B.; Ind. Eng. Chem; Vol. 44; pp: 1292-1298; 1952.

152. Neuhaus, A.; Z. Electrochem.; Vol. 56; pp: 453-458; 1952.

153. Neuhaus, A.; Fortschr. Mineral.; Vol. 28; pp: 58-63; 1949.

154. Mason, B.J. and van den Heuvel, A.P.; Proc. Phys. Soc.; Vol. 74; pp: 744-755; 1959.

155. Schulz, L.G.; Acta. Cryst.; Vol. 5; pp: 264-265; 1952.

156. Edwards, G.R. and Evans, L.F.; Trans. Farad. Soc.; Vol. 58; pp: 1649-1655; 1962.

157. Fletcher, N.H.; Jou. Chem. Phys.; Vol. 29 (3); pp: 572-576; 1958.

158. Fletcher, N.H.; Jou. Chem. Phys.; Vol. 38 (1); pp: 237-240; 1963.

159. Willems, J.; Z. Krist.; Vol. 105; pp: 53-68; 1943.

160. Sloat, C.A. and Menzies, A.W.C.; Jou. Phys. Chem.; Vol. 35; pp: 2005-2021; 1931.

161. Johnson, G.W.; Jou. Appl. Phys.; Vol. 22 (6); pp: 797-805; 1951.

162. Schulz, L.G.; Acta. Cryst.; Vol. 4; pp: 483-486; 1951.

163. Shaskolskii, M. and Shubnikov, A.; Z. Krist.; Vol. 85; pp: 1-6; 1933.

164. Triche, H.; Anal. Chim. Acta.; Vol. 4; pp: 12-20; 1950.

165. Miller, C.H. and Benge, R.J.; British Patent No. 1,333,551; Oct. 1973; assigned to Minister of Aviation, London; 1973.

166. Donnay, J.D.H., Donnay, G. and Cox, E.G.; (editors); Crystal Data - Determinitive Tables; 2nd edition; American Crystallographic Association; 1963.

167. Pistorius, C.W.F.T. and Pistorius, M.C.; Z. Krist.; Vol. 117; pp: 259-271; 1962.

168. Wyckoff, R.W.G.; Crystal Structures, Vol. 2; 2nd edition; Interscience, New York; 1964.

169. Weast, R.C. (ed.); C.R.C. Handbook of Chemistry and Physics; 61 st edition; C.R.C. Press, Florida; 1980.

170. Bourgeois, L.; Compt. Rend.; Vol. 88; pp: 382-383; 1879.

171. Shidlovskii, A.A., Voskresenskii, A.A. and Balakireva, T.N.; Russ. Jou. Phys. Chem.; Vol. 45 (7); p. 1067; 1971.

172. Sax, N.I. et al; Dangerous Properties of Industrial Materials; 5th Edition; Van Nostrand Reinhold, New York; 1979.

173. Basset, J., Denney, R.C., Jeffrey, G.H. and Mendham, J.; Vogel's Textbook of Quantitative Inorganic Analysis; 4th edition; Longman, London; p: 453; 1978.

174. Tennent, R.M. (ed.); Science Data Book; Oliver & Boyd, Edinburgh; 1971.

175. Dean, J.A. (ed.); Lange's Handbook of Chemistry; 12th edition; McGraw-Hill, New York; 1979.

176. Wyckoff, R.W.G.; Crystal Structures, Vol. 1; 2nd edition; Interscience, New York; 1963.

177. Pye Unicam Ltd. (agents for Philips); Instructions for Use - Philips PW9409 Digital pH Meter; 1979.

178. National Research Council, U.S.A.; International Critical Tables, Vol. 7; McGraw-Hill, New York; p. 301; 1930.

179. Kohlrausch, F.; Z. Phys. Chem.; Vol. 64; pp: 129-169; 1908.

180. Stephen, H. and Stephen, T. (editors); Solubilities of Inorganic and Organic Compounds, Vol. 1; Pergamon, Oxford; 1963.

181. Waddell, J.; Analyst; Vol. 43; pp: 287-289; 1918.

182. Beyer, G.L. and Rieman, W.; Jou. Am. Chem. Soc.; Vol. 65; pp: 971-973; 1943.

183. Osawa, T.; Bunseki Shiyaka; Vol. 2; pp: 250-257; 1948; (MOD translation no.: TN243 (DRIC-T-4929)).

184. Wyman, J.; Jou. Am. Chem. Soc.; Vol. 55; pp: 4116-4121; 1933.

185. Robinson, R.A. and Stokes, R.H.; Electrolyte Solutions; 2nd edition; Butterworths, London; 1970.

186. Zimmerman, H.K.; Chem. Rev.; Vol. 51; pp: 25-65; 1952.

187. Kertes, A.S., Levy, O. and Markovits, G.Y.; in: Experimental Thermodynamics, Vol. 2; ed: Le Neindre, B. and Vodar, B.; Butterworths, London; pp: 725-748; 1975.

188. James, A.M.; Practical Physical Chemistry; 2nd edition; Churchill, London; pp: 116-128; 1967.

189. Dundon, M.L.; Jou. Am. Chem. Soc.; Vol. 45; pp: 2658-2666; 1923.

190. Rao, C.N.R.; Ultraviolet and Visible Spectroscopy; 3rd edition; Butterworths, London; 1975.

191. Koryta, J.; Ion-selective Electrodes; Cambridge University Press, Cambridge; 1975.

192. Moody, G.J. and Thomas, J.D.R.; Selective Ion Sensitive Electrodes; Merrow, Watford; 1971.

193. Philips' Gloeilampenfabriken; Guide to the Use of Ion Selective Electrodes; Eindhoven; 1975.

194. Marlow, J.S. and Chapman, B.; Pye Unicam Ltd., (Agents for Philips); Private Communications; 1980, 1981.

195. Harned, H.S. and Owen, B.B.; The Physical Chemistry of Electrolyte Solutions; 3rd edition; Reinhold, New York; 1958.

196. Wolfe, M.A.; Numerical Methods for Unconstrained Optimisation: An Introduction; Van Nostrand Reinhold, New York; pp: 130-141; 1978.

197. Nelder, J.A. and Mead, R.; Computer Jou.; Vol. 7 (4); pp: 308-313; 1965.

198. Schnabel, B.K.; M.Sc. Thesis; University of Leeds; 1966.

199. Parkinson, J.M. and Hutchinson, D.; in: Proc. Conf. on Numerical Methods for Non-linear Optimisation; ed.: Lootsma, F.A.; Academic Press, London; pp: 115-135; 1972.

200. Simons, T.J., De Silva, R.L. and Creasy, D.E.; Jou. Chem. Tech. Biotechnol.; Vol. 32; pp: 518-524; 1982.

201. Himmelblau, D.M.; Process Analysis by Statistical Methods; Wiley, New York; pp: 176-207; 1970.

202. Hawksley, P.G.W.; B.C.U.R.A. Bulletin; Vol. 15 (4); pp: 105-146; 1951.

203. Hawksley, P.G.W.; B.C.U.R.A. Bulletin; Vol. 16 (4); pp: 117-147; 1952.

204. Hawksley, P.G.W.; B.C.U.R.A. Bulletin; Vol. 16 (5); pp: 181-209; 1952.

205. Allen, T.; Particle Size Measurement; 3rd edition; Chapman and Hall, London; 1980.

206. Allen, T.; Lab. Equip. Digest; Feb. 1980; pp: 81-87; 1980.

207. Heywood, H.; Proc. Inst. Mech. Eng.; Vol. 140; pp: 257-347; 1938.

208. Coulson, J.M. and Richardson, J.F.; Chemical Engineering, Vol. 2; 3rd edition; Pergamon, Oxford; pp: 1-12; 1978.

209. Leschonski, K.; Powder Tech.; Vol. 24; pp: 115-124; 1979.

210. British Standards Institution; Test Sieving; BS 1796; 1976.

211. British Standards Institution; Specification for Test Sieves; BS 410; 1969.

212. Coulter Electronics Ltd.; Instruction Manual for Coulter Counter Model Z_B (Industrial); 1975.

213. Samartzopoulos, C.G.; Lab. Practice; Jan. 1964; pp: 39-42; 1964.

214. Allen, T. and Marshall, K.; The Electrical Sensing Zone Method of Particle Size Measurement; University of Bradford; 1972.

215. Allen, T.; Proc. Conf. Particle Size Analysis; Sept. 1966; Soc. Anal. Chem.; pp: 110-153; 1966.

216. Lines, R.W.; Powder Tech.; Vol. 7; pp: 129-136; 1973.

217. Yarde, H.R.; Jou. Sci. Instrum.; Vol. 42; p.711; 1965.

218. Krebs, R.D.; Jou. Sci. Instrum.; Vol. 42; p.891; 1965.

219. Chaffin, E.P.; Proc. 5th Brit. Coulter Counter Users' Meeting, London; March 16-17; 1967.

220. Ullrich, W.J.; in: Recent Developments in Powder Metallurgy, Vol. 1; ed.: Hausner, H.; Plenum Press, New York; pp: 125-143; 1966.

221. Harfield, J.G.; Coulter Electronics Ltd.; Private Communications; 1980, 1981.

222. Harfield, J.G., et al; in: Particle Size Analysis; ed.: Groves, M.J.; Heyden, London; pp: 378-394; 1978.

223. Coulter Electronics Ltd.; Coulter Counter Calibration Standards, Assay Sheets; 1980, 1981.

224. Lloyd, P.J., Stenhouse, J.I.T. and Buxton, R.E.; in: Particle Size Analysis; ed.: Groves, M.J.; Heyden, London; pp: 367-377; 1978.

225. Wales, M. and Wilson, J.N.; Rev. Sci. Instrum.; Vol. 32 (10); pp: 1132-1136; 1961.

226. Princen, L.H. and Kwolek, W.F.; Rev. Sci. Instrum.; Vol. 36 (5); pp: 646-653; 1965.

227. Edmundson, I.C.; Nature; Vol. 212; pp: 1450-1452; 1966.

228. Harris, C.C. and Jowett, A.; Nature; Vol. 208; pp: 175-176; 1965.

229. Sopp, O.I. and Moum, J.; Nature; Vol. 210; pp: 724-725; 1966.

230. Eckhoff, R.K.; Nature; Vol. 210; pp: 765-766; 1966.

231. Kubitschek, H.E.; Rev. Sci. Instrum.; Vol. 33 (5); pp: 576-577 ; 1962.

232. Gwyn, J.E., Crosley, E.J. and Marshall, W.R.; Ind. Eng. Chem. (Fundam.); Vol. 4 (2); pp: 204-208; 1965.

233. British Standards Institution; The Determination of Particle Size of Powders, Part 2: Liquid Sedimentation Methods; BS 3406, Pt. 2; 1963.

234. Svarovsky, L. and Allen, C.J.; in: Particle Size Analysis; ed.: Groves, M.J.; Heyden, London; pp: 441-450; 1978.

235. Chuffart, R.C.; British Patent 851, 067; Oct. 1960; assigned to I.C.I. Ltd.; 1960.

236. King, W.G. and Burrus, H.L.; G.E.C. Jou. Sci. & Tech.; Vol. 39 (2); pp: 76-84; 1972.

237. Grimes, G.R.; Paper presented at a local American Chemical Society Meeting; 1961.

238. Mistler, R.E., Muccigrosso, A.T. and Ploetz, G.L.; paper presented at 63rd Annual Meeting of the American Ceramic Society; 1961.

239. Mullin, J.W. and Ang, H.M.; Powder Tech.; Vol. 10; pp: 153-156; 1974.

240. Rosen, H.N. and Hulburt, H.M.; Ind. Eng. Chem. (Fundam.); Vol. 9 (4); pp: 658-661; 1970.

241. Shah, M.B.; Ph.D. Thesis; University College, London; 1980.

242. Garside, J., Mullin, J.W. and Das, S.N.; Ind. Eng. Chem. (Proc. Des. Dev.); Vol. 12 (3); pp: 369-371; 1973.

243. Harris, C.C.; Nature; Vol. 187; pp: 401-403; 1960.

244. Randolph, A.D. and Larson, M.A.; Theory of Particulate Processes; Academic Press, New York; 1971.

245. Ang, H.M. and Mullin, J.W.; Trans. Instn. Chem. Engrs.; Vol. 57; pp: 237-243; 1979.

246. Hulburt, H.M.; in: Proc. 6th Symp. Ind. Cryst.; ed.: Mullin, J.W.;Plenum Press, New York; pp: 343-351; 1976.

247. Hulburt, H.M. and Katz, S.; Chem. Eng. Sci.; Vol. 19; pp: 555-574; 1964.

248. Canning, T.F. and Randolph, A.D.; AIChE Jou.; Vol. 13 (1); pp: 5-10; 1967.

249. Bransom, S.H.; Brit. Chem. Eng.; Vol. 5; pp: 838-844; 1960.

250. van Oosterhout, G.W. and van Rosmalen, G.M.; Jou. Cryst. Growth; Vol. 48; pp: 464-468; 1980.

251. van Rosmalen, G.M., van der Leeden, M.C. and Gouman, J.; Krist. Tech.; Vol. 15 (10); pp: 1213-1222; 1980.

252. Bransom, S.H. and Dunning, W.J.; Disc. Farad. Soc.; No. 5; pp: 96-103; 1949.

253. Liao, P.F. and Hulburt, H.M.; Proc. 69th Annual Meeting of AIChE, Chicago; pp: G1-G14; 1976.

254. von Smoluchowski, M.; Z. Physik. Chem.; Vol. 92; pp: 129-168; 1917.

255. von Smoluchowski, M.; Z. Physik.; Vol. 17; pp: 557-571 and 585-599; 1916.

256. Sastry, K.V.S. and Fuerstenau, W.; Ind. Eng. Chem. (Fundam.); Vol. 9 (1); pp:145-149; 1970.

257. Wahl, E.F. and Baker, C.G.J.; Can. Jou. Chem. Eng.; Vol. 49; pp: 742-746; 1971.

258. Halfon, A. and Kaliaguine, S.; Can. Jou. Chem. Eng.; Vol. 54; pp: 168-172; 1976.

259. Sarig, S., Eidelman, N., Glasner, A. and Epstein, J.A.; Jou. Appl. Chem. Biotech.; Vol. 28; pp: 663-667; 1978.

260. Wang, C.S.; Ph.D. Thesis; California Institute of Technology, Pasadena; 1966; (in: Dissert. Abs.; Vol. 27B; pp: 1575-1576; 1966/67).

261. Packter, A.; Krist. Tech.; Vol. 9 (3); pp: 249-256; 1974.

262. Packter, A. and Saunders, D.F.; Z. Phys. Chem. (Leipzig); Vol. 249 (5/6); pp: 353-358; 1972.

263. Packter, A.; Krist. Tech.; Vol. 12 (7); pp: 729-735; 1977.

264. Gunn, D.J. and Murthy, M.S.; Chem. Eng. Sci.; Vol. 27; pp: 1293-1313; 1972.

265. Mullin, J.W. and Osman, M.M.; Krist. Tech.; Vol. 8 (4); pp: 471-481; 1973.

266. Sohnel, O. and Mullin, J.W.; Krist. Tech.; Vol. 14 (2); pp: 217-228; 1979.

267. Gill, P.E. and Murray, W.; Jou. Inst. Maths. Applics.; Vol. 9; pp: 91-108; 1972.

268. Tong, J.Y. and Johnson, R.L.; Inorg. Chem.; Vol. 5 (11); pp: 1902-1906; 1966.

269. Lukkari, O.; Suomen Kemistilehti B ; Vol. 43 (10); pp: 347-351; 1970.

270. Haight, G.P., Richardson, D.C. and Coburn, N.H.; Inorg. Chem.; Vol. 3 (12); pp: 1777-1780; 1964.

271. Tong, J.Y. and King, E.L.; Jou. Am. Chem. Soc.; Vol. 75; pp: 6180-6186; 1953.

272. Tong, J.Y.; Inorg. Chem.; Vol. 3; pp: 1804-1805; 1964.

273. Lukkari, O.; Ann. Univ. Turku. Ser. A1; No. 100; 57 pp.; 1967.

274. Sherrill, M.S.; Jou. Am. Chem. Soc.; Vol. 29; pp. 1641-1650; 1907.

275. Spitalsky, E.; Z. Anorg. Chem.; Vol. 54; pp: 265-314; 1907.

276. Lundberg, J.; Z. Anorg. Chem.; Vol. 55; pp: 426-436; 1907.

277. Neuss, J.D. and Rieman, W.; Jou. Am. Chem. Soc.; Vol. 56; pp: 2238-2243; 1934.

278. Galea, J. and Haladjian, J.; Rev. de. Chim. Miner.; Vol. 7 (3); pp: 623-634; 1970.

279. Linge, H.G. and Jones, A.L.; Austr. Jou. Chem.; Vol. 21; pp: 2189-2198; 1968.

280. Sasaki, Y.; Acta. Chem. Scand.; Vol. 16 (3); pp: 719-734; 1962.

281. Arnek, R. and Johansson, S.R.; Acta. Chem. Scand.; Vol. 26 (7); pp: 2903-2906; 1973.

282. Jain, D.V.S. and Jain, C.M.; Jou. Chem. Soc. (A); pp: 541-542; 1967.

283. Moore, P., Kettle, S.F.A. and Wilkins, R.G.; Inorg. Chem.; Vol. 5; pp: 220-223; 1966.

284. Davies, W.G. and Prue, J.E.; Trans. Farad. Soc.; Vol. 51; pp: 1045-1051; 1955.

285. Kortum, G.; Z. Phys. Chem. B ; Vol. 33; pp: 243-264; 1936.

286. Lukkari, O.; Suomen Kemistilehti B ; Vol. 38 (5/6); pp: 121-122; 1962.

287. Kokenge, B.R.; Ph.D. Thesis; Ohio University; 1966. (in: Dissert. Abs.; Vol. 27B; pp: 2639-2640; 1966/67).

288. Lukkari, O.; Suomen Kemistilehti B ; Vol. 35 (5/6); p. 91; 1962.

289. Scrutton, A. and Grootscholten, P.A.M.; Trans. Instn. Chem. Engrs.; Vol. 59; pp: 238-246; 1981.

290. Nancollas, G.H. and Purdie, N.; Trans. Farad. Soc.; Vol. 59; pp: 735-740; 1963.

291. Liu, S.T., Nancollas, G.H. and Gasiecki, E.A.; Jou. Cryst. Growth; Vol. 33 (1); pp: 11-20; 1976.

292. Davies, C.W. and Jones, A.L.; Trans. Farad. Soc.; Vol. 51; pp: 812-817; 1955.

293. Davies, C.W. and Nancollas, G.H.; Trans. Farad. Soc.; Vol. 51; pp: 818-823; 1955.

294. Davies, C.W. and Nancollas, G.H.; Trans. Farad. Soc.; Vol. 51; pp: 823-829; 1955.

295. Smith, B.R. and Sweett, F.; Jou. Coll. Interf. Sci.; Vol. 37 (3); pp: 612-618; 1971.

296. Nancollas, G.H. and Gardner, G.L.; Jou. Cryst. Growth; Vol. 21; pp: 267-276; 1974.

297. Garside, J., Brecevic, L. and Mullin, J.W.; Jou. Cryst. Growth.; Vol. 57 (2); pp: 233-240; 1982.

298. Furedi-Milhofer, H., Brecevic, L. and Pugaric, B.; Disc. Farad. Soc.; No. 61; pp: 184-193; 1976.

299. Marshall, R.W. and Nancollas, G.H.; Jou. Phys. Chem.; Vol. 73 (11); pp: 3838-3844; 1969.

300. Packter, A., Alleem, A., Chauhan, P. and Uppaladini, S.C.; Cryst. Res. Tech.; Vol. 16 (12); pp: 1419-1424; 1981.

301. Numerical Algorithms Group; NAG FORTRAN Library Manual Mark 7, Vol. 2; NAG, Oxford; 1978.

302. Broyden, C.G.; in: Numerical Methods for Unconstrained Optimisation; ed.: Murray, W.; Academic Press, London; pp: 87-106; 1972.

303. Murray, W.; in: Numerical Methods for Unconstrained Optimisation; ed.: Murray, W.; Academic Press, London; pp: 107-122; 1972.

304. Buckley, H.E.; Crystal Growth; Wiley, New York; 1951.

305. Nielsen, A.E.; Pure & Appl. Chem.; Vol. 53; pp: 2025-2039; 1981.

306. Garside, J.; Chem. Eng. Sci.; Vol. 26; pp: 1425-1431; 1971.

307. De Silva, R.L., Falangas, E. and Creasy, D.E.; Trans. Instn. Chem. Engrs.; Vol. 58; pp: 135-137; 1980.

308. Garside, J. and Mullin, J.W.; Trans. Instn. Chem. Engrs.; Vol. 46; pp: 11-18; 1968.

309. Reich, R. and Kahlweit, M.; Ber. Bunsenges. Physik. Chemie.; Vol. 72 (1); pp: 66-69; 1968.

310. Reich, R. and Kahlweit, M.; Ber. Bunsenges. Physik. Chemie.; Vol. 72 (1); pp: 70-74; 1968.

311. Eigen, M. and Maas, G.; Z. Physik. Chem. (Frankfurt); Vol. 49 (4/5); pp: 163-177; 1966.

312. Glasstone, S. and Lewis, D.; Elements of Physical Chemistry; 2nd edition; Macmillan, London; pp: 631-639; 1974.

313. Kavanau, J.L.; Water and Solute-Water Interactions; Holden-Day Inc., San Francisco; 1964.

314. Padova, J.; Jou. Chem. Phys.; Vol. 39 (6); pp: 1552-1557; 1963.

315. Padova, J.; Jou. Chem. Phys.; Vol. 40 (3); pp: 691-694; 1964.

316. Muirhead-Gould, J.S. and Laidler, K.J.; Trans. Farad. Soc.; Vol. 63 (4); pp: 944-952; 1967.

317. Laidler, K.J. and Muirhead-Gould, J.S.; Trans. Farad. Soc.; Vol. 63 (4); pp: 953-957; 1967.

318. Goldman, S. and Bates, R.G.; Jou. Am. Chem. Soc.; Vol. 94 (5); pp: 1476-1484; 1972.

319. Tremaine, P.R. and Goldman, S.; Jou. Phys. Chem.; Vol. 82 (21); pp: 2317-2321; 1978.

320. Rideal, G.; Lab. Equip. Digest; Vol. 20 (6); pp: 83-87 and 90; 1982.

321. Creasy, D.E.; Crystallisation and Other Topics; TR 14; Department of Chemical Engineering; University of Aston in Birmingham; 1972.

322. Creasy, D.E. and Skander, J.L.; Crystal Growth of Low Solubility Materials; Sixth Progress Report - First Series; TR 18(6); Department of Chemical Engineering; University of Aston in Birmingham; 1977.

323. Allen, T.; Particle Size Measurement; 1st edition; Chapman and Hall, London; pp: 62-64; 1968.